Relative Permeability Estimation in a CO_2/Heavy Oil system

By

Olufemi Saliu

B.Sc., MSc.

Submitted for the Degree of Doctor of Philosophy

Heriot-Watt University

School of Energy, Geoscience, Infrastructure and Society

Institute of Petroleum Engineering

December 2017

Abstract

With the decline in the world reserves of conventional hydrocarbon resources, attention is shifting to the exploitation of unconventional resources like heavy oil. Though the thermal recovery method is quite common with heavy oil, studies and field trials have shown that in certain situations, non-thermal methods like CO_2-flooding could be more appropriate in exploiting heavy oil reservoirs. Relative permeability for oil, water, and gas are necessary requirements in carrying out numerical simulation for the purpose of predicting and optimizing recovery from these non-thermal methods. The scarcity of information on heavy oil relative permeability often leads to the erroneous application of the conventional oil relative-permeability assumptions in the simulation of heavy oil processes. Studies have shown that viscous fingering, oil swelling, and drastic reduction of viscosity due to dissolution of gas in oil are common phenomena in the recovery processes of heavy oil, thus it is expected that the properties of the relative permeability of heavy oil should be different from the relative permeability from conventional oil which clearly has a different recovery mechanism.

In this work, the results of series of coreflood unsteady-state two-phase displacement experiments were used to investigate the characteristics of two phase relative permeability in heavy oil production processes. The experiments were carried out on two different heavy oils with different viscosity on cores of similar characteristics. Firstly, two phase relative permeability of the heavy oil processes were estimated by the history matching and the analytical approach for oil-water, and oil-gas systems. Also, in order to investigate the suitability of existing three phase models in simulating three phase flow in heavy oil systems, the two phase relative permeability curves from the history matching technique were used to generate three phase relative permeability curves. Also investigated was the appropriateness of the analytical method to generate three phase relative permeability curves.

In this work, the relative permeability curves from several heavy oil core flood experiments using 1D and 2D models is estimated. These experiments involve different heavy oil viscosities, and different core orientations. This study shows that when gas or water is injected to improve the recovery of heavy oil, the values of the residual oil saturation vary with oil viscosity. As a result of these effects, the relative permeability curves estimated from these core flood experiments are also found to vary with the oil viscosity. Besides the effect

of oil viscosity on the relative permeability curves of heavy oil systems, the relative permeability curves obtained from cores in the vertical direction during flooding are also observed to be different from those obtained from cores placed in the horizontal direction.

The performance of the correlation-generated three-phase relative permeability models were assessed by comparing the results of the simulation against the experimental data. From the results, it is seen that there could be large prediction errors if an inappropriate three-phase relative permeability model is used for the simulation. The analytical method was also found deficient in estimating three-phase relative permeability curves for heavy oil systems. An automatic history matching of the three phase experimental results of heavy oil was then used to give very accurate relative permeability results, though this could be laborious and time-consuming.

The main conclusions derived from this work are that (1) while the relative permeability from conventional oil are only dependent on saturation, the relative permeability from heavy oil (in addition to saturation), is dependent on oil viscosity and direction of flow; (2) once there is a proven case of instability in the heavy oil system, a 2D grid system should be used to estimate relative permeability curves in order that the viscous fingering in the system can be modelled; (3) The analytical corrected Nitrogen-heavy oil relative permeability can be used as a substitute relative permeability to model CO_2/heavy oil system; (4) The three phase relative permeability models in existing reservoir simulation packages are not adequate in modelling three phase flow in heavy oil; the three phase relative permeability for modelling heavy oil processes should be instead estimated from the automatic history matching of the three phase experimental results of the heavy oil.

Dedicated to the Almighty God, the father of lights, with whom there is no variableness, nor shadow of turning.

Acknowledgements

I would like to express my gratitude to my supervisor Professor Mehran Sohrabi for the opportunity he gave me to fulfil an ambition, and for his guidance and fatherly role throughout the course of my work on this thesis. My appreciation also goes to Professor Mahmoud Jamiolahmady and Dr Hamidreza Shahverdi for their technical support during the course of this research. I also owe my friend and partner in the EOR team, Dr Alireza Emadi, a big debt of gratitude for conducting the micro-model and core-flood experimental works of the heavy oil project.

I am also appreciative of the support and encouragement I got from Norida Kechut, Jalal Foroozesh, Pedram Mahzari, Seyi Awodele, Akindolu Dada, Pastor Christiana Longe and the RCCG Open Heavens family, and Pastor Victor Francis and the RCCG Livingston Assembly family. They all made my stay in Edinburgh memorable.

My gratitude also goes to the following: my dear wife, Omobolawa Anike Femi-Saliu for her sacrifice, endurance, prayers and love; to my daughters, Omoyeni Femi-Saliu and Omolade Femi-Saliu for their love and patience; to my siblings for their love and understanding; and lastly to my parents Mr Suraju Ade Saliu, and Mrs Risikat Ajoke Saliu for their prayers and best wishes.

ACADEMIC REGISTRY
Research Thesis Submission

Name*:*	Olufemi Saliu		
School:	Energy, Geoscience, Infrastructure and Society		
Version: *(i.e. First, Resubmission, Final)*	Final	Degree Sought:	PhD in Petroleum Engineering

Declaration

In accordance with the appropriate regulations I hereby submit my thesis and I declare that:

1) the thesis embodies the results of my own work and has been composed by myself
2) where appropriate, I have made acknowledgement of the work of others and have made reference to work carried out in collaboration with other persons
3) the thesis is the correct version of the thesis for submission and is the same version as any electronic versions submitted*.
4) my thesis for the award referred to, deposited in the Heriot-Watt University Library, should be made available for loan or photocopying and be available via the Institutional Repository, subject to such conditions as the Librarian may require
5) I understand that as a student of the University I am required to abide by the Regulations of the University and to conform to its discipline.
6) I confirm that the thesis has been verified against plagiarism via an approved plagiarism detection application e.g. Turnitin.

* *Please note that it is the responsibility of the candidate to ensure that the correct version of the thesis is submitted.*

Signature of Candidate*:*		Date:	01/12/2017

Submission

Submitted By *(name in capitals):*	
Signature of Individual Submitting:	
Date Submitted:	

For Completion in the Student Service Centre (SSC)

Received in the SSC by *(name in capitals):*			
Method of Submission *(Handed in to SSC; posted through internal/external mail):*			
*E-thesis Submitted (**mandatory for final theses**)*			
Signature:		Date:	

Table of Contents

Chapter 1: Introduction

1.1 Background

Heavy oil development around the world is getting a lot of attention as a result of the decline in conventional oil reserves, and the steady increase in the world demand for petroleum. Figure 1.1 shows a projection of World Oil Supply against World Oil Demand by the International Energy Agency (IEA) indicating that as at 2014, world oil demand has already outgrown world oil supply (Alboudwarej et al., 2006).

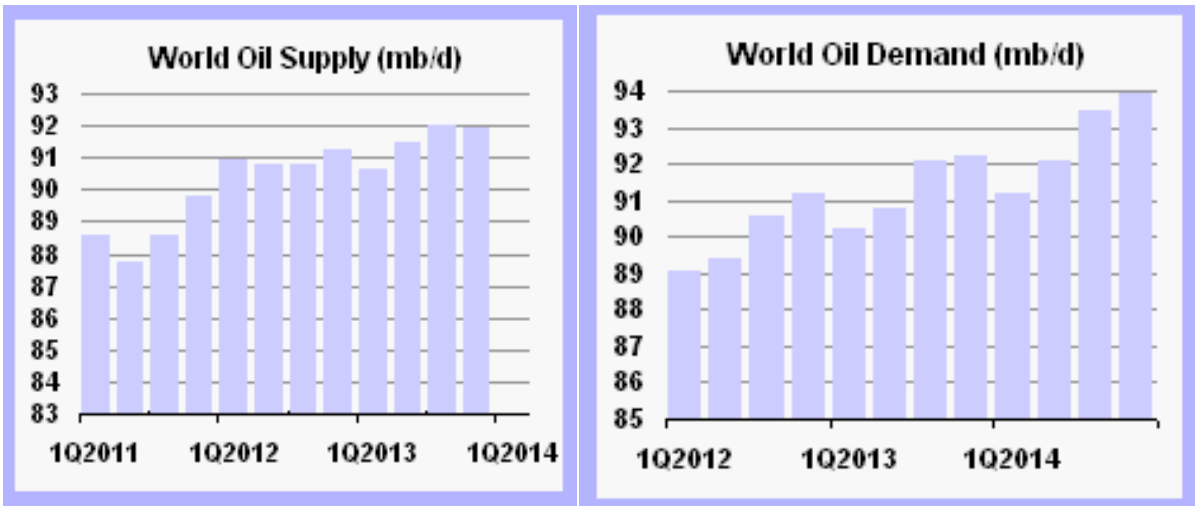

Figure 1.1: World Oil Supply vs World Oil Demand (Alboudwarej et al., 2006).

The persistent shortfall between the oil demand and supply, which is a result of economic development activities in places like China, India, and Brazil, has pushed the oil price to an unprecedented height for more than ten years. This lasting high price is however an incentive to investment in research and development of unconventional resources like heavy oil. Heavy Oil development has the potential to meet the world energy demand as a result of its reserve size and diversity. According to (Alboudwarej et al., 2006), heavy oil accounts for approximately 70% of the world's petroleum resources (9-13 trillion barrels); figure 1.2 shows the distribution of the world energy resources.

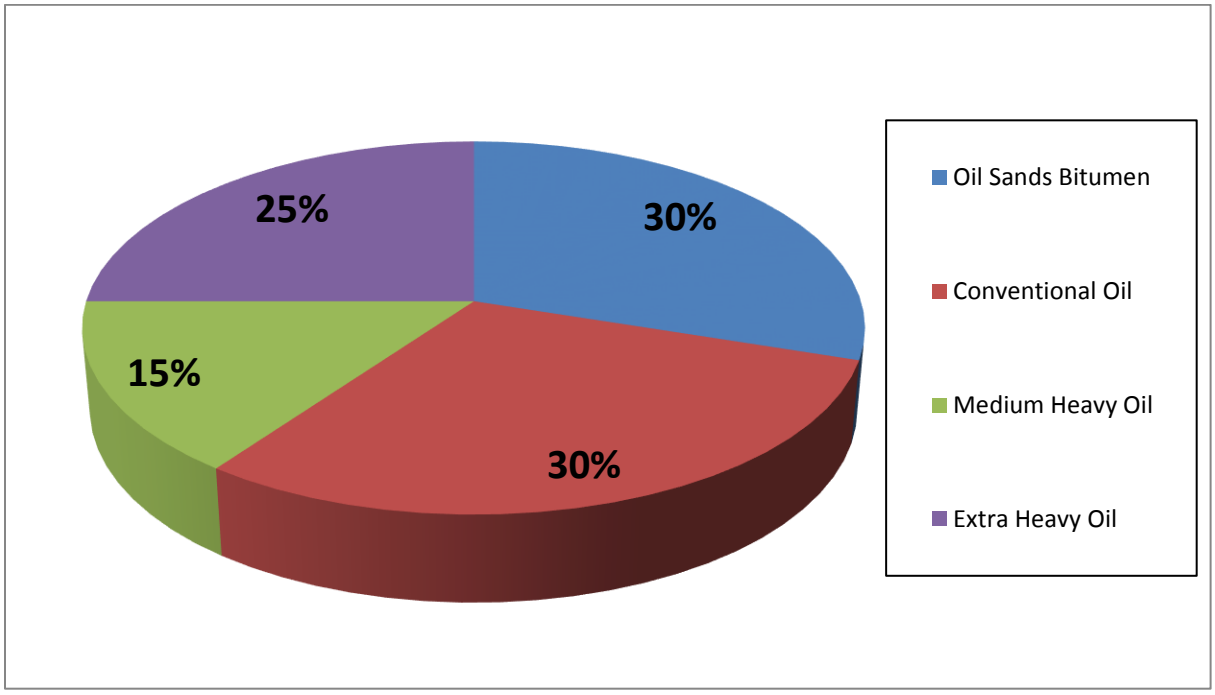

Figure 1.2: Heavy oil (medium heavy, extra heavy and bitumen) about 70% of the word total resources (Alboudwarej et al., 2006).

1.2 Heavy Oil

Heavy oils are oil with high viscosity (resistance to flow) and high density (low API gravity) as a result of the presence of large fractions of high molecular weight compounds. These compounds (usually consisting of Asphaltenes) have very low volatility and high melting point thereby giving heavy oil its unique characteristics. Compared to light oil (conventional oil), heavy oils are oils with maximum API gravity of 22° and a viscosity greater than 100 cp. Heavy oils are created when lighter molecular weight components in conventional oil are removed due to activities of bacteria, water washing, and evaporation during migration and entrapment; thereby leaving the remaining oil denser and more viscous (Emadi, 2012).

Heavy oils are often found in shallow reservoirs of about 4000ft or less (Brown et al., 2001). This is explained as the consequence of the escape of gas and light molecular weight components from oil due to ineffective reservoir seals occasioned by low pressure at these depths. Although it is an important resource, the economic development and production of heavy oil reservoirs can be very challenging due to their high density and viscosity.

Heavy oil production from the reservoir, just like in conventional oil production, can be through any of primary, secondary, and tertiary recovery method. While the energy in the reservoir is used to drive production in the primary recovery stage, water or gas is injected into the reservoir to displace oil towards producing wells and to maintain the reservoir pressure in the secondary recovery stage. Commercial production with the primary recovery method in heavy oil reservoirs is often not practicable as the recovery factor can be very small due to poor oil mobility. And using water flooding comes with the challenge of unfavorable mobility ratio between water and oil thereby leading to viscous fingering and very poor recovery.

1.3 EOR in Heavy Oil Reservoirs

The enhanced oil recovery method (or the tertiary recovery method) refers to all activities embarked upon to lower the residual oil saturation at the end of natural depletion and sometimes, after secondary recovery processes. These activities usually target the modification of interfacial tensions and wettability, the mobility of the driving fluid, and the alteration of the reservoir fluid properties in such a way that there is an overall improvement of oil recovered. The parameters used in measuring the success or otherwise of an EOR are mobility ratio (M) and the capillary number (Ca):

1.3.1 Mobility Ratio

Mobility ratio is the ratio of the mobility of the displacing fluid to the mobility of the displaced fluid

$$M = \frac{k_d/\mu_d}{ko/\mu o} \tag{1.1}$$

Where kd is the effective permeability of the displacing fluid, μd is the viscosity of the displacing fluid, ko is the effective permeability of the oil, and μo is the viscosity of the oil.

For good displacement efficiency, the mobility ratio has to be favorable ($M \leq 1$); that means, under an imposed pressure differential, the oil travels faster than the displacing fluid. If $M > 1$, this is unfavorable because the displacing fluid travels faster than the displaced fluid giving rise to viscous fingering where most of the oil is by-passed. So an EOR project would be technically successful if it lowers the viscosity of the oil, or it increases the viscosity of

the displacing fluid, or it increases the effective permeability to oil, or it decreases the effective permeability to the displacing fluid; or any combination of the above scenarios.

1.3.2 Capillary Number

Capillary number is ratio between the viscous and the capillary forces

$$Ca = \frac{\mu V}{\sigma} = K\frac{\frac{\Delta P}{L}}{\sigma} \tag{1.2}$$

Where μ is displacing fluid viscosity, V is the pore velocity, σ is the interfacial tension between the oil and displacing fluid, ΔP/L is the pressure gradient across a distance L, and K is the effective permeability to oil.

Capillary force is the force responsible for trapping oil in the reservoir hence high capillary force leads to high residual oil saturation. Any increase in capillary number as a result of an EOR process therefore means the process is at least a technical success. From equation 1.2, residual oil saturation of a certain oil can be decreased by any or combination of increasing the displacing fluid viscosity, increasing the pressure gradient, and decreasing the interfacial tension (IFT).

Enhanced heavy oil recovery mostly targets the reduction of oil viscosity through thermal processes as the viscosity of the oil is the most sensitive parameter to the recovery of heavy oil reservoirs. In this method, the application of heat energy into the reservoir lowers the oil viscosity by several orders of magnitude thus making the oil more mobile, and thereby enhancing its recovery. There are however non-thermal methods which can also be employed to enhance heavy oil recovery. These methods involve the injection of certain fluids that interact with the oil and the reservoir in such ways that favour additional oil recovery. Every heavy oil reservoir is unique so a recovery method that is successful in one may not be successful in another. Apart from oil properties like density and viscosity, reservoir geological properties like depth, areal extent, permeability, rock strength, and reservoir thickness must be taken into consideration when considering an optimum recovery technique for a heavy oil reservoir.

1.3.3 Thermal Recovery Methods

The thermal oil recovery methods have traditionally been used in the development of heavy oil in countries like Venezuela, Canada, and the United States where significant heavy oil production activities exist. Compared to conventional oil, heavy oil has very high viscosity, hence the thermal recovery process is used to reduce the in situ viscosity of the oil (which can be up to a couple of millions cp) and thus enhance the oil recovery. The different types of thermal recovery methods are discussed below:

I. In Situ Combustion

This is where a fire front is created in the reservoir with the aid of air injection. As the oil burns, the heat reduces oil viscosity, and the fire front moves in the reservoir displacing the fluids ahead of it towards the production wells. In situ combustion works best when the oil saturation and porosity are high. In this method, significant amount of heat is lost to the surroundings.

II. Hot Water Flooding

In this method, the hot water is injected into the reservoir to help in heating up the oil and bringing down its viscosity. However, the method does not have the capacity for significant oil recovery due to its associated poor volumetric sweep efficiency resulting in early breakthrough of water.

III. Steam Injection

This involves injecting high pressure and high temperature steam into the reservoirs thereby reducing oil viscosity and increasing recovery. The steam oil ratio (SOR) defined as the volume of steam needed in cold water equivalent per unit volume of produced oil is a measure of the efficiency of the oil recovery (Chang et al., 1990). Thus a steam injection project is assessed for feasibility by considering steam cost vis-a- vis the additional revenue from oil recovery due to steam injection. The cyclic steam stimulation, continuous steam injection, and steam-assisted gravity drainage (SAGD) are different steam injection schemes that have been implemented with high success rate.

1.3.4 Non-thermal Recovery Methods

The thermal heavy oil recovery methods, in addition to being capital intensive and environmentally unfriendly (as it generates high CO_2 footprint which has negative environmental impact), may be unsuitable in certain heavy oil reservoirs (e.g. thin reservoirs and deep reservoirs). As a result of these unfavorable conditions, research into non-thermal (cold) heavy oil recovery methods has been on the increase. Examples of non-thermal methods that have potential to efficiently produce a heavy oil reservoir are discussed below:

I. Miscible Flooding

This is an injection process where a gas or a mixture of gases that is miscible with the reservoir oil at the reservoir pressure and temperature is injected into the reservoir. In this process, the interface between the injected gas and the oil is removed, thus allowing for one phase flow of highly reduced viscosity, and total displacement efficiency. Gases used in this process include natural gas, Nitrogen and Carbon dioxide; but the choice of the injected gas in a particular reservoir case is a function of technical and economic feasibility in the case. In general, miscibility is a function temperature, pressure, and oil composition. Minimum Miscibility Pressure (MMP) of an oil reservoir system is the minimum pressure required at the reservoir temperature for the injected gas to be completely miscible with the oil. As most heavy oil reservoirs are found in shallow reservoirs with reservoir pressure lower than the minimum miscibility pressure, miscible flooding is hardly possible in heavy oil reservoirs.

II. Immiscible Gas Flooding

This is a process where gas is injected to displace the reservoir oil towards the producing well in conditions where the gas cannot achieve total miscibility with the oil. As this process is often hampered by unfavorable mobility ratio leading to viscous fingering and poor areal sweep efficiency, the attraction for its application is in the oil viscosity reduction, oil swelling, and gas-oil interfacial tension reduction. This attraction is more pronounced in CO_2 flooding of heavy oil where close to two orders of magnitude viscosity reduction has been observed (Klins, 1984).

III. CO_2 Flood

Carbon dioxide injection into heavy oil reservoirs has been found to reduce significantly the viscosity of the oil in a manner that is similar to what is obtainable in the heavy oil thermal recovery processes; hence CO_2 injection processes are very viable alternative to thermal heavy oil recovery. For conventional oil, CO_2 tends to be miscible in the oil thus offering very great recovery potential; whereas in a heavy oil system, CO_2 is not miscible with the oil as a result of the presence of heavier components, and due to the characteristic low reservoir pressure (usually lower than the minimum miscibility pressure) in heavy oil reservoirs. Thus, the recovery of heavy oil using CO_2 injection is through an immiscible displacement process where the main recovery mechanisms are viscosity reduction and oil swelling.

The suitability of CO_2 injection as an EOR technique in heavy oil production is as a result of high solubility of CO_2 in crude oil compared to other gases. The reason for this is that at the same temperature and pressure, CO_2 has the highest dissolution rate (lowest equilibrium ratio) among the gases. Due to this high dissolution rate, the oil viscosity reduces greatly improving the mobility of the oil towards the producing well; and the oil swells and expands out of dead end pores, bringing about significant addition to oil recovery. In addition, at high pressures, CO_2 density has a density close to that of a liquid making CO_2 less prone to gravity segregation. A major disadvantage of CO_2 flooding of heavy oil reservoirs, however, is the presence of viscous fingering in the immiscible displacement process. The viscous fingering is caused by flow instability at the displacement front resulting from a less viscous (and more mobile) fluid displacing a viscous fluid. This makes the recovery process inefficient and suffers from low recovery.

The potential benefits offered by CO_2 non-thermal heavy oil recovery method around the world are very huge. In Saskatchewan, Canada, it is estimated that development of enhanced oil recovery processes applicable to thin, unconsolidated sand reservoirs could recover as much as about 4 billion barrels of heavy oil. A CO_2-EOR project expected to inject 18 million ton CO_2 to recover 130 million barrels of oil was established in Weyburn Oil Field in south Saskatchewan in 2000 (Green et al., 1998). The use of CO_2 in EOR projects is also a potential means of reducing the contribution of fossil fuel emissions to global warming and

ocean acidification. CO_2 is first captured from fossil fuel power plants and other industries, and then transported to a storage site from where it could be retrieved for EOR purposes.

IV. Water Alternate Gas Flooding

In view of the poor sweep efficiency in immiscible CO_2 flooding, there are injection strategies that can be employed to tame viscous fingering in heavy oil recovery. One of them is the Water Alternate Gas flooding (WAG) where the CO_2 injection can be alternated with water injection, with the water sweeping the swollen, less viscous oil towards the production well; and redistributing the fluid in the porous medium thereby reducing the CO_2 relative permeability and increasing the oil recovery.

V. CO_2-Foam Flood

Another injection strategy employed to mitigate the effect of the poor sweep efficiency in CO_2 flooding is the CO_2-foam Flood to displace the oil. It has been found that in the presence of a suitable surfactant strong foam can be formed when CO2 and water are injected, either simultaneously or individually into the reservoir. Due to foam's high viscosity, it can help in improving mobility ratio in the reservoir when used as a displacing agent in heavy oil reservoirs.

1.4 Thesis Objective

The objective of this thesis is the numerical simulation of CO_2-EOR processes in heavy oil, resting on the overall project objective of investigating and developing non-thermal enhanced heavy oil recovery methods using CO_2, water, chemicals, and CO_2-foam at the Institute of Petroleum Engineering, Heriot Watt University.

The thesis objective is achieved by analysing data from a series of Micro-model and core-flood experiments that were performed in the laboratory at Heriot Watt by research staff. The micro-model experiments are visualization studies that show the underlying pore-scale mechanisms in the CO_2 flood, CO_2 alternate Water flood (WAG), and CO_2-foam flood. The results of these visualization studies can be useful in interpreting the core-flood experiments and in the tuning of the parameters used in the numerical simulation of the processes.

The core-flood experiments, also involving CO_2 flood, CO_2 alternate Water flood (WAG), and CO_2-foam flood, were designed to evaluate the potential in these processes in enhancing heavy oil recovery. They are also useful for estimating the relative permeability curves used in numerical simulation. Figure 1.3 shows the workflow of the joint industry project on Enhanced Heavy Oil Recovery in Heriot Watt University (Emadi, 2012).

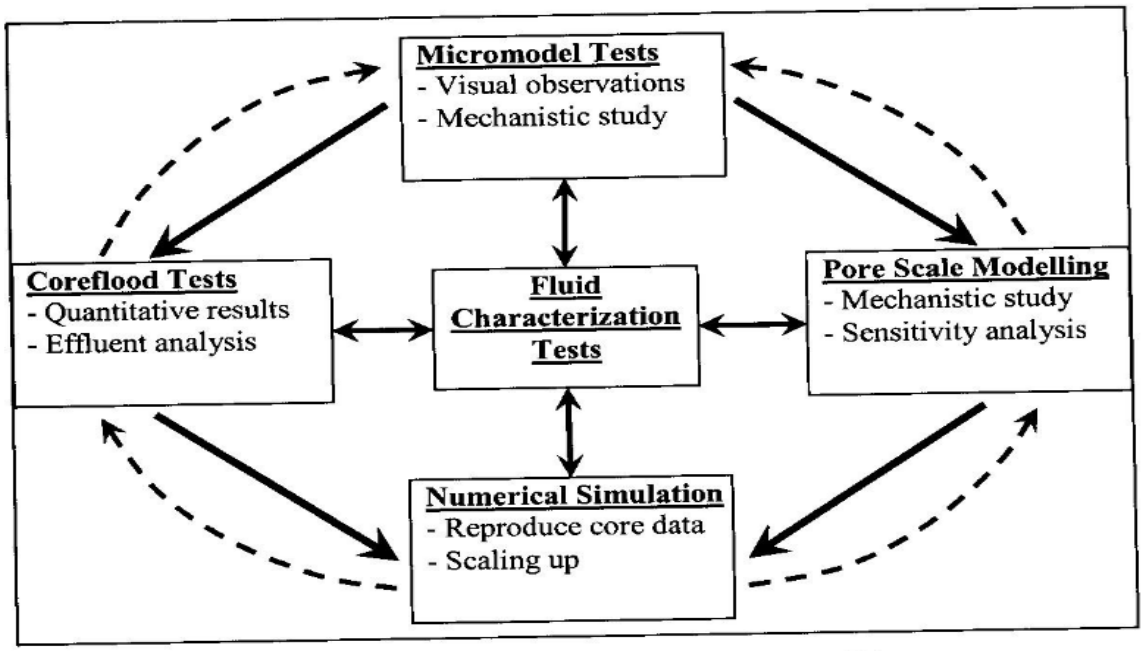

Figure 1.3: Workflow of the joint industry project on Enhanced Heavy Oil Recovery in Heriot Watt University (Emadi, 2012).

A lot of papers have been published by researchers on ways of improving heavy oil recovery processes through CO_2-EOR processes but not so many studies have been done on the numerical simulation of these processes. Since numerical simulation is essential in promoting overall project efficiency, this work is focused on the numerical simulation of the CO_2 flood, CO_2 alternate Water flood (WAG), and CO_2-foam flood of heavy oil reservoirs. The objective of this thesis is to:

1. Investigate the feasibility of the existing commercial reservoir simulators to successfully simulate the non-thermal recovery processes in heavy oil projects.
2. Mathematically model the recovery performance of the non-thermal recovery processes in heavy oil projects.

1.5 Numerical Simulation

As it is the practice in conventional oil projects, where investment decisions and development plans optimization are essential, it is also important to estimate the recoverable oil volume, and forecast production rates through time in heavy oil projects through the use of reservoir simulation. Reservoir simulation combines the concept of material balance and fluid flow theory to predict fluid movement through three-dimensional space over time in the reservoir. And it achieves this by using reservoir rock and fluid properties as input into the resulting partial differential equations, and solving them for the relevant boundary and initial conditions.

1.5.1 Compositional Simulation

The CO_2-flood of heavy oil is most appropriately described by a set multi-phase, multi-component, and multi-mechanism flow equations since the flow involves immiscible fluids, with changes in composition of the fluids as the flow progresses due to more than one mass transport mechanism. Usually, heavy oils contain a very large percentage of asphaltenes and resins, and since in the available laboratory characterization methods, the actual molecular structures of the compounds in the mixture and their concentrations are not easily determined using the simulated distillation techniques, as high as 50% of the composition of the oil may be lumped together as an ill-defined C+ fraction.

Thus, the use of the EOS for phase behaviour modelling for heavy oil becomes very challenging as characterization data for the lumped C+ is unavailable. Another reason why the characterization of heavy oil is challenging is because most of the existing EOS and their associated correlations used in all existing phase behaviour packages have been developed with light oil. The process of splitting and lumping often used in phase behaviour modelling of light oil to manage the number of pseudo-components in the reservoir simulation is very difficult in heavy oil due to the lack of accurate characterization data.

1.6 Thesis Content

Chapter two presents the literature review of numerical simulation in non-thermal processes. In Chapter three, the estimation of the two-phase relative permeability curves from displacement core-flood data using CMOST a commercial computer program is done. And

Chapter four presents the analytical approach to estimate relative permeability of heavy oil systems.

In Chapter five, an equation of state model was generated for an heavy oil, which in conjunction with the right relative permeability (estimated in chapter three), was used in the compositional modelling of the heavy oil/CO_2 displacement processes. And in Chapter six, the numerical simulation of the three phase experiments using both the black oil and the compositional model of Eclipse for the appropriate experiment is reported. These simulations test the capability of the existing three phase correlation models in existing commercial simulators by comparing the simulation results with the experimental results. An in-house three- phase flow computer program was also used to simulate the three phase experiments.

Finally, in chapter seven, conclusions and recommendations on the estimation and use of relative permeability in heavy oil system is presented.

1.7 References

1. Alboudwarej H., Felix J, Taylor S, Badry R, et al., 2006, "Highlighting Heavy Oil," Oilfield Review18, no. 2. 34-53.
2. Al-Hussainy, R. and Ramey, H.J. jr., 1966, "Applications of Real Gas Theory to Well Testing and Deliverability Forecasting," JPT (May), 637-642, 1966.
3. Ali, Farouq S. M., 1974, "Current Status of Steam Injection as a Heavy Oil Recovery Method." Journal of Canadian Petroleum Technology. Volume 13, Number1
4. Chang, S.H., L.A. Owusu, S.B. French, and F.S. Kovarik, 1990, 'The Effect of Microscopic Heterogeneity on CO_2-Foam Mobility: Part 2- Mechanistic Foam Simulation,' SPE/DOE 20191, Proceedings of the SPE/DOE 7th Symposium on Enhanced Oil Recovery, Tulsa, Oklahoma
5. Curtis, C., R. Kopper, E. Decoster, A. Guzman-Garcia, C. Huggins, L. Knauer, M. Minner, N. Kupsch, L.M Linares, H. Rough, and M.Waite, 2002, ' Heavy Oil Reservoirs' Schumberger Oilfield Review, 14(3) pp. 30-51
6. Dake, L.P.,1978, "Fundamentals of Reservoir Engineering" (Elsevier)
7. Emadi, A., 2012, 'Enhanced Heavy Oil Recovery by water and CO_2 Flood' PhD Thesis. IPE, Heriot Watt University, Edinburgh.
8. Farouq Ali, S.M., Thomas, S., 1996, 'The Promise and Problems of Enhanced Oil Recovery Methods' JCPT September, volume 35, No. 7

9. Fergui A., M. Quintard, H. Berttin, and D. Defives, 1995, 'Transient Foam Flow in Porous Media: Experiments and Simulation,' Proceedings of the 8th European IOR Symposium, Vienna Austria

10. Gates, Ian D. and Wang, J., 2011, "Evolution of In Situ Oil Sands Recovery Technology in the Field: What Happened and What's New?" SPE 150686-MS.

11. Green, D.W. and Willhite, G.P., 1998, 'Enhanced Oil Recovery' SPE Textbook Series Vol.6, ISBN: 978-1-55563-077-5

12. Katayouj S. Nejad, EirikAsbjorn, Berg, Jon Knut Ringen, 2011, 'Effect of oil viscosity on water/oil relative permeability,' SCA, Austin, Texas, USA, 18-21 September, 2011.

13. Klins, M. A., 1984, "Carbon-Dioxide Flooding: Basic mechanisms and Project design" International Human Resources Development Corporation, Boston, Massachusetts

14. Kokal, S.L., Sayegh, S.G., 1993, "Phase behaviour and physical properties of CO_2-saturated heavy oil and its constitutive fractions: Experimental data and correlations" Journal of Petroleum Science and Engineering. Vol. 9: 289-302

15. Kovscek, A.R., T.W. Patzek, and C.J. Radke, 1995 'Simulation of Foam Transport in Porous Media,' SPE 26402, Proceedings of the 68th Annual Technical Conference of SPE, Houston, TX.

16. Leverett, M.C., Flow of oil/water mixtures through unconsolidated Sands', Tans. AIME,(1939) 132, 149

17. Meyer, R.F., and Attanasi, E.D., 2003, 'Heavy Oil and Natural Bitumen- Strategic Petroleum Resources,' USGS Fact Sheet 70-03, August.

18. Patzek, T.W. and M.T. Koinis, 1988, 'Kern River Steam-Foam Pilots,' JPT, 42(4) (1990) 496-503.

19. Redlich, O., and Kwong, J.N.S., 1949, 'On the thermodynamic of solutions. V. An equation of state; fugacities of gaseous solutions.' Journal of Natural Sciences, Chem. Rev., Vol. 44, p233.

20. Sayegh, S.G., Rao, D.N., Kokal, S., Najman, J., 1990, 'Phase behaviour and physical properties of Lindbergh heavy oil/ CO_2 mixtures.' Journal of Canadian Petroleum Technology. Vol. 29, No. 6.

21. Speight, J.G. 2009. 'Enhanced Recovery Methods for Heavy Oil and Tar Sands.' Gulf Publishing Company, Houston, TX.

Chapter 2: Literature Review

Heavy oil resources in the world seem to have the potential to meet future petroleum needs of the world. However, compared to conventional oil the development and production of heavy oil comes with a lot of difficulties. As the viscosity of heavy oil is very high, it is usually immobile or partially immobile under reservoir conditions. The effect of the injection of CO_2 and other solvents into heavy oil reservoirs on its recovery potential has been studied extensively, and techniques and processes that can be deployed to enhance the heavy oil recovery have been developed. This work however seeks to investigate the feasibility of using existing commercial simulation software to simulate these processes.

2.1 Overview of Numerical Simulation of Multiphase Flow in Porous Media

As it is the practice in conventional oil projects, where investment decisions and development plans optimization are essential, it is also important to estimate the recoverable oil volume, and forecast production rates through time in heavy oil projects through the use of reservoir simulation. Reservoir simulation combines the concept of material balance and fluid flow theory to predict fluid movement through three-dimensional space over time in the reservoir. And it achieves this by using reservoir rock and fluid properties as input into the resulting partial differential equations, and solving them for the relevant boundary and initial conditions.

The permeability of a producing reservoir, k, relates the pressure gradient, dP, with the macroscopic fluid velocity, U as shown below:

$$U \alpha k\, dP \tag{2.1}$$

In radial coordinates Darcy's law is:

$$q = \frac{2\pi rkh}{\mu}\frac{dp}{dr} \tag{2.2}$$

When the continuity equation and the equation of state is combined with Darcy's law, the expression below is generated:

$$\frac{\partial^2 p}{\partial r^2} + \frac{1}{r}\frac{\partial p}{\partial r} = \frac{\phi \mu c_t}{\mathrm{k}}\frac{\partial p}{\partial t} \tag{2.3}$$

Where c_t is the total system compressibility, t is the time, and ø is the reservoir porosity.

The real gas pseudo-pressure, m(p), defined by Al-Hussainy and Ramey (1966) as:

$$\mathrm{m(p)} = \int_{p_0}^{p} \frac{2\mathrm{p}}{\mu \mathrm{z}} dp \tag{2.4}$$

Using this gives the equivalent gas (compressible) flow equation:

$$\frac{\partial^2 \mathrm{m(p)}}{\partial r^2} + \frac{1}{r}\frac{\partial \mathrm{m(p)}}{\partial r} = \frac{\phi \mu c_t}{\mathrm{k}}\frac{\partial \mathrm{m(p)}}{\partial t} \tag{2.5}$$

Reservoir simulation solves these flow equations respectively for oil and gas by employing numerical methods like the finite difference method. A major disadvantage of the numerical methods however is that the computational cost can be prohibitive; and it is very susceptible to serious convergence difficulties. As a result of these complexities, the processes that are presently implemented in most simulators are the relatively simple ones.

2.2 Darcy's Equation

Although Darcy's law was formerly developed for single phase, laminar, and non-Newtonian flow, there have been some modifications in the law to accommodate cases involving multiphase flow processes, and cases with complex phenomena such as non-Newtonian fluid flow. These cases will be looked into in the following sections.

2.3 Relative Permeability

The concept of relative permeability is introduced to reservoir simulation engineering to account for situations where there are two or more immiscible fluids flowing simultaneously in the reservoir. Relative permeability is hence a measure of the ability of the rock to conduct a fluid through it when two or more fluids are flowing in the reservoir rock. The modified Darcy's equation for multiphase flow processes thus reads:

$$v = -\frac{K k_p}{\mu_p}\frac{\partial P}{\partial x} \tag{2.6}$$

Where k_p and μ_p are the relative permeability and viscosity of phase p respectively. In other words, each fluid has its own effective permeability, which is the product of relative

permeability and the absolute permeability. Relative permeability is a flow property that has the composite effect of pore geometry, porosity, wettability, saturation, and saturation history.

Wettability is a major influence on the shapes of the relative permeability curves, and since every reservoir is unique with respect to prevailing wettability conditions, relative permeability curves estimation from laboratory core flood experiment must be carried out for all reservoirs that require numerical simulation.

Figure 2.1 is a picture illustrating the influence of the presence of water on the flow capacity of oil. For the case of constant total flow rate, the higher the saturation of water in the pore space, the less the flow capacity of oil, hence relative permeability is a representation of the reductions in flow capacity of a fluid as a result of the reduction in the area of flow as a result of the presence of another fluid.

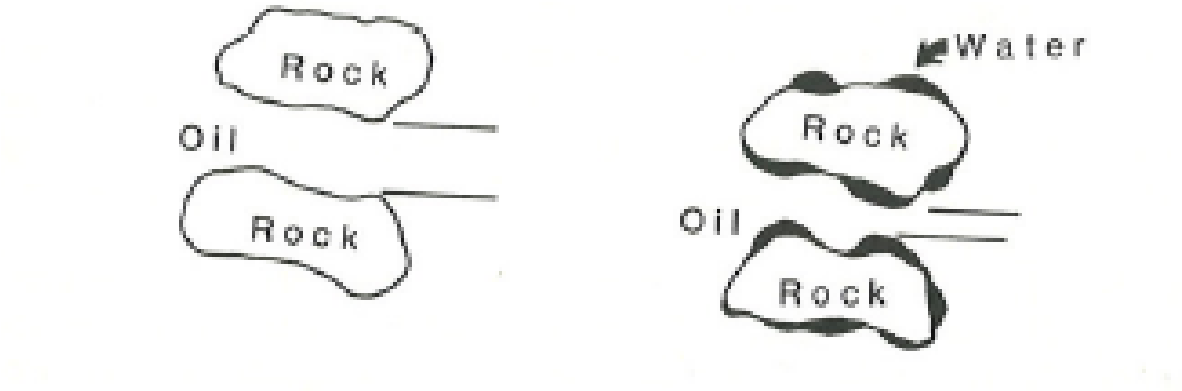

Figure 2.1: Showing the reduction in the pore space available for oil flow due to the presence of water.

In other words, relative permeability of a fluid is a function of the fluid saturation. The higher the saturation of the fluid, the higher is the relative permeability of the fluid. It also follows from this relationship that for an oil-water system, the bigger the value of the residual oil saturation, the smaller is the endpoint water relative permeability. This is aptly captured in Figure 2.2, a typical normalized water-oil relative permeability curve. If the residual oil saturation could be reduced to zero, that is the whole pore space in figure 2.1 is filled with water, then the water end point relative permeability would be 1.0.

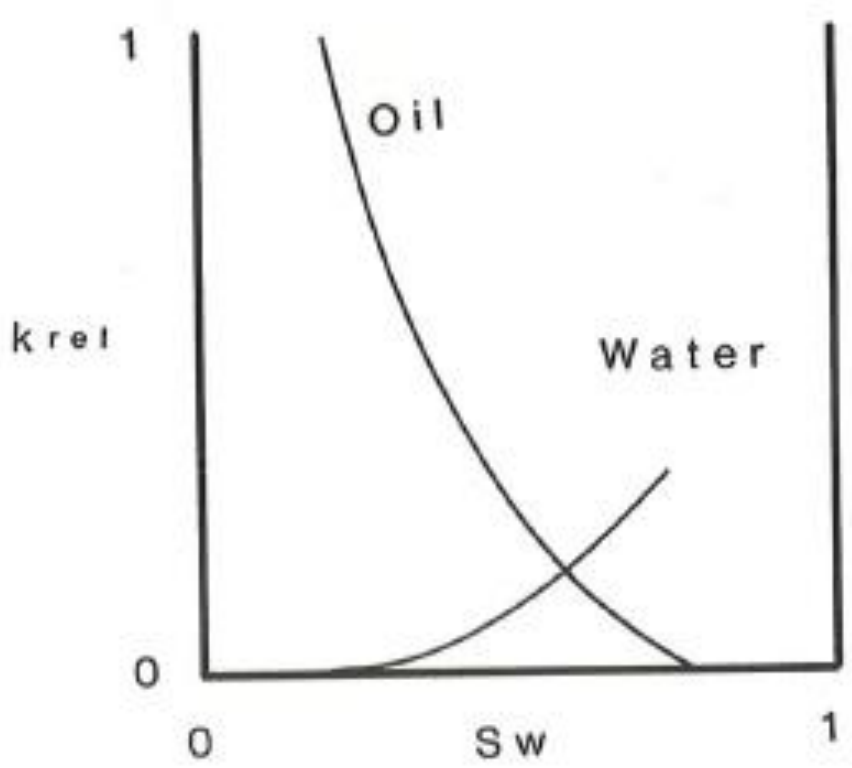

Figure 2.2: Typical normalised water-oil relative permeability curves.

Again, from Figure 2.1, it can be inferred that relative permeability is a function of the wettability of the system, since wettability determines fluid distribution. Wettability determines which fluid is the wetting phase- i.e. sticks to the wall of the rock and flows through a film, and which one is the non-wetting phase – i.e. stays at the center, and flows between the wetting phases on opposite walls. Thus the relative permeability curves of a strongly water wet system would be different from the relative permeability curves of a strongly oil wet system or that of a mixed wet system. And since hysteresis (direction of saturation change) has also been observed to affect fluid distribution, the relative permeability curves in a drainage process would be different from the curves in an imbibition process for the same rock-fluid system.

The Darcy's law for oil and water phases, respectively, for an inclined porous sample, is

$$v_o = -\frac{Kk_{ro}}{\mu_o}\left(\frac{\partial P_o}{\partial x} - \rho_o g \sin\alpha\right) \tag{2.7}$$

$$v_w = -\frac{Kk_{rw}}{\mu_w}\left(\frac{\partial P_w}{\partial x} - \rho_w g \sin\alpha\right) \tag{2.8}$$

And from continuity equations the following equations emerge:

$$\frac{\partial}{\partial x}\left(\frac{Kk_{ro}}{\mu_o}\left(\frac{\partial P_o}{\partial x} - \rho_o g \sin\alpha\right)\right) = \frac{\partial(\Phi S_o)}{\partial t} \quad (2.9)$$

$$\frac{\partial}{\partial x}\left(\frac{Kk_{rw}}{\mu_w}\left(\frac{\partial P_w}{\partial x} - \rho_w g \sin\alpha\right)\right) = \frac{\partial(\Phi S_w)}{\partial t} \quad (2.10)$$

And

$$S_o + S_w = 1 \quad (2.11)$$

$$P_c = P_o - P_w;\ P_o = P_c + P_w \quad (2.12)$$

Where V is the velocity, K is the absolute permeability, kr is the relative permeability, P is the reservoir pressure, x is the distance along the porous sample, Pc is the capillary pressure, ρ is the density, g is the acceleration due to gravity, and subscript o and w, are the oil and water phase respectively.

By rearranging equation 2.7 to 2.12, the general equation of two phase incompressible, immiscible fluid flow written as:

$$\vec{v}.\nabla f_w + \nabla.\left(\frac{Kk_{ro}f_w}{\mu_o}\nabla Pc\right) + \nabla.\left(\frac{Kk_{ro}f_w}{\mu_o}\Delta\rho\nabla z\right) = -\Phi\frac{\partial S_w}{\partial t} \quad (2.13)$$

$$\text{Where } f_w = \frac{k_{rw}/\mu_w}{k_{ro}/\mu_o + k_{rw}/\mu_w};\ v = v_o + v_w;\ \text{and}\ \Delta\rho = \rho_w - \rho_o \quad (2.14)$$

The three terms on the left hand side of equation 2.13 are the viscous, capillary, and gravity terms respectively. These are the three forces influencing multiphase flow in the porous media. The flow regime can be characterized by the capillary number Nc and the bond number Nb. The capillary number is defined as the dimensionless ratio of viscous to capillary forces at the pore scale, while the Bond number is the dimensionless ratio of gravitational to capillary forces at the pore scale. The dimensionless numbers are given below:

$$\text{Capillary number:}\quad Nc = \frac{K}{\sigma}\left|\frac{\Delta P}{\Delta x}\right| = \frac{\mu v}{\sigma} \quad (2.15)$$

Bond Number: $Nb = \frac{\triangle \rho g K}{\sigma}$ (2.16)

Where μ = displacing fluid viscosity, V is the pore velocity, σ is the interfacial tension between the oil and displacing fluid, ΔP/L is the pressure gradient across a distance L, and k is the effective permeability to oil.

Flow in porous media is externally driven by viscous and gravity forces while capillary forces control the flow at the pore scale. For conventional oil reservoir, studies have shown that the capillary forces usually dominate compared to viscous and gravity forces; and the capillary number is always less than 10^{-6} (Green and Willhite, 1986). If the viscous and gravity forces in the reservoir increase and become comparable to the capillary force, the relative permeability in the reservoir is likely to be affected. Therefore, an appreciation of the relative magnitude of these forces in an oil and gas reservoir can be very useful in understanding the mechanisms involved in the recovery process and in interpreting the relative permeability data (Green and Willhite, 1986).

2.3.1 Factors affecting Relative Permeability

The Darcy's equation and its adaptation for multiphase flow was derived for Newtonian, low viscosity fluids hence it is suitable for fluid flow calculations of conventional oil reservoirs. To use the equation for fluid flow calculations, the relative permeability of the reservoir rock to each of the fluid phases in the reservoir are determined in the laboratory through core-flood experiments as a function of the wetting phase saturation. The differential pressure across the core and the production data are measured from the experiment and are then used with the Darcy's equation to estimate relative permeability. The distribution of the different fluids in the interstices of the porous media is a strong function of the wettability characteristics of the reservoir, hence relative permeability is a function of rock wettability. The interfacial tension between fluids determines the residual saturation of the fluids in the reservoir hence it is also a very strong factor affecting the value of the relative permeability. Amaefule and Handy (1982) found that the residual oil saturation decreases with decrease in interfacial tension, hence the oil relative permeability curves decrease and water relative permeability curves increase with decrease in interfacial tension. Increase in temperature reduces the interfacial tension between fluids, thus making relative permeability a function of the temperature in the reservoir. Also as overburden pressure in the reservoir increases, the

sand grains are brought closer together causing a reduction in the pore throat diameters thereby leading to saturation redistribution, and changes in the relative permeability.

Researchers like Odeh (1959) and Johnson et al. (1958) however reported that relative permeability is not a function of factors like viscosity and the displacement rate for the cases involving low-viscosity oils. However, Lefebvre du Prey (1973) reported the impact of viscosity on oil and water relative permeability curves in an unsteady state displacement method. With increasing viscosity of one phase, the relative permeability of the other phase declines. They also reported that at large capillary number, flow rates and viscosity have impact on unsteady state relative permeability curves.

Lo and Mungan (1973) also measured oil-water relative permeability at room temperature and elevated temperatures. Their work showed that with increase in temperature, oil viscosity decreased; residual oil saturation decreased; and oil relative permeability increased. This change in oil relative permeability was attributed to the change of viscosity. Abrams (1975) carried out waterflood tests on core samples, and he observed that as the oil/water viscosity ratio increases, the residual oil saturation also increases, affecting the relative permeability.

Sufi et al. (1982) reported that at a certain high displacement rates or at high oil/water viscosity ratio (which is often used to obtain a wide saturation range, and to eliminate boundary effects and gravity segregation), the displacement process becomes unstable and this affects the relative permeability. Van Meurs (1958) observed displacement patterns with transparent model and found that at viscosity ratio (viscosity of displaced/viscosity of displacing fluid) of unity, the displacement process was piston-like, but at a viscosity ratio of 80, there was viscous fingering in the displacement. Pavone (1992) showed in his 3D experiments of drainage displacement that the width of viscous fingers gets smaller and the displacing fluid relative permeability decreases with increase in viscosity ratio. Since the factors like viscosity ratio and displacement rate that govern the stability of a displacement process have been found to affect the relative permeability, it is then possible that instability is the underlying mechanism that causes this departure from the researchers who concluded that displacement rate and fluid viscosities have no effects on relative permeability.

2.3.2 Instability at the Displacement Front during a Coreflood Study

Wang et al. (2006) carried out some unsteady state displacement experiments to investigate the effect of viscosity on oil-water relative permeability curves. They showed that as viscosity of the oil increases, the residual oil saturation increases and both oil and water relative permeability curves decrease. The result of this study is summarized in Figure 2.1.

In conventional oil, residual oil is left due to capillary trapping after waterflooding (Moore and Slobod, 1956). In heavy oil waterflooding however, the main source of trapping of residual oil is the unfavorable mobility ratio which causes the displacement front to become unstable leading to the formation of fingers thus causing premature water breakthrough and reduction in oil recovery at breakthrough (Mai and Kantzas, 2007).

As mentioned earlier, the performance of a reservoir being flooded by a displacing fluid depends on the interplay between the viscous, capillary and gravitational forces. The viscous force is proportional to viscosity and the frontal velocity, and it is a resistance to the displacement of oil. The capillary force reflects the interfacial tension and wettability, and it either aids or opposes the driving force in effecting oil recovery depending on the contact angle (1718). The gravitational force is a function of density difference between displaced and displacing fluids. It also can either add or oppose the driving force in effecting oil recovery depending on the orientation of the reservoir.

Instability in a displacement process occurs basically when the gravity forces and capillary forces are less than the viscous forces; i.e. when the viscous force is dominant. This then results in different oil water distribution pattern and recovery performance, hence the differences in the estimated relative permeability.

Peters et al. (1987) performed water flood experiments on unconsolidated sand packs saturated with viscous oils. Different levels of instability were observed by varying the displacement rate, sand wettability, and oil viscosity. The results show that the relative permeability curves estimated by the dynamic displacement method are significantly influenced by the degree of instability of the displacement. Peter and Flock (1981) identified parameters controlling the stability of a system as: mobility ratio, wettability, rock permeability, system geometry and interfacial tension. They performed stability analysis in order to identify the conditions under which viscous fingers are formed and developed a

dimensionless stability number for quantitative prediction of the onset of instability in a displacement process. Their instability number for a cylindrical system is:

$$Ns = \frac{(M-1)(v-v_c)\mu_w d^2}{N_w k_{wor}} \tag{2.17}$$

$$v_c = \frac{k_{wor}(\rho_w - \rho_o)g\cos\alpha}{\mu_w(M-1)} \tag{2.18}$$

And

$$M = \frac{k_{wor}\mu_o}{k_{oiw}\mu_w} \tag{2.19}$$

Where

Nw = wettability constant, dimensionless

d = core diameter, m (ft)

k_{wor} = water permeability at residual oil saturation, m^2 (md)

k_{oiw} = oil permeability at initial water saturation, m^2 (md)

μ_o = oil viscosity, Pa.s (cp)

μ_w = water viscosity, Pa.s (cp)

ρ_o = oil density, kg/m^3 (Lbm/gal)

ρ_w = water density, kg/m^3 (Lbm/gal)

α = angle between core axis and vertical, rad (degrees)

v = displacement velocity, m/s (ft/sec)

v_c = critical velocity, m/s (ft/sec)

M = mobility ratio

And the critical value of the stability number was determined to be $13.56(\pi^2)$, below which the displacement process is considered stable.

A review of the literature reveals that researchers like Wyckoff (1936), Leverett (1938) and Odeh (1959) who reported that neither flow rate nor viscosity has any effect on relative permeability conducted their displacement experiments at a stability number that is within

the stable region; while researchers like Al-Shuraiqi (2005), Wang (2006) , and MAI (2009) who concluded that both the flow rate and the viscosity ratio in a coreflood displacement experiment have an impact on the relative permeability data conducted their experiments under stability numbers that are considered to be in the unstable region. Table 2.1 shows a summary of the conclusion of different researchers on the dependency of viscosity ratio on relative permeability.

Table 2.1: A summary of the conclusion of different researchers on the dependency of viscosity on relative permeability.

Title	**Author**	**Year**	**Instability number**	**Conclusion on Relative Permeability**
Effect of viscosity ratio on relative permeability	A.S Odeh	1959	0.46 (<13.56)	Viscosity ratio and rate does not affect RP
Numerical and experimental investigation into the effects of viscosity and injection rate on relative permeability and recovery	H.S Al-Shuraiqi,C.A Grattoni and A.H Muggeride	2005	15 (>13.56)	Viscosity ratio and rate affects RP
Heavy oil Waterflooding: effects of flow rate and oil viscosity	A.Mai and A.Kantazs	2009	1188 (>13.56)	Viscosity ratio and rate affects RP
Effect of viscosity on heavy-oil/water relative permeability curves	J.Wang, M.Dong and K.Asghari	2006	84 (>13.56)	Viscosity ratio and rate affects RP

Core flood experiments are usually performed at the rate of flow in the reservoir; hence the effect of rate on relative permeability does not pose much practical problem. That leaves the viscosity and wettability as the prime parameters controlling the stability of the displacement front during a fluid displacement process. This is also evident in the fact that Al-Shuraiqi, Mai, and Wang all conducted their experiments with relatively high viscosity fluids while Odeh, Wyckoff, and Leverret conducted their experiments with relatively low viscosity fluids. The variation of relative permeability with viscosity in Wang's work is shown in Figure 2.3.

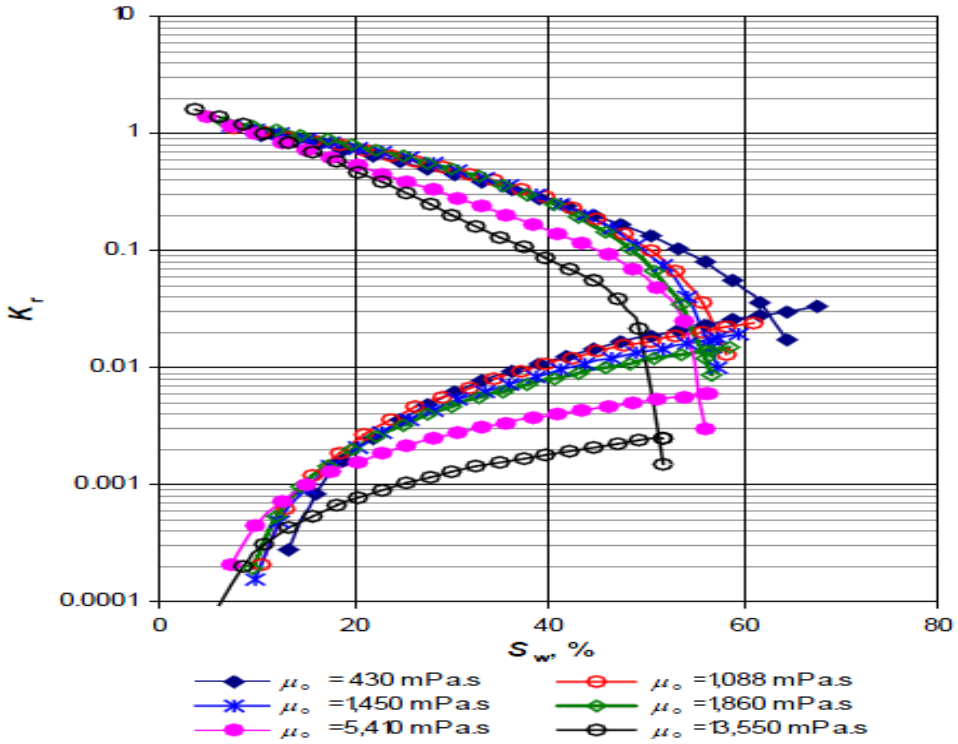

Figure 2.3: Effect of viscosity on relative permeability curves for oil-water system (Wang, 2006).

Thus it can be said that for light oil, the two phase relative permeability curves depend on saturation, wettability and pore structure but not on the fluid viscosities, densities or flow rates. But for heavy oil (μ>100cp), the relative permeability curves in addition to being dependent on saturation, wettability and pore structure, may also be dependent on viscosity

2.4 Non-Newtonian Flow

Newtonian fluids exhibit a proportionality between stress (τ) and strain (γ) in a laminar flow as shown in the equation:

$$\tau = \mu\gamma \tag{2.20}$$

Where μ, is the fluid viscosity, and it is constant for all strain. Any fluid whose rheological behaviour obeys a constitutive equation other than the expression above is a non-Newtonian fluid.

Non-Newtonian fluids can be classified into three main categories: time independent, time dependent, and viscoelastic. In the time independent fluids, the strain rate depends only on the instantaneous stress; in the time dependent fluid, the strain depends both on the

magnitude of the applied stress and its duration; and viscoelastic fluids show partial elastic recovery when the deforming stress is removed and the strain is a function of both time and the magnitude of the stress. The time-independent fluids are further classified as shear thickening and shear thinning fluids. In the shear thickening fluids, the viscosity increases on increasing shear rate, while in the shear thinning (or pseudoplastic) fluids, the viscosity decreases on increasing shear rate. And the fluid is called a yield-stress fluid if it sustains initial stress without flowing, it. Figure 2.4 shows six rheological classes under the time independent category.

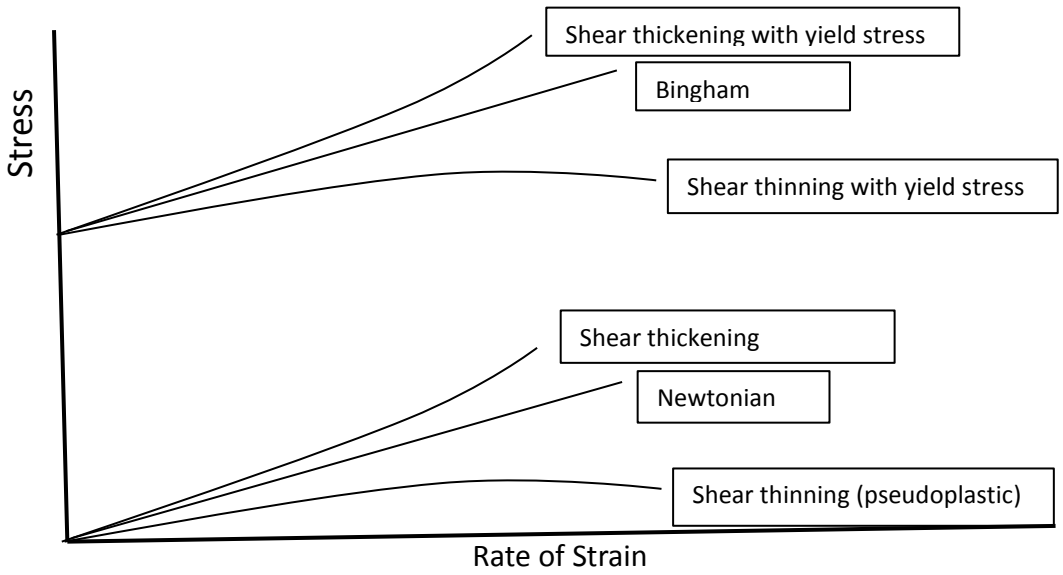

Figure 2.4: The six main classes of the time-independent fluids.

The rheological model is the relationship between shear stress and shear rate in the fluid, and their time derivatives. The power law, Ellis law, Carreau law, and the Herschel-Bulkley law are the principal rheological models used in modeling the time-independent non-Newtonian fluids.

The power law is a two parameter model given as:

$$\mu = C\dot{\gamma}^{n-1} \tag{2.21}$$

Where μ is the viscosity, $\dot{\gamma}$ is the shear rate, is the flow behavior index, and C is constant.

The Ellis law is a three parameter model given as:

$$\mu = \frac{\mu_0}{1+(\frac{\tau}{\tau_{1/2}})^{\alpha-1}} \tag{2.22}$$

Where μ is the viscosity, μ_0 is the low-shear viscosity, τ is the shear stress, $\tau_{1/2}$is the shear stress at which $\mu = \mu_0/2$, and α is an indicial parameter related to the power-law index by α =1/n.

The Carreau law is a four parameter model given as:

$$\mu = \mu_\infty + \frac{\mu_0 - \mu_\infty}{[1+(\dot{\gamma}t_c)^2]^{(1-n)/2}} \tag{2.23}$$

Where μ is the fluid viscosity, μ_0 is the viscosity at zero shear rate, μ_∞ is the viscosity at infinite shear rate, t_c is the characteristic time, $\dot{\gamma}$ is the shear rate, and n is the flow behaviour index.

The Herschel-Bulkley model is a three parameter rheological model that can be used to describe Newtonian and non-Newtonian fluids. It is given as:

$$\tau = \tau_0 + C\dot{\gamma}^n \tag{2.24}$$

Where τ is the shear stress, τ_0 is the yield stress above which substance starts to flow, C is the consistency factor, $\dot{\gamma}$ is the shear rate and n is the flow behaviour index.

Foam and polymers used in enhancing oil recovery from reservoirs have non-Newtonian characteristics. Some heavy oils have been found to have non-Newtonian characteristics. The injection of foam and polymer to an oil reservoir to enhance oil recovery or the injection of water into heavy oil could be an example of non-Newtonian and Newtonian fluid immiscible process in a porous medium. Because very little research looking into the physics of the displacement process on this multi-phase flow involving both non-Newtonian and Newtonian fluids in porous media has been published, the mechanisms of immiscible displacement involving non-Newtonian fluid is not yet well understood. The other factors that affect the flow behaviour of these fluids are adsorption on the pore surfaces of the rock, dispersion, viscous fingering, and lithology of the formation of interest.

2.5 CO_2-Heavy Oil Compositional Simulation

Carbon dioxide injection into heavy oil reservoirs has been found to have a substantial viscosity reduction effect on the oil similar to what is obtainable in the heavy oil thermal recovery processes, hence CO_2 injection processes is a viable alternative to thermal heavy oil recovery (Sayegh et al., 1993). For conventional oil, CO_2 tends to be miscible in the oil thus offering very great recovery potential, whereas in a heavy oil system, CO_2 is not miscible with the oil as a result of the presence of heavier components, and the characteristic low reservoir pressure (usually lower than the minimum miscibility pressure) in heavy oil reservoirs. Thus, the recovery of heavy oil using CO_2 injection is through an immiscible displacement process where the main recovery mechanisms are viscosity reduction and oil swelling (Sayegh et al., 1990).

The suitability of CO_2 injection as an EOR technique in heavy oil production is as a result of high solubility of CO_2 in oil compared to other gases. Due to the high dissolution, the oil viscosity reduces greatly improving the mobility of the oil towards the producing well; and the oil swells and expands out of dead end pores, bringing about significant addition to oil recovery.

The reason why the viscosity reduction reported in a CO_2-saturated heavy oil system is higher than in the cases of other gases like Nitrogen or natural gas is that at the same temperature and pressure, CO_2 has the highest dissolution rate (lowest equilibrium ratio) among the gases. At high pressures, the density of CO_2 is close to that of a liquid and it is higher than that of natural gas or Nitrogen, thereby making it more soluble in oil and less prone to gravity segregation. Also at high pressure the viscosity of CO_2 is higher than that of CH_4 and N_2 making room for better sweep efficiency and mobility control than with other gases.

At low CO_2 concentration, the CO_2 –oil mixture exists essentially as a single phase (CO_2 completely dissolves in the oil) except at extremely low pressure when the mixture exists in the liquid-vapour region. But as the concentration of CO_2 increases, a transition to liquid-liquid equilibrium is seen which is associated with a change in mass transfer mechanism from dissolution of CO_2 in oil to extraction of hydrocarbon components into the CO_2 (Klins, 1984).

For conventional oil, the mechanism of CO_2 displacing crude oil in a reservoir depends on reservoir temperature, pressure and crude oil composition (Klins, 1984). This CO_2-oil phase behaviour is shown in Figure 2.5. It is important to note that boundaries separating the regions vary from oil to oil, with heavier oil shifting the divisions upward. From the figure, there are five possible regions a displacement mechanism can fall into. In region 1, which is a low pressure region, the CO_2 swells the oil, and reduces the viscosity of crude oil. As the pressure of the system increases, there is a cross-over into the region II where hydrocarbon begins to vaporise into the gas phase in addition to the oil swelling and oil viscosity reduction.

At a much higher pressure (region IV) the vaporization or the extraction of hydrocarbon components from the crude oil becomes the dominant mechanism eventually leading to a miscible displacement process (in light oil systems). This is hardly the case in heavy oil reservoirs since heavy oil reservoirs are usually characterized by low reservoir pressures. Region III is a low temperature, low pressure region where the formation of a third phase (CO_2-rich liquid mixtures) is possible as a result of CO_2 extracting the light hydrocarbon ends in the oil. And Region V is a low temperature, high pressure cases where CO_2 exists in the liquid phase. This behaviour can also be replicated in a CO_2-heavy oil system.

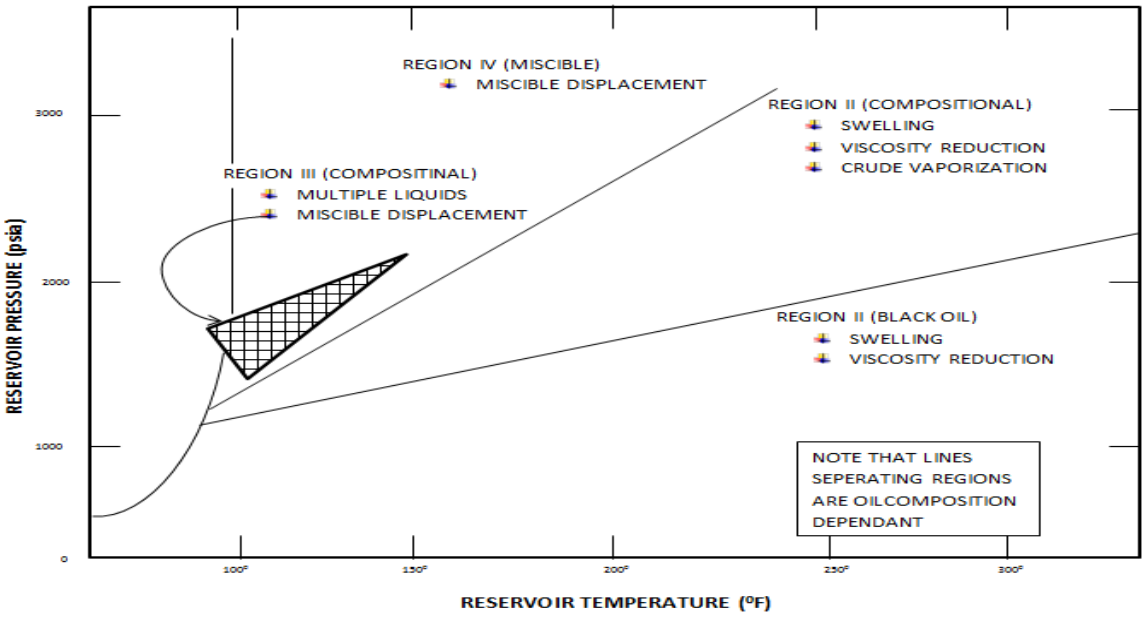

Figure 2.5: The impart of reservoir temperature and pressure on CO_2 injection displacement mechanisms and the applicable simulation techniques (Klins, 1984).

According to Klins (Klins, 1984), the CO_2-flood of heavy oil is most appropriately described by a multi-phase, multi-component, and multi-mechanism flow equations. This is because the flow involves immiscible fluids, with changes in composition of the fluids as the flow progresses and the flow is likely due to more than one mass transport mechanism, in this case, convention and diffusion processes. In other words, the CO_2-heavy oil displacement process is best modelled with compositional simulation while giving due attention to the diffusion flow mechanism. The continuity equation for component i in the flow process is represented as:

$$-\nabla . (\rho_o \omega_{oi} \bar{\upsilon}_{oi} + \rho_g \omega_{gi} \bar{\upsilon}_{gi}) = \frac{\delta}{\delta x} (\boldsymbol{\Phi} S_o \rho_o \omega_{oi} + \boldsymbol{\Phi} S_o \rho_o \omega_{oi}) \quad (2.25)$$

Where the subscript o and g represent the oil and gas phase, ω is the mass fraction, ρ is the phase density, S is the saturation, $\boldsymbol{\Phi}$ is the porosity, and $\bar{\upsilon}_{oi}$ is the velocity of component i in the oil phase is given as:

$$\bar{\upsilon}_{oi} = \bar{\upsilon}_o{}^{\boldsymbol{c}} + \bar{\upsilon}_{oi}{}^{\boldsymbol{d}} \quad (2.26)$$

Where, the superscripts c and d denote convention and dispersion, respectively. The convective velocities are usually assumed to be the Darcy phase velocities, and the dispersive term is usually replaced with the Fick's law.

In solving equation 2.25, it is often assumed that the reservoir fluid and injection gas are at thermodynamic equilibrium in each grid block at each time step. The composition at equilibrium is a function of reservoir temperature, pressure and overall composition, and this is either calculated through the minimization of the Gibbs free energy of the mixture, or through the equality of fugacity for each component at different phases. Existing commercial simulators use tuned Equations-of-State (EOS), like Soave-Redlich-Kwong (Redlich et al., 1949) and Peng-Robinson (Peng et al., 1976), to solve the fugacity equations by first testing for the stability of a single-phase mixture, and then using flash calculations to determine equilibrium compositions in each grid block. The EOS, in addition to calculating the number of phases and the components distribution in the phases is also used to calculate the volume and density of the phases. The EOS model is tuned in a commercial phase behaviour package with phase behaviour experimental data.

An equation of state (EOS) is a physically based algebraic equation which relates volume to pressure and temperature for a single component or a mixture. These easily measured thermodynamic variables make up what is known as a PVT relationship. The Van der Waals' equation of state, shown below, is one of the earliest attempts to represent the behaviour of real gases by an equation (McCain, 1990):

$$(\mathrm{P} + \frac{a}{V^2})\ (\mathrm{V} - b)\ = \mathrm{RT} \tag{2.27}$$

This equation differs from the ideal gas equation by the addition of $\frac{a}{V^2}$ to pressure, P, which corrects pressure for the forces of attraction between the gas molecules; and the subtraction of the constant b, a correction due to the volume occupied by the molecules, from the molar volume, V. Constant a and b are characteristic of the particular gas, while R and T are respectively the universal gas constant and Temperature.

The Peng-Robinson EOS is of the form of the van der Waals equation of state, used to describe the fluid properties of the oil/CO_2 interaction:

$$\mathrm{P} = \frac{RT}{v-b} - \frac{a\alpha(T_R,\omega)}{v(v+b)+b(v-b)} \tag{2.28}$$

$$T_R = \frac{T}{T_C} \tag{2.29}$$

Where P is the pressure, T is the absolute temperature, v is the molar volume, R is the universal gas constant, a and b are the constants related to the attractive and repulsive forces, T_R is the reduced temperature, T_C is the critical temperature,ω is the accentric factor, and α is a function that adjusts the EOS to vapour pressure experimental data.

The attractive and repulsive terms for a pure component are related to its critical properties as follows:

$$a = 0.457235\frac{R^2{T_c}^2}{P_c} \tag{2.30}$$

$$b = 0.0777969\frac{RT_c}{P_c} \tag{2.31}$$

Where, P_c is the critical pressure, the α-function for the Peng-Robinson EOS is given by:

$$\alpha(T_R, \omega) = [1 + m(1 - T_R{}^{0.5})]^2 \quad (2.32)$$

And m is a function of the acentric factor, given by:

$$m = 0.37464 + 1.54226\omega - o.26992\omega^2 \quad (2.33)$$

Equations of State (EOS) are essentially developed for pure components, but using them for mixtures requires the employment of mixing rules to evaluate the EOS parameters for mixtures. So in a mixture, the 'a' and 'b' terms in the EOS are related to its pure component values through the mixing rules. The following mixing rules are used with the Peng-Robinson equation of state (1976):

$$a = \sum_i \sum_j x_i x_j a_{ij} \quad (2.34)$$

$$b = \sum_i \sum_j x_i x_j b_{ij} \quad (2.35)$$

Where x_i is the mole fraction of component i, and a_{ij} and b_{ij} are given by:

$$a_{ij} = \sqrt{a_i a_j}(1 - k_{ij}) \quad (2.36)$$

$$b_{ij} = \frac{b_i + b_j}{2} \quad (2.37)$$

And the term k_{ij} is the binary interaction coefficient between component i and j. The binary interaction coefficients have different values for each binary pair, and the values must be obtained by fitting the equation of state to gas-liquid equilibria data for each binary mixture.

While the application of EOS to a simple mixture is simple and straightforward, using it in a crude oil system comes with some challenges. The method used in the industry today is to use the gas chromatography simulated distillation to divide the fluid into components and pseudo-components. The method involves injecting the oil sample into a heated zone where it is vaporised and transported by a carrier gas (usually Helium) into a column packed with a stationary liquid or solid phase, resulting in partitioning of the injected sample constituents. The partitioning of components is done according to their boiling points; hence compounds are eluted in a similar order as in a distillation (Danesh, 1998). For the intermediate or heavy fractions, they are eluted as a continuous stream containing overlapping compounds, and hence they are treated as pseudo-components. The components and pseudo components

concentrations are determined through their area under the detector response-time curve; and the molecular weight and specific gravity of each component and pseudo-component are estimated with the use of the Whitson correlations constrained by data like the specific gravity of the oil. The molecular weight of the fluid is measured with the CRYETTE^{TM} cryoscopes equipment which uses the estimated value of the freezing point depression for the molecular weight estimation.

Due to the large number of components in a crude oil system, it is not possible to obtain its complete compositional analysis; hence a large group of ill-defined components are lumped together and referred to as the C-plus fraction. And the C-plus pseudo-component is characterized by its average molecular weight and density (Danesh, 1998).

Once the molecular weight, specific gravity and the boiling point of the components and pseudo components are known, the critical properties (Tc, Pc, Vc) and the accentric factor, ω, for each component and pseudo-component required for phase behaviour modelling using EOS are then determined using a set of correlations. Examples of these correlations used in existing phase behaviour packages are the Lee-Kesler, Twu, and the Riazi-Daubert correlations (Danesh, 1998). These properties and the compositions of the fractions are then input into the EOS for phase behaviour modelling where the binary interaction coefficient and the properties of the C-plus fraction are iteratively adjusted until the EOS reproduces the laboratory determined PVT relationship.

Usually, heavy oils contain a very large percentage of Asphaltenes and Resins, and since in the available laboratory characterization methods, the actual molecular structures of the compounds in the mixture and their concentrations are not easily determined using the simulated distillation techniques, as high as 50% of the composition of the oil may be lumped together as an ill-defined C+ fraction. Thus, the use of the EOS for phase behaviour modelling for heavy oil becomes very challenging as characterization data for the lumped C+ is unavailable.

Another reason why the characterization of heavy oil is challenging is because most of the existing EOS and their associated correlations used in all existing phase behaviour packages have been developed with light oil. The process of splitting and lumping often used in phase behaviour modelling of light oil to manage the number of pseudo-components in the

reservoir simulation is very difficult in heavy oil due to the lack of accurate characterization data.

Furthermore, viscosity correlations in the existing commercial simulators have worked well for light oils, but have not been so successful for heavy oil viscosity modelling (Yazdani et al., 2010). The Lohrenz, Bray, and Clark correlation- LBC (Lohrenz et al., 1964), developed based on the residual viscosity concept and the theory of corresponding states, calculates the viscosities of reservoir fluids from their compositions. About 260 different categories of light oils (black oil to highly volatile) were used to develop this correlation:

$$[(\mu-\mu^*)*\xi + 10^{-4}]^{1/4} = 0.1023 + 0.023364\rho_r\ 0.058533\rho_r^2-0.40758\rho_r^3+0.0093324\rho_r^4 \qquad (2.38)$$

Where μ^*, the low pressure mixture gas viscosity is given as:

$$\mu^* = \frac{\sum_{j=1}^{n}(x_j\mu_{j^*}\sqrt{M_j})}{\sum_{j=1}^{n}(\sqrt{M_j})} \qquad (2.39)$$

And ξ, the mixture parameter is given by

$$\xi = \frac{[\sum_{j=1}^{n}(x_jT_{cj})]^{1/6}}{[\sum_{j=1}^{n}(x_jM_j)]^{1/2}[\sum_{j=1}^{n}(x_jP_{cj})]^{2/3}} \qquad (2.40)$$

There have been some studies on the equation of state modelling for heavy oil mixture with solvents like CO_2. Svrcek et al (1982) used the Peng-Robinson (PR) equation of state and Lee-Kesler property correlations to study mixtures of Athabasca and Peace River bitumen with carbon dioxide and ethane. They characterised the oil using 5 pseudo-components, and they were able to fit the solubility data. They, however, found that relatively small differences in estimated critical properties and accentric factor for heavy oil factions can result in significant differences in the equation of state predictions of gas solubility and heavy oil density.

Sayegh and Kokal (Sayegh et al., 1993) also used the Peng-Robinson (PR) equation of state with volume translation and the Lee-Kesler and Twu property correlations to match heavy oil – CO_2 mixtures experimental data of solubility, density, gas oil ratio, and viscosity.

Saber et al (Saber et al, 2011), using a group contribution approach to estimate the critical properties of the pseudo components, also found that the Peng-Robinson equation of state

with the right tuning, can be adequate in modelling the phase behaviour of Athabasca heavy oil and n-decane.

Castellanos et al (Castellanos et al., 2011) also used the PR EOS to model the phase behaviour of heavy oil and solvent mixtures. They found the Lee-Kesler and Twu property correlations suitable for heavy fractions, but the Lee-Kesler correlations provided a better fit to the data, when the binary interaction parameters between the solvent and each heavy oil pseudo-component were regressed to fit experimental data. They also used a rigorous stability procedure to ensure that the correct phase system is applied during the flash calculations.

Yazdani et al. (2010) did a viscosity and phase behaviour modelling of a heavy oil/ butane system. And also in their work, they found the Peng- Robinson EOS model to be the most representative equation of state of their heavy oil/butane phase behaviour. However, they concluded that many of the available correlations in existing commercial phase behaviour packages are not suitable for heavy oil viscosity modelling.

Yang et al (2007) used the LBC correlation to model different category of oil –from gas condensate to heavy oil- and concluded that the LBC viscosity model can work for heavy oil viscosity if the calculated viscosities are tuned to match the experimental viscosities. Tuning of the LBC viscosity model is done by modifying the pseudo-components critical volumes and the LBC coefficients. In addressing the often encountered non-monotonically increasing C7+ fractions, they recommended that instead of using the correlation in the package to calculate critical volumes, the initial critical volumes of the C7+ components should be estimated based on component viscosities calculated from a dead oil empirical correlation. This way, monotonically increasing component viscosities for the C7+ components is ensured during the tuning process. They also recommended that a monotonic relation of viscosity versus reduced density should be maintained during the regression of LBC coefficients.

In the light of the above, the Peng-Robinson (PR) equation of state with volume translation and the Lee-Kesler and Twu property correlations were used to match heavy oil –CO_2 mixtures experimental, and the LBC correlation was used to model and match the experimental viscosities in this phase behaviour study.

2.6 Three Phase Relative Permeability Models

Different models have been developed to describe three phase flow involved in recovery processes like WAG and pressure blow-down after water-flooding. In developing these models, certain assumptions were made. Some models, for example were made with the assumption that oil is always of the intermediate wetting phase, thus these models combine two-phase data to get a three phase data in such a way that relative permeabilities to gas and water are usually made dependent on each phase's saturation, because they are often considered as the non-wetting and wetting phases, respectively. Similar assumptions go for three phase capillary pressure models where gas-oil and oil-water capillary pressures are dependent on gas and water saturations, respectively, and it is assumed that gas-water capillary pressure is the sum of the other two capillary pressures.

2.6.1 Stone 1 Model (Stone)

The development of the Stone model was based on channel flow theory (Stone, 1970). Channel flow theory means that there is only one mobile fluid in a flow channel. This implies that the wetting phase is found in the small pore spaces and the non-wetting phase is found in the large pore spaces, while the intermediate phase separates them. Thus the microscopic fluid distributions at the water-oil interface will be identical in both 2 phase oil-water system and 3 phase water-oil-gas system at a given equal water saturation, provided water saturation change direction is same in both systems. Thus in a water wet system, since the water and the gas (non-wetting phase) are not in contact at all, they do not have any influence on one another. So the relative permeability of the water phase and the gas phase in a three phase flow are functions of their own saturation and are the same as their two phase relative permeability value.

The stone model interpolates between the two sets of two phase data to obtain the three phase relative permeability for oil. The model will yield the correct two phase data when only two phases are flowing.

$$S_o{}^* = \frac{S_o - S_{om}}{1 - S_{wc} - S_{om}} (\text{for } S_o \geq S_{om}) \tag{2.41}$$

$$S_w{}^* = \frac{S_w - S_{wc}}{1 - S_{wc} - S_{om}} \ (\text{for } S_w \geq S_{wc}) \tag{2.42}$$

And

$$S_g{}^* = \frac{S_g}{1-S_{wc}-S_{om}} \text{ (for } S_o \geq S_{om}) \quad (2.43)$$

Since the water and gas are spatially remote the Stone model assumes that the impedance of oil flow by water and gas are mutually independent events, thus

$$K_{ro} = S_o{}^* \beta_w \beta_g \quad (2.44)$$

Where, $\beta_w$as a function of water saturation is obtained from the two phase data as:

$$\beta_w = \frac{K_{row}}{1-S_w{}^*} \quad (2.45)$$

and$\beta_g$as a function of gas saturation, is obtained from the two phase data as:

$$\beta_g = \frac{K_{rog}}{1-S_g{}^*} \quad (2.46)$$

The Stone model assumes that the three phase relative permeability data are independent of viscosity. And it has been found not to be accurate at low oil saturation.

2.6.2 The Stone 2 Model (Stone 2)

This is a modified form of the Stone 1 model for the mixed-wet rock (Stone, 1973) and it is given thus:

$$K_{ro} = (K_{row} + K_{rw})(K_{rog} + K_{rg}) - (K_{rw} + K_{rg}) \quad (2.47)$$

Where $K_{rw}$and K_{rg} are the two-phase water and gas relative perrmeabilities respectively.

The Stone 2 model always predicts too high residual oil values in the region of high water saturation and low gas saturation. So the assumption of water and gas blockage of oil in this region being independent events may not necessarily be correct. Dietrich (Stone, 1973) suggested re-writing the Stone 2 model as:

$$K_{ro} = \frac{1}{K_{rocw}}(K_{row} + K_{rw})(K_{rog} + K_{rg}) - (K_{rw} + K_{rg}) \quad (2.48)$$

WhereK_{rocw} is the oil relative permeability at connate water-saturation. This is to correct for the fact that $K_{row}$and K_{rog} are not equal to one at the connate water saturation.

2.6.3 Saturation Weighted Interpolation

This is also referred to as the Baker model and it is based on saturation weighted interpolation based on water/oil and gas/oil data, given by:

$$K_{ro} = \frac{(S_w - S_{wc})K_{row} + (S_g - S_{gr})K_{rog}}{(S_w - S_{wc}) + (S_g - S_{gr})} \tag{2.49}$$

The linear interpolation in the Baker model is similar to the interpolation shown geometrically on the ternary diagram in Figure 2.6.

2.6.4 Stone 1 Exponents Model

Hustard et al (1995) modified the Stone 1 model to address the inadequacy observed in the Stone's models. The modification was done by introducing an exponent term, n, to the normalised saturations represented by the β parameter, as follows:

$$K_{ro} = \frac{K_{row}(S_w)K_{rog}(S_g)}{K_{rocw}} \beta^n \tag{2.50}$$

Where

$$\beta = \frac{S_o{}^*}{(1 - S_w{}^*)(1 - S_g{}^*)} \tag{2.51}$$

$$S_o{}^* = \frac{S_o - S_{om}}{1 - S_{wir} - S_{om} - S_{gc}} \tag{2.52}$$

$$S_w{}^* = \frac{S_w - S_{wc}}{1 - S_{wir} - S_{om} - S_{gc}} \tag{2.53}$$

And,

$$S_g{}^* = \frac{S_g - S_{gc}}{1 - S_{wir} - S_{om} - S_{gc}} \tag{2.54}$$

β may be interpreted as a variable that varies between zero and one for low and high oil saturation, respectively. The values of 'n' in equation 2.50 causes the low oil isoperms to become more linear between the two phase values.

2.6.5 IKU Model

The IKU method was developed based on the work of Hustard et al (1995) to estimate the three phase relative permeabilities using saturation dependent two phase relative permeability values. Figure 2.6 is a typical ternary diagram where all the oil two phase end point values (S_{org}, S_{gro}, S_{orw}, and S_{wro}) are indicated. All the points can be connected by straight lines; and the lines connect the two phase end points representing the minimum and maximum oil saturations for oil flow. These minimum and maximum oil saturation points are respectively given by:

$$S_{omn} = \frac{S_w S_{orw} + S_g S_{org} + S_{org} S_{orw}(S_o - 1)}{S_g(1 - S_{orw}) + S_w(1 - S_{org})} \tag{2.55}$$

$$S_{omx} = \frac{S_w S_{gro} + S_g S_{wro} + S_{gro} S_{wro}(S_o - 1)}{S_g S_{wro} + S_w S_{gro}} \tag{2.56}$$

And the normalized three-phase oil saturation is then:

$$S_{o^*} = \frac{S_o - S_{omn}}{S_{omx} + S_{omn}}$$

And the representative two phase oil relative permeabilities from the normalized oil saturation are given by:

$$\widehat{K}_{rog} = K_{rog^n}(S_{o^*}) \tag{2.57a}$$

$$\widehat{K}_{row} = K_{row^n}(S_{o^*})$$

And, $\widehat{K}_{row} = K_{row^n}(S_{o^*})$ (2.57b)

The representative two phase oil relative permeability may then be weighted by the saturations in the three phase region to give the three phase oil relative permeability:

$$K_{ro} = \frac{S_w}{S_w + S_g}\widehat{K}_{row} + \frac{S_g}{S_w + S_g}\widehat{K}_{rog} \tag{2.58}$$

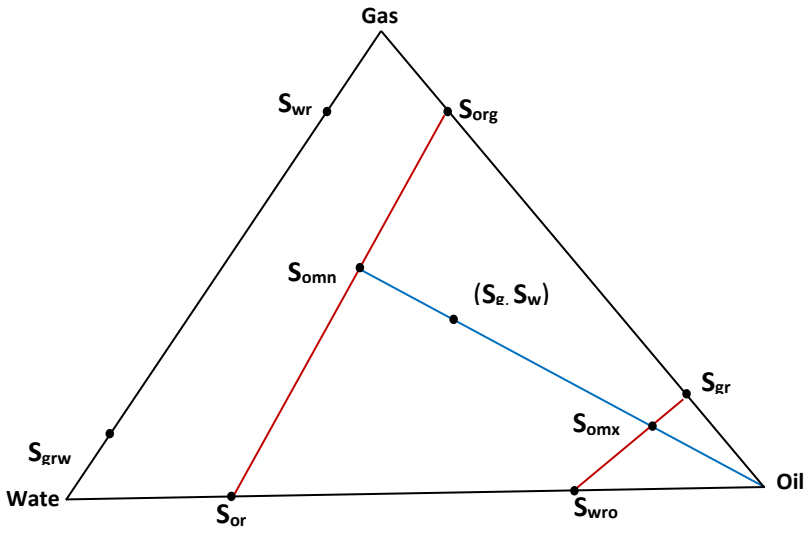

Figure 2.6: A typical three phase ternary diagram showing all the oil two phase end point values.

These methods have been applied with some degrees of success in estimating three phase relative permeability in conventional oil. However, the use of these estimated relative permeability curves in reservoir simulators in some instances have not satisfactorily reproduced coreflooding results, suggesting that the relative permeability curves might be inadequate in simulating processes where their developing assumptions are violated.

2.7 References

1. Abrams, 1975, 'The influence of fluid viscosity. Interfacial Tension, and flow velocity on residual oil saturation left by waterflood' SPEJ 437447.

2. Al-Hussainy, R., and Ramey, H.J., 1966, "Application of Real Gas Flow Theory to Well Testing and Deliverability Forecasting" Journal of Petroleum Technology, May 1966, 637.

3. Amaefule, J.O. and Handy, L.L., 1982, "The effect of interfacial Tension on Relative Oil and Water Permeabilities of consolidated Porous Media," SPEJ 22 (3): 371-381. SPE-9783-PA.

4. Anthony R. Kovscek, 1998, 'Reservoir Simulation of Foam Displacement Processes' the 7th UNITAR International Conference on Heavy Crude and Tar Sands, Beijing, Chin.

5. Baker, L.E., 1998, "Three phase relative permeability correlations," paper SPE 17369 presented at the SPE enhanced oil recovery symposium, Tulsa, Oklahoma.

6. Bernard, G.G. and Jacobs, W.L., 1965, "Effect of Foam on Trapped Gas Saturation and on Permeability of Porous Media to Water," SPEJ5 (4): 195-300; Trans., AIME, 234. SPE-1204-PA. DOI:10.2118/1204-PA.

7. Buckley, S. E., Leverett, M. C., 1942, "Mechanism of Fluid Displacement in Sands", Petroleum Transactions, AIME, Vol. 146, pp 107-116.

8. Corey, A.T., 1954, 'The interrelation Between Gas and Oil Relative Permeabilities.' Producers Monthly 19(November): 38-41.

9. Dake, L.P, (1978),'Fundamentals of Reservoir Engineering.',1st Edition, 100-125 Amsterdam, Elsevier.

10. Danesh, A., 1998, "PVT and phase behaviour petroleum reservoir fluids," ISBN:978-0-444-82196-6.

11. David D. Huang and Matt M. Honarpour, 1996, "Capillary end effects in coreflood calculations" SCA conference Paper number 9634, France.

12. Ekwere, J. P., Khataniar, S., 1987, 'The effect of Instability on relative permeability curves obtained by the dynamic-displacement method '. SPE Formation Evaluation, Volume2, Number 4, pp 469-474.

13. Emera, M.K., Sarma H.K., 2006, "Genetic Algorithm (GA) – based correlations offer more reliable Prediction of CO_2 oil physical properties," Canadian International Petroleum Conference, Calgary, Alberta, Canada, June 13-15.

14. Falls, A.H., Hirasaki, G.J., Patzek, T.W., Gauglitz, D.A., Miller, D.D., Ratulowski, T., 1988, 'Development of a mechanistic Foam simulator: The population Balance and Generation by Snap-off. SPE Reservoir Engineering, August 1988.

15. Green, D.W. and Willhite, G.P., 1998, 'Enhanced Oil Recovery' SPE Textbook Series Vol.6, ISBN: 978-1-55563-077-5.

16. H.S. Al-Shuraiqi, C.A. Grattoni, and A.H. Muggeridge, 2005, 'Numerical and Experimental Investigation into the effects of Viscosity and Injection rate on Relative Permeability and Oil Recovery'. International Symposium of the Society of Core Analysts, Toronto, Canada; August 21−25. SCA2005.

17. Hustard, O.S., & Hansen A.G., 1995, 'A consistent correlation for three phase relative permeabilities and phase pressures based on three sets of two phase data' 8th EAPG Improved Oil Recovery European Symposium, Vienna, 1: 289.

18. Jamaluddin, A.K.M., Kalogerakis, N.E., Chakma A., "Predictions of CO_2 solubility and CO_2 saturated liquid density of heavy oils and bitumens using a cubic equation of state" Fluid Phase Equilibria Volume 64, 1991, page 33-48

19. Jensen, J.A. and Friedmann, F., 1987, 'Physical and chemical effects of an oil phase on propagation of foam in porous media' Paper SPE 16375 presented at the 1987 SPE California regional meeting. Ventura, April 8-10

20. Johnson, E.F., Bossler, D.P., Naumann, V.O., 1958," Calculation of Relative Permeability from displacement Experiments", Petroleum Transactions, AIME, Vol. 216, pp 370-372.

21. Jones, S. C. and Roszelle, W.O "Graphical Techniques for Determining Relative from Displacement Experiments", J. Pet. Tech. (May 1978) *807*

22. Kovscek, A. R. and Radke, C. J. (1993), 'Fundamentals of Foam Transport in Porous Media', Topical report prepared, Earth Sciences Division of Lawrence Berkeley Laboratory and Department of Chemical Engineering/ University of California, Berkeley, USA

23. Kovscek, A.R. and Radke, C.J., 1994, "Fundamentals of Foam Transport in Porous Media' Advances in Chemistry, Vol. 242, Chapter 3, pp 115–163

24. Lefebvre du Prey, 1973, 'Factors Affecting Liquid-Liquid Relative Permeabilities of a Consolidated Porous Medium' SPE Journal, Volume13, Number 1, page 39-47.
25. Levrett, M.C., (1938) ' Flow of oil-water mixtures through unconsolidated sands, Trans. AIME 132, 149-171.

26. Lo, H. Y., and Mungan, N. (1973): Effect of Temperature on Water-Oil Relative Permeabilities in OilWet and Water-Wet systems," 48th Annual SPE of AIME Fall Meeting, Las Vegas, Sept. 30-0ct. 3, 1973. Preprint No. SPE 4505 (1973).

27. Lohrenz, J., Bray, B.C., and Clark, C.R., 1964, "Calculating viscosities of Reservoir fluids from their composition' Journal of Petroleum Technology. 1171

28. Mai, A., Kantzas, A (2008) 'Improved Heavy Oil Recovery by Low Rate Water flooding,' International Thermal Operations and Heavy Oil Symposium, Calgary, Alberta, Canada; October 20−23 SPE Paper 117648.

29. Mai, A., Kantzas, A, 2007 'Heavy oil Waterflooding: Effects of Flowrate and Oil viscosity,' 8th Canadian International Petroleum Conference, Calgary, Alberta, Canada; June 12-14.

30. Maini, B.B., 1995 'Is It Futile to Measure Relative Permeability for Heavy Oil Reservoirs?', In the proceedings of the 46th Annual Technical Meeting, Petroleum Society of CIM, Banff, Canada, May 14-17.

31. McDougall S.R., Salino P.A., Sorbie, K.S., 1997, "The effect of Interfacial Tension upon Gas-Oil Relative Permeability Measurements: Interpretation using pore-scale models," SPE Annual Technical Conference and Exhibition, 5-8 October, San Antonio, Texas, SPE-38920-MS.

32. Mehdi H. Leonard K., Herbert Harvey A., 1986, "Relative permeability of Petroleum Reservoirs," C R C press LLC, 1986

33. Moore, T. F., and Slobod, R. L., 1956, "The Effect of Viscosity and Capillarity on the Displacement of Oil by Water," Prod. Monthly 20.

34. Norman D.H. Munroe, Denver F. Cheddie, William Mendez and Puneet K. singh Gill ,2008, 'Mathematical Model of Fluid Injection in Heavy Oil Reservoirs' International Latin American and Caribbean Conference for Engineering and Technology. 04 June – 06 June, Tegucigalpa, Honduras.

35. Norman D.H. Munroe, Maria C. Bravo and Puneet K. singh Gill, 2007, "Advances in Heavy Oil Recovery" International Latin American and Caribbean Conference for Engineering and Technology.29 May – 1 June, Tampico, Mexico.

36. Odeh, A.S., 1959, 'Effect of Viscosity Ratio on Relative Permeability.' Trans. AIME 216: page 346-353.

37. Paul Wilhite G. 'Waterflooding' SPE textbook series Vol. 3.

38. Peng, D.Y., and Robinson, D.B., 1976, 'A new Two-Constant Equation of State,' Industrial & Engineering Chemistry Fundamentals, Vol. 15, N0. 1, p. 59-64.

39. Radke, C.J. and Ransohoff, T.C., 'Mechanisms of Foam Generation in Glass Bead Packs', paperSPE 15441 presented at the 61st Annual Technical Conference and Exhibition of the society of Petroleum Engineers, New Orleans, October 5-8, 1986

40. Rajan, R.R., 1986, "Theoretical Correct Analytical Solution for Calculating Capillary Pressure-Saturation from Centrifuge Data" paper presented at the 1986 SPWLA logging symposium, June 9-13.

41. Rapoport L.A and Leas, W.J (1953) 'Proprties of Linear waterfloods' Trans. AIME, 198, 139-148. 3.

42. Rose, W., and Witherspoon, P.A., 1956. "Studies of waterflood performance II. - Trappingoil in a pore doublet"; Illinois Geological Survey Circ. 224.

43. Sharverdi, H., (2012), Characterization of three phase flow and WAG injection in oil reservoirs' PhD thesis, Heriot Watt University, IPE.

44. Stone, H.L., 1970 ' Estimation of three phase relative permeability and residual oil data, SPE paper 73-04-06.

45. Stone, H.L., 1973 “Probability model for estimating three phase relative permeability” SPE journal of Petroleum Technology, paper SPE 2116.

46. Sufi, A.S., Ramey, H.J., and Brigham, W.E, 1982, ‘Temperature effects on relative permeability of oil-water systems' Paper SPE 11071presented at the annual Technical conference and Exhibition, New Orleans, September 26-29.

47. Svrcek, W.Y. and A.K. Mehrotra, 1982, "Gas solubility, viscosity and density measurements for Athabasca bitumen", Journal of Canadian Petroleum Technology, 21(4), 31-38.

48. Van Meurs, P., Chuoke R. L, Van der Poel, 1958, “The instability of slow, Immiscible, Viscous liquid-liquid displacents in permeable media” Trans. AIME , vol 216: 188-194.
49. Wang, J., Dong, M., and Asghari, K., 2006, ‘Effect of Oil Viscosity on Heavy Oil /Water Relative Permeability Curves ’ Society of Petroleum Engineers. SPE 99763
50. William D. McCain, Jr, 1990. “The Properties of Petroleum fluids” ISBN 0-87814-335-1.

51. Yazdani, B.B Maini, 2010, “Measurements and Modelling of Phase behaviour and viscosity of a heavy oil/Butane system,” Journal of Canadan Petroleum Technology, vol 49.

Chapter 3: Two Phase Relative Permeability Curves for Heavy Oil

3.1 Introduction

The two phase (oil/water or gas/oil or gas/water) relative permeability of a rock to a fluid can be estimated from core flood experiments in the laboratory. The experimental technique could either be steady state or the unsteady state method. The steady state method is when a fixed ratio of fluids is made to go through a core sample until equilibrium of saturation and pressure are reached. An unsteady state method on the other hand is when one fluid is injected into a core already saturated with another fluid. The injected fluid displaces the other fluid, and the production data of both fluids at the producing end and the differential pressure along the core are recorded. The unsteady state technique is a less cumbersome experimental technique for heavy oils, and hence the preferred method for estimating heavy oil relative permeability curves (Maini, 1995).

The general equation of two phase incompressible, immiscible fluid flow in a porous medium is written as:

$$\vec{v}.\nabla f_w + \nabla.\left(\frac{Kk_{ro}f_w}{\mu_o}\nabla \mathrm{Pc}\right) + \nabla.\left(\frac{Kk_{ro}f_w}{\mu_o}\Delta\rho\nabla \mathrm{z}\right) = -\Phi\frac{\partial S_w}{\partial \mathrm{t}} \quad (3.1)$$

Where $f_w = \frac{k_{rw}/\mu_w}{k_{ro}/\mu_o + k_{rw}/\mu_w}$; $\mathrm{v} = \mathrm{v_o} + \mathrm{v_w}$; and $\Delta\rho = \rho_w - \rho_o$ (3.2)

The three terms on the left hand side of equation 3.1 are the viscous, capillary, and gravity terms respectively, showing the three forces governing multiphase flow through porous media. The viscous force is proportional to the viscosity, while the capillary force is a function of interfacial tension and wettability, and depending on the contact angle, it either enhances the driving force in effecting oil recovery or it opposes it. The gravitational force is a function of density difference between displaced and displacing fluids. It also can either enhance or oppose the driving force in effecting oil recovery depending on the orientation of the reservoir.

The flow regime of a multiphase flow in a reservoir can thus be characterized by the Capillary number Nc and the Bond number Nb. A scenario where the viscous and gravity forces in the reservoir increase in such a manner that the dominance of capillary force is reduced or neutralized generates a different oil water distribution pattern from the capillary-dominant regime (Emadi, 2012), thus giving a different recovery performance. This is also likely to affect the relative permeability in the reservoir, hence an appreciation of the relative magnitude of these forces in an oil and gas reservoir can be very useful in understanding the mechanisms involved in the recovery process and in interpreting the relative permeability data (Green and Willhite, 1986).

Emadi (2012) carried out some micro-model experiments where water displaces a 0.4cp oil (conventional oil), a 600cp heavy oil, and a 8700cp heavy oil. The glass material designed to model a porous medium was initially saturated with oil before the injection of the oil from one end (injection point) of the glass model. The result of the experiment reveals that for the conventional oil, the water evenly displaces the oil throughout the width and length of the glass model leaving behind immovable disconnected oil ganglia in the model after the breakthrough of water. In the case of the two heavy oils however, the displacing water fingers through the oil leaving behind a connected, and movable oil body at water breakthrough. The difference in the production pattern between the two heavy oils however, is that the more viscous oil produces a smaller finger and records a shorter water-breakthrough time than the less viscous heavy oil. This result shows a clear difference in the water oil distribution and recovery pattern in the three cases. The summary of the micro model experiments is shown in Figure 3.1 and Figure 3.2. Figure 3.1 shows the state of the micro-model before and after a water flood in conventional oil (A) and in heavy oil (B); while figure 3.2 shows the difference in the fingers between the two heavy oils.

The conventional oil displacement is capillary dominated while the heavy oils displacement are dominated by viscous forces thereby generating different water oil distribution patterns. Furthermore, it should be expected from this result that due to the difference in recovery pattern between conventional oil and heavy oil, the relative permeability for heavy oil would be different from that of conventional oil.

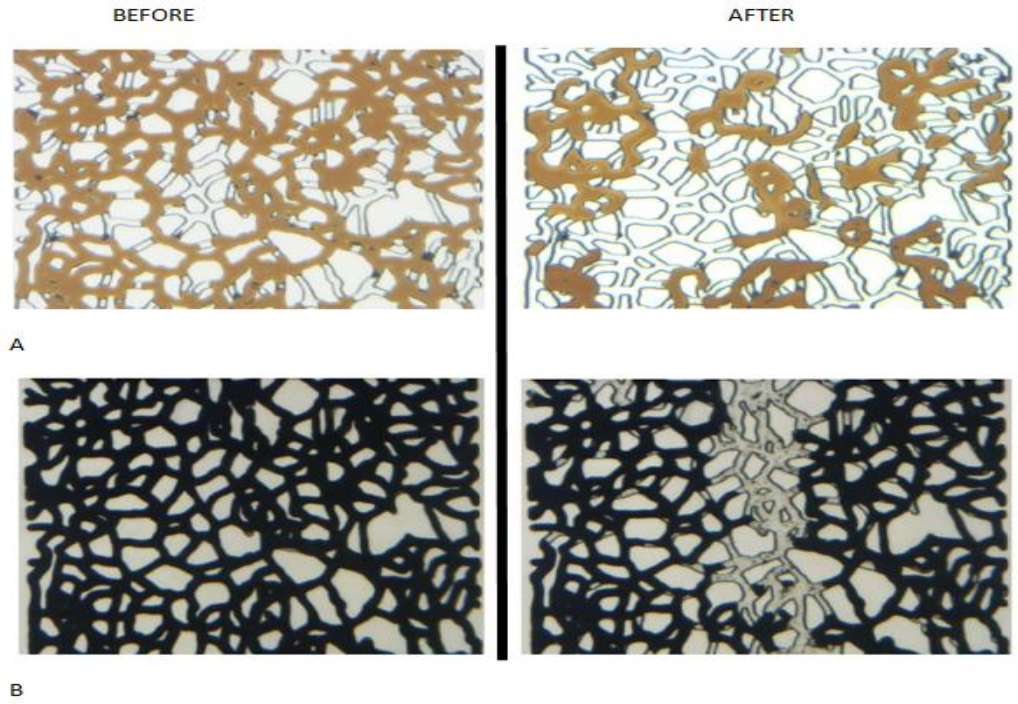

Figure 3.1: An enlarged section of the micro model detailing the recovery characteristics of both the conventional oil (A), and heavy oil (B)- Emadi (2012).

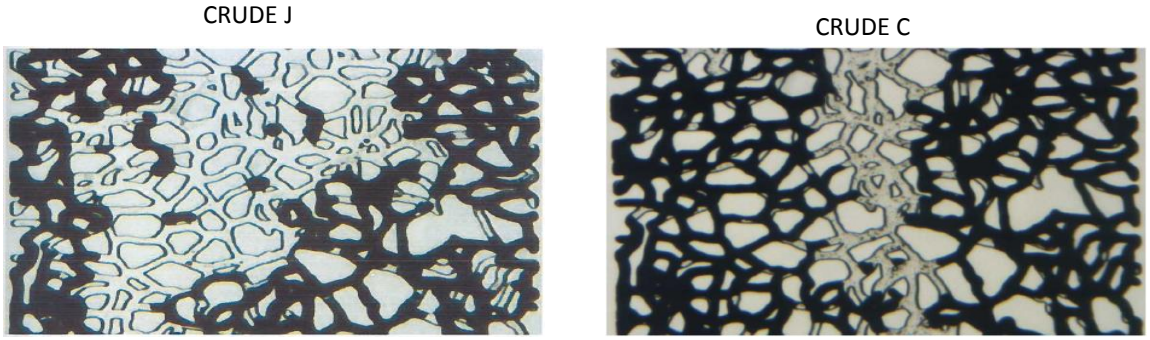

Figure 3.2: An enlarged section of the micro model at water breakthrough showing the displacement patterns from crude J (617 cp), and crude C (8670 cp) (Emadi, 2012).

The objective of this chapter is to estimate two phase relative permeability curves for heavy oil recovery processes and to investigate the impact of a non-capillary dominated heavy oil flow on its relative permeability estimation.

3.2 Relative Permeability Estimation

The implicit method of estimating realistic relative permeability curves from unsteady state core-flood tests using an injection rate that reflects the field flow rate is used in this work.

The implicit method uses a history matching technique where the pressure drop and production data from the experiment are matched by adjusting the relative permeability parameters. An iterative procedure is employed where the values of the parameters defining the shape of the relative permeability curve are adjusted to obtain the match between experimental data and the calculated values of the production and the pressure drop. The main advantage of using the implicit method to estimate relative permeability of heavy oil reservoirs is that it gives room for accounting for the effect of capillary pressure. In its simplest form, the implicit method uses the Corey model (Corey A.T, 1954) to represent the relative permeability function:

$$K_{rw} = K_{rw}^{o}(S_e)^{e_w} \tag{3.3}$$

$$K_{ro} = K_{ro}^{o}(1 - S_e)^{e_o} \tag{3.4}$$

Where

$$S_e = \frac{S_w - S_{wi}}{S_{or} - S_{wi}} \tag{3.5}$$

The objective function, constructed as a weighted sum of squares of the difference between measured and calculated values of production and pressure drop data, is minimized by adjusting e_w, e_o, and K_{rw}^{o}. The K_{ro}^{o} , S_{wi}, and S_{or} are usually measured experimentally.

The core flood experiment data used in this thesis is based on the experimental study performed by Emadi (2012). The properties of the fluids used in the core flood experiment are shown in Table 3.1

Table 3.1: Basic properties of the crude oil samples used in this study.

Crude Name	API	Viscosity	Asphaltene content (%)	Interfacial Tension with water (dyne/cm)	Capillary number (in a water flood)	Interfacial Tension with water (dyne/cm)	Reservoir Temp.	Reservoir Pressure
J	16	617	2.60	23	0.0023	23	28	1500
C	10	8670	11.6	17	0.048	17	50	600

CMOST, CMG's 'Computer Assisted History Matching, Optimization and Uncertainty Assessment tool was employed for history matching the core-flood experiment recovery data

where the Corey parameters (defining the relative permeability curves) are iteratively adjusted until the pressure and production data from the coreflood experiment are matched.

An image of the reservoir grid is presented in Figure 3.3, and the model definitions are shown in Table 3.3. Ideally, a 1-D model (in the direction of flow) should be adequate for relative permeability estimation through the history matching of the experimental data, however, since it has been shown that heavy oil is prone to viscous fingering, a 2-D model would capture its flow behavior better than a 1-D model hence the choice of a 2-D model in this work.

The reservoir grid has 28 blocks in the i-direction, 1 block in the j-direction and 198 blocks in the k-direction. Actually, the core being simulated by the model is a cylindrical section with diameter and height equal to 5.1cm x 32cm, respectively. However, the Cartesian model is used in this work hence the circular surface of diameter 5.1cm has been converted to an equivalent square surface of size 4.52cm by 4.52 cm. Thus each of the 28 blocks in the i-direction is defined as 0.16 cm, and the j block is defined as 4.52 cm, and each of the 198 blocks in the k-direction is defined as 0.16 cm. And both the production and injection wells are placed in the middle of the reservoir grid in the first and last position.

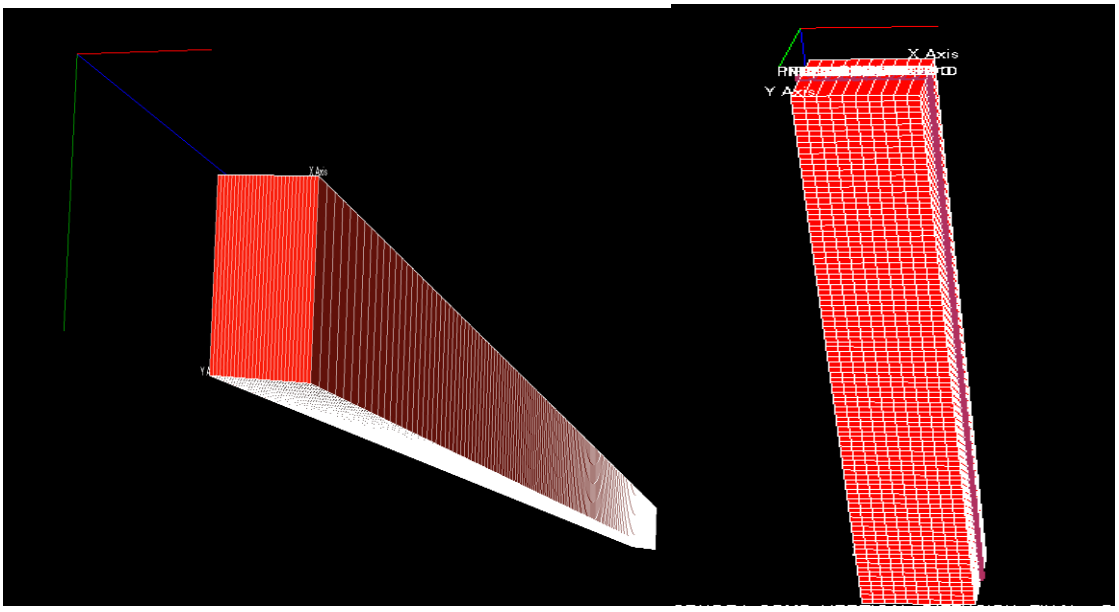

Figure 3.3: A grid system for a two dimensional simulation of water-floods and gas-floods.

The input porosity is 0.2474 with a permeability of 2.5D in X, Y and Z directions for all the grids. In this work, numerical dispersion in the simulation is controlled by using a relatively

large number of grid blocks (NZ = 198) which was tested and found to be adequate from the result of sensitivity study conducted on the core-flood. The capillary end effect was taken into consideration in the simulation by placing one small-thickness extra grid block at both ends of the core, and ignoring capillary pressure on them while the other grid blocks have capillary pressure. This helps to create the capillary discontinuity observed in core flood experiments at the inlet and outlet face of the core.

The model was initialized based on the conditions of the experiments by defining fluid saturation and pressure of each cell explicitly. The initial condition is generally a fixed initial saturation and pressure in the core. And the boundary condition at the inlet is a constant injection rate, and a constant pressure at the outlet. The model is initialized with oil in place in the core seen after the oil flood.

Table 3.2 shows the core and fluid properties for the six two-phase core flood experiments in this study. The table shows the fluid and core data used in the experiment. Each experiment starts with first establishing the initial water saturation of the core by injecting the oil into a brine-saturated core until there is no more water production from the core. Then after the oil flood period, the core is allowed to age before the commencement of the injection of the displacing fluid into the core at a constant rate of 7cm^3/hr (equivalent to a frontal velocity of 1 ft/day); and the differential pressure, and production data is recorded.

Table 3.2: List of all the two phase core flood experiments used in this study.

Exp.	**Type**	**Core orientation**	**Displacing fluid viscosity**	**Oil Viscosity**	**Q**	**Swi**	**Perm. (md)**	**Por.**	**Core dimension**	
									D cm	**L cm**
1	Water flood	Vertical	0.86	617	0	0.15	2500	24.74	5.1	32
2	Water flood	Horizontal	0.86	617	0	0.13	2500	24.74	5.1	32
3	Water flood	Vertical	0.56	8670	0	0.10	2500	24.74	5.1	32
4	CO_2 flood	Vertical	0.05	617	0	0.14	2500	24.74	5.1	32
5	N_2 flood	Vertical	0.02	617	0	0.18	2500	24.74	5.1	32
6	Pre-equilibrated CO_2 flood	Vertical	0.05	617	0	0.18	2500	24.74	5.1	32

Table 3.3: Model definitions used in this study.

Model definitions	
Model	**Cartesian model**
Length	4.52 cm
Width	4.52 cm
Height	32 cm
Initial Oil in Place	162 cm^3

3.2.1 Non-Newtonian Tendencies in Heavy Oil

The Darcy equation used in flow performance calculation was developed for Newtonian fluids (constant viscosity with shear rate), but some heavy oil exhibit non-Newtonian tendencies due to the presence of high asphatene content hence their simulation would require significant change to the traditional Darcy flow equation. The Eclipse simulator employs the Herschel-Bulkley model where the rheology of the fluid can be described by an apparent or effective viscosity. This viscosity may be a non-linear function of the flow rate and it may as well depend on the rock properties such as the permeability and the porosity. In order to remain as close to the Darcy form as possible, a multiplier that modifies the mobility of the fluid depending on the cell properties and local flow rate is used.

According to the Eclipse Technical manual, the Darcy equation for multiphase is hence modified as follows:

$$Q = AK(\frac{k_w}{\mu})B\Delta P \tag{3.6}$$

Where A is area, K is permeability, and B is a complex function, involving grid properties, flow rate or pressure drop, and the rheology of the fluid, i.e.,

$$B = B(\mathrm{d}, \mathrm{K}, \phi, \mathrm{Q}, \Delta P, \mu) \tag{3.7}$$

Heavy crude oils are known to contain high asphaltene content. Asphaltene can cause structural viscosity in heavy oil at low shear rate (due to the self-assemble of the asphaltene molecules) leading to high viscosity; and at high shear rate, the structural viscosity of the oil breaks down leading to decrease in viscosity. This phenomenon is called shear-thinning, and it is a non-Newtonian fluid behavior (Wang, 2006). For a Newtonian fluid, the viscosity does not change with shear rate

In this work, crude J and crude C were examined for non –Newtonian tendencies. This was done by measuring and plotting the viscosity of the fluids at the different shear rates – this was done by another PhD student in the institute. The plots of the viscosity of crude J and C against shear rate at atmospheric pressure are shown in Figures 3.4 and 3.5 respectively. The plots show that crude J is a Newtonian fluid while crude C is a non-Newtonian fluid with a shear thinning flow characteristics. This different fluid rheology of the two crude oils is attributed to the difference in their asphaltene content. Table 3.1 shows that while crude J has an asphaltene content of 2.6%, crude C has an asphaltene content of 11.6%. The relatively high asphaltene content in crude C is responsible for its non-Newtonian nature.

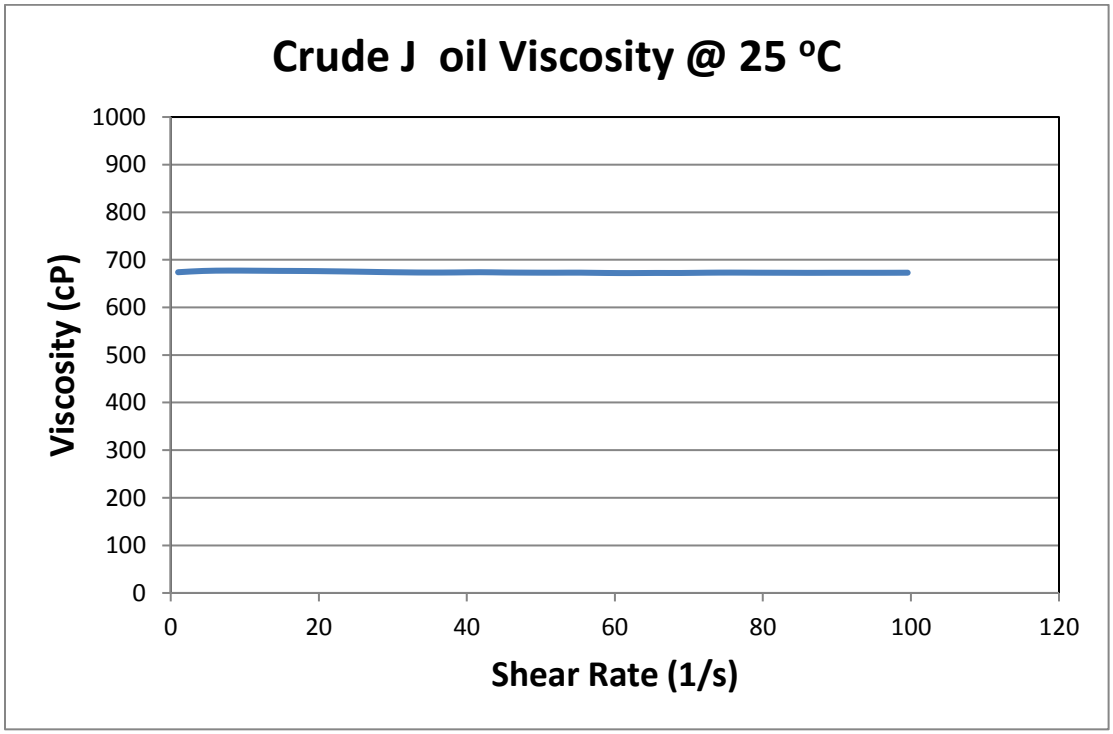

Figure 3.4: Viscosity of crude J versus shear rate at 25 ^{o}C and atmospheric pressure.

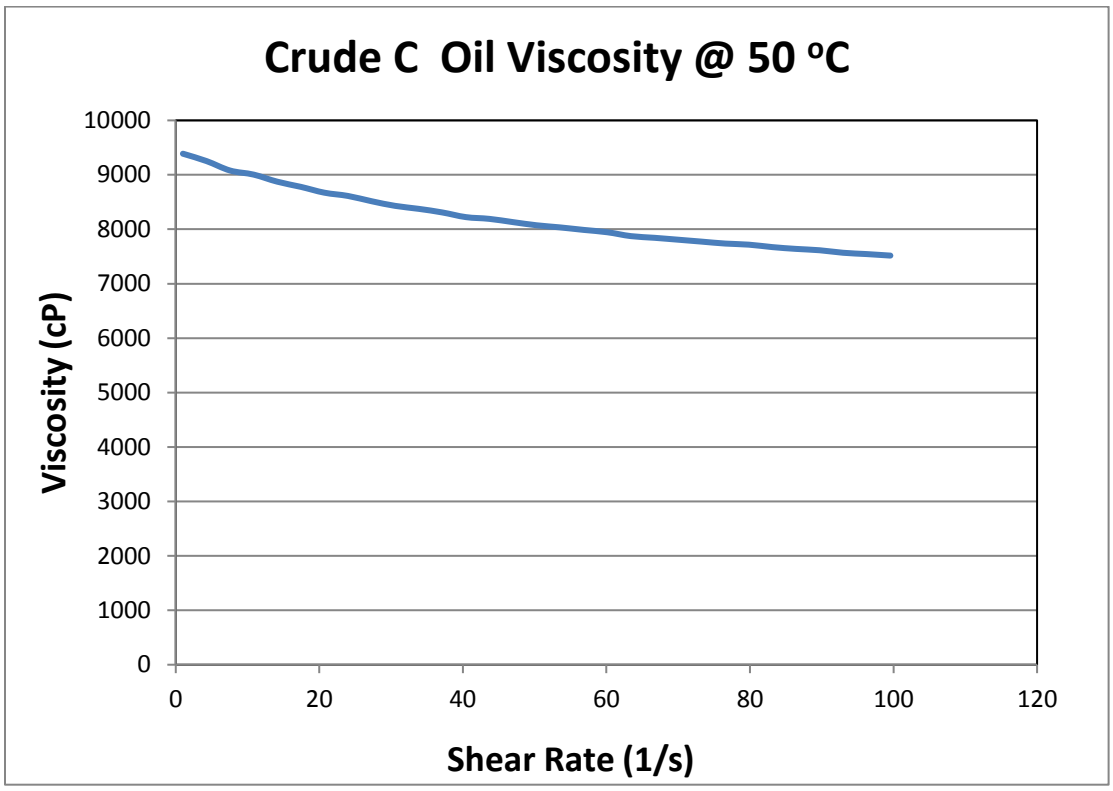

Figure 3.5: Viscosity of crude C versus shear rate at 50 °C and atmospheric pressure.

3.2.2 Capillary Pressure

Capillary pressure is an important parameter for characterizing multiphase fluids distribution and flow in porous media. The oil-water and the gas-oil capillary pressure for the core used in this simulation were estimated from an air-brine centrifuge experiment in our laboratory, where brine is the wetting phase. The Rajan parameter estimation method (Rajan,1986) was used to obtain the capillary pressure curve from equilibrium centrifuge data.

The air-brine capillary pressure data needs to be converted into the oil-brine and CO_2-oil capillary pressure curves by accounting for the corresponding interfacial tensions and contact angles. This conversion is done using the Leverett conversion:

$$Pc_{ow} = Pc_{aw} * (\gamma\text{-}\cos\theta)_{ow} / (\gamma\text{-}\cos\theta)_{aw} \quad (3.8)$$

Where Pc_{aw} is air brine capillary pressure, Pc_{ow} is oil-brine capillary pressure, γ is interfacial tension and θ is contact angle.

The interfacial tension for the air-brine at the lab condition is 72 dynes/cm, and the air-brine contact angle has been assumed to be zero. The measured interfacial tension and contact angle for the crude oil and water system at the test conditions are 30.84 mN/m and 25 respectively. PVTi (Shlumberger Equation of State software) was used to estimate Oil-CO_2 interfacial tension at the test condition as 1.33 dynes/cm and its contact angle has been assumed to be zero.

The results of the measured capillary pressures for water-oil and CO_2-oil systems used in this study are shown in Figure 3.6 and 3.7 respectively. As can be seen, the Pc curves show very small and flat capillary pressure values which are not unexpected as the core is very permeable and homogenous.

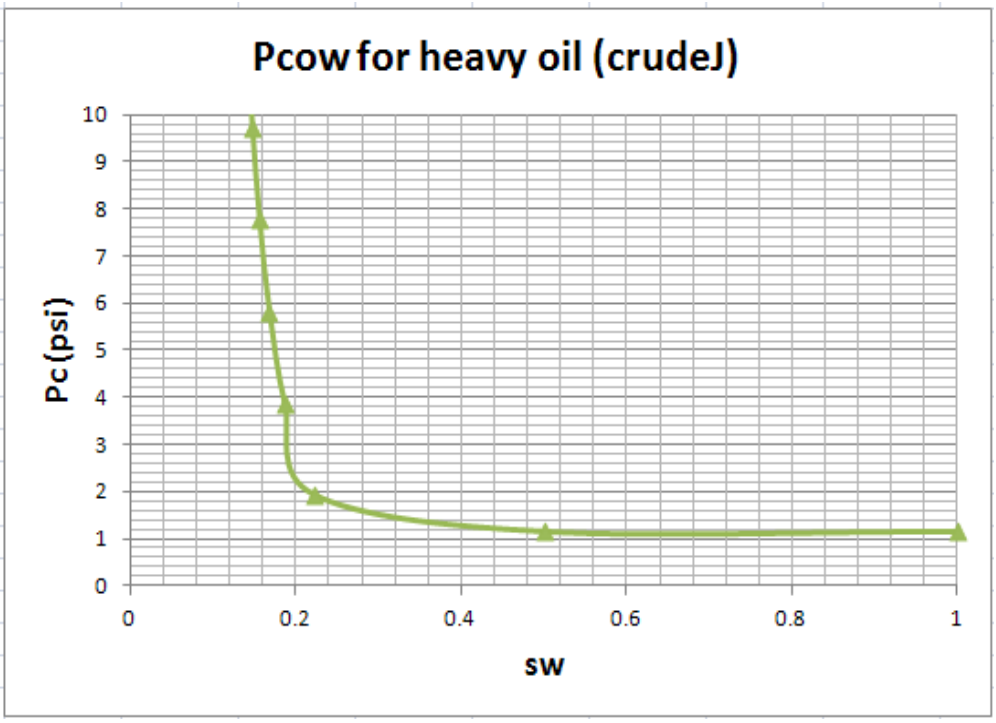

Figure 3.6: Oil/brine capillary pressure of crude J in 2500md homogenous core estimated from a centrifuge method.

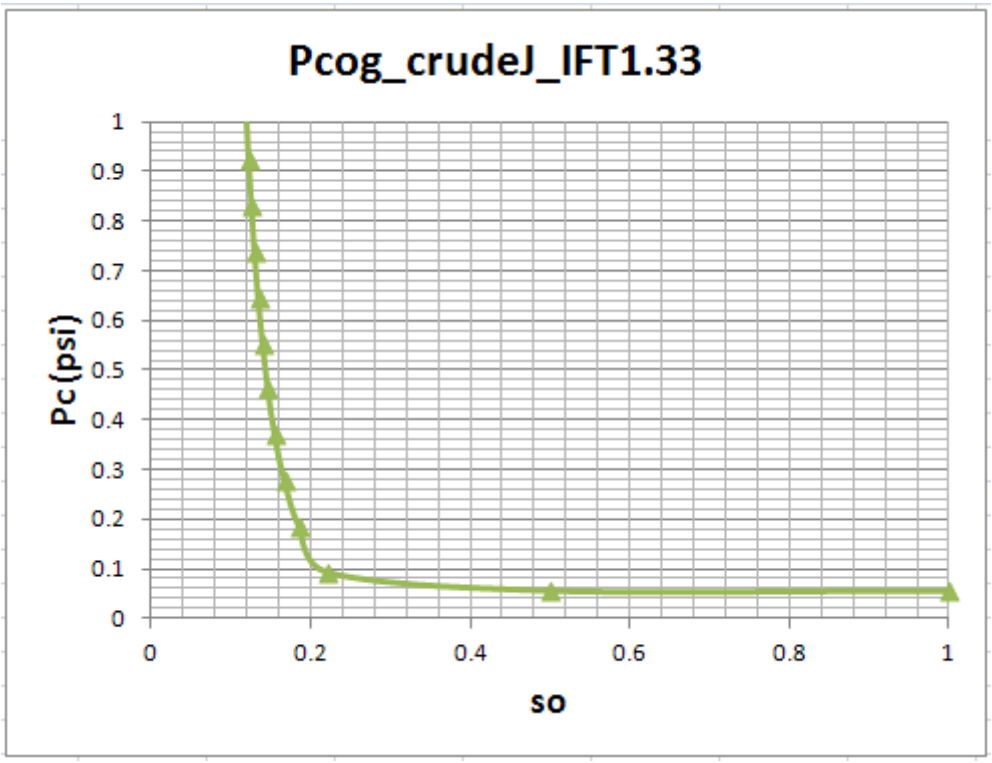

Figure 3.7: Oil/CO_2 capillary pressure of crude J in a 2500md homogenous core estimated from a Centrifuge method.

3.3 Results and Description of the Relative Permeability Curves

As mentioned earlier in this chapter, all the coreflood experiments (Table 3.2) whose results are being matched for the estimation of two phase relative permeability in this work were performed and documented by another PhD researcher in the institutute (Emadi, 2012). Figure 3.8 to 3.10 are the matches between the experiment and simulation results for cumulative oil production, cumulative water production, and the differential pressure across the vertical 2500 md core in the secondary water flood crude J. As can be seen from the figure, the matches are very good hence the relative permeability data generated from them would be considered adequate to describe the processes in the core flood. Figure 3.11a shows the estimated relative permeability data from the matched experiment and Figure 3.12 shows the displacement patterns of crude J oil by secondary water flood at different times in a section of the vertical 2500 md core. The section shows how the viscous finger in crude J forms and increases with time, and ultimately leading to early breakthrough of water after about 5 hours of water injection which is consistent with the water production plot in Figure 3.9.

On the other hand, Figure 3.11b demonstrates the importance of using a 2-D model over a 1-D model. The 2-D model is able to capture phenomena like viscous fingering and hence gives a more realistic relative permeability values than in a 1-D model. This behavior is actually more evident in crude C, the higher viscosity fluid, as shown in figure 3.21b. It follows then that the more pronounced the viscous fingering phenomena, the more pronounced is the difference in the relative permeabilities of the 1-D from the 2-D models.

Figure 3.13 to 3.15 are the matches between the experiment and simulation results for cumulative oil production, cumulative water production, and the differential pressure across the horizontal 2500 md core in the secondary water flood crude J. The matches in this case are also very good hence the relative permeability data generated (shown in Figure 3.16) from them are considered adequate to describe the processes in the core flood. Figure 3.17 is the comparison of the oil and water relative permeability of crude J from the vertically oriented core and the horizontally oriented core in a secondary water flood experiment. What can be seen clearly from this comparison is that the vertical core flood experiment gives lower residual oil saturation than in the horizontal core flood experiment, which translates to a higher recovery. The reason for this difference in relative permeability between horizontal and vertical core is more likely to be the difference in the degree of viscous fingering in the two core-floods. This means the gravity force in the vertical core flood helps in stabilizing the flow and reducing the tendency for viscous fingering.

Figure 3.18 to 3.20 are the matches between the experiment and simulation results for cumulative oil production, cumulative water production, and the differential pressure across the vertical 2500 md core in the secondary water flood crude C. The matches here are also good hence the relative permeability data therein generated (shown in figure 3.21a) are adequate to describe the processes in the core flood. Figure 3.22 shows a comparison of the relative permeabilities obtained from the secondary water-flood of crude C and crude J in the vertical 2500 md core. This figure reveals that the oil relative permeability in crude J (617 cp) is higher than in crude C (8670 cp). This is expected in a viscous dominated displacement where water breakthrough appears earlier in crude C than in crude J. Furthermore, in the spontaneous imbibitions process which takes place after water breakthrough in both displacements, it is much easier for the imbibed water to displace a 617 cp oil than a 8670 cp

oil, thereby producing more of the 617 cp oil (crude J), and hence the higher the crude J oil relative permeability.

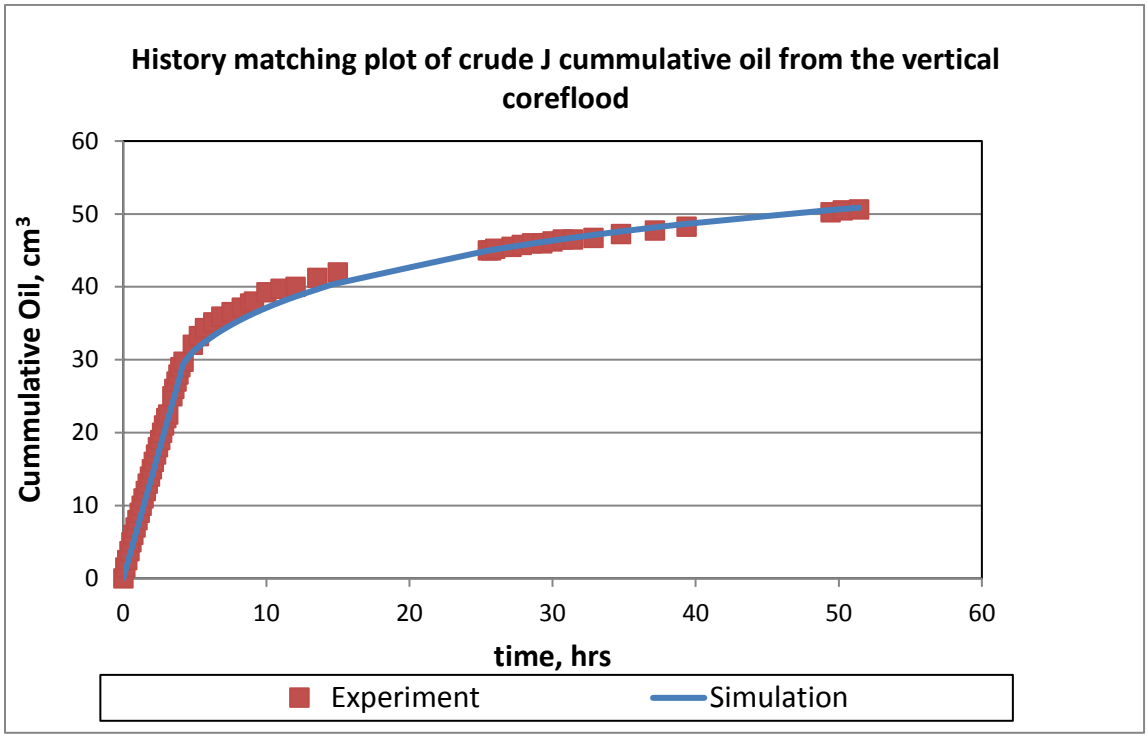

Figure 3.8: Comparison between experiment and simulation results for cumulative oil production in the vertical 2500 md core in the secondary water flood crude J.

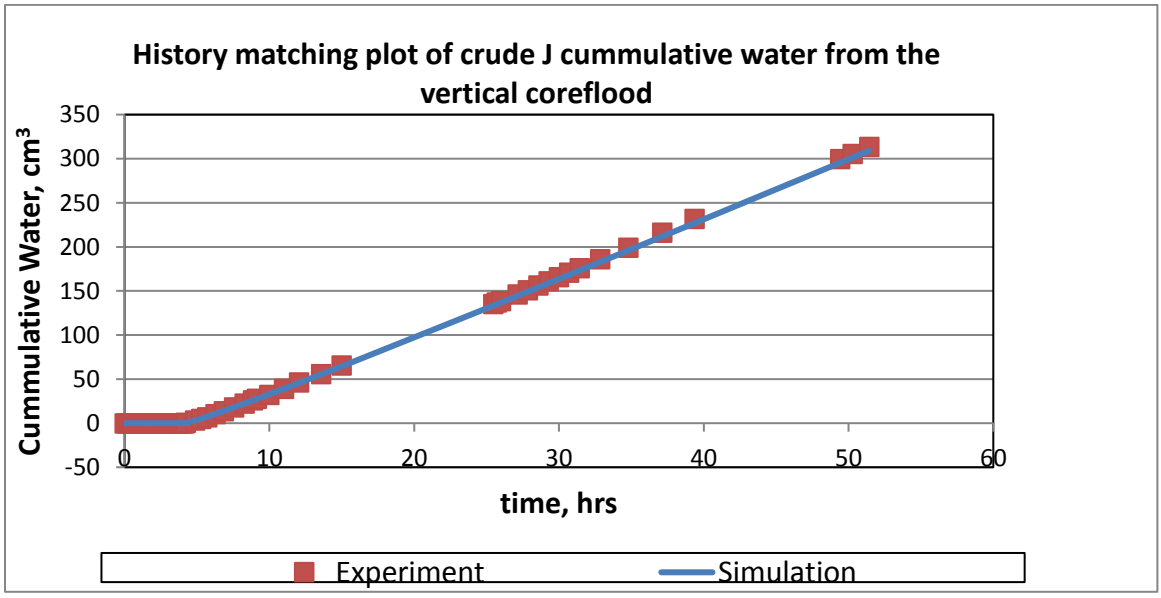

Figure 3.9: Comparison between experiment and simulation results for cumulative water production in the vertical 2500 md core in the secondary water flood crude J.

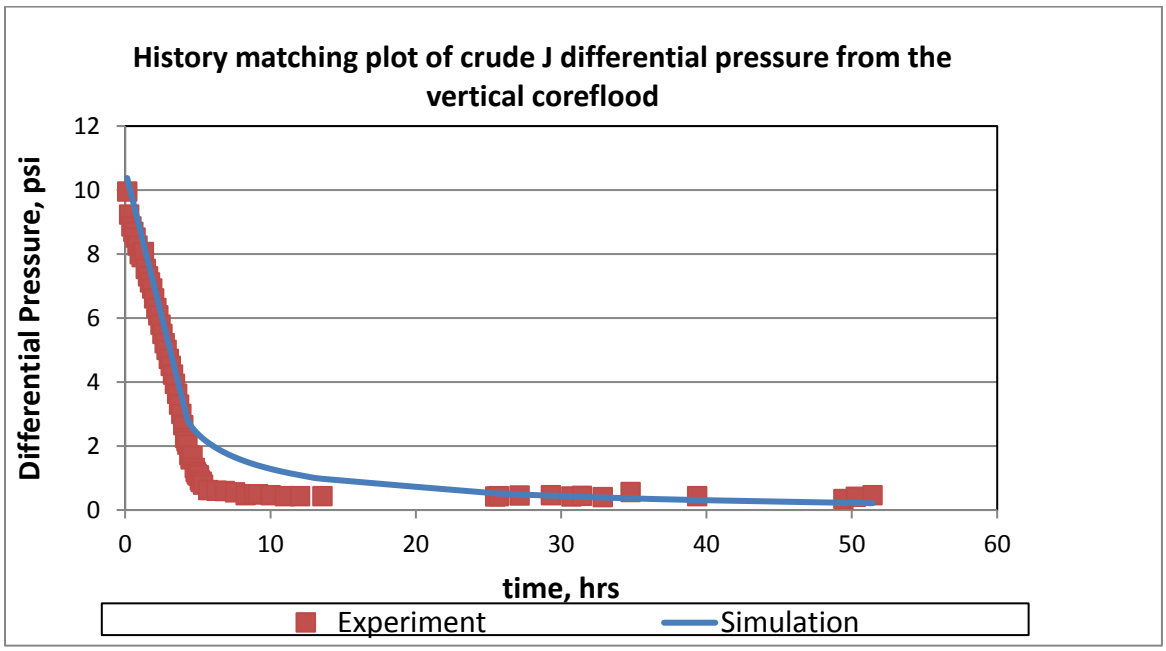

Figure 3.10: Comparison between experiment and simulation results for differential pressure across the vertical 2500 md core in the secondary water flood of crude J.

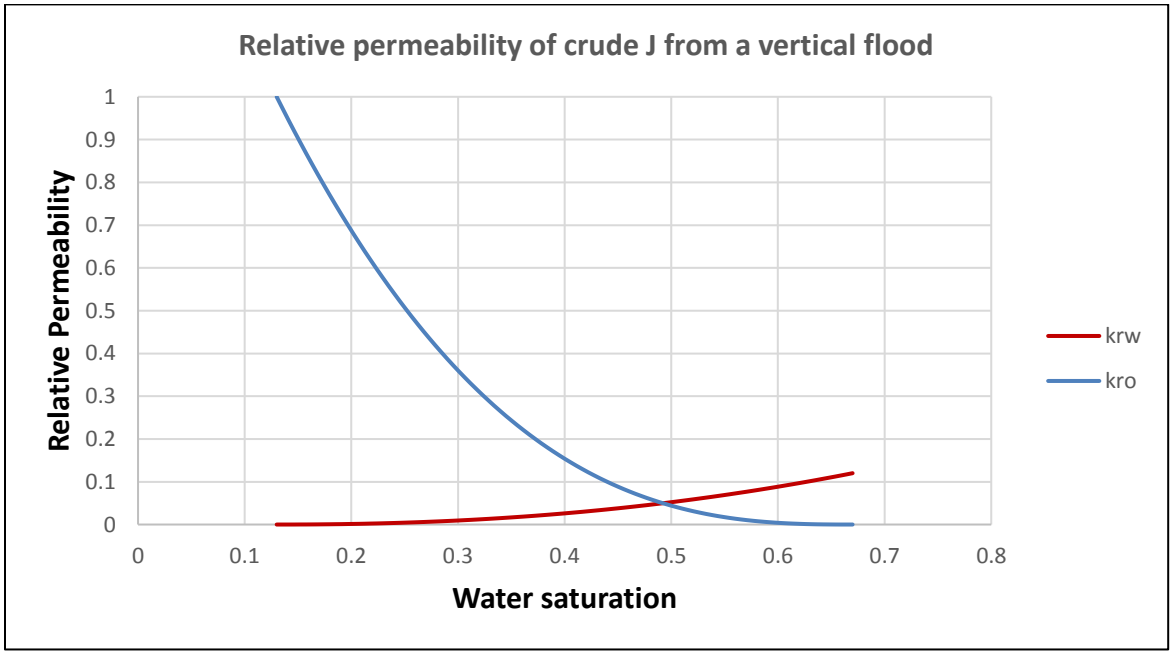

Figure 3.11a: Crude J oil and water relative permeability versus water saturation obtained from the secondary water-flood of crude J in vertical orientation of 2500 md core.

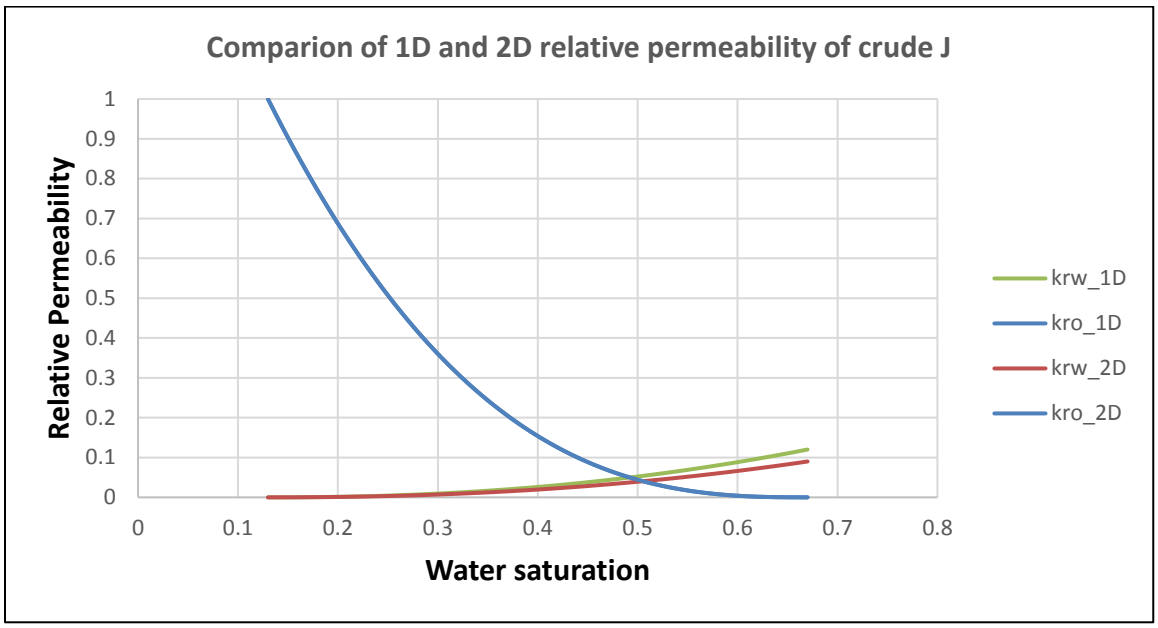

Figure 3.11b: Comparison of the relative permeabilities of the 1-D and 2-D gridding obtained from the secondary water-flood of crude J in the 2500 md core.

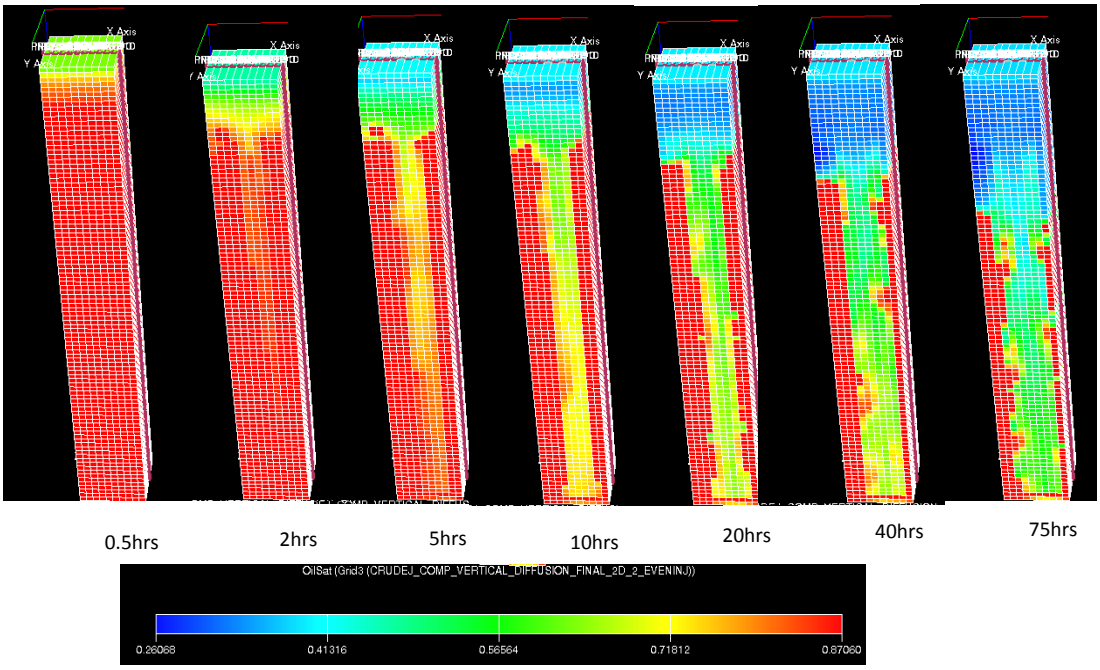

Figure 3.12: A section of 2500 md (vertical orientation) core showing the displacement patterns of crude J oil by secondary water flood at different times.

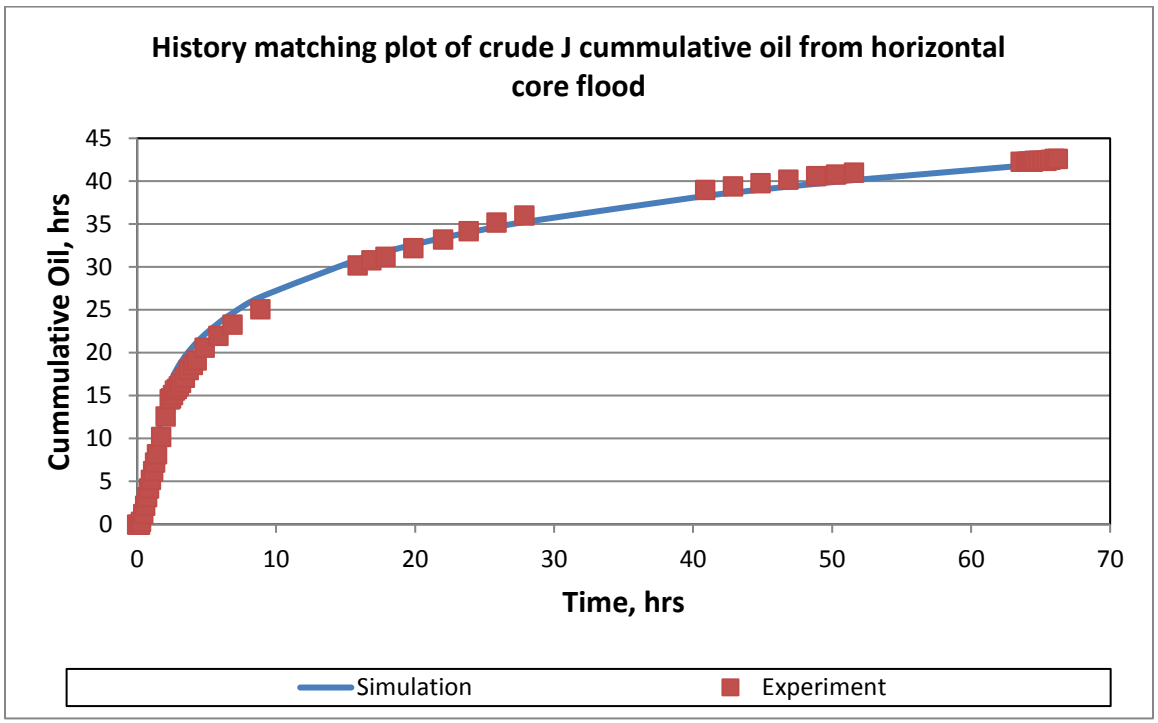

Figure 3.13: Comparison between experiment and simulation results for cumulative oil production in the horizontal 2500 md core in the secondary water flood of crude J.

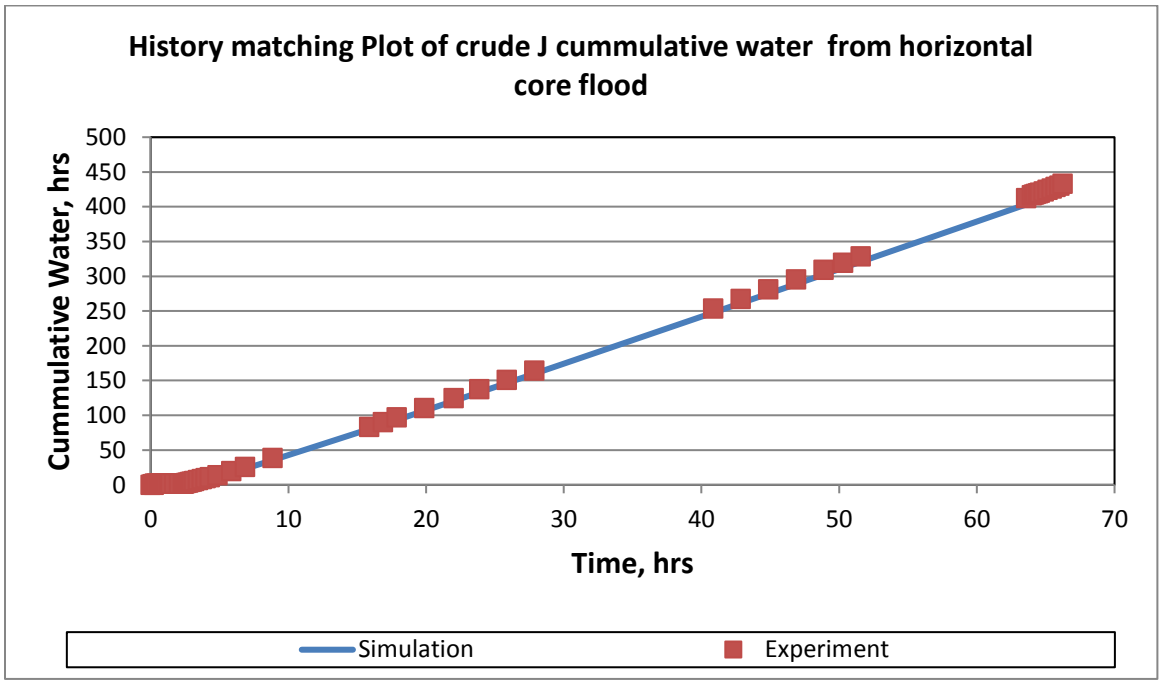

Figure 3.14: Comparison between experiment and simulation results for cumulative water production in the horizontal 2500 md core in the secondary water flood of crude J.

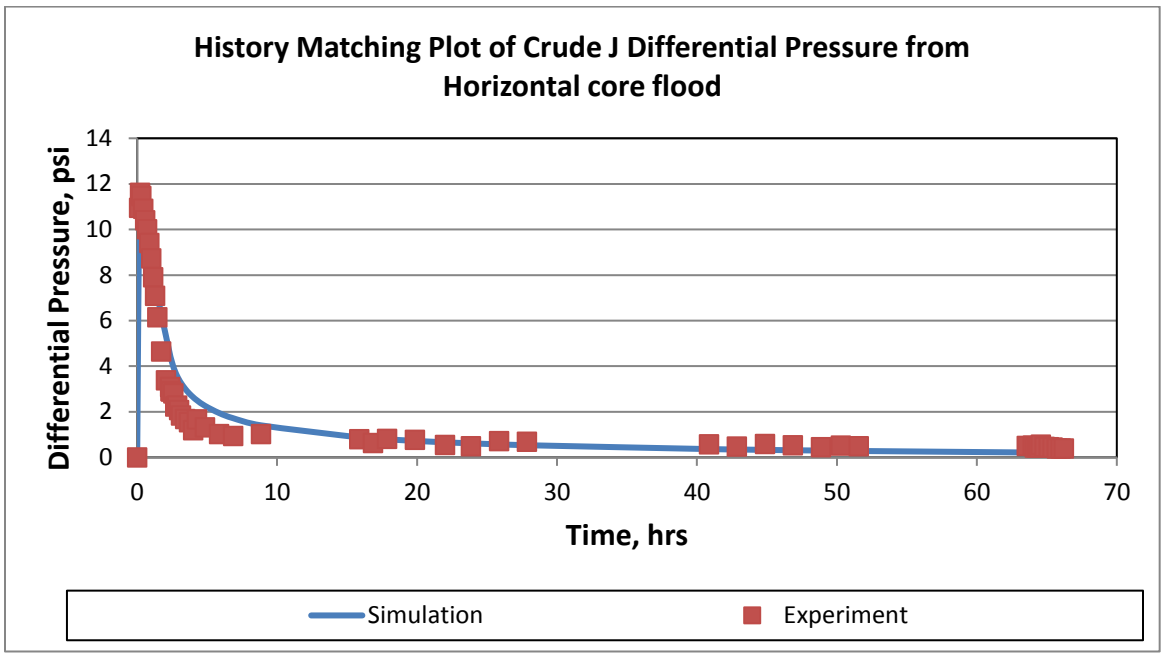

Figure 3.15: Comparison between experiment and simulation results for differential pressure across the horizontal 2500 md core in the secondary water flood of crude J.

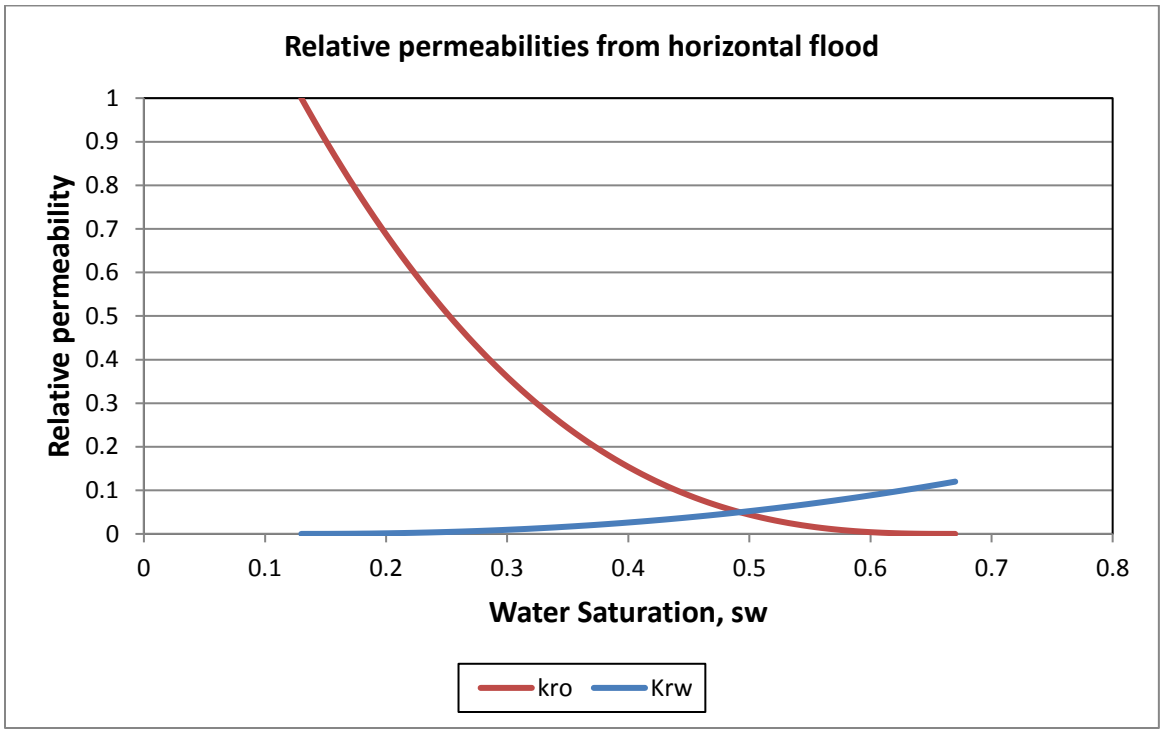

Figure 3.16: Crude J oil and water relative versus water saturation obtained from the secondary water-flood of crude J in horizontal orientation of 2500 md core.

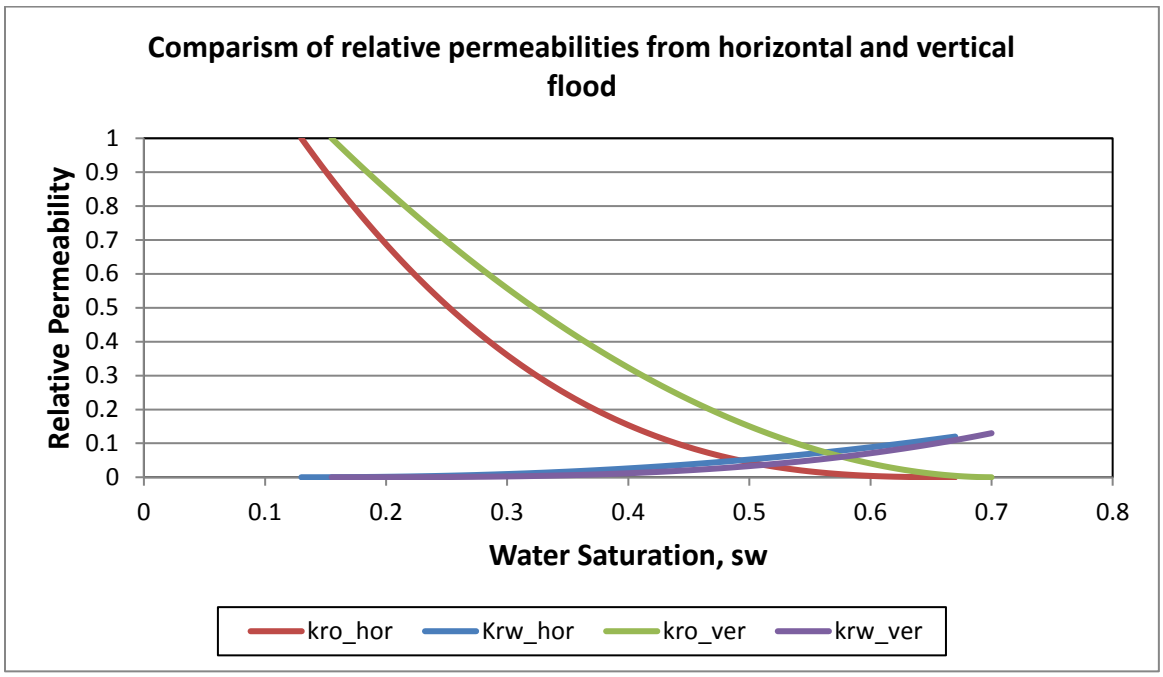

Figure 3.17: Comparison of the relative permeabilities of the horizontal and vertical flood obtained from the secondary water-flood of crude J in the 2500 md core.

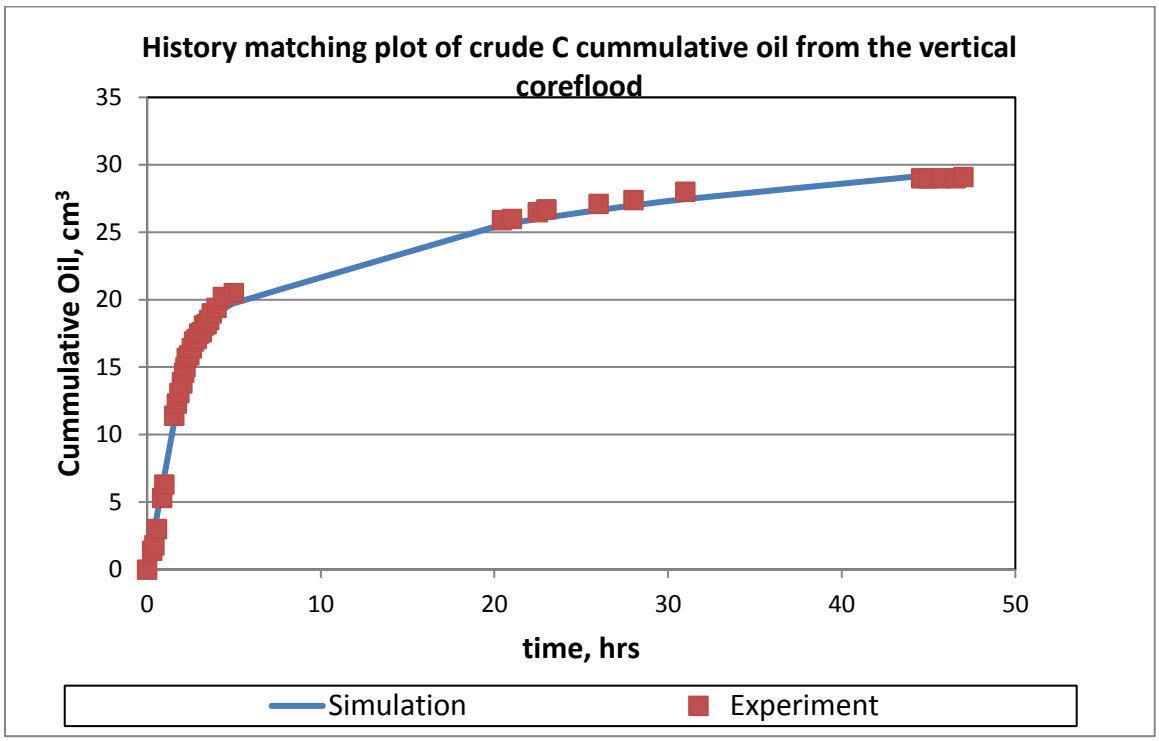

Figure 3.18: Comparison between experiment and simulation results for cumulative oil production in the vertical 2500 md core in the secondary water flood of crude C.

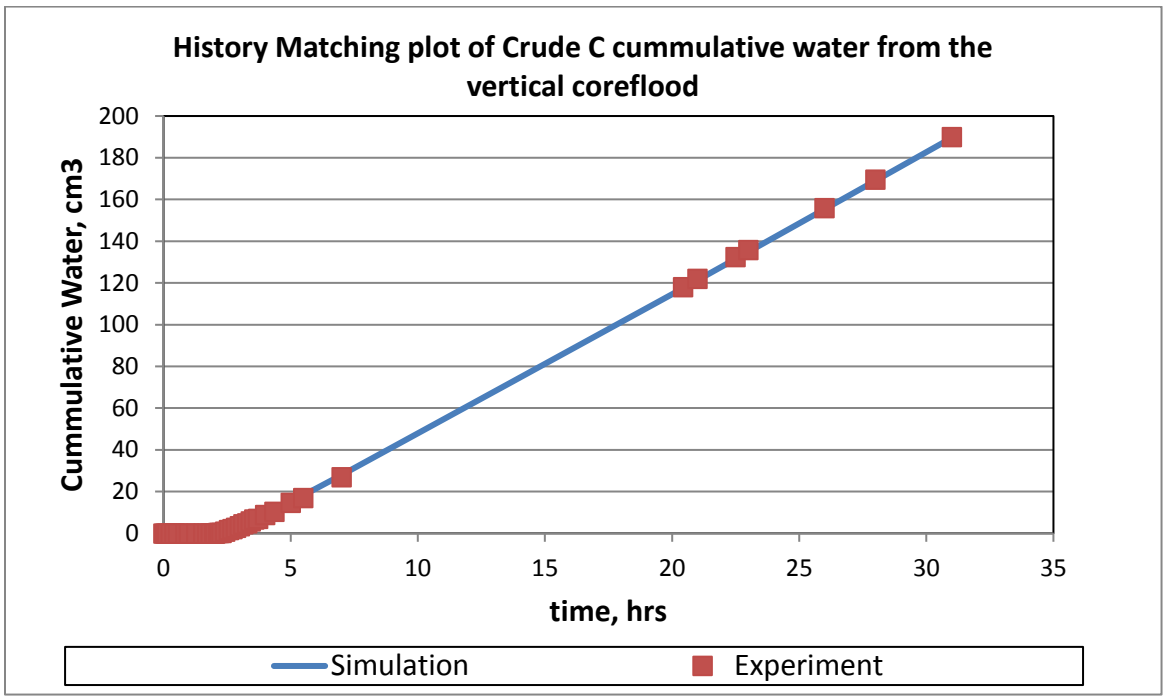

Figure 3.19: Comparison between experiment and simulation results for cumulative water production in the vertical 2500 md core in the secondary water flood of crude C.

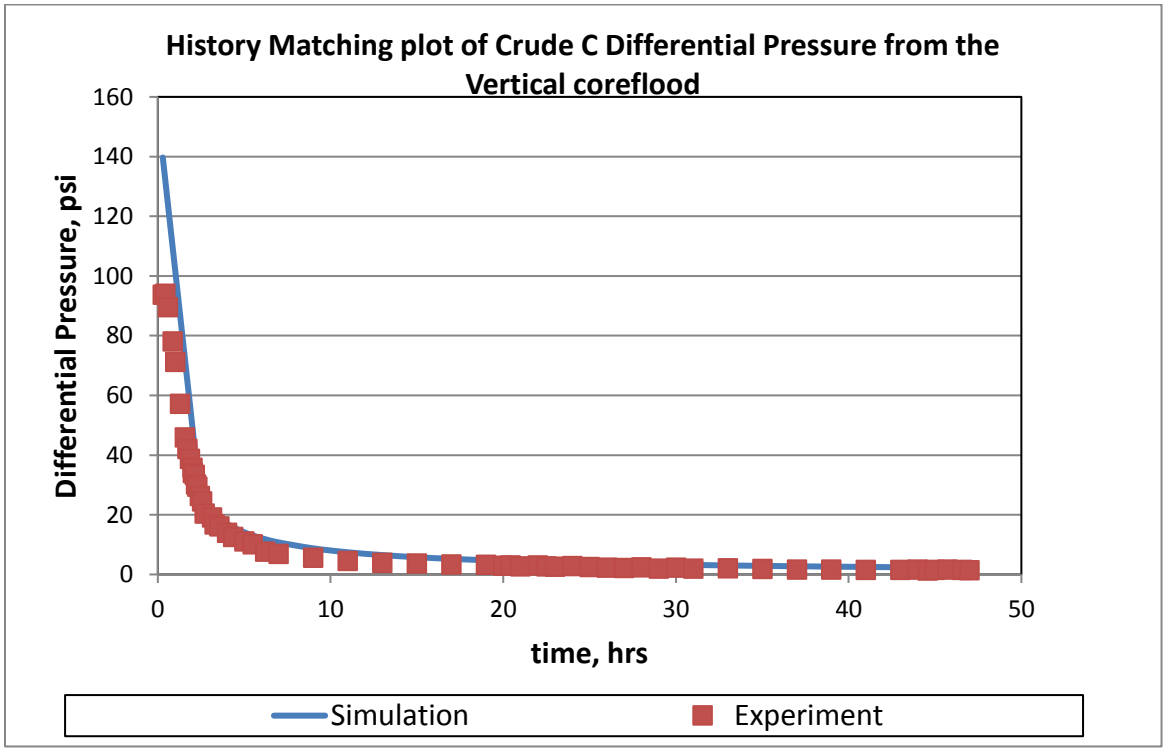

Figure 3.20: Comparison between experiment and simulation results for differential pressure across the vertical 2500 md core in the secondary water flood of crude C.

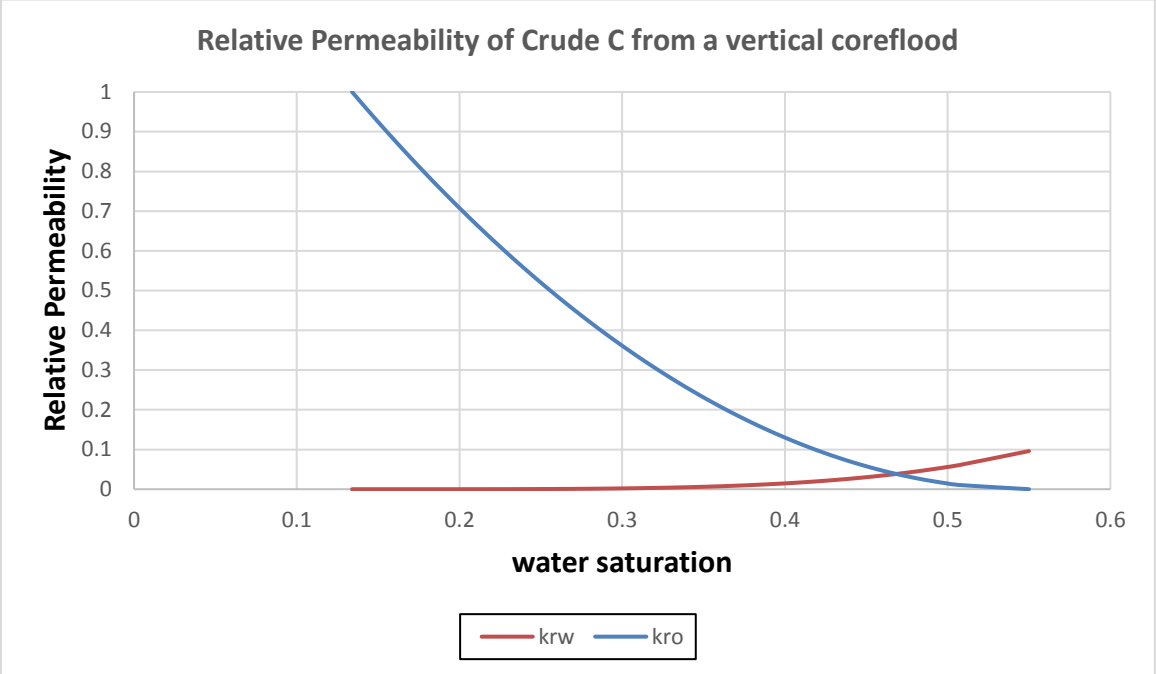

Figure 3.21a: Crude C oil and water relative versus water saturation obtained from the secondary water-flood of crude C in vertical orientation of 2500 md core.

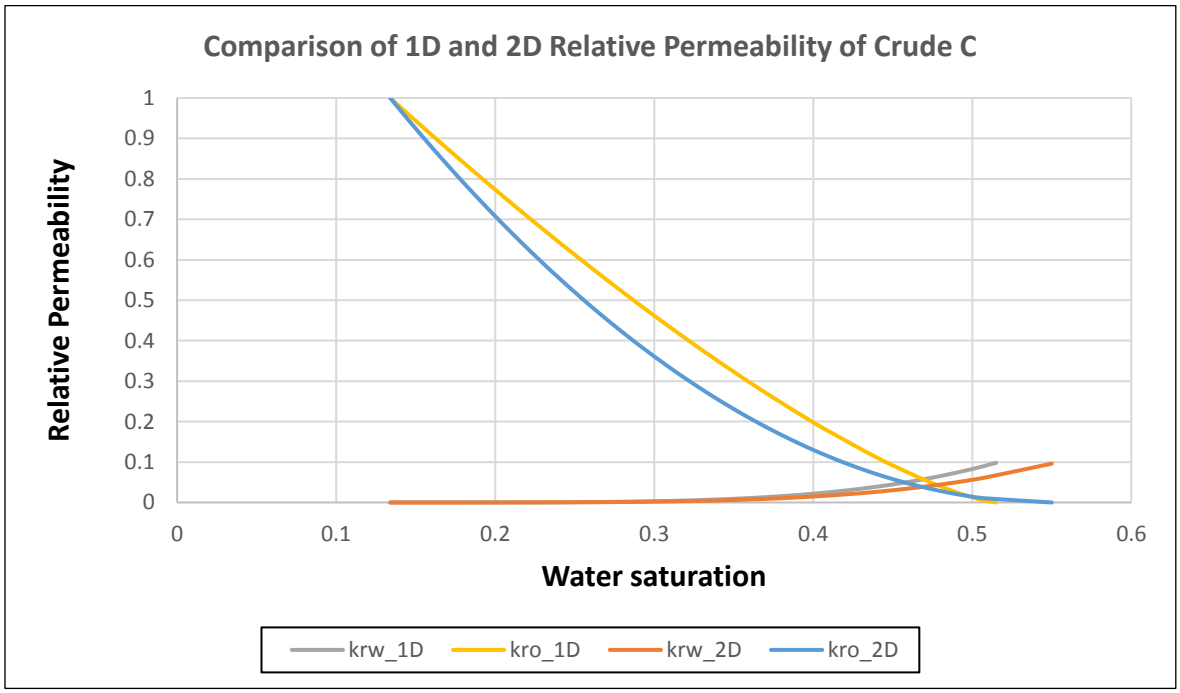

Figure 3.21b: Comparison of the relative permeabilities of the 1-D and 2-D gridding obtained from the secondary water-flood of crude C in the 2500 md core.

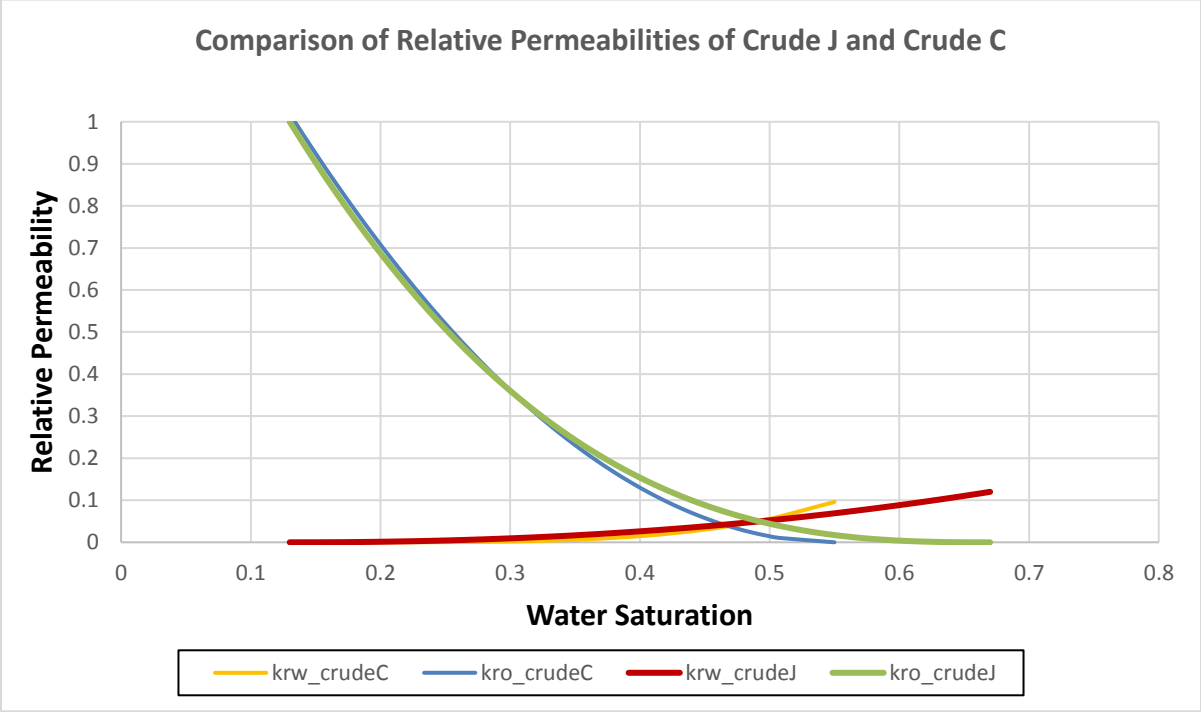

Figure 3.22: Comparison of the relative permeabilities obtained from the secondary water-flood of crude C and crude J in the vertical 2500 md core.

3.3.1 CO_2 Relative Permeability

When CO_2 is used to displace oil in a coreflood experiment, it dissolves in the oil bringing about reduction in the interfacial tension, reduction in oil viscosity, and oil swelling. All these have huge impacts on the estimated CO_2 and oil relative permeability (McDougall, 1997). As both interfacial tension and oil viscosity decrease with increase in CO_2 dissolution, the viscous/ capillary force balance constantly changes over the experimental range considered, with different displacements effectively lying in different flow regimes.

Thus a different method of estimating the CO_2 oil relative permeability has to be used. The use of pre-equilibrated CO_2-flood, where oil is pre-equilibrated with CO_2, and the CO_2 is pre-equilibrated with oil prior to displacement process in the core and the use of Nitrogen flood have been suggested in the literature as alternative approaches to estimate CO_2 and oil relative permeability.

The pre-equilibrated experiment though has minimal mass exchange between CO_2 and the oil, cannot give a representative CO_2 and oil relative permeability. The viscosity of the pre-

equilibrated oil used in this experiment is 15 cp, which is more mobile and has lower residual oil saturation than the 617 cp crude J, and hence will have a higher oil relative permeability than the real one. Also the reduction of interfacial tension of the oil as a result of the pre-equilibration will cause an exaggerated oil relative permeability. Nitrogen on the other hand has a negligible effect on interfacial tension and oil viscosity, and does not bring about oil swelling, thus making Nitrogen flood experiment of the oil more acceptable approach of estimating the CO_2 and oil relative permeability.

Figure 3.23 to 3.25 are the matches between the experiment and simulation results for cumulative oil production, cumulative water production, and the differential pressure across the vertical 2500 md core in the secondary water flood crude C. The matches here are also good hence the relative permeability data generated from them (shown in figure 3.26) are adequate to describe the processes in the core flood.

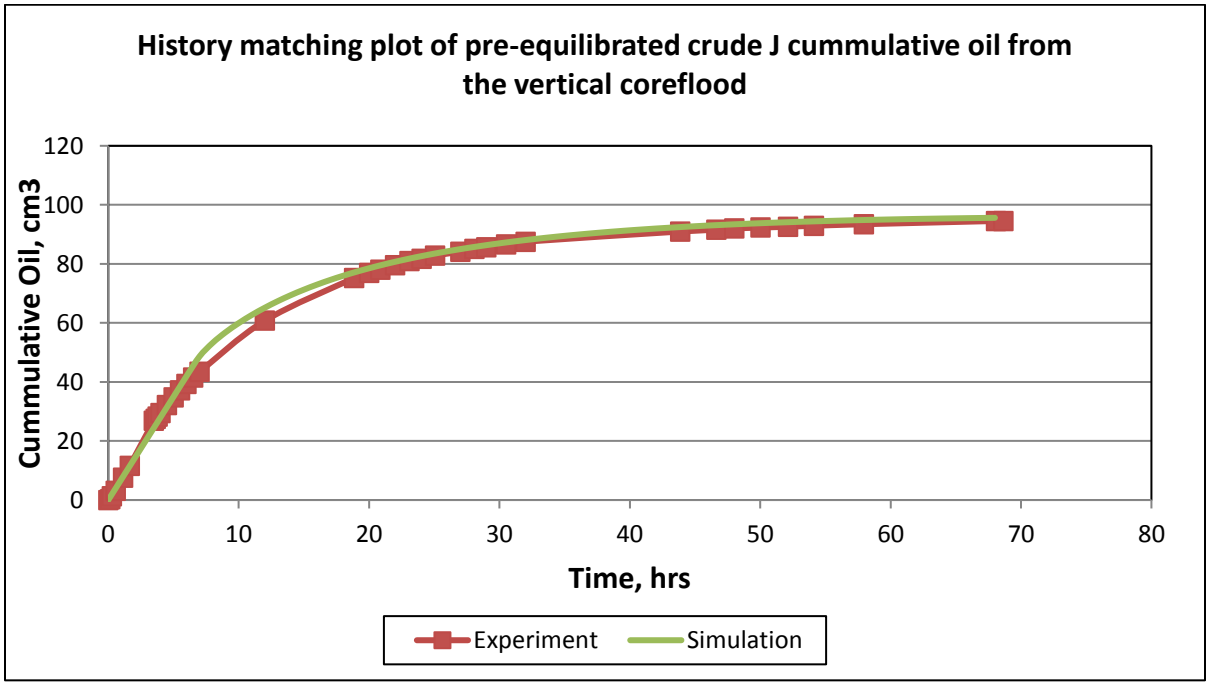

Figure 3.23: Comparison between experiment and simulation results for cumulative oil production in the vertical 2500 md core in the secondary CO_2 flood of pre-equilibrated crude J.

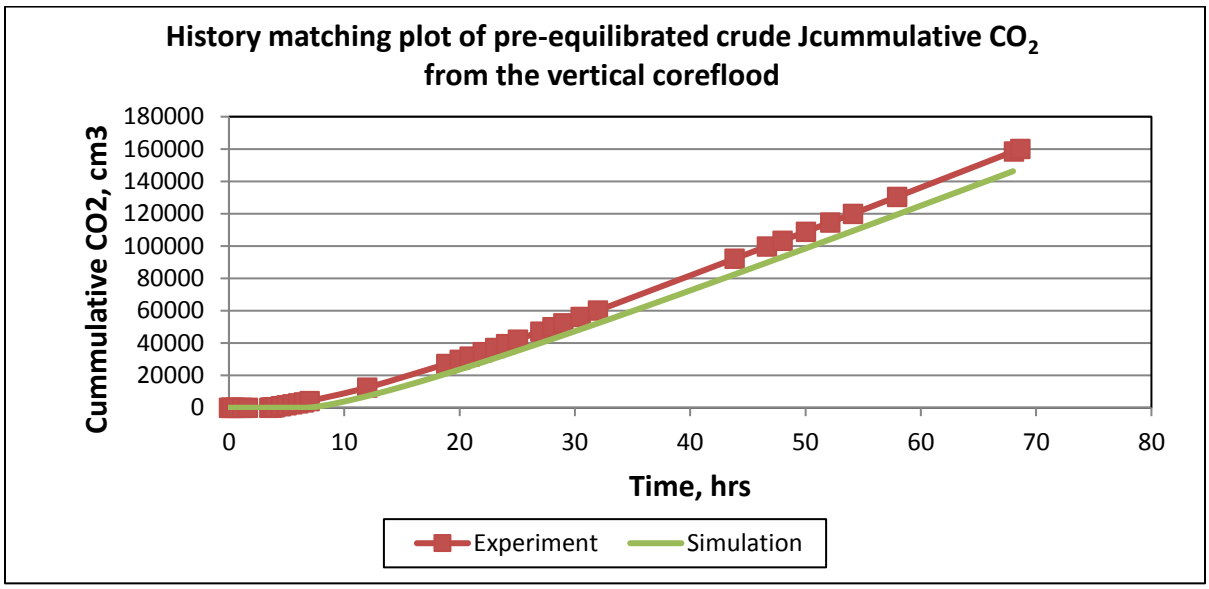

Figure 3.24: Comparison between experiment and simulation results for cumulative CO_2 production in the vertical 2500 md core in the secondary CO_2 flood of pre-equilibrated crude J.

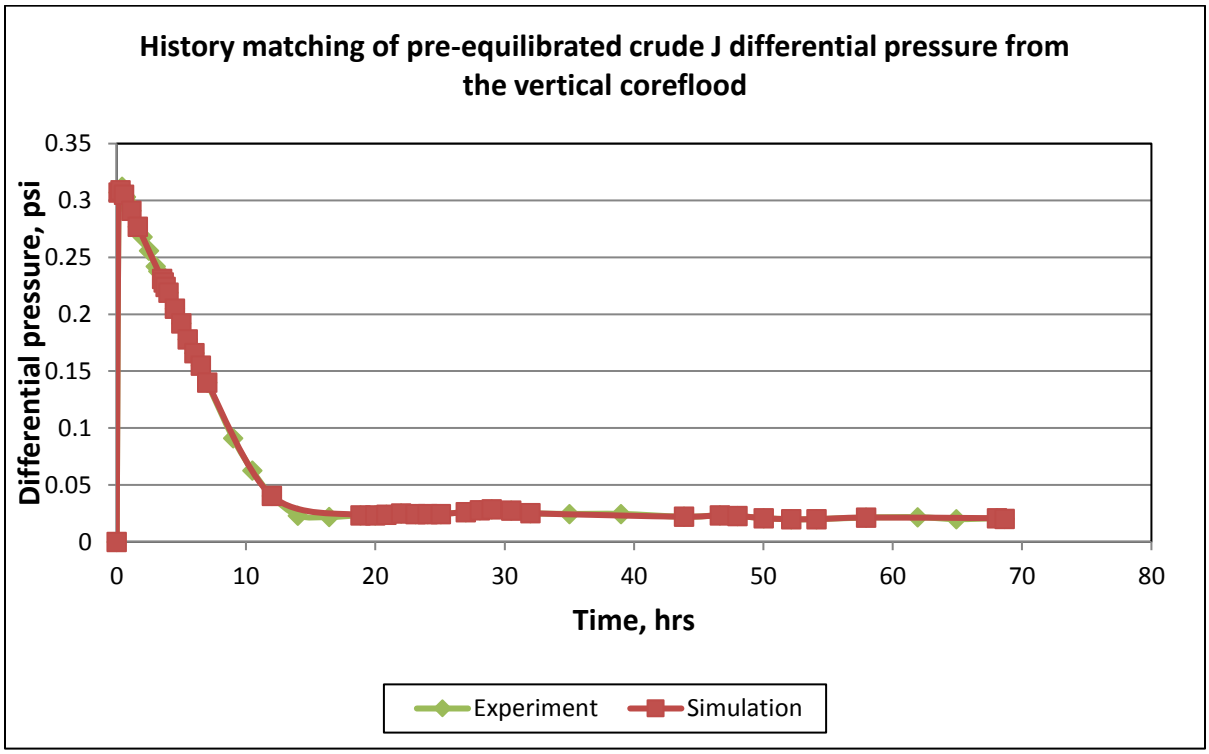

Figure 3.25: Comparison between experiment and simulation results for differential pressure in the vertical 2500 md core in the secondary CO_2 flood of pre-equilibrated crude J.

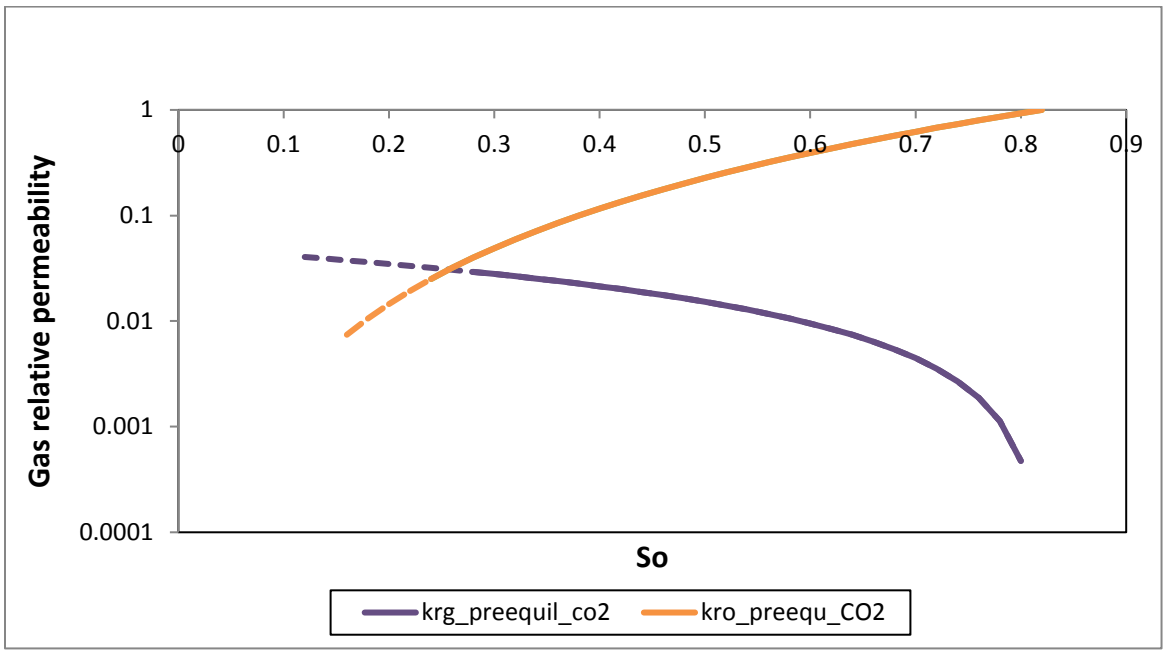

Figure 3.26: Crude J oil and CO_2 relative permeability versus oil saturation obtained from secondary pre-equilibrated CO_2-flood of crude J in vertical orientation 2500 md core.

Figure 3.27 shows the relative permeabilities as estimated from the history matching of the production and differential pressure data from the secondary Nitrogen-flood of crude J in a vertical orientation of the 2500md core. Figure 3.28 shows a comparison between the oil-N_2 relative permeability curves and the oil-CO_2 relative permeability curves. Though the oil relative permeability curves are close, the CO_2 relative permeability is clearly higher than the N_2 relative permeability. The reason for this is that because unlike CO_2, N_2 does not dissolve into oil, the interfacial tension (IFT) and the viscosity of the oil in both cases are different.

Though the Nitrogen flood gives a more practicable estimation of the relative permeability, there is the danger that it still does not adequately estimate a non-swelling, and a non-viscosity reducing CO_2-oil relative permeability because there is a slight swelling and viscosity reduction observed in the oil when mixed with Nitrogen. Ghoodjani (2011) carried out an experimental study looking at the effects of CO_2 on relative permeability with the objective of calculating CO_2-oil relative permeability from a base relative permeability like N_2-oil relative permeability. Based on the effects that fluid viscosities, interfacial tension, and oil swelling have on gas-oil relative permeability, they developed two dimensionless numbers to correlate CO_2-oil to N_2-oil relative permeability and vice versa. The dimensionless numbers are:

$$RBF_o = \sqrt{\frac{(IFT_{CO2}).(\mu_{o_{CO_2}}).(SF_{N2})}{(IFT_{N2}).(\mu_{o_{N2}}).(SF_{CO2})}} \quad (3.9)$$

$$RBF_g = \sqrt{\frac{(IFT_{CO2}).(\mu_{g_{CO_2}}).(SF_{CO2})}{(IFT_{N2}).(\mu_{g_{N2}}).(SF_{N2})}} \quad (3.10)$$

Where, RBF_o and RBF_g stand for relative permeability boost factor for oil and gas, respectively. And IFT is the interfacial tension, μ is the viscosity, and SF is the swelling factor. The following relations were then used to calculate Corey's exponent and residual oil saturation in CO_2 injection from N_2 relative permeability data:

$$e_{oCO2} = RBF_o . e_{oN2} \quad (3.11)$$

$$e_{gCO2} = RBF_g{}^2 . e_{gN2} \quad (3.12)$$

$$S_{or_{CO2}} = \sqrt{RBFo} . S_{or_{N2}} \quad (3.13)$$

These relationships were then used to generate a new CO_2 and oil relative permeability from the N_2 relative permeability data. These estimations of CO_2 and oil relative permeability were done for both crude J and crude C. Table shows the Ghoodjani correlation's parameters for both crude J and crude C. It has been assumed that the interfacial tension for the three gas and oil systems is 1.33 dyne/cm.

Table 3.4: The Ghoodjani correlation's parameters used in this study.

	Crude J_N2	Crude J_CO2	Crude C_CO2
Interfacial Tension, IFT	**1.33**	**1.33**	**1.33**
Gas Viscosity, μ_g	**0.0188**	**0.0151**	**0.0162**
Oil Viscosity, μo	**8670**	**15**	**660**
Swelling Factor, SF	**1**	**1.18**	**1.05**
Oil exponent, e_o	**3**	**0.11**	**0.81**
Gas exponent, e_g	**1.5**	**1.42**	**1.34**
Oil Relative Permeability Boost Factor, RBF_o	**1**	**0.03829**	**0.2693**
Gas Relative Permeability Boost Factor, RBF_g	**1**	**0.9735**	**0.9512**

Figure 3.29 shows a comparison between the N_2-oil relative permeability and the CO_2-oil relative permeability estimated from Ghoodjani's dimensionless boost factor correlations.

The closeness between the two relative permeability data would suggest that N_2-flood generated relative permeability data is, for all intent and purposes, a good representation of the CO_2-oil relative permeability data.

Figure 3.30 shows the CO_2-oil relative permeability estimated from Ghoodjani's dimensionless boost factor correlations for crude C.

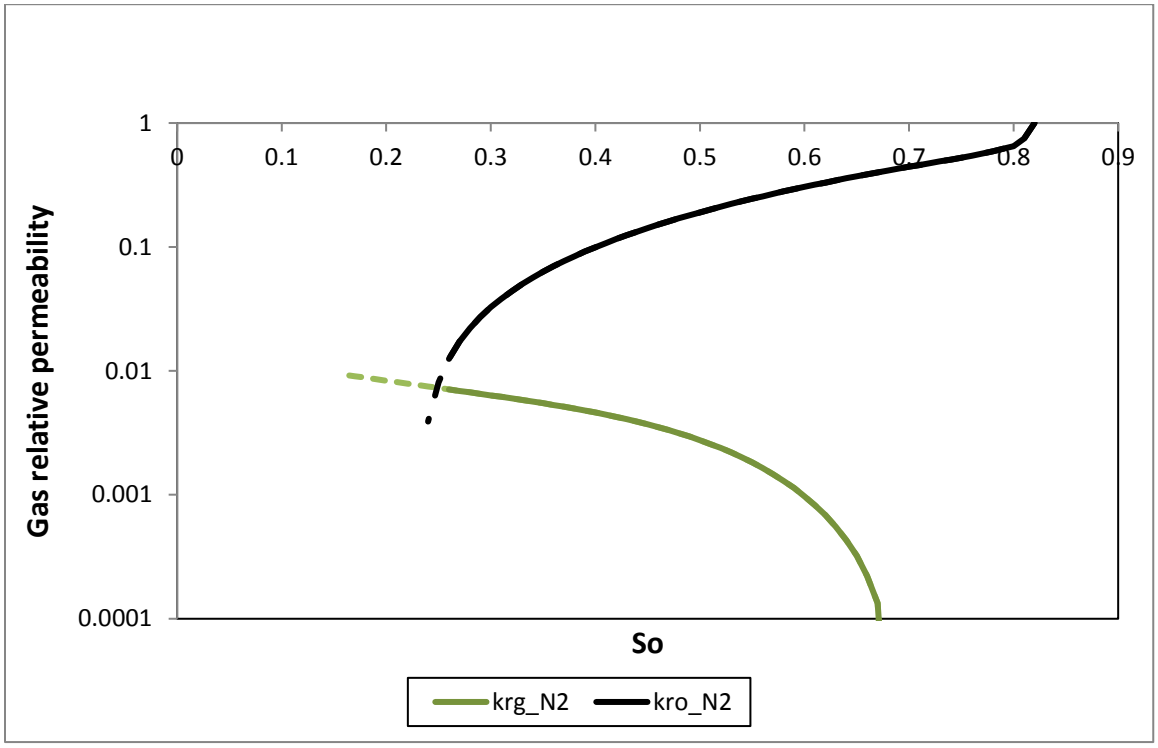

Figure 3.27: Crude J oil and N_2 relative permeability versus oil saturation obtained from secondary pre-equilibrated N_2-flood of crude J in vertical orientation 2500 md core.

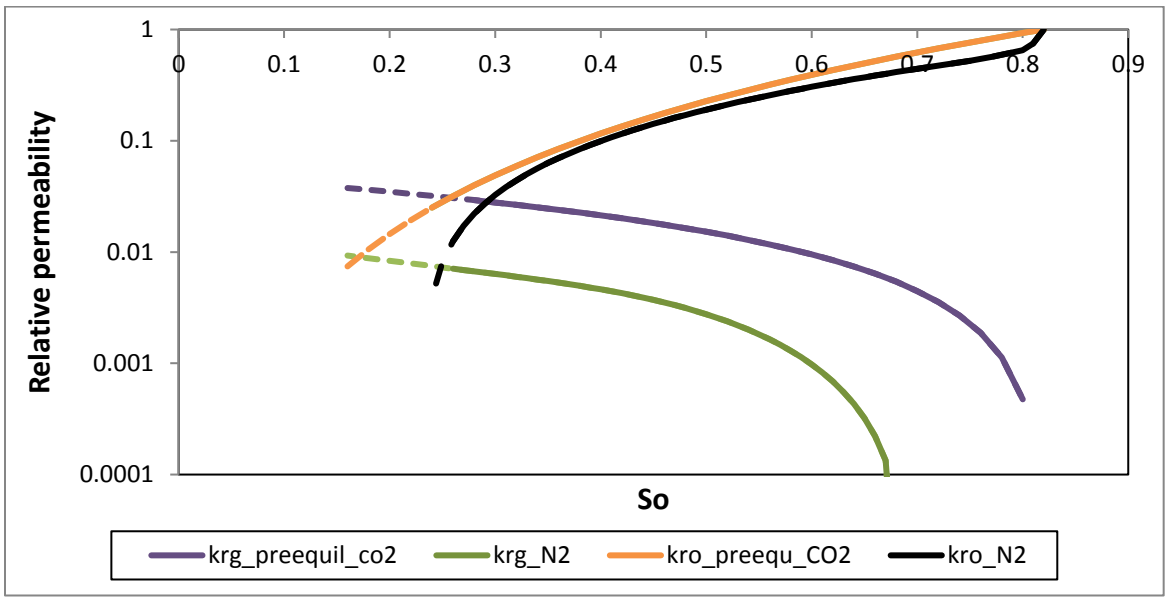

Figure 3.28: Comparison between the oil-N_2 relative permeability of crude J as estimated from history matching of the production and differential pressure data from the secondary N_2-flood and pre-equilibrated CO_2-flood respectively of crude J in a vertical orientation of the 2500 md core.

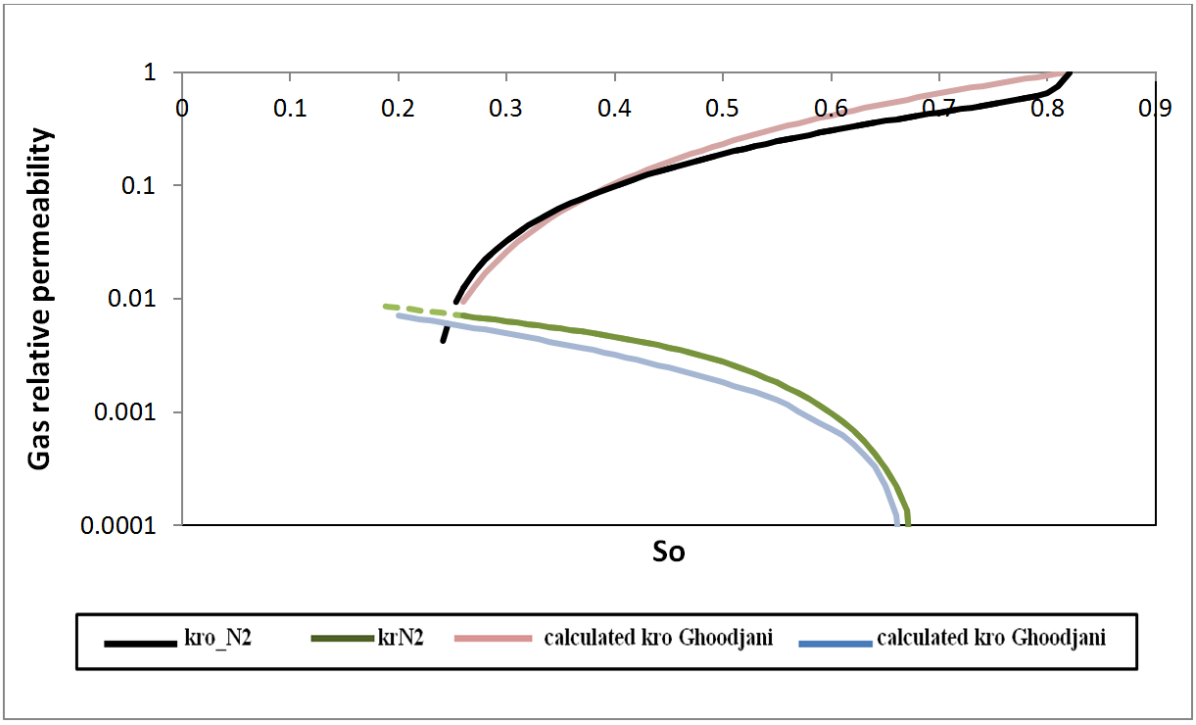

Figure 3.29: Comparison between the oil-N_2 relative permeability of crude J and the CO_2-oil relative permeability of Crude J estimated from Ghoodjani's dimensionless boost factor correlation.

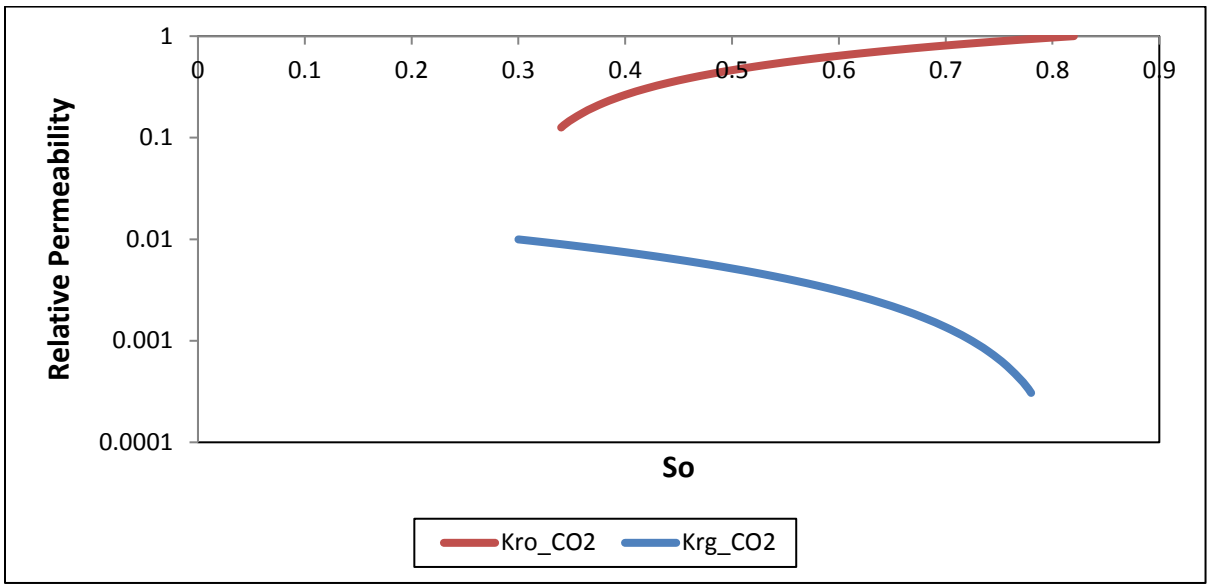

Figure 3.30: Crude C oil and CO_2 relative permeability versus oil saturation obtained from Ghoodjani's dimensionless boost factor correlation.

3.4 Conclusion

The peculiar characteristics of heavy oil relative permeability has been studied in this work, and close attention was paid to the impact of displacement parameters like viscosity ratio, core orientation, interfacial tension, and stability at the displacement front has on the estimated relative permeability. For stable displacement process as often seen in conventional oil, the estimated relative permeability is only a function of the saturation of the fluid whereas, for unstable displacement processes as often seen in heavy oil, the estimated relative permeability is also a function viscosity ratio and the rates, in addition to saturation. The following conclusions can also be drawn from this work:

1. Experiments for estimating relative permeability curves should be performed at the exact condition in the reservoir as reservoir simulation studies results can be very sensitive to small changes in heavy oil relative permeability curves. This is due to the viscous instability in heavy oil displacement process.

2. Increasing the displacement rate or increasing the viscosity of the displaced fluid in a coreflood experiment tends to shift the flow regime from a capillary dominated flow to a viscous dominated flow thereby aggravating instability at the displacement front with the consequent inefficient displacement.

3. The higher the instability at displacement front, the worse is the resulting viscous fingering, and the smaller is the relative permeability of the displacing fluid.

4. The water relative permeability from vertical coreflood is higher than the one from the horizontal corefloods. This is because gravity forces help in stabilizing coreflood experiments.

5. For stable displacement process, relative permeability is only a function of the saturation of the fluid; whereas, for unstable displacement process, relative permeability is also a function viscosity ratio.

6. The relative permeability curves for heavy oil with a tendency for instability are apparent relative permeability, and must be estimated at the exact reservoir condition, else may not be useful

3.5 References

1. Abrams ,1975, 'The influence of fluid viscosity. Interfacial Tension, and flow velocity on residual oil saturation left by waterflood' SPEJ 437447.

2. Al-Shuraiqi, H.S., Grattoni, C.A., and Muggeridge, A.H. ,2005, 'Numerical and Experimental Investigation into the effects of Viscosity and Injection rate on Relative Permeability and Oil Recovery'. In the proceedings of the International Symposium of the Society of Core Analysts held in Toronto, Canada; August 21−25. SCA2005-

3. Amaefule, J.O. and Handy, L.L., 1982, The effect of interfacial Tension on Relative Oil and Water Permeabilities of consolidated Porous Media. SPEJ 22 (3): 371-381. SPE-9783-PA.

4. Buckley, S. E., Leverett, M. C., 1942, "Mechanism of Fluid Displacement in Sands", Petroleum Transactions, AIME, Vol. 146, pp 107-116.

5. Corey, A.T., 1954, 'The interrelation Between Gas and Oil Relative Permeabilities.' Producers Monthly 19(November): 38-41.

6. Dake, L.P, 1978,'Fundamentals of Reservoir Engineering.',1st Edition, 100-125 Amsterdam, ELSEVIER.

7. Didler Pavone ,1992, 'Observation and correlation for immiscible viscous-fingering experiments.

8. Ekwere J. Peters, Donald L. Flock ,1981, 'The onset of Instability During Two-phase Immiscible Displacement in Porous Media' Society of Petroleum Engineers. SPE 8371.

9. Ekwere, J. P., Khataniar, S ,1987, 'The effect of Instability on relative permeability curves obtained by the dynamic-displacement method '. SPE Formation Evaluation, Volume2, Number 4, pp 469-474.

10. Emadi ,2012, 'Enhanced heavy oil recovery by water and carbon-dioxide' PhD thesis. Institute of Petroleum engineering, Heriot Watt University.

11. Fassihi M.R. ,1989, 'Estimation of relative permeability from low rate, unsteady state tests- a simulation approach;

12. Ghoodjani, E., Bolouri, S.H., 2011, 'Experimental Study and Calculation of CO2-oil relative permeability' Petroleum and Coal 53 (2) 123-131, 2011.

13. Green and Willhite, (1986) 'Enhaced Oil Recovery.

14. Johnson, E.F., Bossler, D.P., Naumann, V.O., 1958" Calculation of Relative Permeability from displacement Experiments", Petroleum Transactions, AIME, Vol. 216, pp 370-372.

15. Jones, S. C. and Roszelle, W.O., 1978, "Graphical Techniques for Determining Relative from Displacement Experiments", J. Pet. Tech. (May 1978) *807*

16. Lefebvre du Prey ,1973, 'Factors Affecting Liquid-Liquid Relative Permeabilities of a Consolidated Porous Medium' SPE Journal, Volume13, Number 1, pp 39-47.

17. Levrett, M.C., 1938, "Flow of oil-water mixtures through unconsolidated sands," Trans. AIME 132, 149-171.

18. Lo, H. Y., and Mungan, N., 1973), "Effect of Temperature on Water-Oil Relative Permeabilities in OilWet and Water-Wet systems," 48th Annual SPE of AIME Fall Meeting, Las Vegas, Sept. 30-0ct. 3, 1973. Preprint No. SPE 4505 (1973).

19. Mai, A., Kantzas, A, 2007, 'Heavy oil Water-flooding: Effects of Flowrate and Oil viscosity'. In the proceedings of the 8th Canadian International Petroleum Conference, Calgary, Alberta, Canada; June 12-14.

20. Mai, A., Kantzas, A., 2008, 'Improved Heavy Oil Recovery by Low Rate Water flooding'. In the proceedings of the International Thermal Operations and Heavy Oil Symposium, Calgary, Alberta, Canada; October 20−23 SPE Paper 117648.

21. Maini, B.B., 1995, 'Is It Futile to Measure Relative Permeability for Heavy Oil Reservoirs?', In the proceedings of the 46th Annual Technical Meeting, Petroleum Society of CIM, Banff, Canada, May 14-17.

22. McDougall S.R., Salino P.A., Sorbie, K.S., 1997, 'The effect of Interfacial Tension Upon Gas-Oil Relative Permeability Measurements: Interpretation using pore-scale models," SPE Annual technical conference and exhibition, San Antonio, Texas.

23. Mehdi H. Leonard K., Herbert Harvey A. (1986), "Relative permeability of Petroleum Reservoirs," CRC Press, Inc. Boca Raton, Florida.

24. Moore, T. F., and Slobod, R. L., 1956, "The Effect of Viscosity and Capillarity on the Displacement of Oil by Water," Prod. Monthly (Aug 1956).

25. ODEH A.S., 1959,'Effect of Viscosity Ratio on Relative Permeability.' Society of Petroleum Engineers.

26. Paul Wilhite G., 1986, 'Waterflooding' SPE textbook series Vol. 3. ISBN:878-1-55563-005-8.

27. Rajan, R.R., 1986, "Theoretical Correct Analytical Solution for Calculating Capillary Pressure-Saturation from Centrifuge Data" paper presented at the 1986 SPWLA logging symposium, June 9-13.

28. Rapoport L.A and LEAS, W.J., 1953, 'Properties of linear waterfloods,' Pet Trans AIME 198:139-148 SPE 213-G.

29. Rose, W., and Witherspoon, P.A., 1956. "Studies of waterflood performance II. – Trapping oil in a pore doublet," Illinois Geological Survey Circ. 224.

30. Sufi, A.S., Ramey, H.J., and Brigham, W.E, 1982, 'Temperature effects on relative permeability of oil-water systems' Paper SPE 11071presented at the annual Technical conference and Exhibition, New Orleans, September 26-29.

31. Van Meurs, P., Chuoke R. L, Van der Poel, 1958, "The instability of slow, Immiscible, Viscous liquid-liquid displacents in permeable media" Trans. AIME, vol 216: 188-194.

32. Wang, J., Dong, M., and Asghari, K, 2006, 'Effect of Oil Viscosity on Heavy Oil /Water Relative Permeability Curves ' Society of Petroleum Engineers. SPE 99763.

33. Wang, S., Huang, Y. and Civan, F,, 2006, "Experimental and theoretical investigation of the Zaoyuan field heavy oil flow through porous media," Journal of Petroleum Science and Engineering, 50, 83-101.

34. Wyckoff, R.D., and H.G. Botset, 1936, 'The flow of gas liquid mixture through unconsolidated sand'. Physics 7: 325-345.

Chapter 4: Estimating Heavy Oil Relative Permeability with Analytical Methods

4.1 Introduction

The relative permeability of rocks to oil, water and gas flow in the reservoir is an important parameter in analyzing and predicting the reservoir behavior. In a two phase system, the Kozeny-Carman equation can be used to explain the relationship between the oil relative permeability and the relative permeability of the other fluid (gas or water). The Kozeny-Carman equation used in calculating pressure drop of a laminar flow of a Newtonian and incompressible fluid flowing through a porous medium is

$$\frac{dP}{L} = \frac{180\mu}{{\phi_s}^2 {D_p}^2} \frac{(1-\epsilon)^2}{\epsilon^3} v_s \tag{4.1}$$

Where

dP is the pressure drop

L is the total length of the medium

v_s is the superficial velocity of the fluid through the medium

μ is the viscosity of the fluid

ϵ is the porosity of the medium

ϕ_s is the sphericity of the particles in the medium

D_p is the diameter of the related spherical particle

This equation is comparable to the Darcy's law:

$$v_s = \frac{K}{\mu} \frac{dP}{L} \tag{4.2}$$

Or

$$\frac{dP}{L} = \frac{\mu}{K} v_s \tag{4.3}$$

Where, K is the permeability of the medium.

If equation 4.1 and 4.3 are compared

$$\frac{180\mu}{{\phi_s}^2 {D_p}^2} \frac{(1-\epsilon)^2}{\epsilon^3} = \frac{\mu}{K} \tag{4.4}$$

Or

$$K = \frac{{\phi_s}^2 {D_p}^2}{180} \frac{\epsilon^3}{(1-\epsilon)^2} \tag{4.5}$$

From equation 4.5, it can be said that the permeability of a porous material is a function of the product of the tortuosity, and the parameter that evaluates the mean hydraulic radius of channels through which the fluid flows. For a multiphase system the tortuosity parameter was approximated by a simple fluid saturation term in Burdine's equation as:

$$K_{ro} = \left(\frac{S_o - S_{or}}{1 - S_{or}}\right)^2 \frac{\int_0^{S_o} dS_0/{P_c}^2}{\int_0^1 dS_0/{P_c}^2} \tag{4.6}$$

$\left(\frac{S_o - S_{or}}{1 - S_{or}}\right)^2$ is a parameter called tortuosity coefficient; and the ratio of the integrals is a function of the mean hydraulic radii of the oil channel at any saturation , S_o.

And for gas relative permeability,

$$K_{rg} = \left(1 - \frac{S_o - S_{or}}{S_m - S_{or}}\right)^2 \frac{\int_{S_o}^1 dS_0/{P_c}^2}{\int_0^1 dS_0/{P_c}^2} \tag{4.7}$$

Where the ratio of the integrals in equation 4.7 is a function of the mean hydraulic radii of the oil channel at any saturation, S_o; and S_{or} is the residual oil saturation; S_m is the lowest oil saturation at which the gas tortuosity is infinite; and P_c is the capillary pressure. The ratio of the integral in both equations 4.6 and 4.7 can be evaluated by finding the areas under the curves of the $1/{P_c}^2$ against oil saturation, and thus both oil and gas relative permeability as a function of saturation can be estimated if S_{or} and S_m are known.

Two phase relative permeabilities for oil-water and gas-oil systems have always been estimated from unsteady state core flood experimental data because the unsteady state flow core flood experiment gives flow characteristics that are more representative of the flow characteristics in the reservoir than the flow characteristics from steady state flow core flood experiments. Estimating the relative permeability of oil and water from an unsteady state core flood experiment would involve first saturating a small linear core with water, then oil-flood it to irreducible water saturation. Subsequently, water is injected through one end of

the core, and during this process, pressure drop across the core, oil and water recovery at the other end of the core are measured. These measured data, with the knowledge of the pore volume of the core, its absolute permeability, and the viscosities of both the oil and water are sufficient to estimate the relative permeability curves.

The JBN analytical method of calculating relative permeability from displacement experiments was developed by Johnson, Bossler, and Nauman in 1952. It is the most widely used analytical method for calculating relative permeability in conventional oil. There is however no record in the literature of the use of the JBN method in calculating relative permeability in heavy oil. Another popular analytical method is the graphical technique which also, like the JBN method, has no record of being used in estimating heavy oil relative permeability curves. The two methods are used in this work to evaluate the relative permeabilities in a heavy oil water flood processes.

The estimation of relative permeability curves using both the JBN and the graphical methods requires the determination of the saturation at a point in the core. Fortunately, the Welge equation estimates the saturation at the effluent end of the core if the average saturation history in the core is known. The average saturation at any time in the displacement process can be determined from a simple material balance.

Consider displacement of oil by water in a system of dip angle Θ as shown in Figure 4.1:

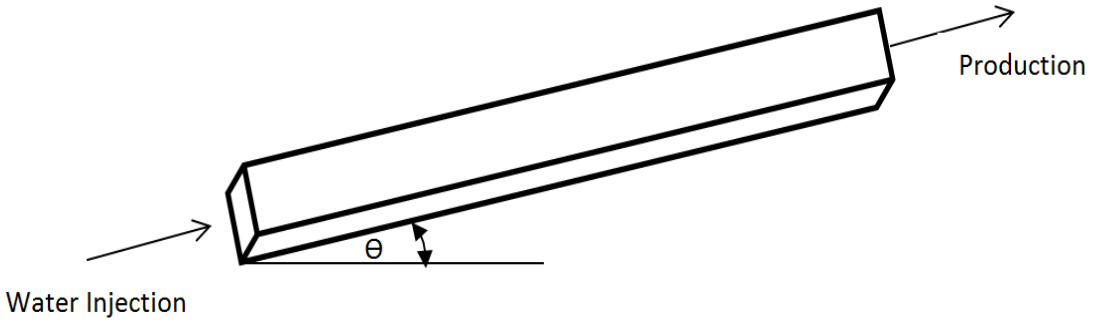

Figure 4.1: A section showing the displacement of oil by water in a system of dip angle Θ

Starting with Darcy's equation, the oil rate is given by:

$$q_o = -\frac{Kk_{ro}A}{\mu_o}\left(\frac{\partial P_o}{\partial x} + \rho_o\, g\, sin\theta\right) \tag{4.8}$$

Rearranging,

$$\frac{q_o\mu_o}{Kk_{ro}} = -A\left(\frac{\partial P_o}{\partial x} + \rho_o\, g\, sin\theta\right) \tag{4.9}$$

And the water rate:

$$q_w = -\frac{Kk_{rw}A}{\mu_w}\left(\frac{\partial P_w}{\partial x} + \rho_w\, g\, sin\theta\right) \tag{4.10}$$

Rearranging,

$$\frac{q_w\mu_w}{Kk_{rw}} = -A\left(\frac{\partial P_w}{\partial x} + \rho_w\, g\, sin\theta\right) \tag{4.11}$$

The Capillary pressure expression is given by:

$$P_c = P_o - P_w \tag{4.12}$$

By subtracting equation 4.11 from 4.9, and substituting for capillary pressure

$$\frac{q_o\mu_o}{Kk_{ro}} - \frac{q_w\mu_w}{Kk_{rw}} = -A\left(\frac{\partial P_c}{\partial x} - \Delta\rho\, g\, sin\theta\right) \tag{4.13}$$

And by substituting

$$q_o = q_t - q_w \tag{4.14}$$

$$\frac{(q_t - q_w)\mu_o}{Kk_{ro}} - \frac{q_w\mu_w}{Kk_{rw}} = -A\left(\frac{\partial P_c}{\partial x} - \Delta\rho\, g\, sin\theta\right) \tag{4.15}$$

$$\frac{-q_w\,\mu_o}{Kk_{ro}} - \frac{q_w\mu_w}{Kk_{rw}} = -\frac{q_t\mu_o}{Kk_{ro}} - A\left(\frac{\partial P_c}{\partial x} - \Delta\rho\, g\, sin\theta\right) \tag{4.16}$$

$$q_w\left(1 + \frac{k_{ro}\mu_w}{k_{rw}\mu_o}\right) = q_t + \frac{Kk_{ro}A}{\mu_o}\left(\frac{\partial P_c}{\partial x} - \Delta\rho\, g\, sin\theta\right) \tag{4.17}$$

And by substituting the fraction of water flowing:

$$f_w = q_w/q_t \tag{4.18}$$

$$f_w = \frac{1+\frac{Kk_{ro}A}{q_t\mu_o}\left(\frac{\partial P_c}{\partial x} - \Delta\rho\, g\, sin\theta\right)}{1+\frac{\mu_w}{k_{rw}}.\frac{k_{ro}}{\mu_o}} \tag{4.19}$$

And if the capillary pressure can be neglected:

$$f_w = \frac{1-\frac{Kk_{ro}A}{q_t\mu_o}(\Delta\rho\ g\ sin\theta\ )}{1+\frac{\mu_w}{k_{rw}}.\frac{k_{ro}}{\mu_o}} \tag{4.20}$$

And for the simplest case of horizontal flow, with negligible capillary pressure:

$$f_w = \frac{1}{1+\frac{\mu_w}{k_{rw}}.\frac{k_{ro}}{\mu_o}} \tag{4.21}$$

4.2 Buckley-Leverett One Dimensional Displacement

In an oil-water system where water is displacing oil, Buckley and Leverett (1942) describes an equation that determines the velocity of a plane of constant water saturation travelling in a one dimensional system.

Mass In – Mass out = Rate of increase of mass in the volume element

$$q_w\rho_w|_x - q_w\rho_w|_{x+dx} = A\phi dx\ \frac{\partial(\rho_w S_w)}{\partial t} \tag{4.22}$$

$$q_w\rho_w|\mathrm{x} - (\ q_w\rho_w|\mathrm{x} + \frac{\partial(\rho_w q_w)}{\partial x}\mathrm{dx}\ ) = A\phi dx\ \frac{\partial(\rho_w S_w)}{\partial t} \tag{4.23}$$

$$\frac{\partial(\rho_w q_w)}{\partial x} = -A\phi\ \frac{\partial(\rho_w S_w)}{\partial t} \tag{4.24}$$

For an incompressible fluid, it means the density is constant:

$$\frac{\partial(q_w)}{\partial x} = -A\phi\ \frac{\partial(S_w)}{\partial t} \tag{4.25}$$

$$\left.\frac{\partial(q_w)}{\partial x}\right|_t = -A\phi\ \left.\frac{\partial(S_w)}{\partial t}\right|_x \tag{4.26}$$

This is the Buckley-Leverett equation.

Since S_w is a function of distance, x, and time, t, i.e S_w(x,t), thus:

$$dS_w = \left.\frac{\partial S_w}{\partial x}\right|_t \mathrm{dx} + \left.\frac{\partial S_w}{\partial t}\right|_x \mathrm{dt} \tag{4.27}$$

For a constant water saturation, $dS_w = 0$, hence:

$$\left.\frac{\partial S_w}{\partial t}\right|_x = -\left.\frac{\partial S_w}{\partial x}\right|_t \left.\frac{\partial x}{\partial t}\right|_{S_w} \tag{4.28}$$

and

$$\left.\frac{\partial q_w}{\partial x}\right|_t = \left(\frac{\partial q_w}{\partial S_w}\frac{\partial S_w}{\partial x}\right)_t \tag{4.29}$$

Substituting 4.28 and 4.29 into 4.26:

$$\left(\frac{\partial q_w}{\partial S_w}\frac{\partial S_w}{\partial x}\right)_t = A\phi \left.\frac{\partial S_w}{\partial x}\right|_t \left.\frac{\partial x}{\partial t}\right|_{S_w} \tag{4.30}$$

$$\left.\frac{\partial q_w}{\partial S_w}\right|_t = A\phi \left.\frac{dx}{dt}\right|_{S_w} \tag{4.31}$$

Since $q_w = q_t f_w$

$$v_{S_w} = \left.\frac{dx}{dt}\right|_{S_w} = \left.\frac{q_t}{A\phi}\frac{df_w}{dS_w}\right|_{S_w} \tag{4.32}$$

Integrating for the time of injection gives:

$$\int_0^t \frac{dx}{dt}dt = \int_0^t \frac{q_t}{A\phi}\frac{df_w}{dS_w}dt \tag{4.33}$$

$$X_{S_w} = \frac{1}{A\phi}\frac{df_w}{dS_w}\int_0^t q_t dt \tag{4.34}$$

Or

$$X_{S_w} = \left.\frac{W_i}{A\phi}\frac{df_w}{dS_w}\right|_{S_w} \tag{4.35}$$

This is the position of the fluid front, which is also called the frontal advance equation.

If $Q = \frac{W_i}{A\phi L}$, the number of pore volume is substituted into equation 4.35 for the special case at breakthrough, where X_2 is L, equation 4.35 becomes:

$$\frac{1}{Q} = \frac{A\phi L}{W_i} = \left.\frac{df_w}{dS_w}\right|_{S_w} \tag{4.36}$$

Then,

$$Q = \frac{1}{\left.\frac{df_w}{dS_w}\right|_{S_w}} \tag{4.37}$$

Equation 4.37 is the expression for the number of pore volume injected into the core, where W_i is the cumulative fluid injected into the core. In a core flood study, the volume of oil produced is equal to the volume of water injected before breakthrough. Applying a simple

material balance on the core, the volume of water injected, Wi, and the total oil recovered, N_p, can be expressed as:

$$W_i = N_p = A\phi L(S_{wavg} - S_{wc}) \tag{4.38}$$

Where S_{wavg} is the average water saturation in the core after the injection of Wi; S_{wc} is the irreducible water saturation in the core, and L is the total length of the core. V_p , the pore volume is $A\phi L$, thus equation 4.38 becomes:

$$N_p = V_p(S_{wavg} - S_{wc}) \tag{4.39}$$

Or

$$S_{wavg=} S_{wc} + N_p/V_p \tag{4.39b}$$

Welge (1952) in an attempt to develop a solution for a water-flood performance expresses the average water saturation as:

$$S_{wavg} = \frac{\int_0^{x2} S_w \, A\phi dx}{\int_0^{x2} A\phi dx} \tag{4.40}$$

For a constant cross-sectional area, A, and porosity, ϕ, equation 4.40 reduces to:

$$S_{wavg} = \frac{\int_0^{x2} S_w \, dx}{X_2} \tag{4.41}$$

By employing the product rule

$$\int_0^{x2} S_w \; dx = X_2 S_{w2} - \int_0^{x2} x \; dS_w \tag{4.42}$$

Equation 4.41 becomes

$$S_{wavg} = S_{w2} \quad - \frac{1}{X_2} \int_0^{x2} x \; dS_w \tag{4.43}$$

If $X_2 = L$, at the outlet end of the core, then equation 4.43 becomes:

$$S_{wavg} = S_{w2} \quad - \frac{1}{L} \int_0^{L} x \; dS_w \tag{4.44}$$

And S_{w2} is the water saturation at the outlet end of the core.

By substituting for x (using equation 4.35) in equation 4.44 gives:

$$S_{wavg} = S_{w2} - \frac{W_i}{A\phi L} \int_1^{f_{w2}} df_w \quad (4.45)$$

$$S_{wavg} = S_{w2} + \frac{W_i}{A\phi L} (1 - f_{w2}) \quad (4.46)$$

If the pore volume, $V_p = A\phi L$, then number of pore volume , is given as, $Q = \frac{W_i}{V_p}$, hence :

$$S_{wavg} = S_{w2} + Q (1 - f_{w2}) \quad (4.47)$$

$$S_{wavg} = S_{w2} + Q f_{o2} \quad (4.48)$$

4.3 JBN Methods

The use of the JBN method assumes that capillary pressure effect is negligible. Due to the effect of the large viscosity for heavy oil, the capillary pressure and gravity terms become negligible in equation 4.19, thus making equation 4.21 adequate in describing fractional flow for heavy oil flow processes. The second assumption for the use of the JBN method is that the flow velocity through the core is constant. This is possible if the different phases flowing through the core behave as immiscible incompressible fluids, hence the application of the JBN method is more suitable for water flood processes in heavy oil than gas flood processes. In this chapter therefore, the JBN method, and its graphical technique alternative by Jones and Roszelle will be used to estimate the oil and water relative permeability curves from a water flood experiment of heavy oil crude J. Figure 4.2 shows the plot of the cumulative oil recovery and the differential pressure across the core versus the cumulative brine injected in the water-flood of crude J in a horizontal core. The basic properties of crude J, and the core used is shown in Table 4.1, and the core-flood experiment's result in a tabular for is shown in table 4.2.

Table 4.1: Basic Properties of Crude J and the Core used in this Study

Crude Name	Porosity	Perm. (md)	Core Orientation	Core Diameter (cm)	Core Length (cm)	Viscosity (cp)	Reservoir Temp. (deg. C)	Reservoir Pressure (psi)
J	0.24	2500	Horizontal	5.1	32	617	28	1500

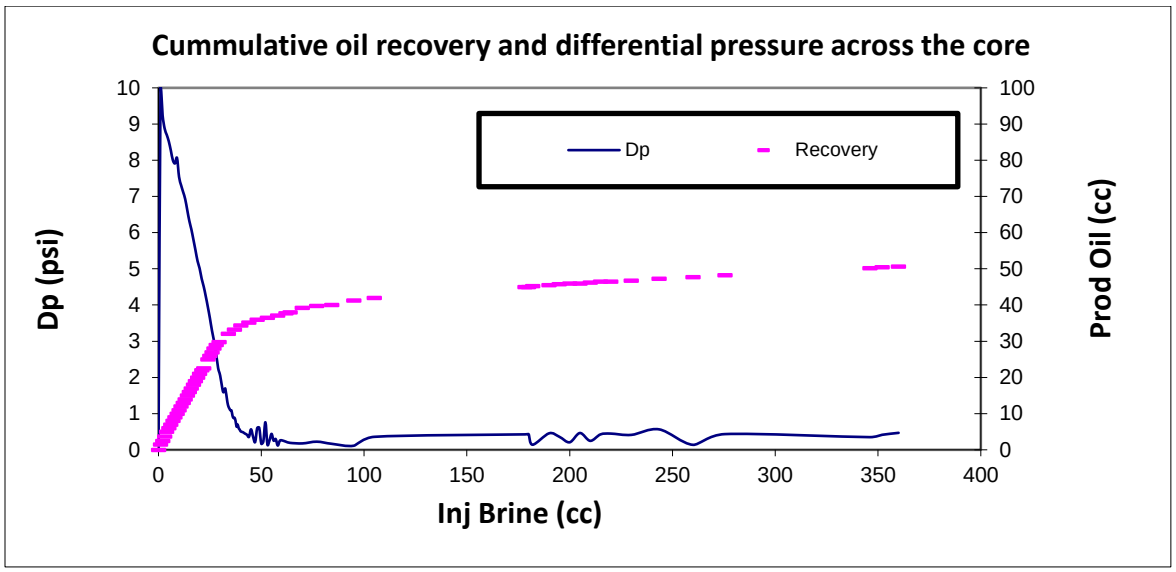

Figure 4.2: A plot of Cumulative Oil Recovery and Differential Pressure across the core vs cumulative Brine injected in the Water-flood of crude J in a Horizontal Core.

Table 4.2: Recorded Constant Rate Water-flood Results showing Total oil produced, Total Brine Produced, and the Differential Pressure across the Core.

Total Water Injected (cm^3)	**Number of Pore Volume (Q)**	**Time (Hour)**	**Total Brine produced (cm^3)**	**Total Oil Produced (cm^3)**	**Differential Pressure (psi)**
0	0.00	0.00	0.00	0.00	0.00
1	0.01	0.14		1.50	9.96
2	0.01	0.29	0.00	2.50	9.24
5	0.03	0.71	0.00	6.00	8.52
6	0.04	0.86	0.00	7.00	8.27
70	0.43	10.00	32.15	39.25	0.47

77	0.47	11.00	38.90	39.75	0.44
84	0.52	12.04	46.15	40.00	0.44
230	1.41	32.86	186.15	46.75	0.41
243.5	1.49	34.79	199.15	47.25	0.57
346	2.12	49.43	299.65	50.25	0.35
352	2.16	50.29	305.65	50.50	0.42
360	2.21	51.43	313.50	50.65	0.47

The presentation of the equations used in this section is presented below:

From equation 4.36

$$Q = \frac{1}{\frac{df_w}{dS_w}\Big|_{S_w}} \tag{4.49}$$

From equation 4.21

$$f_o = \frac{\frac{\mu_w}{k_{rw}}.\frac{k_{ro}}{\mu_o}}{1+\frac{\mu_w}{k_{rw}}.\frac{k_{ro}}{\mu_o}} \tag{4.50}$$

$$\frac{f_w}{f_o} = \frac{\mu_o}{k_{ro}}.\frac{k_{rw}}{\mu_w} \tag{4.51}$$

From equation 4.47

$$S_{wavg} = S_{w2} + Qf_{o2} \tag{4.52}$$

$$f_{o2} = \frac{dS_{wavg}}{dQ} \tag{4.53}$$

$$u_o = -\frac{Kk_{ro}}{\mu_o}\frac{\delta P}{\delta x} \tag{4.54}$$

$$f_{o2}u = -\frac{Kk_{ro}}{\mu_o}\frac{\delta P}{\delta x} \tag{4.55}$$

From 4.55

$$\frac{\delta P}{\delta x} = -\frac{u\mu_o}{K}\frac{f_{o2}}{k_{ro}} \tag{4.56}$$

The pressure drop across the system of length L may be expressed in form of the integral of $\frac{\delta P}{\delta x}$ as:

$$\Delta P = -\int_0^L \frac{\delta P}{\delta x}\, dx \tag{4.57}$$

Substituting for $\frac{\delta P}{\delta x}$ by equation 4.56:

$$\Delta P = \frac{u\mu_o}{K}\int_0^L \frac{f_{o2}}{k_{ro}}\, dx \tag{4.58}$$

If the volumetric rate of injection is constant, equation 4.34 can be rewritten as

$$X_{S_w} = \frac{\Delta t q_t}{A\phi}\frac{df_w}{dS_w} \tag{4.59}$$

Or, where $\frac{df_w}{dS_w} = f_w{}'$

$$X_{S_w} = \frac{\Delta t q_t}{A\phi} f_w{}' \tag{4.60}$$

At a particular instant, A, according to equation 4.60, the various distances that have been moved along the length of the core can be compared and expressed:

$$\frac{X_{S_w}}{L} = \frac{f_w{}'}{f_{w2}{}'} \tag{4.61}$$

Thus,

$$dx = \frac{L df_w{}'}{f_{w2}{}'} \tag{4.62}$$

Substituting for dx in equation 4.58 gives:

$$\int_0^{f_{w2}{}'} \frac{f_o}{k_{ro}}\, df_w{}' = \frac{\Delta P K f_{w2}{}'}{Lu\mu_o} = f_{w2}{}' \frac{u_s/\Delta P_s}{u/\Delta P} = \frac{f_{w2}{}'}{I_r} \tag{4.63}$$

The symbol $I_{r,}$ is the relative injectivity of the core, describing how the injectivity into the core changes with cumulative injection. It is the ratio of injctivity index , $u/\Delta P$ at any time during the flood, to the injectivity index at the initiation of the flood (when only oil is flowing in the core).

Differentiating equation 4.63 with respect to f_w, gives

$$\frac{f_o}{k_{ro}} = \frac{d(\frac{f_{w2}{}'}{I_r})}{df_{w2}{}'} \tag{4.64}$$

From equation 4.49, $f_{w2}{}'$ is equal to the reciprocal of the cumulative volume injection, Q, thus:

$$\frac{f_o}{k_{ro}} = \frac{d(\frac{1}{QI_r})}{d(\frac{1}{Q})} \tag{4.65}$$

$$S_{w2} = S_{wavg} - Q\, f_{o2} \tag{4.66}$$

Equation 4.47 can be combined with 4.65 to evaluate the oil relative permeability at the outlet face saturation S_{w2}. This was used to evaluate the oil relative permeability from the water flood experiment of heavy oil crude J whose result is presented in figure 4.2. The estimated oil relative permeability is shown in figure 4.3.

And the equivalent water relative permeability at the outlet face for the same water flood experiment of heavy oil crude J is evaluated from equation 4.51. The estimated oil relative permeability is shown in figure 4.4. Table 4.3 shows the tabular presentation of the estimation of oil/water relative permeabilities from JBN method.

Table 4.3: Estimated Values for Oil/Water Relative Permeabilities from JBN method.

Q	$1/Q$	S_{av}	S_{w2}	I_r	f_{02}	f_{w2}	k_{ro}	k_{rw}
0.000		0.130	0.130	0.000				
0.006	163.020	0.141	0.130	1.000				
0.012	81.510	0.148	0.136	0.928	1.000	0.000	0.893	0.0000
0.031	32.604	0.174	0.143	0.856	1.000	0.000	0.893	0.0000
0.037	27.170	0.181	0.144	0.831	1.000	0.000	0.893	0.0000
0.429	2.329	0.415	0.326	0.047	0.208	0.792	0.186	0.0012
0.472	2.117	0.419	0.385	0.044	0.071	0.929	0.064	0.0014

0.517	1.934	0.421	0.403	0.044	0.034	0.966	0.031	0.0014
1.411	0.709	0.470	0.435	0.041	0.025	0.975	0.022	0.0015
1.494	0.669	0.474	0.419	0.057	0.037	0.963	0.033	0.0014
2.122	0.471	0.495	0.435	0.035	0.028	0.972	0.025	0.0014
2.159	0.463	0.497	0.407	0.042	0.042	0.958	0.037	0.0014
2.208	0.453	0.498	0.457	0.047	0.019	0.981	0.017	0.0015

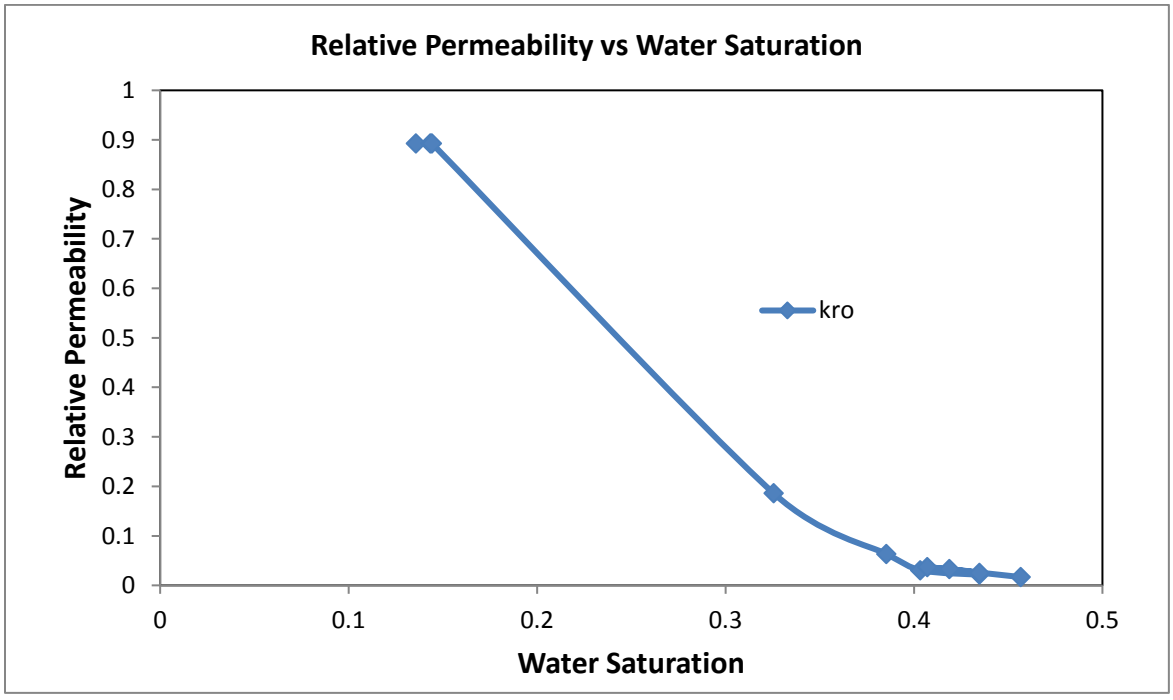

Figure 4.3: Oil Relative Permeability Curve estimated with the JBN method on the Results of Water-flood of crude J in a Horizontal Core.

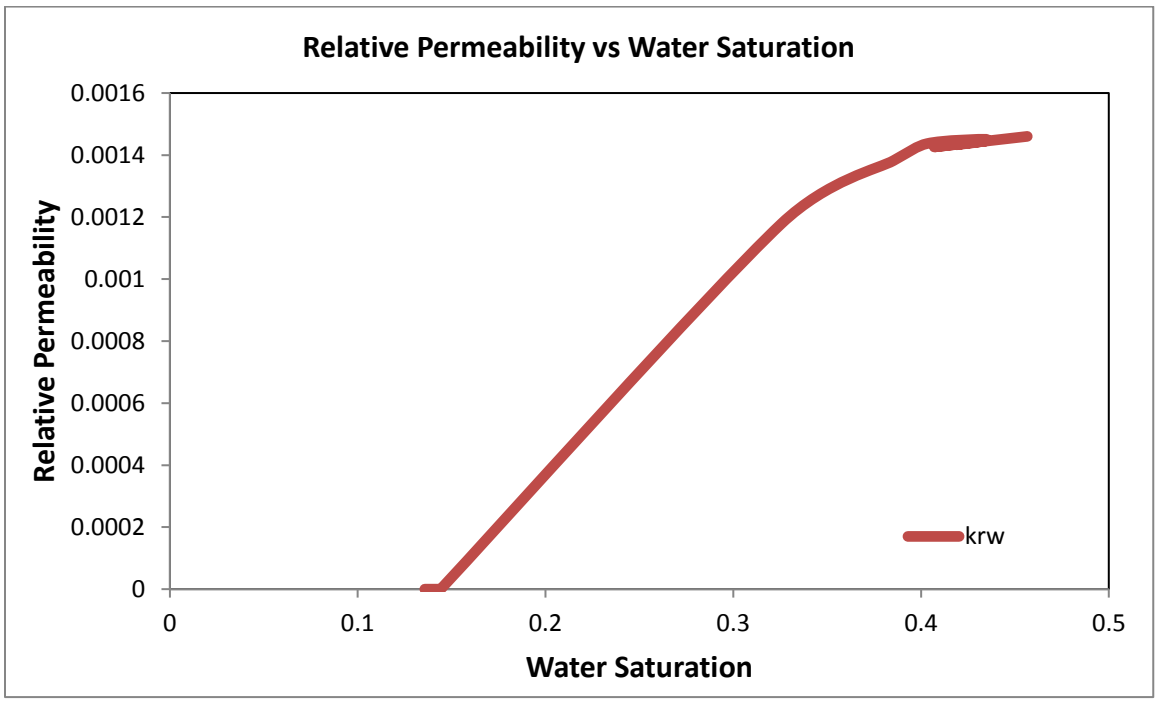

Figure 4.4: Water Relative Permeability Curve estimated with the JBN method on the Results of Water-flood of crude J in a Horizontal Core.

4.4 Graphical Techniques for Determining Relative Permeability from Displacement Experiments

Though the JBN method and the Welge equation have been used for years to estimate analytically the relative permeability curves from a core-flood displacement test, the evaluation of derivatives often introduces errors to the process. Jones and Roszelle (1978) used a graphical technique that is easier to use, less prone to errors, and is very suitable for constant rate displacements.

From equation 4.21, when gravity and capillary pressure are ignored, the water/oil relative permeabilities respectively are:

$$k_{rw} = \frac{\mu_w f_w}{\lambda_2} \tag{4.67}$$

$$k_{ro} = \frac{\mu_o f_o}{\lambda_2} \tag{4.68}$$

Where fw and fo, the fractional flow of water and oil respectively must be expressed as functions of saturation; and λ, the effective viscosity, must also be expressed as a function of saturation. Since these values must be point values (not average values), their values are

determined at the outlet end of the core because the fractional flow of oil and water at this end is the produced oil fraction and the water cut respectively.

Table 4.2 presents the injected water volume, converted to pore volume, Q. And by using equation 4.39b, and the starting water saturation, S_{wc} the average water saturation, $S_{wavg,}$ is calculated as a function of Q. Table 4.3 presents the calculated the average water saturation, $S_{wavg,}$ the pore volume, Q. The Welge equation shows that the water saturation at the outlet end, S_{w2}, is can be related to the average water saturation, $S_{wavg,}$ as shown below:

$$S_{w2} = S_{wavg} - Q \frac{dS_{wavg}}{dQ} \tag{4.69}$$

Thus the water saturation at the outlet end S_{w2}, is the intercept of a line tangent to the curve at any pore volume, Q. Figure 4.5 is a plot of the average water saturation, $S_{wavg,}$ against the number of injected pore volume, Q, hence S_{w2} at different Q can be estimated from the plot. Figure 4.6 shows the plot of water saturation at outlet end of the core against the number of injected pore volume, Q.

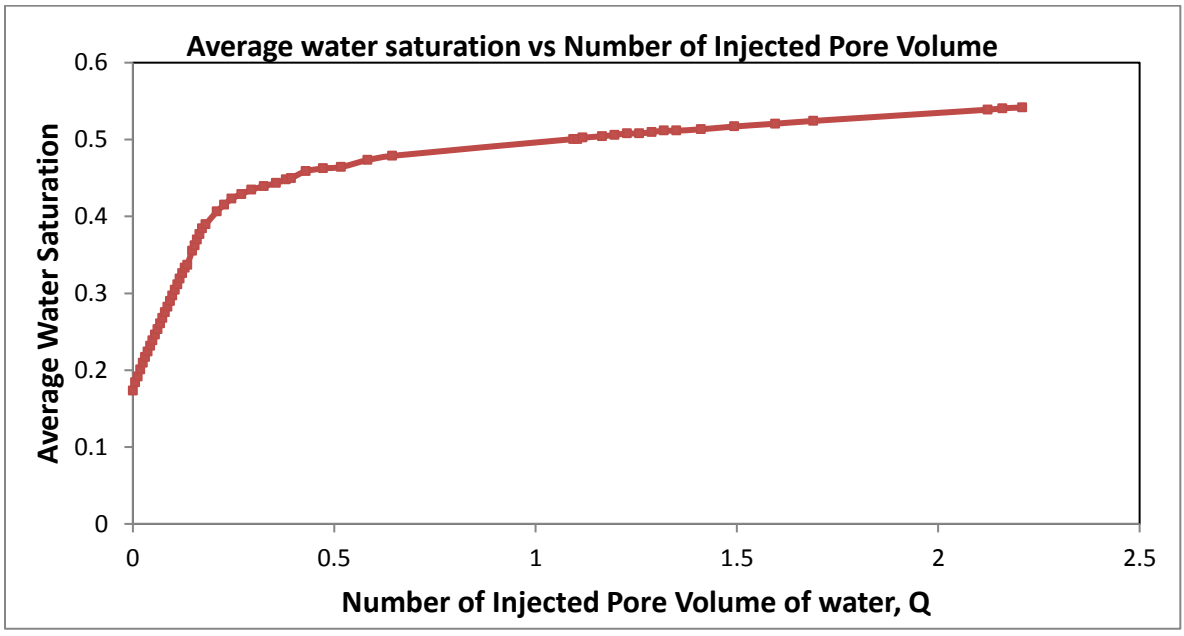

Figure 4.5: The Average Water Saturation Plot used in Constructing Point Saturation.

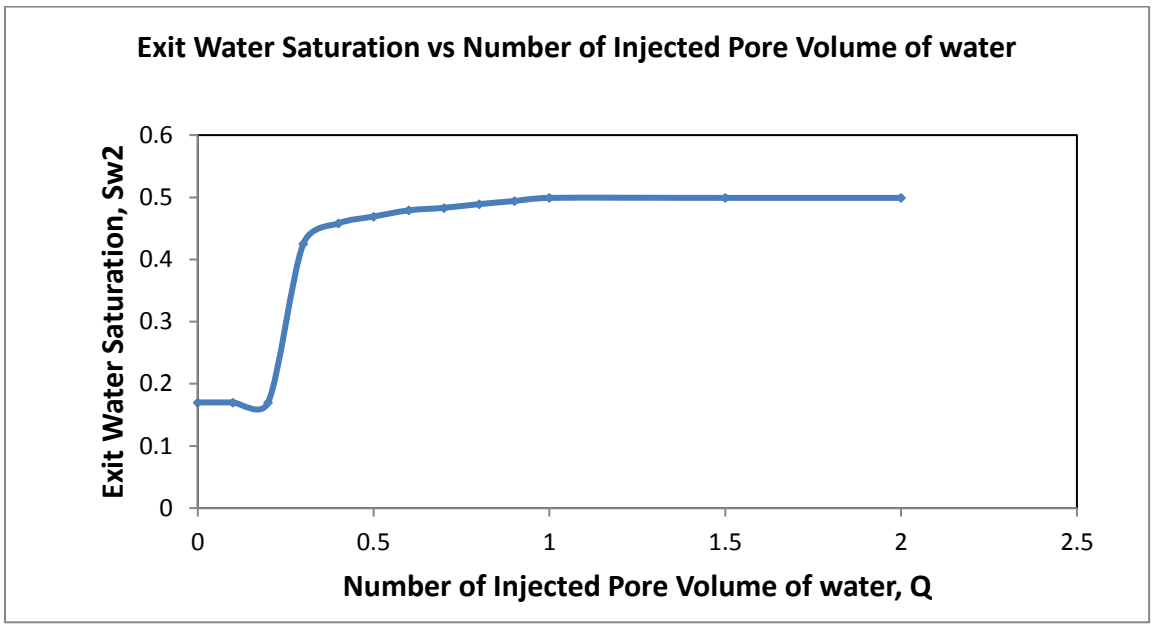

Figure 4.6: The Plot of water saturation at outlet end of the core.

Equation 4.48 shows that the fractional flow of oil, f_{o2} is the same as the slope of the tangent line in figure 4.5 at any number of injected pore volume, Q; thus it is calculated as follows:

$$f_{o2} = (S_{wavg} - S_{w2})/Q \tag{4.70}$$

And the fractional flow of water, f_{w2} is calculated thus:

$$f_{w2} = 1 - f_{o2} \tag{4.71}$$

An advantage of the graphical method over other methods is that it could be used to extrapolate $(1 - S_{or})$ from a plot of average saturation; S_{wavg} against the reciprocal of number of pore volume injected$\left(\frac{1}{Q}\right)$. Figure 4.9 shows how this plot is used to extrapolate to $(1 - S_{or})$ at infinite throughput$\left(\frac{1}{Q} = 0\right)$.

With reference to equation 4.67 and 4.68, the effective viscosity (as a function of saturation) at the outlet end, λ, must be determined to calculate the relative permeability curves. First, the average effective viscosity is calculated by dividing the $\frac{dP}{q}$ measured during the water

flood by the $(\frac{dP}{q})_w$ measured in the single phase flow used to find the absolute permeability of the core. i.e.:

$$\lambda = \mu_w(\frac{dP}{q})/(\frac{dP}{q})_w \tag{4.72}$$

The average effective viscosities for the water-flood used in this study are shown in figure 4.7. And the same method of extending the tangents (to the average viscosity) to the axis, as was done for the saturation point values, was employed to estimate the effective viscosity at the outlet end. Figure 4.8 shows the calculated effective viscosity at the outlet end of the core.

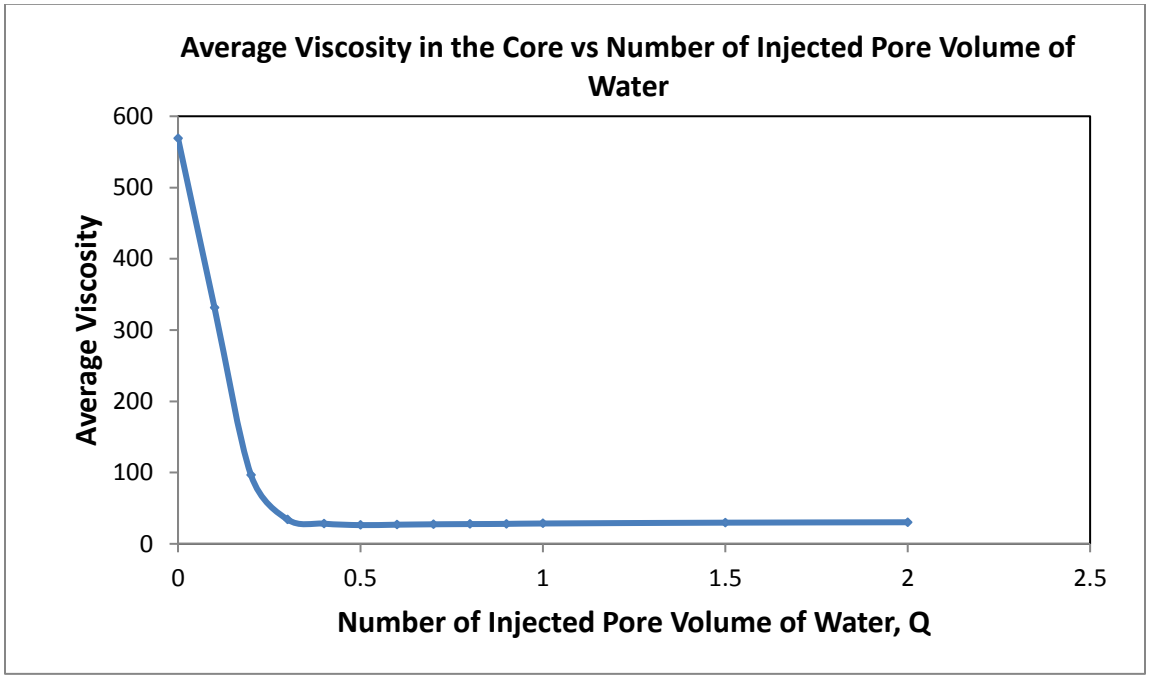

Figure 4.7: The Average Viscosity Plot used in Constructing Outlet End Effective Viscosity.

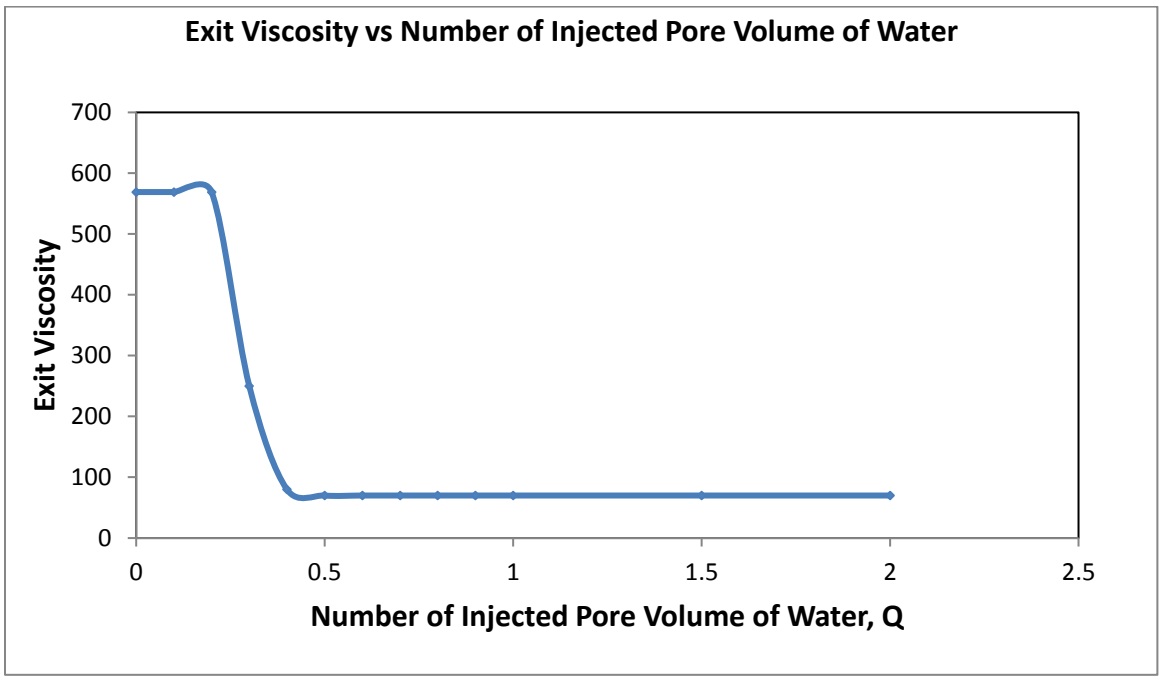

Figure 4.8: The Plot of Effective Viscosity at Outlet End of the Core.

Table 4.4 shows the saturation, effective viscosity, fractional flow of oil and water, and the calculated relative permeability for oil and water. The plot of relative permeability for oil and water from this graphical method is also shown in figure 4.10 and figure 4.11.

Table 4.4: Estimated Values for Oil/Water Relative Permeabilities from the Graphical Method.

Q_i	S_{wavg}	S_{w2}	V_{is_avg}	V_{is2}	f_{02}	f_{w2}	k_{ro}	k_{rw}
0	0.13	0.13	569	569	1.000	0.000	1.000	0.000
0.1	0.2	0.13	331	569	1.000	0.000	1.000	0.000
0.2	0.3	0.13	97	569	1.000	0.000	1.000	0.000
0.3	0.40	0.39	34	250	0.050	0.950	0.100	0.002
0.4	0.42	0.40	28	80	0.005	0.995	0.030	0.005
0.5	0.45	0.43	26	70	0.002	0.998	0.020	0.006
0.6	0.48	0.479	27	70	0.002	0.998	0.010	0.006

0.7	0.484	0.483	27	70	0.001	0.999	0.008	0.0065
0.8	0.49	0.489	28	70	0.001	0.999	0.006	0.007
0.9	0.495	0.494	28	70	0.001	0.999	0.005	0.0075
1	0.50	0.499	29	70	0.001	0.999	0.004	0.008
1.5	0.52	0.499	30	70	0.000	1.000	0.003	0.0085
2	0.535	0.499	30	70	0.000	1.000	0.002	0.009
	0.6	0.6			0.000	1.000	0.000	0.0095

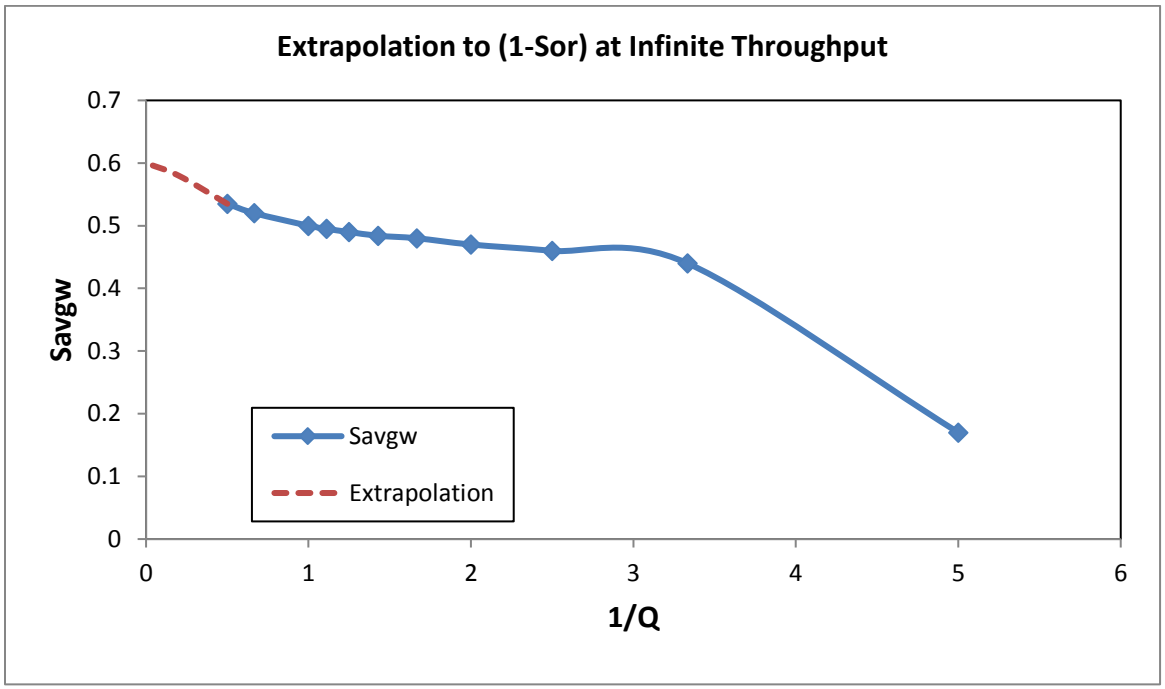

Figure 4.9: The Plot Showing the Estimation of the End Point Saturation S_{or} *by the graphical method.*

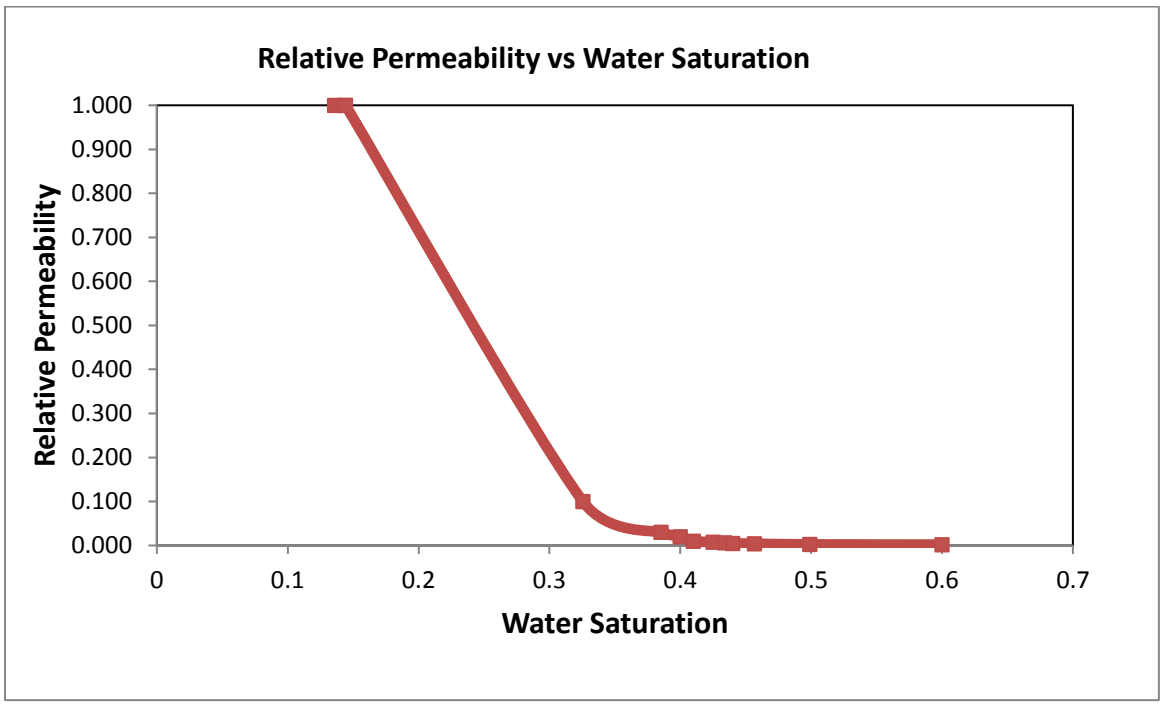

Figure 4.10: Oil Relative Permeability Curve estimated with the Graphical method on the Results of Water-flood of crude J in a Horizontal Core.

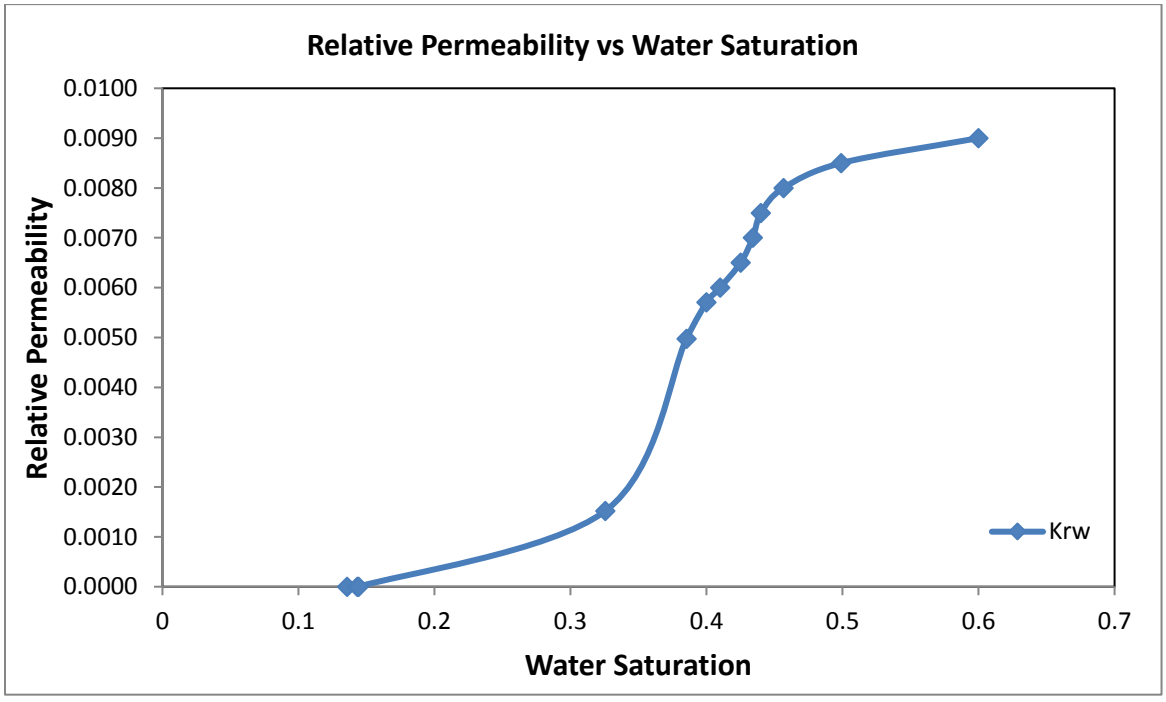

Figure 4.11: Water Relative Permeability Curve estimated with the Graphical method on the Results of Water-flood of crude J in a Horizontal Core.

4.5 Discussion of Results

Table 4.4 shows a list of the average saturations, exit point saturations, average effective viscosities, exit point effective viscosities, the oil and water fractional flow values, and the oil and water relative permeability values. One thing that stands out in the table is that apart from the average saturations, all the aforementioned have the same values for all cases of number of pore volume injected before water breakthrough. This is the reason why it is impossible to obtain relative permeabilities for saturations between breakthrough and initial values.

Figure 4.12 and figure 4.13 show the comparison of the oil relative permeability curves from the JBN, graphical, and the history-matched methods; and the water relative permeability curves from the JBN, graphical, and the history-matched methods, respectively. The oil relative permeability curves from the three methods are close, but this is not the situation for the water relative permeability curves. An explanation for this difference in the values of the water relative permeability from the three methods is that, though capillary pressure in heavy oil recovery system may be less important when compared to its role in conventional oil recovery system, but they should not be completely ignored in the estimation of relative permeability curves. Capillary pressure was used in the estimation of relative permeability from the history-matched method but was not used in the estimation of relative permeability from the JBN and the graphical method.

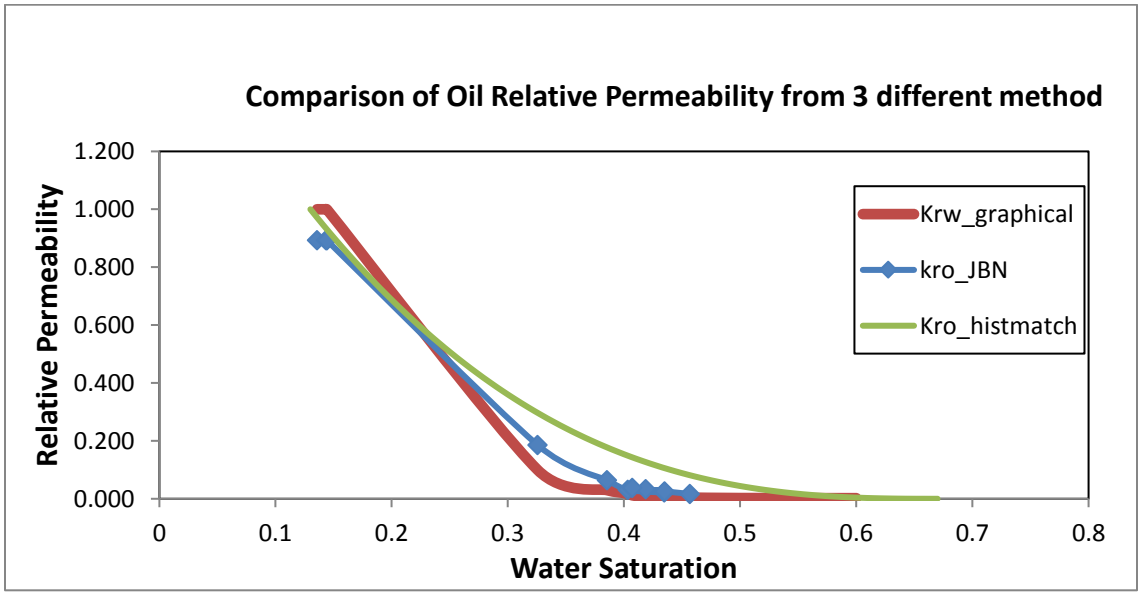

Figure 4.12: Comparison of the Oil Relative Permeability Curves estimated from 3 different Methods: 1. JBN Method 2. The Graphical method and 3. The History-Match Method.

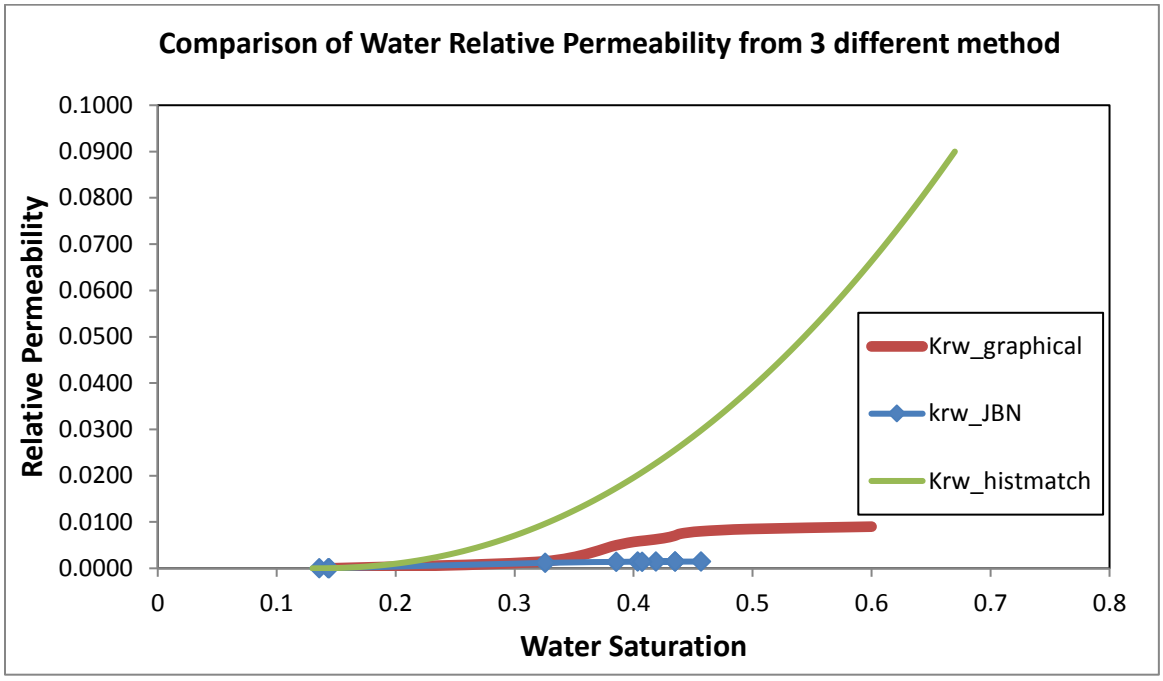

Figure 4.13: Comparison of the Water Relative Permeability Curves estimated from 3 different Methods: 1. JBN Method 2. The Graphical method and 3. The History-Match Method.

4.6 Conclusion

This work on the analytical method of estimation relative permeability may be summarized as follows:

- The JBN method can be easily used for estimating relative permeability for heavy oil but the lack of capillary pressure in the estimation makes the relative permeability from this method less accurate.
- The use of the graphical method makes it easy to estimate the true end-point saturation Sor for the water flood
- The oil relative permeability from the JBN method and the graphical method are similar, but they are both lower than the estimated oil relative permeability from history matching.

- The estimated water relative from the JBN method and the graphical method are lower than the water relative permeability estimated from history matching.

4.7 References

1. Buckley, S.E. and Leverett, M.C., 1942, 'Mechanism of Fluid Displacement in Sands,' Trans., AIME 146, 107-116.
2. Dake, L.P., 1878, 'Fundamental of Reservoir Engineering'Developments in Petroleum Science, 8.
3. Johnson, E.F., Bossler, D. P., and Nauman, V.O, 1959, 'Calculation of Relative Permeability from Displacement Experiments' Trans, AIME 216, 270-372.
4. Jones, S.C., and Roszelle W.O., 1978, 'Graphical Techniques for Determining Relative Permeability from Displacement Experiments' Journal of Petroleum Technology, May.
5. Welge, H.J., 1952, 'Simplified Method for Computing Oil Recovery by Gas or Water Drive'Trans. AIME 195, 91.

Chapter 5: Compositional Simulation of CO_2 –Injection into Heavy Oil

5.1 Introduction

Carbon dioxide injection into heavy oil reservoirs has been found to have a substantial viscosity reduction effect on the oil similar to what is obtainable in the heavy oil thermal recovery processes hence the CO_2 injection processes is a viable alternative to thermal heavy oil recovery (Sayegh et al.,1993). For conventional oil, CO_2 tends to be miscible in the oil thus offering very great recovery potential whereas in a heavy oil system, CO_2 is not miscible with the oil as a result of the presence of heavier components, and the characteristic low reservoir pressure (usually lower than the minimum miscibility pressure) in heavy oil reservoirs. Thus, the recovery of heavy oil using CO_2 injection is through an immiscible displacement process where the main recovery mechanisms are reduction of viscosity and oil swelling (Sayegh et al., 1990).

The suitability of CO_2 injection as an EOR technique in heavy oil production is a result of high solubility of CO_2 in crude oil compared to other gases. Due to the high dissolution, the oil viscosity reduces greatly improving the mobility of the oil towards the producing well and the oil swells and expands out of dead end pores, bringing about significant addition to oil recovery.

A major disadvantage of CO_2 flooding of heavy oil, however, is the presence of viscous fingering in the immiscible displacement process. The viscous fingering is caused by flow instability at the displacement front resulting from a less viscous (and more mobile) fluid displacing a viscous fluid. This makes the recovery process inefficient and suffers from low recovery. However, as will be shown in this thesis, there are injection strategies that can be employed to limit viscous fingering in heavy oil recovery.

The reason why the viscosity reduction reported in a CO_2-saturated heavy oil system is higher than the cases of other gases like Nitrogen or natural gas is that at the same temperature and pressure, CO_2 has the highest dissolution rate (lowest equilibrium ratio) among the gases. At high pressures, CO_2 density has a density close to that of a liquid and is much higher than that of natural gas or Nitrogen, making CO_2 less prone to gravity

segregation and more soluble in oil compared to the other gases. Also at high pressure the viscosity of CO_2 is higher than that of other gases making room for better sweep efficiency and mobility control than with the other gases.

In order to maximise the benefit of CO_2 injection in a heavy oil system, it is important to carry out numerical simulation and phase behaviour studies. The numerical simulation of the CO_2 injection process is performed on a compositional simulator because of the compositional changes in the CO_2-heavy oil process. The simulation is useful for field implementation feasibility investigation, and for process optimisation. The phase behaviours studies are necessary to understand the mechanism of oil displacement by CO_2 and to provide experimental PVT data to fine-tune the phase behaviour (EOS) model used in the compositional modelling.

In this study, a core flood and a PVT experiment were performed with the view of (1) understanding the CO2-heavy displacement mechanism in the reservoir and (2) obtaining data with which to investigate the feasibility of existing commercial simulators to adequately simulate the CO2-heavy oil interaction in the reservoir.

5.2 Phase Behaviour Measurement

All the experimental measurement mentioned here were performed in the HWU laboratory by laboratory staff. The heavy oil used in this study is called crude J with viscosity of 617cp.

CO_2 dissolution and diffusion in heavy oils is usually slow as a result of the high viscosity of heavy oil hence, a major fraction of the oil in the reservoir might be only partially saturated with CO_2 during CO_2 flooding. It is then necessary to measure the phase behaviour of these partial CO_2-saturated oils. In this study, the viscosity of Crude J at different saturation level with CO_2 was measured.

Figure 5.1 presents the measured viscosity data of the partially CO_2-saturated samples of crude "J" at 1500 psig and 28 °C (reservoir conditions of this crude). A substantial viscosity reduction close to 97.5% - from 617 cp to only 15.2 cp – was achieved when crude "J" was fully saturated with CO_2. However, the viscosity reduction was more pronounced at low fractions of CO_2 dissolution. As can be seen in the figure, viscosity of CO_2 saturated oil

dropped to 28.2% and 11.7% of the dead oil viscosity as a result of the partial CO_2 dissolution of only 20% and 40 %.

Table 5.1: Dynamic viscosity of crude "J" at different saturation fraction of CO_2 as measured in the laboratory at a pressure of 1500psi, and a temperature of 28 °C.

CO_2 Content (saturation fraction)	**CO_2 Content (mol %)**	**Viscosity(μ)**	**Viscosity ratio (μcso/ μdo)**
0%	0	617 (cP)	100.0%
20%	22	174 (cP)	28.2%
40%	36	72.1 (cP)	11.7%
70%	50	30.8 (cP)	5%
100%	58	15.2 (cP)	2.5%

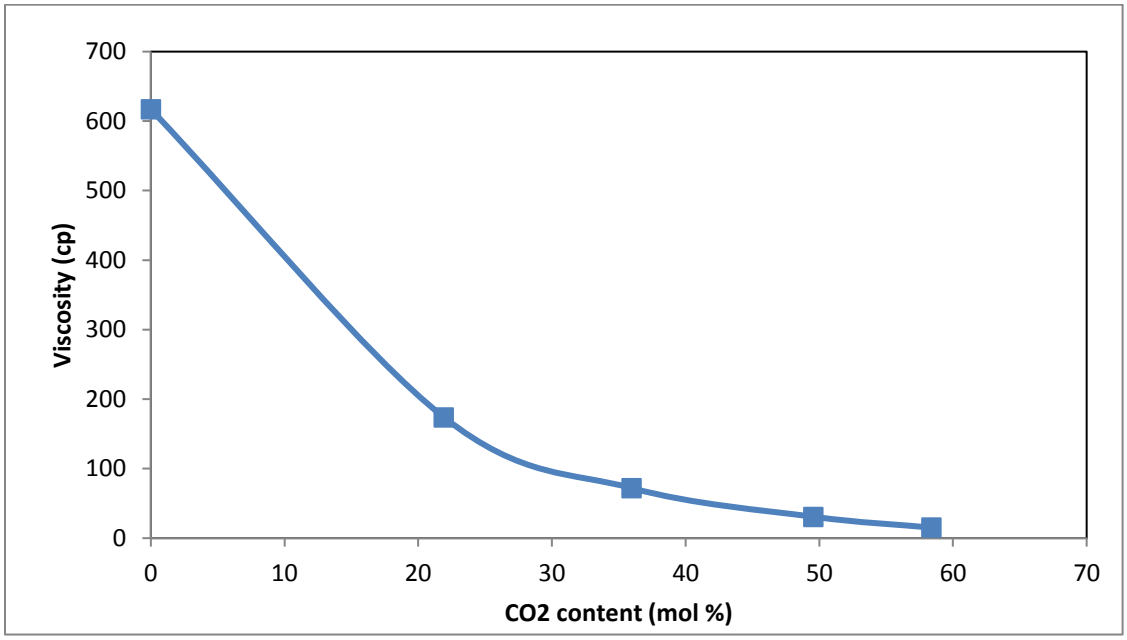

Figure 5.1: Measured Viscosity of crude J at 1500psig and 28 °C at various level of CO_2 Content (CO_2 content at saturation = 82 ccCO_2/ ccOil, T =28 ^{0}C, P=1500 psi)

The measured viscosity data in this study will not be sufficient to adequately tune the Equation of State (EOS) model constructed to characterize the fluid properties and the phase behaviour interaction between CO_2 and the oil. Thus it is necessary to use CO_2-heavy oil

physical properties correlations that have been successfully used in past studies to generate data that will be used in addition to the measured viscosity data to tune the phase behaviour model for this study.

5.2.1 CO_2 Oil Physical Properties Correlation

The saturation pressure, swelling factor, and the density at different CO_2 saturation of the oil can be estimated from existing correlations. The swelling factor and density of the CO_2/heavy oil mixture can be estimated using the Emera and Sarma (2006), Simon and Graue (1965), Mehrotra and Svrcek (1982) and Chung et al (1986). The saturation pressure can be estimated with the Vasquez & Beggs, and the Simon and Graue (1965). And the viscosity of the CO_2/heavy oil mixture can be estimated using the Beggs and Robinson (1975), Mehrotra and Svrcek (1982), the Quail et al (1988), and the Emera and Sarma (2006). The correlations are further discussed below:

1. **Simon and Graue (1965)**

Simon and Graue presented correlations for predicting solubility, swelling, and viscosity behavior of CO_2/crude-oil systems.

Correlations developed from their experimental data are the principal correlations currently used in reservoir engineering presented in a graphical form. The main weakness of the Simon-Graue correlations is that they are not presented in mathematical form therefore, they are not readily implemented in a computer simulator.

2. **Beggs and Robinson (1975)**

This is a correlation used in estimating the viscosity of a CO_2-oil mixture. It neglects the dependence of oil viscosity on composition and pressure. It is presented as follows:

For oil with dissolved gas:

$$\mu = A\,(10^{x} - 1)^{B} \tag{5.1}$$

Where

$$x = 10^{(3.0324 - 0.02023 Yo)}\,(1.8T + 32)^{-1.163} \tag{5.2}$$

$$A = 10.715\,\left(\frac{Sol\,(\frac{m3}{m3})}{5.615} + 100\right)^{-0.515} \tag{5.3}$$

$$B = 5.44 \left(\frac{Sol\ (\frac{m3}{m3})}{5.615} + 150\right)^{-0.33} \quad (5.4)$$

Where

T = temperature, ^{o} F

Y_o=oil gravity, ^{o} API

3. Vaqsquez and Beggs (1980)

$$R_s = C_1 Y_{gs} P^{C2} \exp\{C_3 [Y_o/(T+460)]\} \quad (5.5)$$

Where

R_s = dissolved GOR, SCF/STB

Y_{gs} = gas gravity (air =1)

P= pressure, psia

T = temperature, ^{o} F

Y_o=oil gravity, ^{o} API

And values for the coefficients are given in Table 5.2 follows:

Table 5.2:Vaqsquez and Beggs coefficients

Coefficient	**Yo < 30**	**Yo > 30**
C_1	0.0362	0.0178
C_2	1.0937	1.187
C_3	25.724	23.931

Table 5.3 shows a summary of the measured properties of the CO_2-heavy oil mixture, and Figure 5.2 to figure 5.5 show the comparison of the result of the different correlations in the plot of properties against CO_2 saturation.

Table 5.3: Comparison of correlations and experiment for viscosity, swelling factor, Saturation pressure, and density for CO_2-heavy oil mixture.

Experiment						Beggs and Robinson	Simon & Graue		
CO2 content (saturation fraction %)	GOR (cc/cc)	CO2 content (mol %)	viscosity (cp)	Saturation Pressure (psi)	Swelling Factor	viscosity (cp)	Saturation Pressure (psi)	Swelling Factor	Density (g/cc)
0	0	0	617			617	0	1	0.96
20	16.4	22	174			169	350	1.04	0.952
40	32.8	36	72.1			79	650	1.08	0.945
70	57.4	50	30.8			37	1100	1.15	0.927
100	82	58	15.2	1500	1.2	22	1500	1.2	0.919

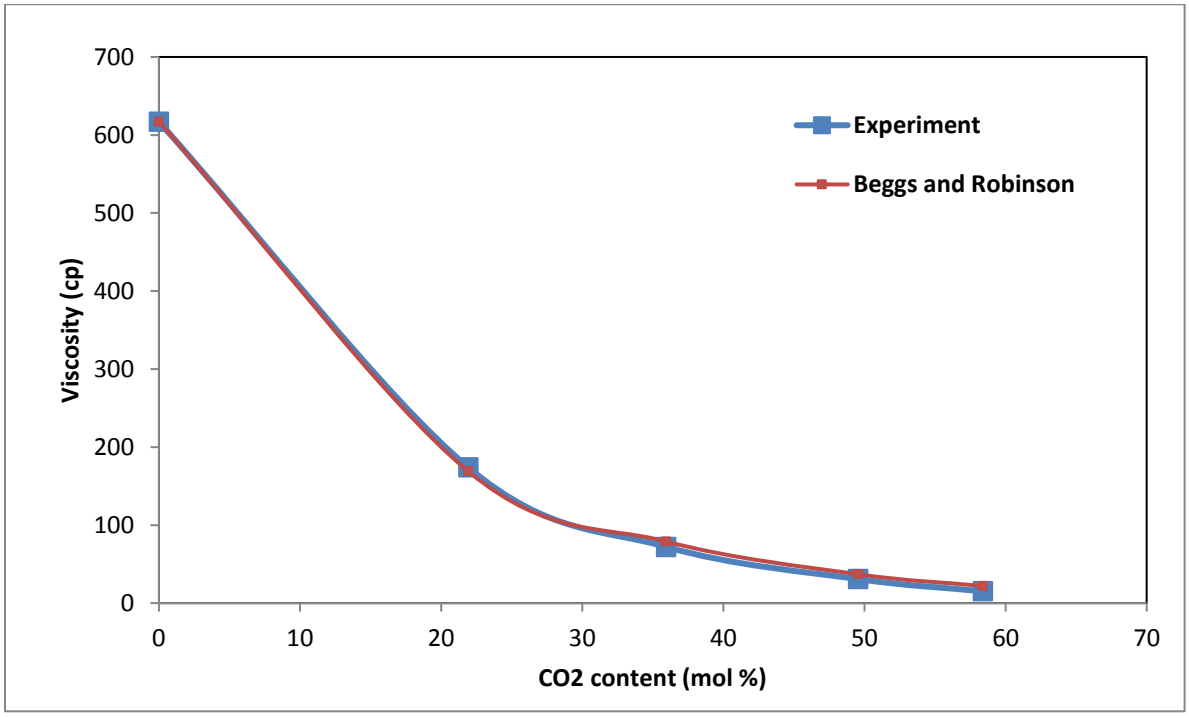

Figure 5.2: Comparison of viscosity of CO_2 saturated oil between the experimental data and Beggs & Robinson correlation (CO_2 content at saturation = 82 ccCO_2/ccOil, T =28 ^{0}C, P=1500 psi)

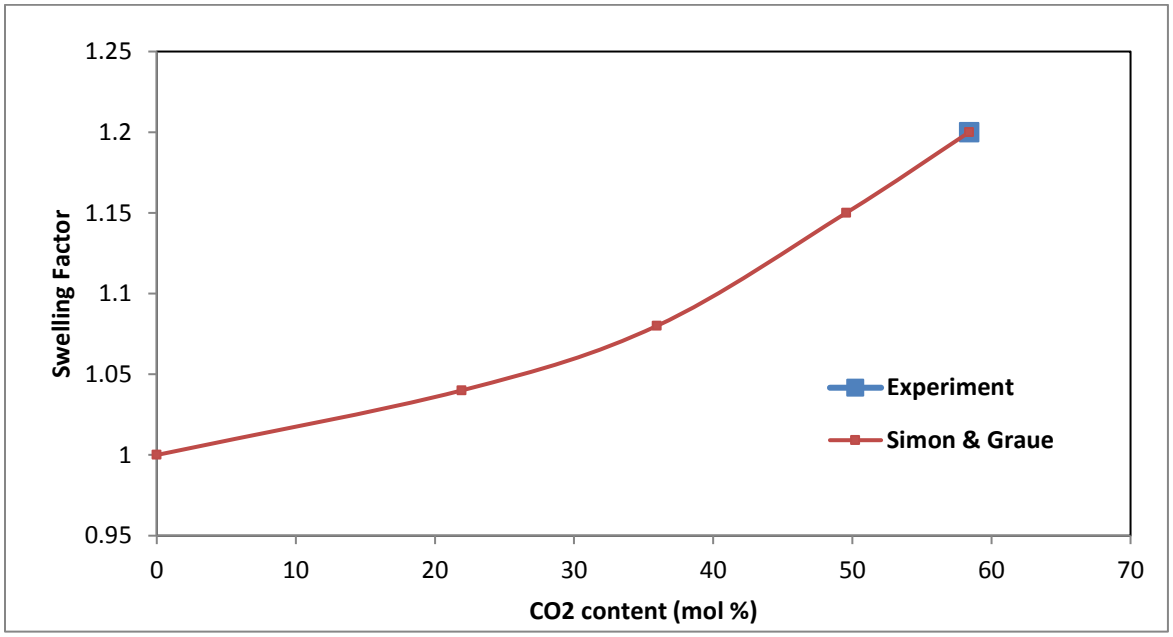

Figure 5.3: Comparison of swelling factor of a CO_2 saturated oil between the experimental data and Simon & Graue and Vasquez & Beggs correlations (CO2 content at saturation = 82 ccCO_2/ccOil, T =28 ^{0}C, P=1500 psi).

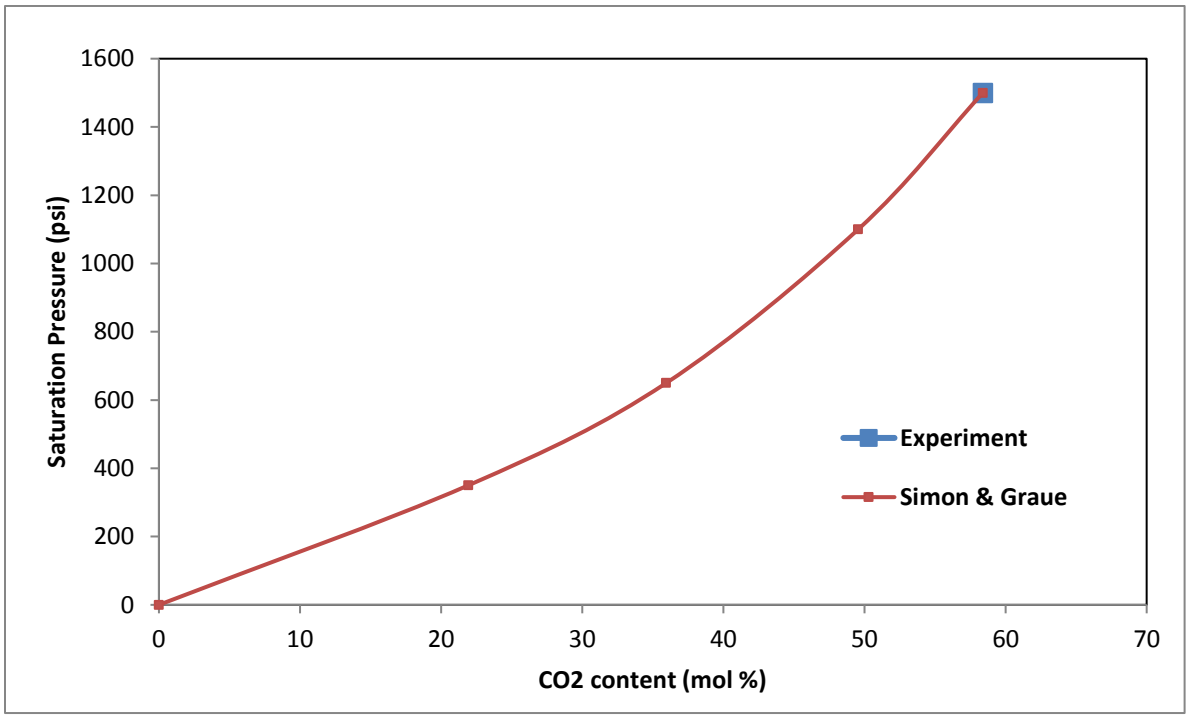

Figure 5.4: Comparison of saturation pressure of a CO_2 saturated oil between the experiment data and Simon & Graue and Vasquez & Beggs correlations (CO_2 content at saturation = 82 ccCO_2/ ccOil, T =28 ^{0}C, P=1500 psi).

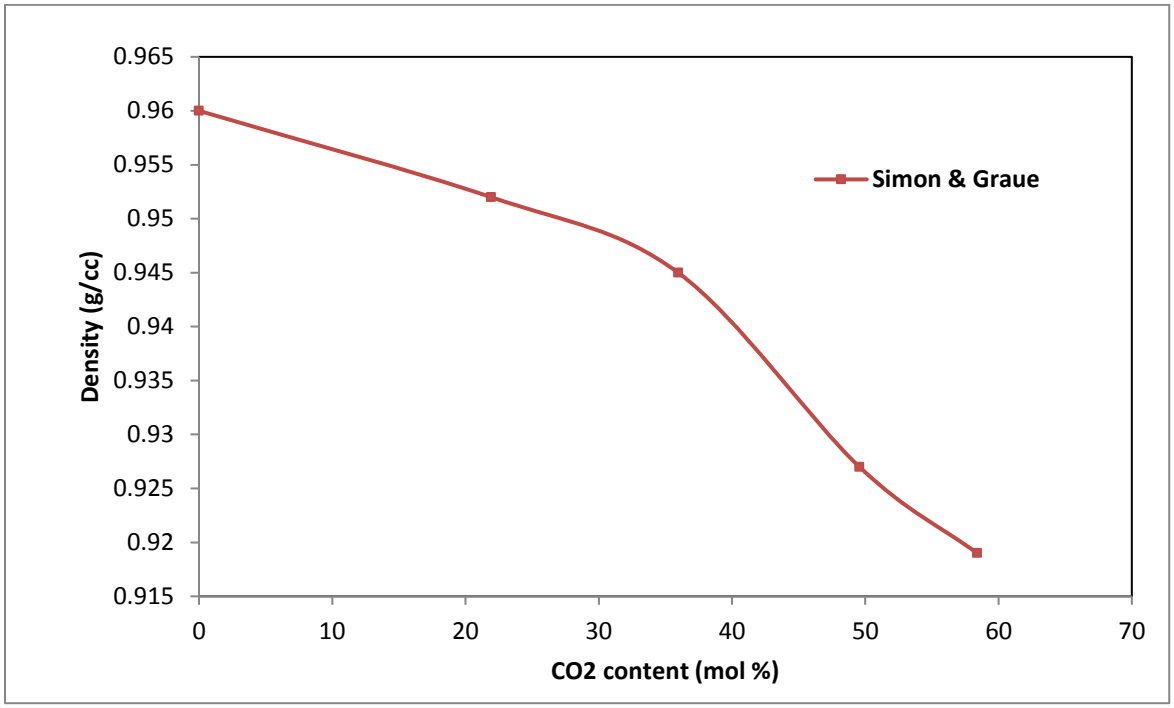

Figure 5.5: The density profile a CO_2 saturated oil using the Simon & Graue correlations (CO_2 content at saturation= 82ccCO_2/ ccOil, T =28 ^{0}C, P=1500 psi).

5.2.2 Compositional Analysis

A compositional analysis of the crude J using Gas Chromatography (GC) technique was performed in HWU laboratory and the result is shown in table 5.4a. The table shows that about 41% (wt %) of the hydrocarbon belongs to the C40+, which implies that there is still a lot room for improving the compositional analysis. The high temperature gas chromatography column, if used, can further analyse the C40+ fraction thus reducing the proportion of the C+ fraction to an acceptable level. The lower this proportion, the more accurate and more representative is the tuned equation of state (EOS), and the compositional numerical simulation of the CO2 injection process.

A comparison of the compositional analysis of crude J (table 5.4a) and crude C (table 5.4b) reveals that while the C1-C20 in crude J is about 27%, it is only about 13.5% in crude C. And while the C26+ in crude J is 62%, it is about 76% in crude C. While this difference is expected between crude J (617 cp) and crude C (8670 cp), it does not completely explain the huge difference in their viscosities.

The high difference in their viscosities can be attributed to the difference in their asphaltene content as earlier shown in Table 3.1. While Crude J has 2.6% asphaltene content (wt%), Crude C has 11.6 % asphaltene content (wt%). This difference in asphaltene content is also responsible for Crude J having a Newtonian flow tendency while crude C has a non-newtonian flow tendency as shown in figure 3.4 and figure 3.5 respectively.

Table 5.4a: Compositional analysis of crude J.

HRM 'Oil-J'

Extended HP-1 Composition
(Whitson's Generalised MWs)

Comp	MWs	Weight%	Mole%
C1	16.04	0.00	0.00
C2	30.07	0.00	0.00
C3	44.1	0.00	0.00
iC4	58.12	0.00	0.00
nC4	58.12	0.00	0.02
iC5	72.15	0.02	0.10
nC5	72.15	0.01	0.06
C6s	84	0.07	0.32
C7s	96	0.14	0.56
C8s	107	0.37	1.29
C9s	121	0.72	2.23
C10s	134	1.12	3.13
C11s	147	1.39	3.54
C12s	161	1.88	4.37
C13s	175	2.23	4.79
C14s	190	2.28	4.51
C15s	206	2.90	5.27
C16s	222	2.92	4.94
C17s	237	2.61	4.13
C18s	251	2.87	4.29
C19s	263	2.68	3.82
C20s	275	2.74	3.73
C21s	291	2.27	2.92
C22s	300	2.36	2.95

HRM 'Oil-J'

Extended HP-1 Composition
(Whitson's Generalised MWs)

Comp	MWs	Weight%	Mole%
C23s	312	2.26	2.72
C24s	324	2.05	2.37
C25s	337	1.98	2.21
C26s	349	2.21	2.37
C27s	360	1.44	1.50
C28s	372	2.12	2.13
C29s	382	1.68	1.64
C30s	394	2.02	1.92
C31s	404	1.37	1.27
C32s	415	1.94	1.75
C33s	426	1.01	0.89
C34s	437	1.42	1.22
C35s	445	1.33	1.12
C36s	456	1.26	1.04
C37s	464	0.84	0.68
C38s	475	1.28	1.01
C39s	484	1.05	0.82
C40+	942.8297	41.16	16.37
NB Overall MW(C40+) ex matching with Cryoscopic measurement.		100	100
		100	100
		MW	375
		MW-calcd	375

Table 5.4b: Compositional analysis of crude C.

Oil 'C'			
Composition (Whitson's Generalised MWs)			
Comp	**MWs**	**Weight%**	**Mole%**
C1	16.04	**0.00**	**0.00**
C2	30.07	**0.00**	**0.00**
C3	44.10	**0.00**	**0.00**
iC4	58.12	**0.00**	**0.00**
nC4	58.12	**0.00**	**0.00**
iC5	72.15	**0.00**	**0.00**
nC5	72.15	**0.00**	**0.00**
C6s	84	**0.01**	**0.09**
C7s	96	**0.02**	**0.09**
C8s	107	**0.09**	**0.46**
C9s	121	**0.12**	**0.52**
C10s	134	**0.23**	**0.94**
C11s	147	**0.40**	**1.48**
C12s	161	**0.68**	**2.30**
C13s	175	**1.01**	**3.13**
C14s	190	**1.14**	**3.24**
C15s	206	**1.46**	**3.85**
C16s	222	**1.66**	**4.06**
C17s	237	**1.54**	**3.53**
C18s	251	**1.81**	**3.90**
C19s	263	**1.79**	**3.68**
C20s	275	**1.85**	**3.64**
C21s	291	**1.80**	**3.35**
C22s	300	**1.67**	**3.02**
C23s	312	**1.79**	**3.11**
C24s	324	**1.71**	**2.86**
C25s	337	**1.63**	**2.62**
C26+	**839**	**77.59**	**50.12**
NB MW measured by Cryette (Hooman) c.17.09.10 MW(C26+)ex matching		100.00	**100.00**
		MW	**542**
		Measd MW	**542**

5.3 Phase Behavior Modelling

PVTi of Eclipse phase behaviour package was used to build the phase behaviour model for the heavy oil. To perform phase equilibrium calculations, the critical pressure (Pc), critical temperature (Tc), acentric factor (ω) for each component and the interaction coefficients between different components (dij) are required. The volume shifts and the molecular weight of each component are also required.

Once the properties of the components representing the fluid model have been estimated, a grouping scheme is performed essentially to speed up the simulation running time. Grouping eases the process of simulation by decreasing the number of material balance calculations that will be performed at each grid block at each time step during compositional simulation. The grouping must however be done in such a way that the fluid properties do not change too much as a result of the grouping.

In this study, all the grouping techniques in PVTi (Mole Fraction, Molecular Weight, and Mixing Rule) were considered but the Mole fraction technique was found most suitable in grouping the 40 components fluid system into a ten pseudo-components fluid system. This was done by comparing the phase envelopes generated after the grouping from the various techniques with the phase envelope of the original 40 components fluid system; and the mole fraction technique generating 10 pseudo-components was found most adequate. Shown in Table 5.5 are the new pseudo components and their estimated component's properties.

The Peng-Robinson (PR) equation of state with volume translation was used in conjunction with the viscosity LBC correlation in this study to match the saturation pressures, swelling factors, and the viscosities of the heavy oil –CO_2 mixtures at different CO_2 saturations in the viscosity experiment. The PR EOS model was tuned by the repeated regression of the pseudo-component properties like critical pressure, critical temperature, binary interaction coefficients, and the adjustment of the LBC viscosity coefficients until the experimental data were reasonably matched.

Figure 5.6 to Figure 5.8 present the experimental data and the simulated data after tuning the EOS parameters.

Table 5:5: New pseudo components of crude J after the grouping exercise.

Mole Fractions for Sample ZI

Row	Components	ZI (percent)	Weight fraction (percent)	Mol Weight	Spec Gravity
1	CO2	0	0	44.01	0.777
2	C1+	0.18004	0.033818	70.592	0.582
3	C6+	2.1704	0.58198	100.77	0.73166
4	C9+	5.3611	1.8344	128.59	0.78002
5	C11+	12.693	5.4838	162.37	0.80758
6	C14+	14.703	8.0778	206.47	0.83703
7	C18+	12.232	8.1378	250.01	0.85603
8	C21+	9.6019	7.3862	289.09	0.87262
9	C24+	7.2915	6.4107	330.41	0.88667
10	FR1	17.884	20.683	434.64	0.9
11	FR2	17.884	41.37	869.36	0.93976
12					
13					
14					
15					

Mole fraction total 100 percent

Enter weight fractions

OK Apply Cancel Help

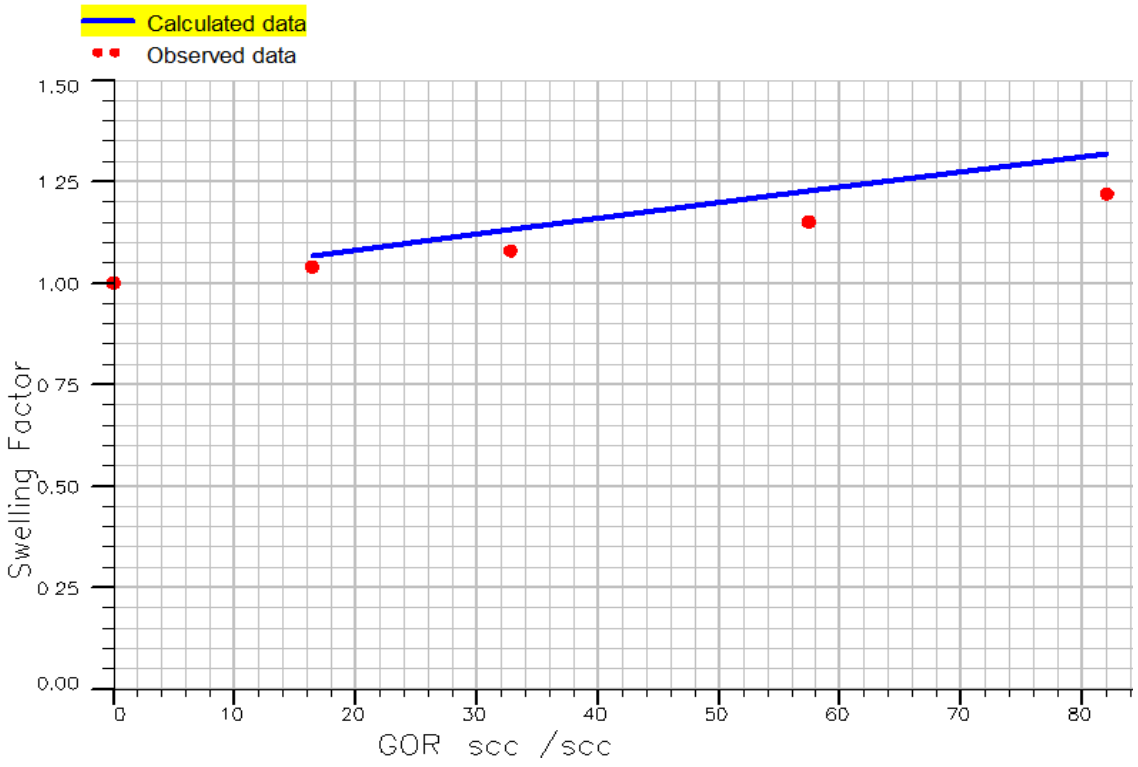

Figure 5.6: Comparison of the effect of CO_2 solubility on swelling factor at 28oC in the tuned EOS model and experiment.

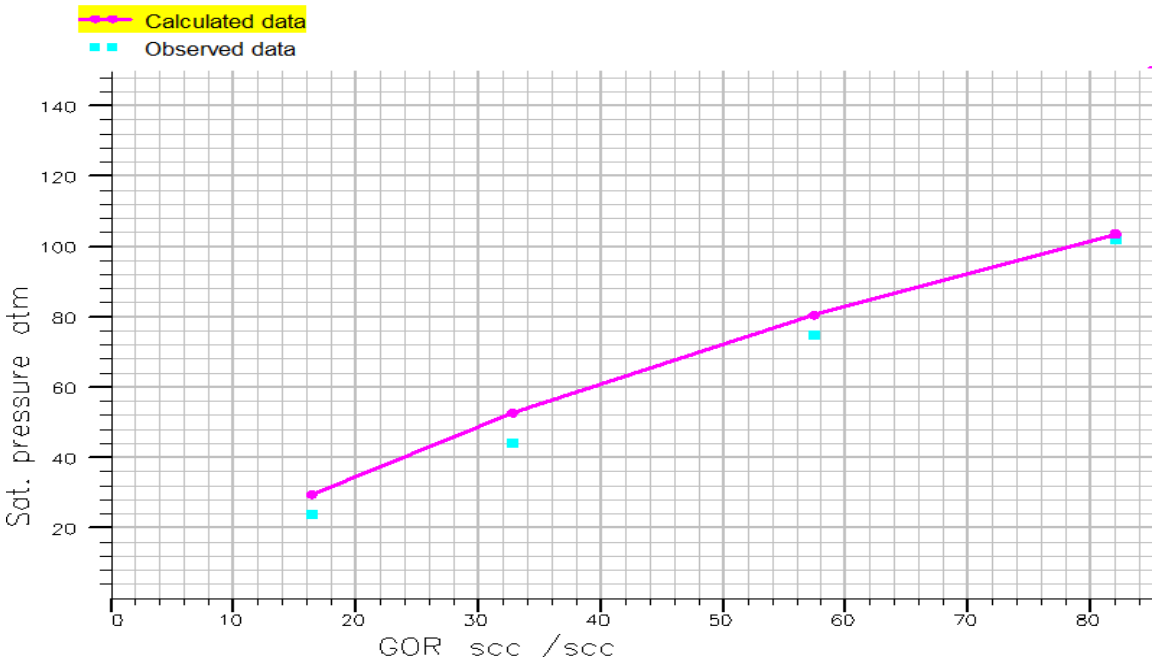

Figure 5.7: Comparison of the effect of CO_2 solubility on saturation pressure in the tuned EOS model and experiment.

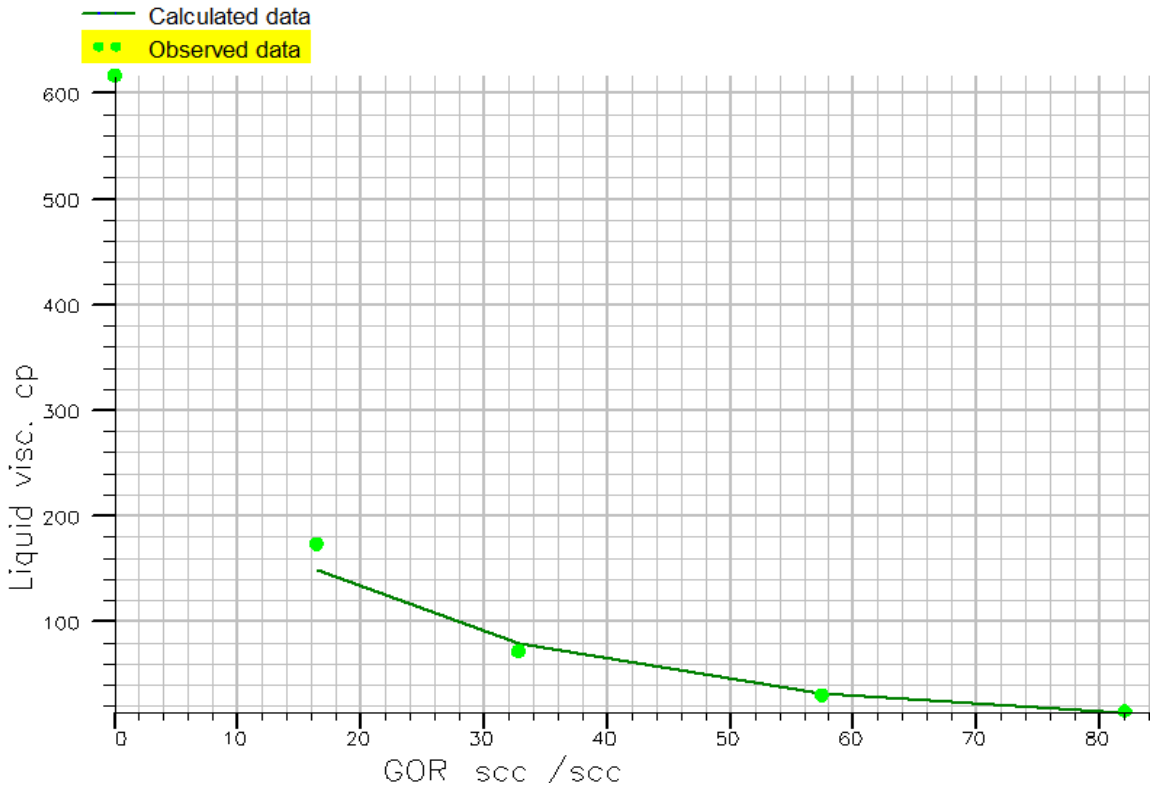

Figure 5.8: Comparison of the effect of CO_2 solubility on oil-CO_2 mixture viscosity in the tuned EOS model and experiment.

5.4 Gas Diffusion Coefficient Estimation

The point has already been made that when CO_2 is injected into a heavy oil reservoir, the miscibility pressure of the heavy oil is usually higher than their reservoir pressure as a result of their high molecular weight. Hence CO_2 enhances heavy oil recovery only by immiscible drive through swelling of oil and the reduction of its viscosity and that as much as twenty percent swelling and two order of magnitude reduction in viscosity reduction can be achieved in some heavy oils. It has also been earlier mentioned in this work that channels (or fingers) are created as a result of unfavourable mobility ratio that is typical in heavy oil reservoirs hence the success of the injection process relies on the diffusion of gas in the channels into oil in the matrix.

The four factors that contribute to mass transfer in a CO_2 heavy oil process are pressure, gravity, diffusion, and capillary drive. The pressure or displacement factor is dominant and important when there is a differential pressure across the path of flow. However, this factor loses its dominance and importance when differential pressure is almost zero due to the formation of fingers in CO_2 heavy oil displacement processes. The importance of the effect of gravity on oil recovery also cannot be overemphasized especially in reservoirs with very a high oil column. If the bypassed fluid and the displacing fluids are first contact miscible (FCM), there is no capillary cross-flow hence capillary forces become unimportant, but when the fluids are multi-contact miscible (MCM) or immiscible, there would be capillary-driven cross-flow and hence capillary forces begin to play important role in the recovery process. The roles that pressure, gravity, and capillary forces play in oil recovery have been well studied and documented, hence the need to study the role that diffusion plays in the mass transfer between the finger and the un-swept zone.

Gas diffusivity is an important parameter in determining the rate of dissolution of the injection gas in oil and hence the recovery rate in a secondary or tertiary recovery project. Accurate estimation of this parameter is required for reservoir simulation and prediction of oil recovery. Simplified analytical solutions obtained under special conditions can be used to estimate the diffusion coefficient. There are also existing models used in estimating gas diffusivity coefficients, however the accuracies of available models are limited by their inherent simplifying assumptions. Alternatively, the coefficient of diffusion of gas into oil

can be inferred indirectly by matching the prediction of a suitable mathematical model involving gas diffusion processes with the experimental data.

Zhang et al (2000) have determined the diffusion coefficient of gas into heavy oil using a transient state diffusion model. This is a laboratory measurement of gas diffusivity done through the measurement of the gas pressure in contact with the liquid. Their interpretation is based on the measurement of the gas-pressure decline during the dissolution of gas in oil.

5.4.1 Developing the diffusion model based on the Zhang approach

The objective of this section of the work is to use the Zhang approach to develop a mathematical model which describes the dynamic process of CO_2 diffusion into heavy oil at the pore level. As mentioned earlier, when a gas is injected into a core saturated with heavy oil, a finger is created where the gas preferentially flows through. (This is evident in the drastic drop of differential pressure often seen in all CO2/heavy oil core-flood experiments.) As the gas flows through the finger, a direct contact between the gas and the heavy oil happens at the interface, and the gas subsequently gradually dissolved in the oil bringing about oil viscosity reduction and swelling of the oil.

A schematic diagram of the CO_2 heavy oil system is shown in Figure 5.9 where the CO_2-heavy oil interface is at B_1 (x=0.) The end of the core plug is at B_2 (x=L); L would equal to the diameter of the core plug if we assume the width of the finger is negligible.

The dissolution of gas into heavy oil is modelled by assuming that during the diffusion phase, the difference between the inlet and outlet pressure is strictly due to the diffusion of CO_2 into the un-swept zone. Since the CO_2 system is a single component system, the mass density is given by:

$$\rho_g = \frac{M_g P}{ZRT} \tag{5.6}$$

Where M_g is the molecular weight, P and T are the pressure and temperature of the gas respectively. Z is the real gas deviation factor, and R is the universal gas constant.

The volume V and mass m of the gas is given thus:

$$V = A*H \tag{5.7}$$

$$m = \rho_g V \tag{5.8}$$

Where A denotes cross-sectional area of the core, and H denotes the thickness of the gas column. The cumulative mass of dissolved gas in the liquid phase per unit cross-sectional area, Q, is thus given as:

$$Q = \frac{M_g H}{RT}\left(\frac{P_0}{z_0} - \frac{P}{z}\right) \tag{5.9}$$

According to Civan (2001), an alternative expression for Q is:

$$Q(t) = \int_0^L [C(x,t) - C_0]\, dx \tag{5.10}$$

Where C is the dissolved gas concentration in the oil, [kgmole m^{-3}], and L is the length of the liquid column (in the direction of diffused gas).

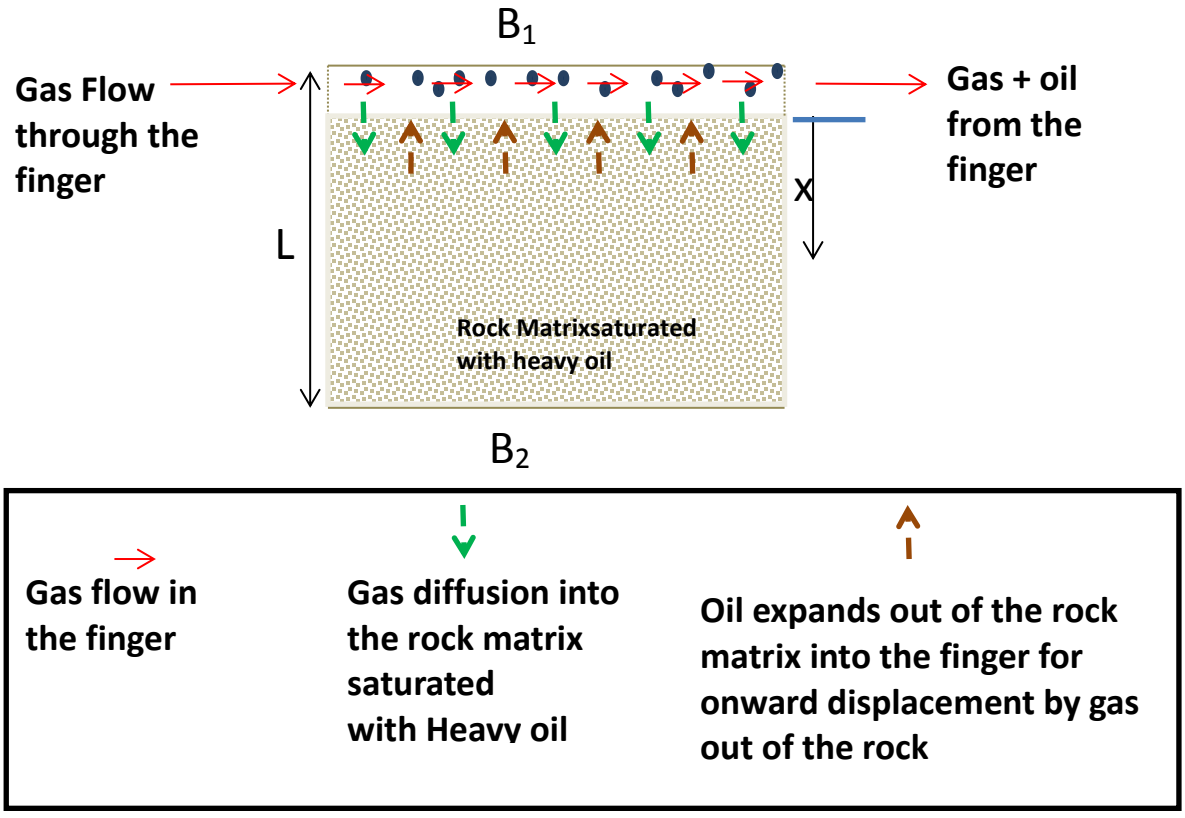

Figure 5.9: 1-dimensional Schematic of a core plug with a finger showing CO_2 diffusivity into heavy oil.

When a solute moves from a region of high concentration to a region of low concentration, diffusion is said to have happened, and the law that describes the process is Fick's law:

$$J = -D\frac{\partial C}{\partial x} \tag{5.12}$$

Where J is, the diffusion flux, [kgmole m^{-2} s^{-1}], is the mass (or mole) of the solute diffusing through unit area per unit time; and D is the diffusion coefficient or diffusivity in [m^2s^{-1}].

By using the Fick's law and the continuity equation, the molecular diffusion process for a one-dimensional system can be represented by:

$$(\frac{\partial C}{\partial t})_{CO2} = (\frac{\partial J}{\partial x})_{CO2} = -\frac{\partial}{\partial x}(D\frac{\partial C}{\partial x})_{CO2} \tag{5.13}$$

Where t is the time[s], and subscript CO_2 refers to the CO_2 phase.

If the diffusion coefficient is assumed to be constant, then Equation 5.13 becomes:

$$(\frac{\partial C}{\partial t})_{CO2} = -(D\frac{\partial^2 C}{\partial x^2})_{CO2} \tag{5.14}$$

The assumptions are:

1. The capillary pressure at the interface is neglected (interface is flat)
2. The heavy oil and CO_2 are at equilibrium conditions at the heavy oil/CO_2 interface

5.4.2 Boundary and Initial Conditions

At the initial condition, the heavy oil was dead oil; that means the initial CO_2 concentration in oil is zero hence

$$\text{At } t=0,\quad C(x)=0, \text{ and } \frac{\partial C}{\partial x}=0,\quad 0 \leq x \leq L \tag{5.15}$$

The boundary conditions are:

1. At the B_2 boundary of the oil domain, it is a no flow boundary without any diffusion.

$$\text{At } x=L,\quad \frac{\partial C}{\partial x}=0,\quad t>0 \tag{5.16}$$

2. Concentration of CO_2 at the CO_2/heavy oil boundary is known; and the concentration of CO_2 in heavy oil is obtained from solubility data.

$$\text{At } x=0, D\frac{\partial C}{\partial x} = k(C_{sat} - C)\quad t>0 \tag{5.17}$$

Equation 5.17 is the gas/liquid interface hindered gas mass-transfer boundary condition where k is the film mass-transfer coefficient at the gas/liquid interface. The symbol C_{sat}represents the saturation (or equilibrium) gas concentration of the oil phase.

As the value of k becomes very large, i.e. k→∞, then Equation 5.17 simplifies to the case for surface Dirichlet-type boundary condition:

At x=0, $C = C_{sat}$,t>0 (5.18)

The Equation 5.13 to 5.18 can be made dimensionless if the dimensionless form of concentration, distance, and time shown below are introduced:

$$C_D = \frac{C}{C_{sat}} \tag{5.19}$$

$$X_D = \frac{x}{L} \tag{5.20}$$

$$t_D = \frac{Dt}{L^2} \tag{5.21}$$

Hence Equation 5.13 to 5.18 can be transformed into the following dimensionless form:

$$\frac{\partial C_D}{\partial t_D} = \frac{\partial^2 C_D}{\partial {x_D}^2}, 0 \leq x_D \leq 1, t_D > 0 \tag{5.22}$$

$$C_D = 0, \ 0 \leq x_D \leq 1, t_D = 0 \tag{5.23}$$

$$\frac{\partial C_D}{\partial t_D} = -k_D(1 - C_D), \ x_D = 0 \ , t_D > 0 \tag{5.24}$$

$$C_D = 0, \ x_D \to \infty, \ t_D > 0 \tag{5.25}$$

Or

$$\frac{\partial C_D}{\partial x_D} = 0, \ x_D = 1 \ , t_D > 0 \tag{5.26}$$

Where k_D, given as

$$k_D = kL/D \tag{5.27}$$

And it is referred to as the mass transfer Biot number because of its analogy with heat transfer problems.

The mass accumulation function Q(t) can also be expressed as a non-dimensional variable:

$$Q(t) = L(C_{sat} - C_o)Q_D(t_D) \tag{5.28}$$

Where $Q_D(t_D) = \int_0^1 C(x_D, t_D)\, dx_D$ (5.29)

Hence

$$Q_D(t_D) = \frac{M_g H}{RTL(C_{sat} - C_o)}\left(\frac{P_0}{z_0} - \frac{P}{z}\right) \tag{5.30}$$

For a reference pressure, P_r, measured at a dimensionless time t_{Dr}, then:

$$Q_D(t_{Dr}) = \frac{M_g H}{RTL(C_{sat} - C_o)}\left(\frac{P_0}{z_0} - \frac{P_r}{z_r}\right) \tag{5.31}$$

Equation 5.30 and 5.31 when combined give:

$$\frac{Q_D(t_D)}{Q_D(t_{Dr})} = \frac{\frac{P_0}{z_0} - \frac{P(t_D)}{z(t_D)}}{\frac{P_0}{z_0} - \frac{P_r}{z_r}} \tag{5.32}$$

If it is assumed that after a long time, saturation (or equilibrium) is reached, then the pressure becomes P_{sat} , $and\ Q_D(t_D)_{sat}$ = 1.0. If we take the $P_r = P_{sat}$, then

$$Q_D(t_D) = \frac{\frac{P_0}{z_0} - \frac{P(t_D)}{z(t_D)}}{\frac{P_0}{z_0} - \frac{P_{sat}}{z_{sat}}} \tag{5.33}$$

Equation 5.22 can be solved for a short time solution using the initial and boundary conditions in equation 5.23 through 5.25, and it can be solved for a long time solution using the initial and boundary conditions in equation 5.23 through 5.26.

1. The analytical solution for the short time solution is:

$$Q_D{}^{ST}(t_D) = \frac{1}{k_D}\left[\exp\left(k_D{}^2 t_D\right) erfc(k_D\sqrt{t_D}) - 1 + 2k_D\sqrt{\frac{t_D}{\pi}}\right] \tag{5.34}$$

As $k_D \to \infty$, Equation 5.34 becomes

$$Q_D{}^{ST}(t_D) = 2\sqrt{\frac{t_D}{\pi}} \tag{5.35}$$

On the other hand, when t_D is very large, $k_D\sqrt{t_D}\rightarrow\infty$, and hence the short time approximation in Equation 5.34 becomes:

$$Q_D{}^{ST}(t_D) = -\frac{1}{k_D} + 2\sqrt{\frac{t_D}{\pi}} \tag{5.36}$$

This large time characteristic of the short time approximation should, in practice, be applied to some mid-range of the overall time variation.

2. The analytical solution for the long time solution

According to Wallas, 1991, when L is finite, a Fourier series analytical solution that is valid for large times and impractical for small times can be obtained as:

$$C_D = 1 - 4\sum_{m=1}^{\infty}\frac{\sin\lambda_m}{2\lambda_m+\sin(2\lambda_m)}\exp\left(-\lambda_m{}^2 t_D\right)\cos[\lambda_m(1-x_D)] \tag{5.37}$$

Where λ_m denotes the roots of

$$\lambda_m \tan\lambda_m = k_D \tag{5.38}$$

When C_D is substituted in Equation 5.29 and the integration is applied, the result becomes:

$$Q_D(t_D) = 1 - 4\sum_{m=1}^{\infty}\frac{\sin\lambda_m}{2\lambda_m+\sin(2\lambda_m)}\exp\left(-\lambda_m{}^2 t_D\right) \tag{5.39}$$

When t_D is large, only the leading term in the infinite series solution is significant hence Equation 5.34 simplifies to:

$$Q_D{}^{LT}(t_D) = 1 - Q_1(\lambda_1)\, e^{-\lambda_1{}^2 t_D} \tag{5.40}$$

Where

$$Q_1(\lambda_1) = \frac{4\,sin^2\,\lambda_1}{\lambda_1\,[2\lambda_1+\sin(2\lambda_1)]} \tag{5.41}$$

Taking the natural log of Equation 5.39 gives:

$$\ln[1 - Q_D{}^{LT}(t_D)] = \ln[Q_1(\lambda_1)] - \lambda_1{}^2 t_D \tag{5.42}$$

Thus plotting $\ln[1 - {Q_D}^{LT}(t_D)]$ against t_D in a given pressure-decline is expected to give a straight line with a slope of $-{\lambda_1}^2$. From the value of λ_1, the values of the coefficients D and K can then be extracted.

Table 5.6 shows the properties and conditions of the fluid and core used in the laboratory experiment for the CO_2 flood of crude J at the Institute of Petroleum Engineering, Heriot Watt University. This information will be used in the estimation of the Diffusivity constant and the interface mass transfer coefficient. Shown in Figure 5.9 is a 1-dimensional schematic of CO_2 diffusion process at the core level when CO_2 is in direct contact with heavy oil. *Table 5.6: Properties of the fluids and core used in the Core-flood experiment.*

Crude J	API=16; Viscosity=617cp; density = 0.948 g/cm^3
Brine	Brine (10000 ppm); viscosity = 0.85 cp;
CO2	viscosity=0.85cp; density = 0.798
Core Diameter	5.12 cm
Core Length	32 cm
Core Porosity	24.74
Core Permeability	2.5 Darcy
Temperature	28 ^{o}C
Pressure	1500 psig

The time used in flooding the heavy oil with CO_2 is about three days and the production characteristic of the produced oil (Figure 5.10) suggests that even after the three pore volume of injection, there is still room for recovery hence it is safe to assume that the oil in the core was not fully saturated with CO2 at the end of the CO_2 flooding. Thus the estimation of the diffusion coefficient D and the interface mass transfer coefficient is better done with large time characteristic of the short time analysis using the data in Table 5.6.

By means of Equation 5.36, this short time analysis solution can be expressed as:

$${Q_D}^{ST}(t_D) = -a_{ST} + b_{ST}\sqrt{t} \tag{5.43}$$

In which the intercept is given as:

$$a_{ST} = \frac{1}{k_D} \tag{5.44}$$

And the slope of the straight line is

$$b_{ST} = \frac{2}{L}\sqrt{\frac{D}{\pi}} \tag{5.45}$$

Figure 5.10 to 5.12 show the recovery plot of the CO_2 flood of crude J (heavy oil) in a core plug. A careful analysis of the figures reveals that at the initial stage, the recovery was dominated by displacement (viscous force), and that diffusion becomes the dominant recovery mechanism after the injection of about 1.5 pore volume of CO_2.

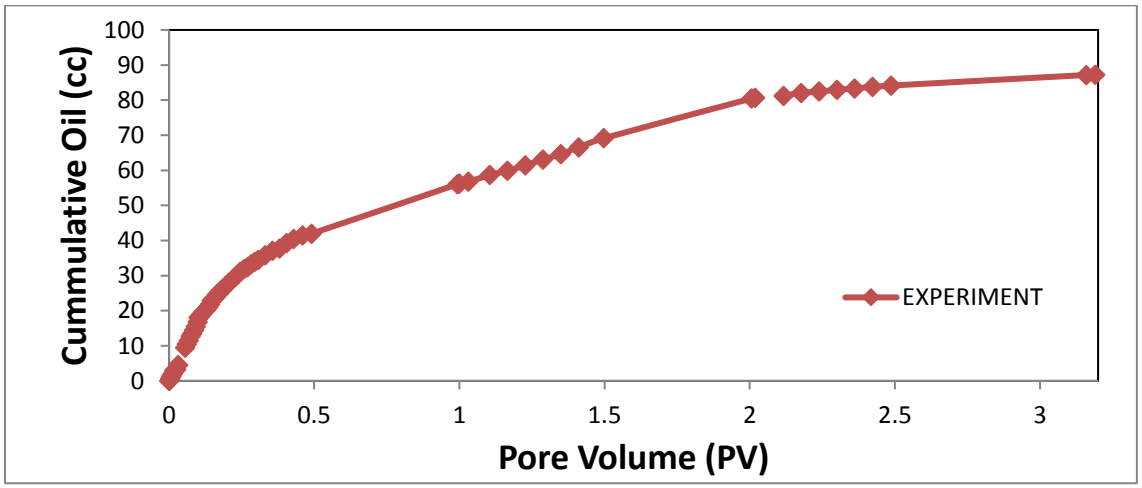

Figure 5.10: Cumulative oil recovery from the unsteady state CO2-core flood of crude J.

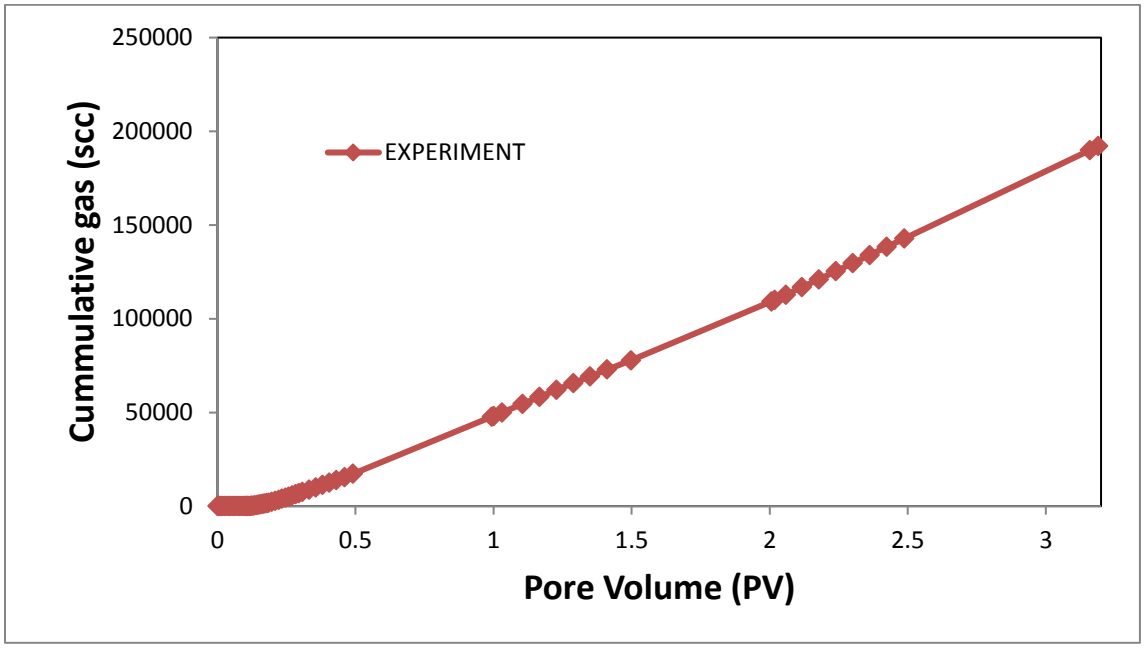

Figure 5.11: Cumulative gas recovery from the unsteady state CO2-core flood of crude J.

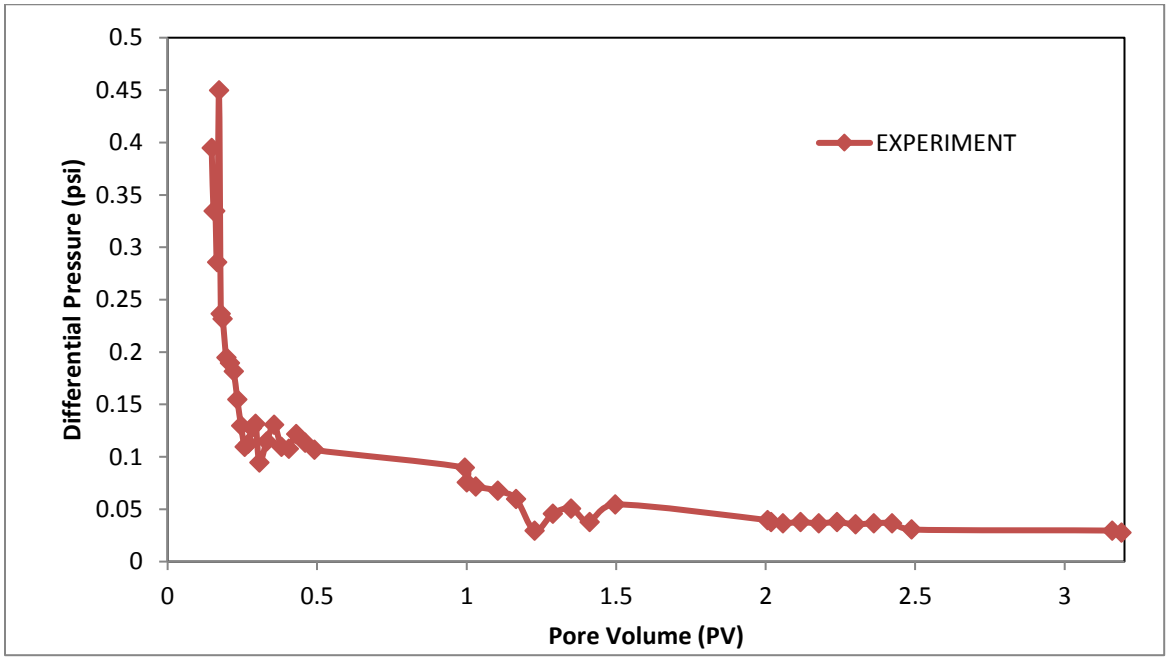

Figure 5.12: Differential pressure from the unsteady state CO2-core flood of crude J

Figure 5.13 shows the measured drop in pressure after 1.5 pore volume of CO_2 has been injected. The objective is to interpret this experimental data and estimate the values of diffusion coefficient D, and the interface mass transfer coefficient k.

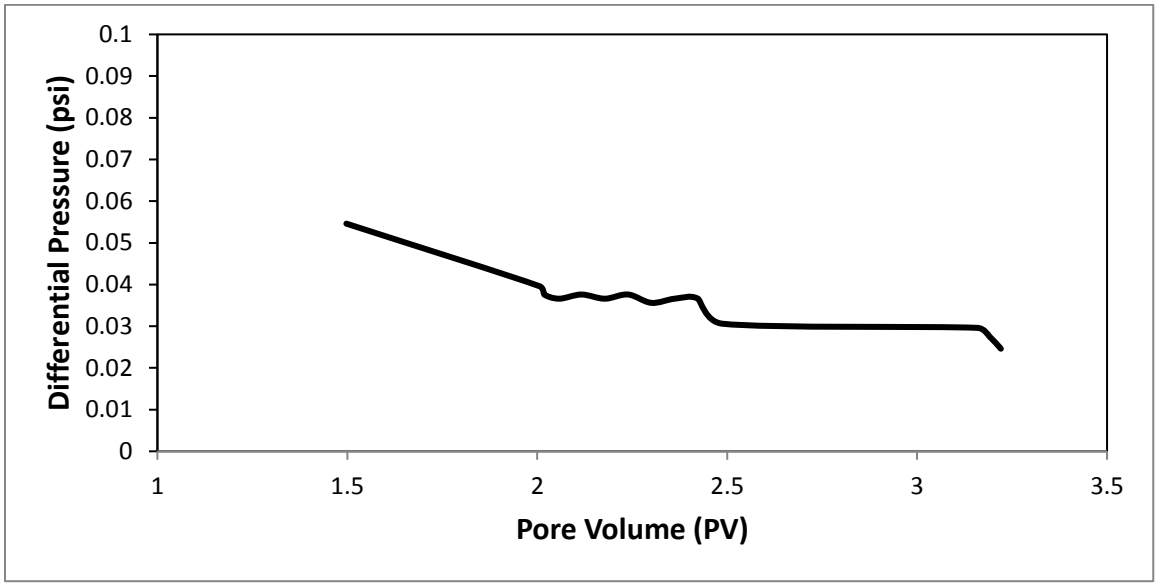

Figure 5.13: Differential pressure plot of the CO_2/heavy oil experimental data during diffusion dominant period.

By employing Equation 5.33 and 5.35 with the experimental data, a plot of Q_D against $t^{1/2}$ was made from where the diffusion coefficient, D, and the interface mass transfer coefficient, k, were extracted. Figure 5.15 shows the plot of Q_{Dn} against $t^{1/2}$, and Table 5.7 shows the parameters of the CO_2 diffusion test.

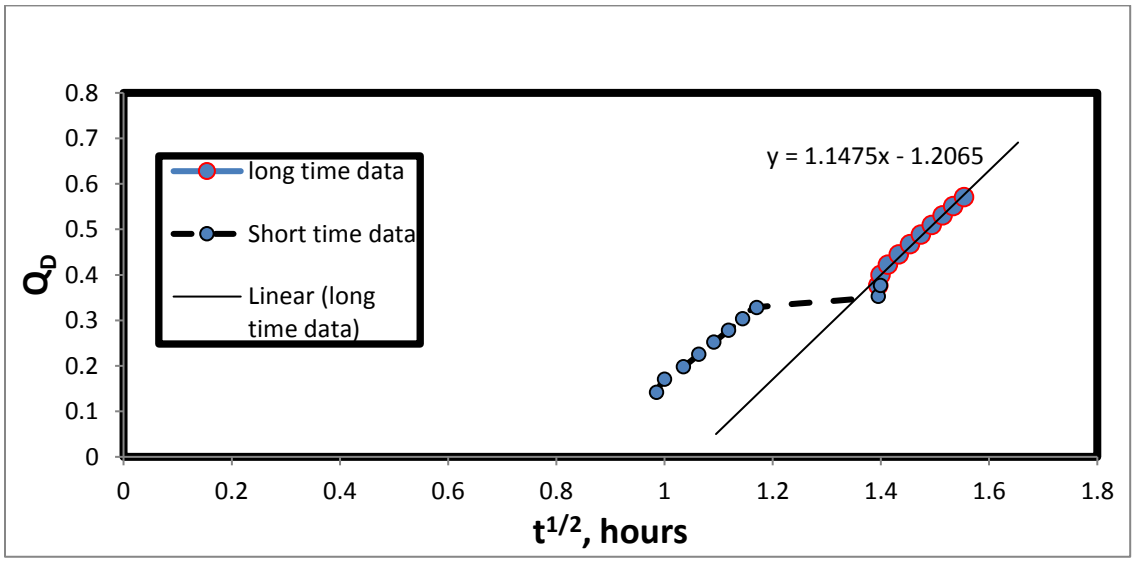

Figure 5.14: A Q_D vs $t^{1/2}$ plot of the CO_2/heavy oil experimental data showing a short and long time approximations used in CO_2 diffusivity constant estimation.

Table 5.7: Parameters of the CO_2 diffusion test.

Solute	Heavy oil (CRUDE J)
Solvent	CO2
Length (m)	0.0512
Temperature (deg. C)	28
Injection pressure(psi)	1500
a_{ST} (dimensionless)	1.147
b_{ST} ($hour^{-1/2}$)	1.206
k_D (dimensionless)	0.8292
D (m^2/s)	$7.53x10^{-7}$
K (m/s)	$1.22x10^{-5}$

5.4.3 CO_2 Diffusion Coefficient Estimation with the Correlation

As CO_2 diffuses into heavy oil causing swelling and viscosity reduction, McManamey and Woollen (1973) showed that the CO_2 diffusion coefficient in oil varies significantly as the oil viscosity changes. According to the conclusion of their work, the CO_2 diffusion coefficient in oil ($D_{co2,oil}$) is related to oil viscosity (μ_{oil}) by the empirical correlation given below:

$$D_{co2,oil} = 1.41 \times 10^{-10}\mu_{oil} \quad (5.46)$$

In the case where the heavy oil was dead oil before the initiation of diffusion into it, the Beggs and Robinson (1975) correlation can be used to estimate the live oil viscosity from the corresponding dead oil value and the solution gas oil ratio:

$$\mu_{oil} = 0.001A\,(\mu_{oilD})^B \quad (5.47)$$

Where

$$A = 10.715(R_s + 100)^{-0.515} \quad (5.48)$$

$$B = 5.44(R_s + 150)^{-0.338} \quad (5.49)$$

R_s is the dissolved gas GOR in scf/STB, μ_{oilD} is the viscosity of gas-free oil in cp, μ_{oil} is the viscosity of gas saturated oil in Pa.s.

By using the laboratory-generated viscosity values reported in Table 5.1 in Equation 5.46, the CO_2 diffusion coefficients at different viscosities are reported in Table 5.8.

Table 5.8: CO_2 diffusion coefficient as measured by the Mcmanamey and Woollen correlation.

Pressure & Temperature	**CO2 Content**	**Viscosity(μ)**	**CO2 diffusion coefficient (m^2/s)**
1500 psig, 28 °C	0%	617 (cP)	8.6997E-08
1500 psig, 28 °C	20%	174 (cP)	2.4534E-08
1500 psig, 28 °C	40%	72.1 (cP)	1.0166E-08
1500 psig, 28 °C	70%	30.8 (cP)	4.3428E-09
1500 psig, 28 °C	100%	15.2 (cP)	2.1432E-09

From the analytical model, an effective diffusion coefficient was calculated to be $7.53 \times 10^{-7} m^2/s$ while the McManamey and Woollen correlation gave comparably lower diffusion coefficient values at all CO_2 contents. In the next section a numerical simulation will be performed with Eclipse 300 and these diffusivity coefficients will be used to match the result of the core flood experiment.

5.5 Compositional Simulation

A core-flood model was created in compositional model simulator of ECLIPSE 300 from the ECLIPSE package and the 10-components phase behaviour (EOS) model of the reservoir fluid was imported into it from PVTi, the Eclipse phase behaviour package. The core flood was represented by a one dimensional model using 100 grid blocks. The model consists of a single well producer and an injector with a grid distribution of 1x1x100 (DX= 4.5376 cm, DY= 4.5376 cm, DZ= 0.32 cm). The input porosity is 0.2474 with a permeability of 2.5D in X, Y and Z directions. In this work, numerical dispersion in the simulation is controlled by using a relatively large number of grid blocks (NZ = 100). The number of grid blocks of

NZ= 100 was chosen as the optimum from the result of sensitivity study conducted on the core-flood.

The model was initialized based on the conditions of the experiments by defining fluid saturation and pressure of each cell explicitly. The initial condition is generally a fixed initial saturation and pressure in the core. The model is initialised with oil in place of 134 cm^3; and an initial water saturation of 14 % and an initial pressure of 1500 psi in each grid cell. The boundary condition at the inlet is a constant CO_2 injection rate of 7cm^3/hr, and a constant pressure of 1500 psi at the outlet.

Figure 5.15 and 5.16 show the relative permeability curves and the capillary pressure respectively used in these core-flood simulations. These curves were estimated in Chapter Two.

The molecular diffusion of gas and oil is activated in Eclipse 300 by using the diffusion keywords. Diffusion is driven by the gradient of the chemical potential as shown in the equation below:

$$J_i = -cDi^a x_i \frac{1}{RT}\frac{\partial}{\partial x}[\mu_i - M_i g(h - h_o) + M_i Di^T i \ln(T)] \quad (5.50)$$

Where:

$J_i$is the molar flux of component per unit area,

c is the total molar concentration given by c = $1/v_m$,

$v_m$is the molar volume of the mixture,

$Di^a$is the activity-corrected diffusion coefficient of component i,

$Di^T$is the thermal diffusion coefficient of component i,

$x_i$is the mole fraction of component i,

$\frac{\partial}{\partial x}$is the gradient in the direction of flow,

$M_i$the molecular weight of component ,

g is the acceleration due to gravity,

h is the height,

h_o is the reference height,

T is the temperature,

R is the gas constant, and

μ_i is the chemical potential of component i, given by

$$\mu_i = \mu_{i0} + RT \ln (f_i) \quad (5.51)$$

Where:

μ_{i0} is the reference chemical potential, and f_i is the component fugacity.

Equilibrium is obtained when the component chemical potential is equal to the gravity potential, which are the first two terms in equation 5.45. The third term is a non-equilibrium term and represents diffusion driven by a temperature gradient, so in an isothermal system, as in this case, the third term in equation 5.45 disappears.

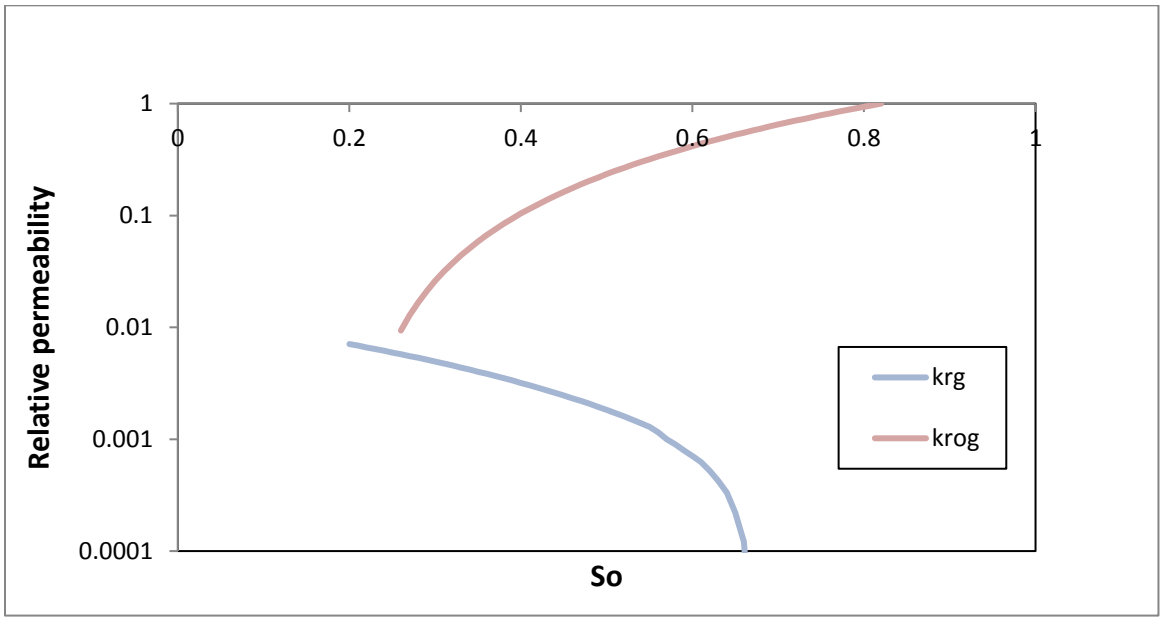

Figure 5.15: Crude J oil and CO_2 relative permeability versus oil saturation obtained from a secondary CO_2-flood of crude J in a vertical orientation 2500md core.

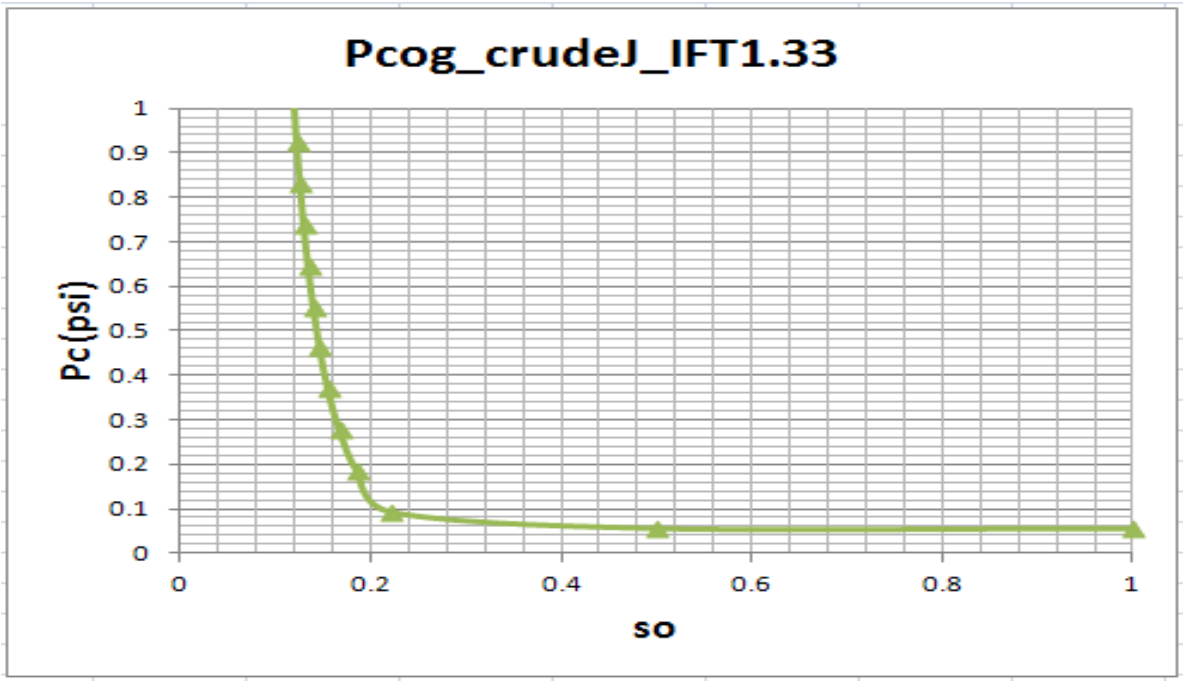

Figure 5.16: Oil/CO_2 capillary pressure of crude J in a 2500md homogenous core estimated from a Centrifuge method.

5.6 Result and Discussion

Figure 5.17 to 5.19 are the matches between the experiment and simulation results for cumulative oil production, cumulative CO_2 production, and the differential pressure across the 2500 md core in the vertical core-flood experiment. The oil recovery match is good in terms of overall cumulative oil recovery (about 1% off), but a bit poor at the early phase of the displacement process (error is 20%). An improvement in the match was sought by performing a sensitivity study with the grid system, knowing that CO_2–heavy oil system is heavily influenced by the magnitude of instability at the displacement front and the ensuing viscous fingering. Figure 5.19 shows that while increasing the number of grids in the X and Y direction appears to improve the match at the early phase of the displacement process, the overall recovery decreases with increase in the number of grid cells in the X and Y direction. The grid system of 1x1x100, in Figure 5.20, thus appears to be the best for this study.

The match can be improved with further study into viscous fingering modelling. The instability at the displacement front and the ensuing viscous fingering is a function of the size of the medium.

Figure 5.21 and 5.22 show the viscosity and gas saturation, respectively, in selected grid cells at different times during the gas injection process. It is observed that in each cell, the viscosity first reduces, then starts to increase with time, suggesting that the mechanism of CO_2 dissolution in oil and the resulting viscosity reduction happens first, followed by the mechanism of extraction of lighter components from the oil. A comparison between Figure 5.18 and 5.19 shows that the transition from the first observed mechanism to the second is occurs with increase in CO_2 saturation in the grid cells.

The compositional analyses of the produced oil samples at the different times revealed differences in the composition of the oil samples.

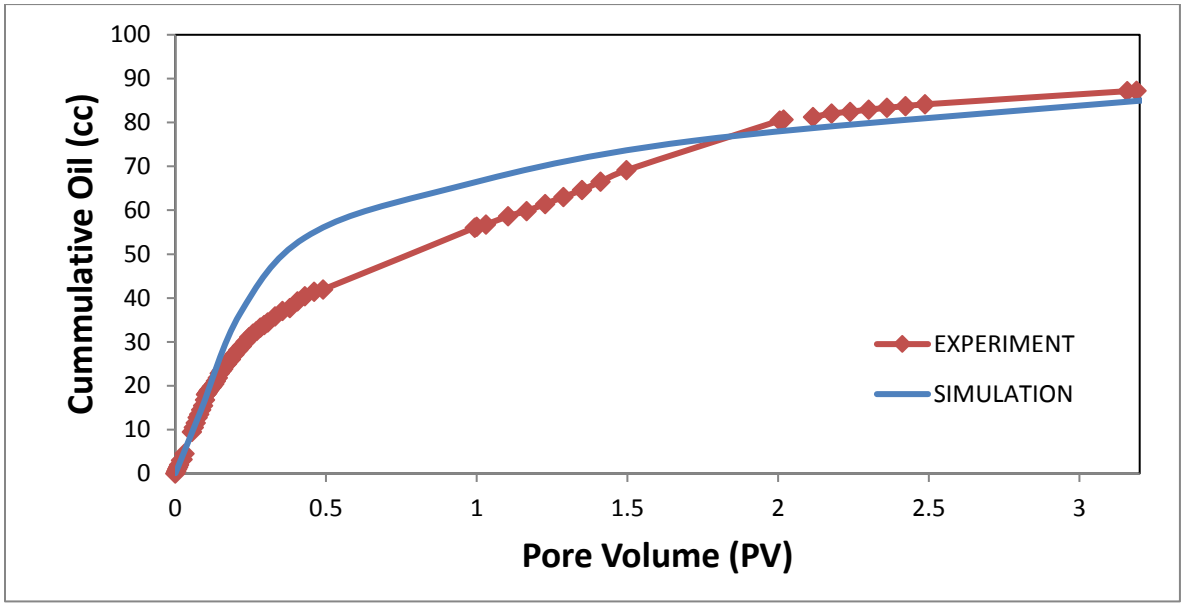

Figure 5.17: Cumulative oil recovery from the experiment and simulation in the unsteady state core flood of crude J.

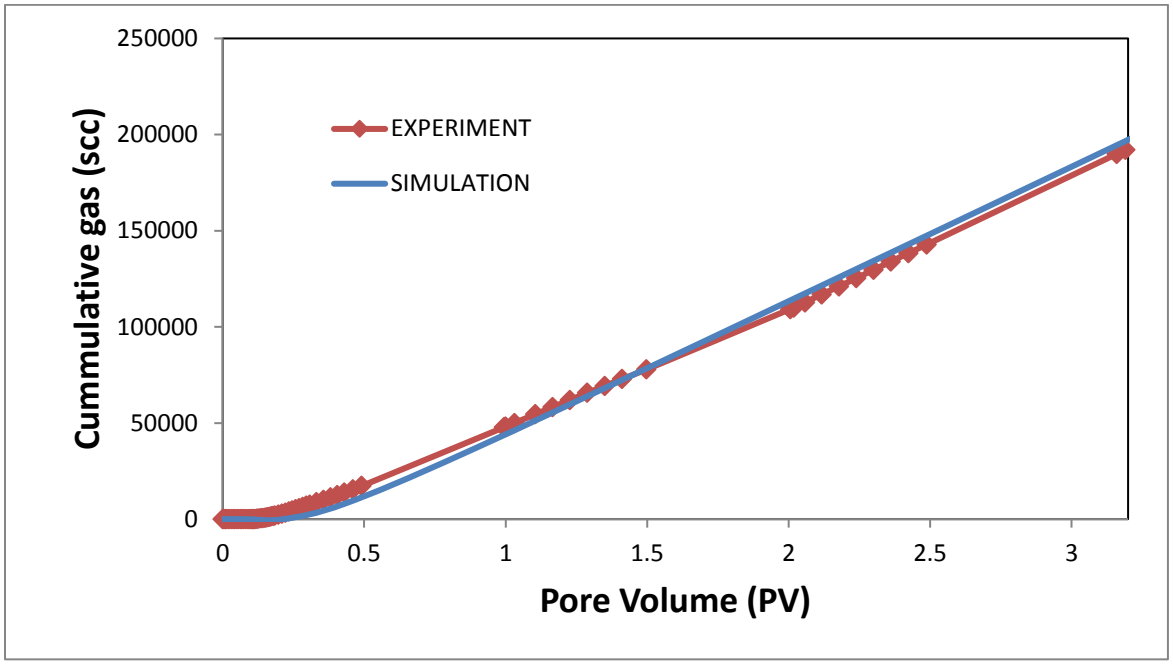

Figure 5.18: Cumulative gas recovery from the experiment and simulation in the unsteady state core flood of crude J.

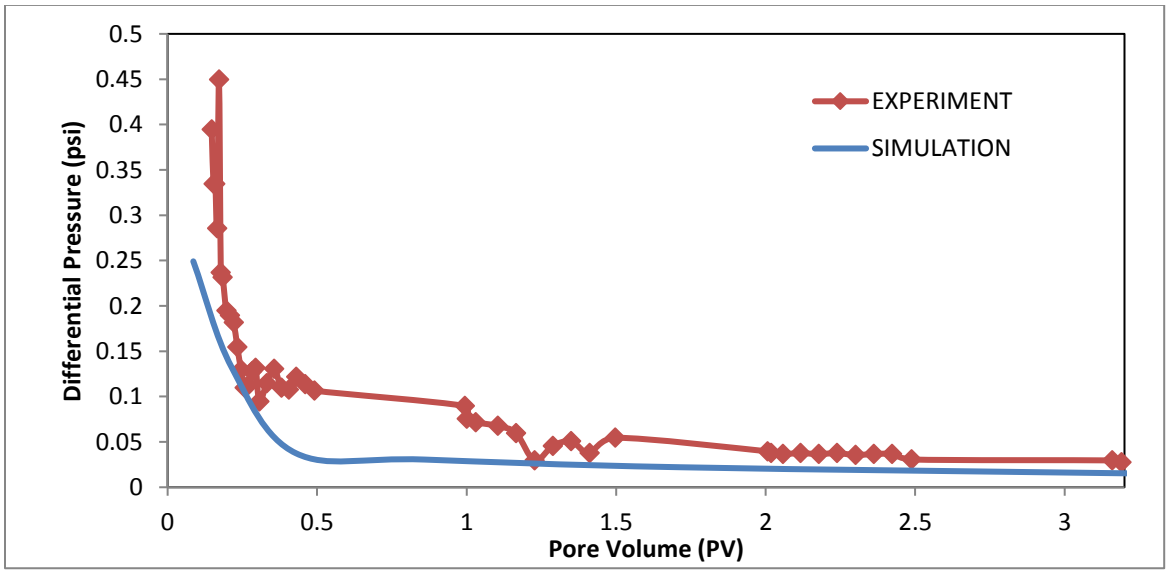

Figure 5.19: Differential pressure from the experiment and simulation in the unsteady state core flood of crude J.

Table 5.9: Oil viscosity (cp) in selected grid-blocks at different times (hours) during CO_2 injection

	Time(hours)						
Grid Number	**0**	**0.5**	**2**	**5**	**10**	**20**	**72**
1	**600**	**325**	**3450**	**9370**	**10700**	**10700**	**10700**
5	**600**	**46**	**115**	**627**	**4770**	**10700**	**10700**
10	**600**	**600**	**56**	**150**	**580**	**5500**	**10700**
20	**600**	**600**	**44**	**64**	**147**	**560**	**10700**
30	**600**	**600**	**600**	**48**	**83**	**249**	**10700**
40	**600**	**600**	**600**	**44**	**64**	**147**	**4745**

50	**600**	**600**	**600**	**44**	**52**	**105**	**1992**
60	**600**	**600**	**600**	**44**	**46**	**80**	**947**
70	**600**	**600**	**600**	**600**	**44**	**72**	**746**
80	**600**	**600**	**600**	**600**	**44**	**64**	**460**
90	**600**	**600**	**600**	**600**	**44**	**57**	**345**
100	**600**	**600**	**600**	**600**	**44**	**51**	**333**

Table 5.10: CO_2 saturation in selected grid-blocks at different times (fraction) during CO_2 injection

	Time(hours)						
Grid Number	**0**	**0.5**	**2**	**5**	**10**	**20**	**72**
1	**0**	**0.3**	**0.45**	**0.54**	**0.55**	**0.55**	**0.55**
5	**0**	**0.16**	**0.29**	**0.43**	**0.54**	**0.56**	**0.56**
10	**0**	**0**	**0.21**	**0.33**	**0.43**	**0.55**	**0.57**
20	**0**	**0**	**0.17**	**0.24**	**0.33**	**0.43**	**0.54**
30	**0**	**0**	**0**	**0.21**	**0.27**	**0.38**	**0.48**
40	**0**	**0**	**0**	**0.18**	**0.24**	**0.33**	**0.44**
50	**0**	**0**	**0**	**0.18**	**0.21**	**0.3**	**0.4**
60	**0**	**0**	**0**	**0.17**	**0.19**	**0.26**	**0.38**
70	**0**	**0**	**0**	**0**	**0.18**	**0.25**	**0.34**
80	**0**	**0**	**0**	**0**	**0.18**	**0.24**	**0.33**

90	**0**	**0**	**0**	**0**	**0.18**	**0.22**	**0.32**
100	**0**	**0**	**0**	**0**	**0.17**	**0.17**	**0.18**

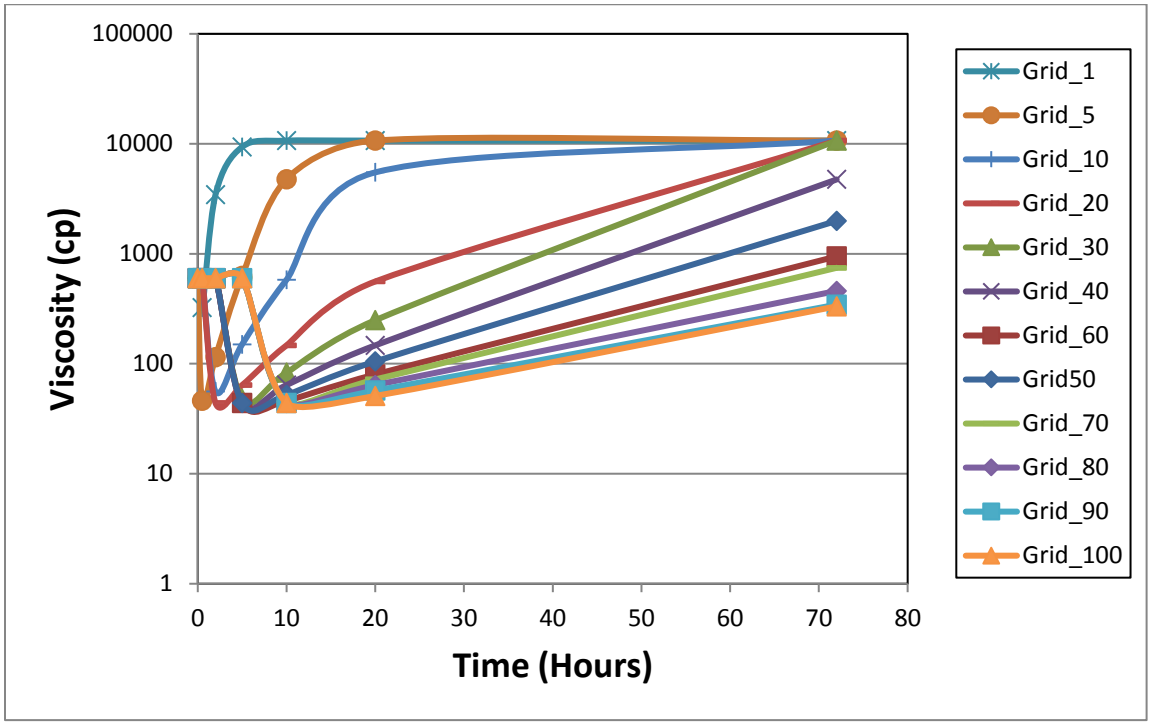

Figure 5.20: Change in viscosity with time in different grid-blocks during CO_2 injection into CO_2-injection process.

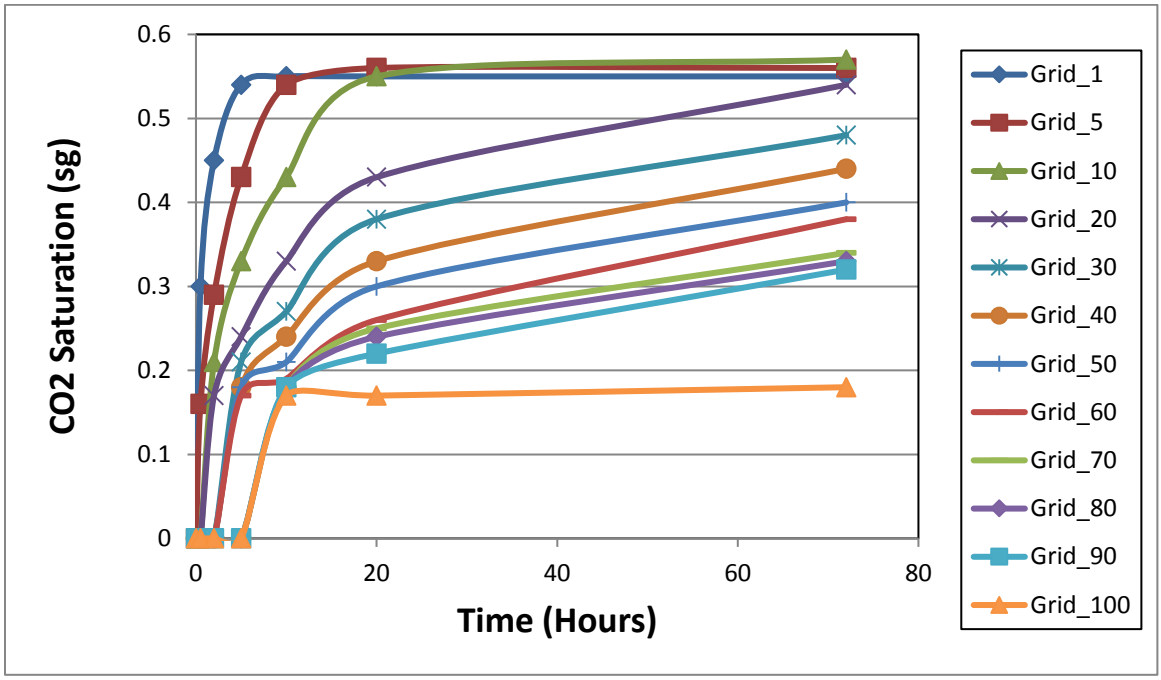

Figure 5.21: Change in CO_2 saturation with time in different grid-blocks during CO_2 injection into Crude J in the vertically positioned core.

5.7 Conclusion

In this study, measurements including CO_2 solubility in oil and the viscosity of the mixture of CO_2 and oil at a particular pressure were carried out. To simulate the phase behaviour of the system, an equation of state (Peng-Robinson) was tuned using the measured experimental data and the PVTi phase behaviour package to regressing parameters like critical properties, acentric factors, and binary interaction coefficients in the Peng –Robinson equation of state model. A mixing viscosity correlation (LBC) was also tuned with the measured data and found to be representative for describing the viscosity of the system.

The following conclusion can be drawn from this study:

- A twelve-fold reduction in oil viscosity was achieved in the near-miscible region with CO_2 injection.
- The model is able to capture solubility, viscosity reduction and the extraction mechanism observed in the micro-model studies.

- The recovery process starts with the direct displacement of oil during which CO_2 dissolves in the oil, bringing about reduction in the oil viscosity and thus boosting recovery. But as the oil is being produced and the CO_2 saturation increases, the extraction of the lighter components begins.
- The Nitrogen-heavy oil relative permeability estimated in Chapter 3 is adequate in the compositional modelling of crude J

5.8 References

1. Baker, L. E., Pierce, A. C., Luks, K. D., 1982, 'Gibbs Energy Analysis of phase Equilibria' Society of Petroleum Engineers Journal, 22, pp. 731-742.
2. Danesh, A., 1998, "PVT and phase behaviour petroleum reservoir fluids," ISBN:978-0-444-82196-6.
3. Diaz, O. Castellanos, Modaresghazani, J., 2011, 'Modelling of phase behaviour of heavy oil and solvent mixtures' Fluid phase equilibria, vol 304. Issues 1-2.
4. Emera, M.K., Sarma H.K., 2006, 'Genetic Algorithm (GA) – based correlations offer more reliable Prediction of CO_2 oil physical properties,' Canadian International Petroleum Conference, Calgary, Alberta, Canada, June 13-15.
5. Frank T.H., Chung, R., Jones, A., Nguyen, H.T., 1988, 'Measurements and Correlations of the Physical properties of CO_2/ heavy –crude oil mixtures' SPE-15080-PA, Society of Petroleum Engineers Journal, SPE Reservoir Engineering, Vol 03, Issue 3.
6. Jamaluddin, A.K.M., Kalogerakis, N.E., Chakma A., "Predictions of CO_2 solubility and CO_2 saturated liquid density of heavy oils and bitumens using a cubic equation of state" Fluid Phase Equilibria Volume 64, 1991, page 33-48
7. Klins, M. A., 1984, "Carbon-Dioxide Flooding: Basic mechanisms and Project design" International Human Resources Development Corporation, Boston, Massachusetts
8. Kokal, S.L., Sayegh, S.G., 1993, 'Phase behaviour and physical properties of CO_2-saturated heavy oil and its constitutive fractions: Experimental data and correlations' Journal of Petroleum Science and Engineering. Vol. 9: 289-302
9. Lohrenz, J., Bray, B.C., and Clark, C.R., 1964, 'Calculating viscosities of Reservoir fluids from their composition' Journal of Petroleum Technology. 1171.
10. McCain, W.D., 1990, 'The Properties of Petroleum fluids'. ISBN 0-87814-335-1.

11. McManamey, W.J., Woollen, J.M., 1973, 'The diffusivity of carbon dioxide in some organic liquids at 25ºC and 50ºC.' Journal of the American Institute of Chemical Engineers, Volume 19, Issue 3, Pp. 667-669.

12. Nima Saber, John M.Shaw, 2011, 'On the phase behaviour of Athabasca vacuum residue+ n-decane' Fluid phase equilibria, vol 302.

13. Peng, D.Y., and Robinson, D.B., 1976, 'A new Two-Constant Equation of State,' Industrial & Engineering Chemistry Fundamentals, Vol. 15, N0. 1, p. 59-64.

14. Redlich, O., and Kwong, J.N.S., 1949, 'On the thermodynamic of solutions. V. An equation of state; fugacities of gaseous solutions.' Journal of Natural Sciences, Chem. Rev., Vol. 44, p233.

15. Sayegh, S.G., Rao, D.N., Kokal, S.L., Najman, J., 1990, 'Phase behaviour and physical properties of Lindbergh heavy oil/ CO_2 mixtures.' Journal of Canadian Petroleum Technology. Vol. 29, No. 6.

16. Shu, W.R., 1984, 'A viscosity correlation for mixtures of heavy oil, bitumen, and petroleum fractions' SPE-11280-PA, Society of Petroleum Engineers Journal, Vol. 24, Issue 03

17. Sohrabi, M., Emadi, A., Jamiolahdy, M., Ireland, S., Brown, C., 2008, 'Mechanisms of Extra-Heavy Oil recovery by Gravity-Stable CO_2 injection' SCAO 2008-20. International Symposium of the Society of Core Analysts held in Abu-Dhabi, UAE, 29 October – 2 November.

18. Strvjek, R., 1989, 'Correlation and evaluation of VLE data for light n-alkane binary mixtures' Pure & Applied Chem., Vol. 61, No. 8, pp. 1419-1427.

19. Svrcek, W.Y., Mehrotra, A.K., 1982, "Gas solubility, viscosity and density measurements for Athabasca bitumen", Journal of Canadian Petroleum Technology, 21(4), 31-38.

20. Wang, S., Huang, Y. and Civan, F, 2006, "Experimental and theoretical investigation of the Zaoyuan field heavy oil flow through porous media," Journal of Petroleum Science and Engineering, 50, 83-101.

21. Yang, T., Fevang, O., Christoffersen, K.R., Ivarrud, E., 2007, LBC viscosity modelling of gas condensate to heavy oil. SPE Annual Technical Conference and Exhibition, 11-14 November. Anaheim California, USA

22. Yazdani, B., Maini, 2010, 'Measurements and Modelling of Phase behaviour and viscosity of a heavy oil/Butane system' Journal of Canadan Petroleum Technology, vol 49.

Chapter 6: Numerical Simulation of Three Phase Flow in Heavy Oil Reservoirs

6.1 Introduction

Water flooding is a common non-thermal enhanced oil recovery technique that has been used, with high success rate, in conventional oil reservoirs. However, it is not a good method for heavy oil on account of the poor mobility ratio between water and oil leading to unfavourable displacement. CO_2 flooding has also been seen to be very successful as an enhanced oil recovery technique in conventional oil reservoirs, especially where CO_2 is completely miscible with the oil. However, given that heavy oils have more of heavy hydrocarbon fractions than light hydrocarbon fractions, and that the reservoir pressure in the typically shallow heavy oil reservoirs are much lower than the minimum miscibility pressure (MMP), miscible displacement is hardly achieved in CO_2 flooding of heavy oil. Nevertheless, the immiscible CO_2 flooding of heavy oil leads to the dissolution of CO_2 into the oil bringing about viscosity reduction and swelling. Despite this obvious advantage in the use of CO_2 flooding, high CO_2 mobility due to its low viscosity leads to unfavourable mobility ratio thereby reducing the macroscopic (areal and vertical) sweep efficiency.

Water-Alternate-Gas (WAG) injection is one of the enhanced oil recovery techniques that can be used to address this inefficient displacement occasioned by viscous fingering prevalent in heavy oil displacement processes. This injection scheme has been used and reported widely in conventional oil reservoirs. Injecting CO_2 and water in an alternating approach would produce a gas permeability reduction effect, thereby improving overall sweep efficiency. In a WAG flooding, the efficiency of the process is controlled by the gas relative permeability since gas is the most mobile phase. In a typical water-wet system for a WAG flooding, gas is the most non-wetting phase while oil is the intermediate phase thus any strategy that reduces the relative permeability of gas in a WAG process automatically increases the relative permeability of oil.

In a secondary gas flood of oil, the gas, being the non-wetting phase occupies the largest pores in the rock and when water is thereafter injected, the water, being the wetting phase occupies the smallest pores, and in the process, displaces oil from the smallest pores thereby

increasing its relative permeability. In a tertiary gas flood, on the other hand, the gas being the most non-wetting phase in a water wet rock occupies the largest pores, and through double drainage, allows the oil to be reconnected as gas is being injected thereby increasing the oil relative permeability. According to Oak (1990), three phase steady state experiments conducted with conventional oil reveal that the three phase relative permeability curves, just like the two phase relative permeability curves are functions of the saturation history.

The alternating of the injection of CO_2 and water into heavy oil enhances oil recovery by altering both the microscopic and macroscopic sweep efficiencies. First, it reduces the negative effect of viscous fingering, and helps in the recovery of bypassed oil in CO_2 and water injection. Secondly, water flooding a reservoir that has been previously flooded with CO_2 benefits from the viscosity reduction due to CO_2 dissolution.

It is necessary to have a good three phase flow simulator for heavy oil if the WAG processes are to be optimized. An accurate simulation of these three phase flow processes enables the control and optimization of the process parameters like injection rates, injection ratio, injection pattern and injection pressure, composition of injection gas, injection pattern and injection pressure. Three phase flow processes require three phase relative permeability curves for numerical simulation.

For conventional oil, there are three main methods of estimating three phase relative permeability. The first one is estimation of three phase relative permeability from steady state displacement experiments. Here, all the three fluids are injected simultaneously into a core until the same proportion of injected fluids are produced (under steady state condition) at the outlet; and the estimation of the relative permeability for each of the three phases is done via Darcy's law. In spite of this ease of estimating three phase relative permeability, the steady state three phase experiments are cumbersome, and may require a long time for steady state to be reached. Equation 6.1 shows how the relative permeability of each of the three phases can be obtained from Darcy's equation.

$$k_{ri} = \frac{(q_i \mu_i L)}{KA\Delta P} \tag{6.1}$$

Where q_i, μ_i, and k_{ri} are the flow rate, viscosity, and relative permeability of phase i respectively and A is the cross-sectional area of the core, L is the length of the core, and Δp is the pressure drop across core during the steady state flow.

The second method is the estimation of three phase relative permeability from unsteady state displacement experiments. In this case, a fluid (displacing fluid) is injected into a core saturated with other fluids (displaced fluids), and the recovery data of all the fluids and the pressure drop across core are measured and recorded for the whole period of injection. Though the unsteady state displacement experiments are not as painstaking and time consuming as its steady state counterpart, the estimation of the three phase relative permeability curves from unsteady state displacement is much more complicated. In this approach, the relative permeability can either be estimated explicitly or implicitly.

The explicit method often used with the unsteady state displacement experiment in the estimation of relative permeabilities is the JBN method (1958) which is based on the Buckley-Leverett solution. The disadvantage of this method though is that it is only appropriate in cases where capillary pressure can be ignored. The major disadvantage of the explicit method is that the calculation of the production data derivatives is susceptible to error, also introducing errors to the relative permeabilities estimation.

The implicit method (or the parameter estimation computation) of relative permeabilities estimation from unsteady state core flood displacement uses optimization techniques where the difference between the measured and simulated values is minimized. This method requires a functional form representing the relative permeability of each phase in which certain selected parameters are tuned iteratively until the experimental data is sufficiently matched. This method is easier to implement in the two phase relative permeabilities estimation because it requires less tuning parameters than in three phase relative permeabilities estimation where divergence problems are often encountered.

And lastly, the third method is the estimation of three phase relative permeability from two phase data using empirical correlations e.g. Stone, Baker, IKU and ODD3P. These different models have been developed to describe three phase flow involved in recovery processes like WAG and pressure blow-down after water-flooding. In developing these models, certain assumptions were made. Some models, for example were made with the assumption that oil

is always of the intermediate wetting phase, and the gas and water are respectively considered as the non-wetting and wetting phases.

The assumptions on which the developments of these three phase relative permeability models were developed were based on the flow characteristics of conventional oil and this, as has been mentioned in this thesis, is different from the flow mechanism of heavy oil. The question hence arises: are the existing three phase relative permeability models suitable for modeling three phase flow in heavy oil WAG processes?

To answer this question, the Eclipse reservoir simulator, employing a variety of three phase relative permeability models, is used to model the WAG core-flood experiments, and the performance for each of the model is compared with the experimental data with the view of determining which of the models best represent the recovery mechanism in heavy oil. The objective of this chapter is therefore to assess the suitability of these models in modeling three phase flow in heavy oil recovery processes.

6.2 Three Phase Relative Permeability Models

6.2.1 Stone 1 Model (Stone)

The development of the Stone model was based on channel flow theory which means that there is only one mobile fluid in a flow channel. This implies that the wetting phase is found primarily in the small pore spaces while the non-wetting phase is found in the large pore spaces, and the intermediate phase spatially separates them. Thus the microscopic fluid distributions at the water-oil interface will be identical in both 2 phase oil-water system and 3 phase water-oil-gas system at a given equal water saturation, provided water saturation change direction is same in both systems. Thus in a water wet system, since the water and the gas (non-wetting phase) are not in contact at all, they do not have any influence on one another. So the relative permeability of the water phase and the gas phase in a three phase flow are functions of their own saturation and are the same as their two phase relative permeability value.

The stone model interpolates between the two sets of two phase data to obtain the three phase relative permeability for oil. The model is such that it will yield the correct two phase data when only two phases are flowing.

$$S_o{}^* = \frac{S_o - S_{om}}{1 - S_{wc} - S_{om}} \text{ (for } S_o \geq S_{om}) \quad (6.2)$$

$$S_w{}^* = \frac{S_w - S_{wc}}{1 - S_{wc} - S_{om}} \text{ (for } S_w \geq S_{wc}) \quad (6.3)$$

and

$$S_g{}^* = \frac{S_g}{1 - S_{wc} - S_{om}} \text{ (for } S_o \geq S_{om}) \quad (6.4)$$

Since the water and gas are spatially remote the stone model assumes that the impedance of oil flow by water and gas are mutually independent events, thus

$$K_{ro} = S_o{}^* \beta_w \beta_g \quad (6.5)$$

Where, β_w as a function of water saturation is obtained from the two phase data as:

$$\beta_w = \frac{K_{row}}{1 - S_w{}^*} \quad \text{(two-phase data)} \quad (6.6)$$

and β_g as a function of gas saturation, is obtained from the two phase data as:

$$\beta_g = \frac{K_{rog}}{1 - S_g{}^*} \quad \text{(two-phase data)} \quad (6.7)$$

The stone model assumes that the three phase relative permeability data are independent of viscosity. And it has been found not to be accurate at low oil saturation.

6.2.2 The Stone 2 Model (Stone 2)

It is a modified form of the Stone 1 model for the mixed-wet rock (Stone, 1973); and it is given thus:

$$K_{ro} = (K_{row} + K_{rw})(K_{rog} + K_{rg}) - (K_{rw} + K_{rg}) \quad (6.8)$$

Where K_{rw} and K_{rg} are the two-phase water and gas relative permeabilities respectively.

The Stone 2 model always predicts too high residual oil values in this region of high water saturation and low gas saturation. So the assumption of water and gas blockage of oil in this

region being independent events may not be necessarily be correct. Dietrich and Bondor (1976) suggested re-writing the stone II model as:

$$K_{ro} = \frac{1}{K_{rocw}}(K_{row} + K_{rw})(K_{rog} + K_{rg}) - (K_{rw} + K_{rg}) \quad (6.9)$$

Where K_{rocw} is the oil relative permeability at connate water saturation. This is to correct for the fact that K_{row} and K_{rog} do not equal to one at the connate water saturation.

6.2.3 Saturation Weighted Interpolation

This is also referred to as the Baker model; and it is based on saturation weighted interpolation based on water/oil and gas/oil data, given by:

$$K_{ro} = \frac{(S_w - S_{wc})K_{row} + (S_g - S_{gr})K_{rog}}{(S_w - S_{wc}) + (S_g - S_{gr})} \quad (6.10)$$

It is well more suitable for oil-wet or intermediate systems.

6.2.4 Stone 1 Exponents Model

Hustard et al (1992) modified the Stone 1 model to address the inadequacy observed in the Stone's models. The modification was done by introducing an exponent term, n, to the normalised saturations represented by the β parameter, as follows:

$$K_{ro} = \frac{K_{row}(S_w)K_{rog}(S_g)}{K_{rocw}}\beta^n \quad (6.11)$$

Where

$$\beta = \frac{S_o{}^*}{(1 - S_w{}^*)(1 - S_g{}^*)} \quad (6.12)$$

$$S_o{}^* = \frac{S_o - S_{om}}{1 - S_{wir} - S_{om} - S_{gc}} \quad (6.13)$$

$$S_w{}^* = \frac{S_w - S_{wc}}{1 - S_{wir} - S_{om} - S_{gc}} \quad (6.14)$$

and

$$S_g{}^* = \frac{S_g - S_{gc}}{1 - S_{wir} - S_{om} - S_{gc}} \tag{6.15}$$

β may be interpreted as a variable that varies between zero and one for low and high oil saturation, respectively. Values of 'n' above one causes the low oil isoperms to become more linear between the two phase values.

All these models have been developed based on the channel flow.

6.3 Three Phase Core-flood Experiments

All the three phase core-flood experiments used in this work were performed and reported by another PhD student in the Institute (Emadi, 2012). Three three-phase experiments are considered in this study: (1) a secondary CO_2-injection into a pre-equilibrated crude J, followed by water injection; (2) a tertiary-CO_2 injection into a water-flood crude J; and (3) a tertiary-CO_2 injection into a water-flood crude C. The pre-equilibrated oil (referred in this work as pre-equilibrated crude J) is of viscosity of 13cp; and crude J, as referred to in earlier chapters, is 617cp; while crude C is 8670cp.

The core used in this experiment is a 2.5darcy cylindrical core of about 32cm long and 5.12 cm. The core porosity and permeability are 24.7% and 2.5D respectively. A summary of the core properties is given in Table 6.1.

Table 6.1 Rock and fluid properties.

----------Core----------	
Diameter, cm	**5.12**
Length, cm	**32**
Porosity, %	**24.7**
Permeability, md	**2500**
----------Fluid----------	
Viscosity of pre-equilibrated crude J, cp	**13**
Viscosity of crude J, cp	**617**
Viscosity of crude C, cp	**8670**
----------Test Conditions ----------	
Pressure (crude J), psig	**1500**
Pressure (crude C), psig	**600**
Temperature (crude J), C	**28**
Temperature (crude C), C	**50**

6.3.1 Pre-equilibrated Crude J: secondary CO_2 injection experiment

In the secondary CO_2 injection experiment, the oil, water and CO_2 were pre-equilibrated at the temperature and pressure of the test condition (28 C, 1500 psi) before being injected into the core. This was done to minimize the effect of mass transfer in the core. The oil and CO_2 were equilibrated in a rocking cell then oil viscosity and CO_2 content in the oil were measured. The oil was then injected into an oil cell, and the gas into a gas cell.

The core was initially saturated with brine and pressurized to 1500 psig at 28 deg C. Then oil was injected into the core to mimic the initial migration of oil in water bearing reservoir and thereby establishing an initial oil and water saturation. In this experiment, the established initial oil saturation was 0.82.

The two phase core-flood experiment started by injecting CO_2 into the oil filled core at a rate of 7cm^3/hr for about 3 days. The differential pressure across the core and the recovered oil and CO_2 were measured.

At the completion of the CO_2 injection (that is when the cumulative oil recovery had reached a plateau), the core was 23% saturated with oil and 59% saturated with CO_2. This was after about three pore volumes of CO_2 were injected.

At this stage, pre-equilibrated brine injection into the core was initiated at a rate of $7cm^3hr^{-1}$. The differential pressure across the core, the recovered CO_2 and brine, oil were all measured and recorded. This continued till the cumulative oil recovery reached a plateau. This was after one pore volumes of brine were injected. Table 6.2 shows the result of the three-phase core-flood for the pre-equilibrated crude J.

Table 6.2: Result of the three-phase core-flood for pre-equilibrated crude J.

TIME (hours)	Pore Volume (PV)	Recovered Oil (cc)	Recovered CO2 (cc)	Recovered WATER (cc)	Differential PRESSURE (psi)	Corrected Recovered Oil (cc)	Corrected Recovered Water (cc)	Corrected Recovered CO2 (cc)
0.00	0.00	0.00	0.00	0.00	0.00	0.00	0.00	0.00
0.43	0.02	0.00	461.54	1.20	0.08	0.00	1.26	425.00
0.57	0.02	0.00	838.11	1.20	0.10	0.00	1.26	801.57
0.71	0.03	0.00	1265.03	1.20	0.09	0.00	1.26	1228.49
0.86	0.04	0.00	1672.03	1.20	0.09	0.00	1.26	1635.49
1.00	0.04	0.20	2065.38	1.10	0.08	0.24	1.16	2011.83
1.14	0.05	0.20	2418.88	1.10	0.09	0.24	1.16	2365.33
1.29	0.06	0.20	2789.16	1.10	0.09	0.24	1.16	2735.61
1.43	0.06	0.20	3238.11	1.10	0.11	0.24	1.16	3184.56
1.93	0.08	0.40	4664.69	1.40	0.12	0.47	1.47	4581.94
2.43	0.10	0.40	6031.47	1.40	0.15	0.47	1.47	5948.72
2.93	0.13	0.40	7422.38	1.60	0.16	0.47	1.68	7333.54
3.43	0.15	0.40	8885.66	1.60	0.18	0.47	1.68	8796.82
4.43	0.19	0.80	11588.81	1.40	0.22	0.94	1.47	11465.94
5.43	0.23	2.20	14091.61	1.40	0.26	2.60	1.47	13828.32
6.43	0.28	3.20	16168.53	1.40	0.30	3.78	1.47	15804.94
6.93	0.30	4.00	17264.69	1.40	0.32	4.72	1.47	16820.86
7.64	0.33	5.50	18647.20	1.80	0.35	6.49	1.89	18040.74
7.86	0.34	5.50	18874.83	2.60	0.35	6.49	2.73	18244.01
8.14	0.35	5.70	19124.48	3.60	0.35	6.73	3.78	18443.15
8.64	0.37	5.90	19381.47	5.90	0.35	6.96	6.20	18610.04
9.14	0.39	6.00	19601.75	9.10	0.35	7.08	9.56	18722.85
9.64	0.41	6.10	19905.94	12.00	0.34	7.20	12.60	18928.71
19.64	0.84	9.60	23074.83	74.00	0.32	11.33	77.70	19858.65
20.64	0.89	9.80	23316.08	80.00	0.31	11.56	84.00	19897.14
21.64	0.93	9.90	23573.08	86.60	0.32	11.68	90.93	19943.14
23.00	0.99	9.90	23961.19	95.70	0.31	11.68	100.49	20054.15
23.64	1.02	10.00	24136.36	99.90	0.31	11.80	104.90	20091.41

6.3.2 Crude J: Tertiary CO_2 injection experiment

In the tertiary CO_2 injection experiment, the core was initially saturated with brine and pressurized to 1500 psig at 28 deg C. Then, oil was injected into the core to mimic the initial migration of oil in a water bearing reservoir and to determine an initial oil and water saturation. In this experiment, the established initial oil saturation was 0.83.

The test started by injecting brine into the oil filled core at a rate of 7cm^3/hr for about 2 days (2.2 pore volume of brine injected). The differential pressure and the recovered oil and CO_2 were measured.

At the end of the brine injection, the core was 53% saturated with oil and 47% saturated with brine. At this stage, CO_2 injection into the core was initiated at a rate of 7cm^{3}hr^{-1}. And the differential pressure and the CO_2, brine and oil recovery were measured and recorded. This continued till the cumulative oil recovery reached a plateau. This was after three pore volumes of CO_2 were injected. Table 6.3 shows the result of the three-phase core-flood for crude J.

Table 6.3: Results of the three-phase core-flood for crude J.

TIME (hours)	Pore Volume(PV)	Recovered Oil (cc)	Recovered Water (cc)	Recovered CO2 (cc)	Differential Pressure (psi)
0.00	0.00	0.00	0.00	0.00	0.46
1.00	0.04	0.25	7.00	0.00	0.57
2.00	0.09	0.50	12.75	0.00	0.50
3.00	0.13	0.50	19.00	0.00	0.40
4.00	0.17	0.75	25.25	0.00	0.30
5.00	0.21	3.25	30.50	0.00	0.25
6.00	0.26	5.50	32.25	1080.00	0.20
7.00	0.30	6.50	32.75	3355.00	0.18
19.00	0.82	20.00	32.75	34230.00	0.05
25.00	1.07	27.50	32.75	50380.00	0.06
32.00	1.37	34.25	32.75	69725.00	0.03
41.50	1.78	39.00	32.75	97800.00	0.01
50.00	2.15	41.50	32.75	124460.00	0.01
70.00	3.01	44.75	32.75	187145.00	0.01

6.3.3 Crude C: Tertiary CO_2 injection experiment

In the tertiary CO_2 injection experiment, the core was initially saturated with brine and pressurised to 600 psig at 50 deg C. Then, oil was injected into the core to mimic the initial migration of oil in a water bearing reservoir and to determine an initial oil and water saturation. In this experiment, the established initial oil saturation was 0.90.

The test started by injecting brine into the oil filled core at a rate of $7cm^3/hr$ for about 2 days (2.1 pore volume of brine injected). The differential pressure and the recovered oil and CO_2 were measured.

At the end of the brine injection, the core was 72% saturated with oil and 28% saturated with brine. At this stage, CO_2 injection into the core was initiated at a rate of $7cm^3hr^{-1}$. And the differential pressure and the CO_2, brine and oil recovery were measured and recorded. This continued till the cumulative oil recovery reached a plateau. Table 6.4 shows the result of the three-phase core-flood for crude C.

Table 6.4: Results of the three-phase core-flood for crude C.

Time (hours)	Pore Volume (PV)	Recovered oil (cc)	Recovered Water (cc)	Recovered CO2 (cc)	Differential Pressure (psi)
0.0	0.00	0.0	0.0	0.0	0.00
0.7	0.03	0.0	0.0	122.5	0.33
1.1	0.05	0.0	0.0	122.5	0.40
1.6	0.07	0.0	7.4	130.0	8.30
1.7	0.07	0.0	11.1	135.0	8.81
1.8	0.08	0.0	14.4	137.5	9.02
3.4	0.15	0.0	18.2	0.0	1.50
5.6	0.24	2.6	20.0	3347.5	0.83
6.5	0.28	3.8	20.0	4522.5	0.68
10.8	0.46	5.6	20.0	11667.5	0.60
15.8	0.68	7.8	20.0	19602.5	0.33
17.7	0.76	8.6	20.0	22632.5	0.21
29.7	1.28	15.2	20.0	41742.5	0.19
50.3	2.16	24.2	20.0	75732.5	0.24
70.3	3.02	32.7	20.0	110552.5	0.09
90.3	3.88	39.8	20.0	145002.5	0.14
101.0	4.34	43.6	20.0	163767.5	0.14
115.4	4.95	49.1	20.0	188402.5	0.15
120.6	5.18	50.9	20.0	197252.5	0.13
126.7	5.44	53.2	20.0	208082.5	0.12
134.3	5.77	55.5	20.0	209132.5	0.12
144.1	6.19	57.6	20.0	218312.5	0.11
144.7	6.22	57.6	20.0	218432.5	0.10
146.0	6.27	57.8	20.0	221117.5	0.11

6.4 Numerical Simulation

All the experiments described above were simulated with Eclipse reservoir simulator. The pre-equilibrated crude J secondary CO_2 injection was modelled as a black oil model, while the crude J tertiary CO_2 injection and the crude C tertiary CO_2 injection were modelled as compositional models. The estimated oil-water and for oil-CO2 two phase relative permeability for each of these different crude oil systems were used to generate three phase relative permeability for each of them using the three phase relative permeability models (Saturated Weighted Interpolation, STONE1, STONE2, STONE1-exponents and ODD3P) in the simulator. The two phase oil-water and for oil-CO2 relative permeability curves for the pre-equilibrated crude J, the crude J, and the crude C were all estimated in chapter three.

The one dimensional models constructed in the simulator consisted of a single well producer and an injector with 100x1x1 (DX= 0.32 cm, DY= 4.5376 cm, DZ= 4.5376 cm). In a grid sensitivity exercise, it was confirmed that the results are independent of the grid size.

6.4.1 Three Phase Simulation for the Pre-Equilibrated Crude J

The measurements of oil and CO_2 production have been done at the standard condition, significant amount of CO_2 has been released which severely affects the recorded oil and gas recovery. Thus, the production data must be corrected to the real amount of fluids produced from the core which should be used for simulation purpose. This correction (used in Table 6.2) can be implemented for oil by multiplying the oil production by the swelling factor of 1.18cc/scc; and water by multiplying the water production by the swelling factor of 1.05cc/scc; and for CO_2 by the following equation:

Real CO_2 production = CO_2 (@ SC) – Oil (@ SC)*CO_2 Solubility (85 scc/cc) – Water (@ SC)*CO_2 Solubility (29 scc/cc). (6.16)

The 2-phase relative permeability in the CO_2-oil system was combined with the 2-phase oil-water relative permeability, and used in black oil simulator (Eclipse 100) to generate a 3-phase relative permeability curves to simulate the 3-phase flow in the experiment. The choice of Eclipse 100 (a Black oil simulator) is because there is no mass transfer involved in the flow as the fluids were pre-equilibrated. The model was initialised with oil in place of 134 cm^3. Simulations were made with different 3-phase relative permeability models

(Saturated Weighted Interpolation, STONE1, STONE2, and STONE1-exponents) and their performances are compared. Figure 6.1 to Figure 6.4 present the experimental and the simulation results of the pre-equilibrated crude J WAG injection using different three phase relative permeability models.

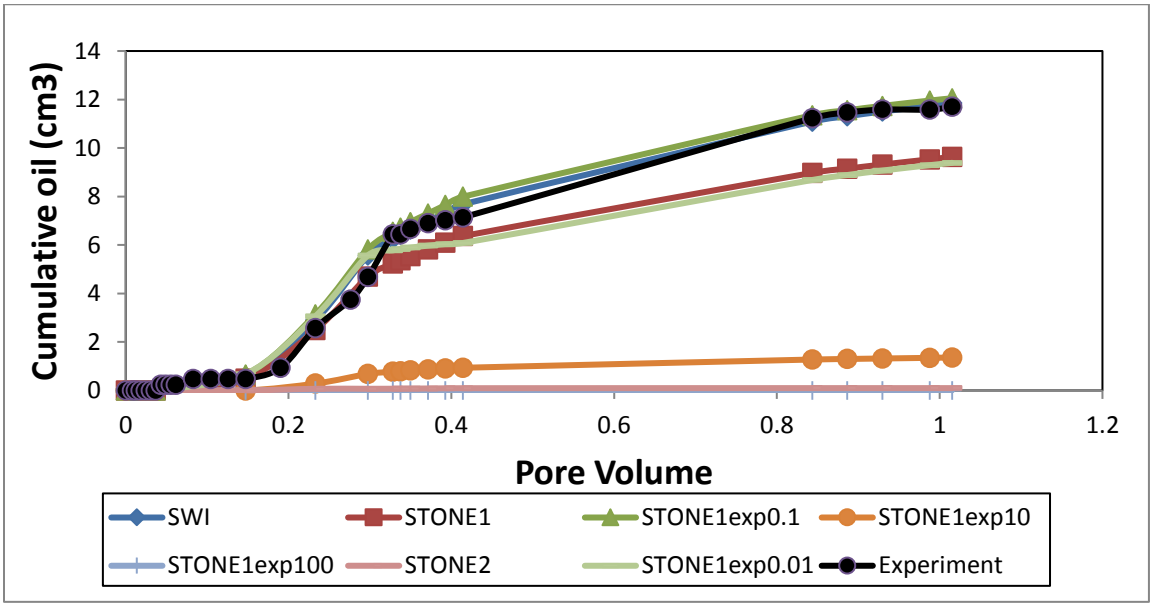

Figure 6.1: Cumulative oil recovery from the experiment and simulation (with different three phase relative permeability models) in the unsteady state core flood of pre-equilibrated crude J.

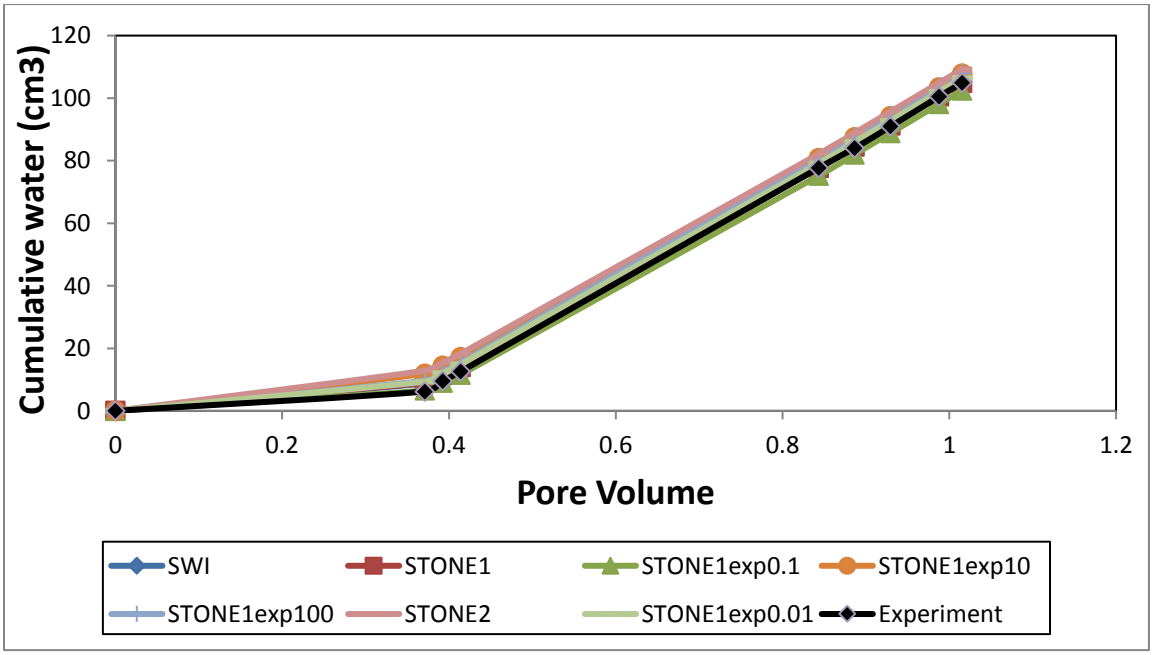

Figure 6.2: Cumulative water recovery from the experiment and simulation (with different three phase relative permeability models) in the unsteady state core flood of the pre-equilibrated crude J.

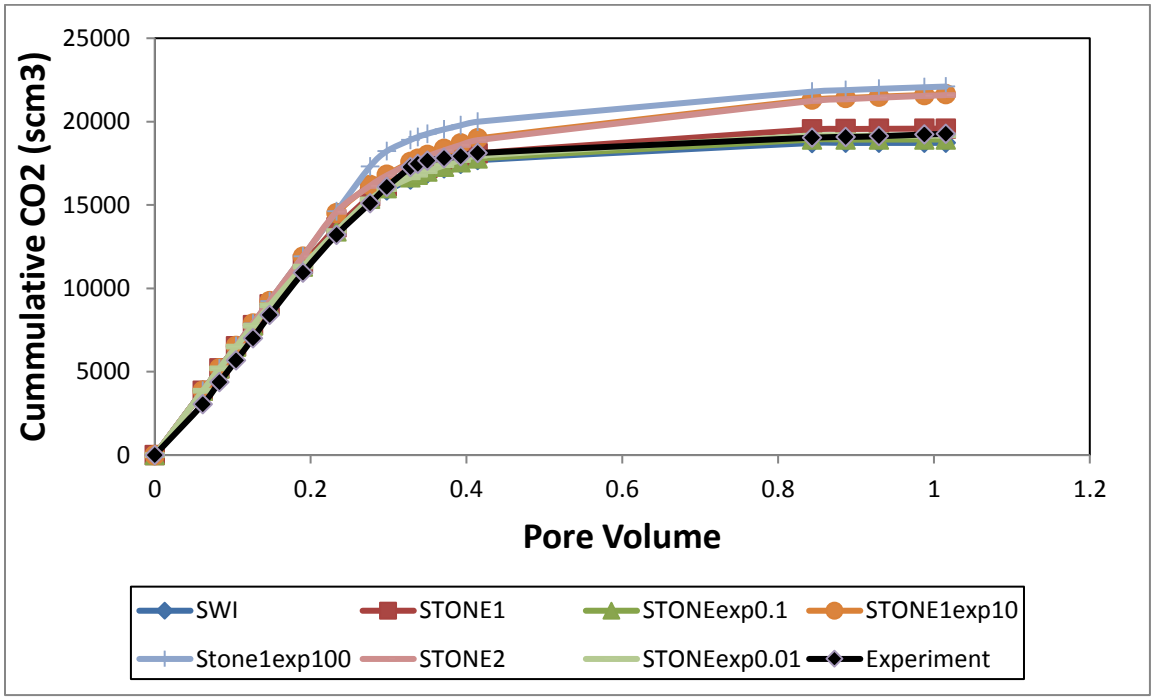

Figure 6.3: Cumulative gas recovery from the experiment and simulation (with different three phase relative permeability models) in the unsteady state core flood of the pre-equilibrated crude J.

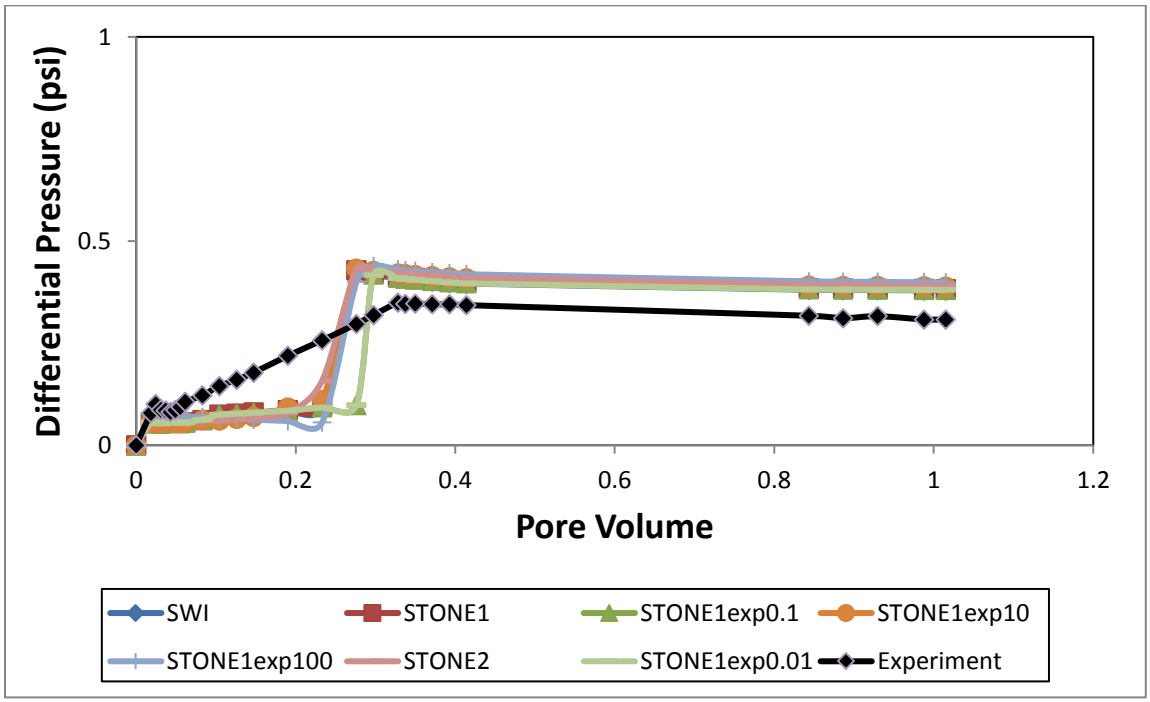

Figure 6.4: Differential pressure from the experiment and simulation (with different three phase relative permeability models) in the unsteady state core flood of the pre-equilibrated crude J .

6.4.2 Three Phase Simulation for Crude J

For the secondary water experiment, the oil and water used were not pre-equilibrated with CO_2 hence the three phase flow in this experiment was simulated as a compositional system with the Eclipse 300 commercial simulator. Figure 6.5 is the PVT regression of the EOS used in the simulation. Simulations were made with different 3-phase relative permeability models (Saturated Weighted Interpolation, STONE1, STONE2, STONE1-exponents and ODD3P) and their performances are compared. Figure 6.6 to 6.9 present the experimental and the simulation results of the crude J WAG injection using different three phase relative permeability models.

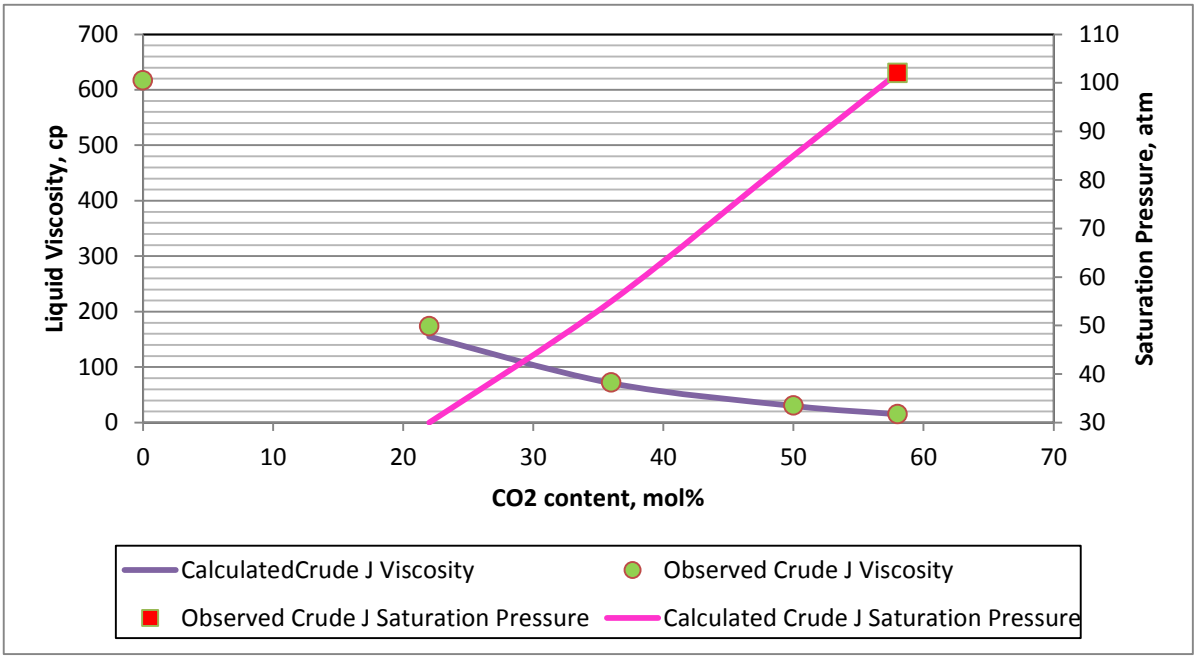

Figure 6.5: viscosity and saturation pressure match of crude J from the tuning of the Peng-Robinson equation of state model.

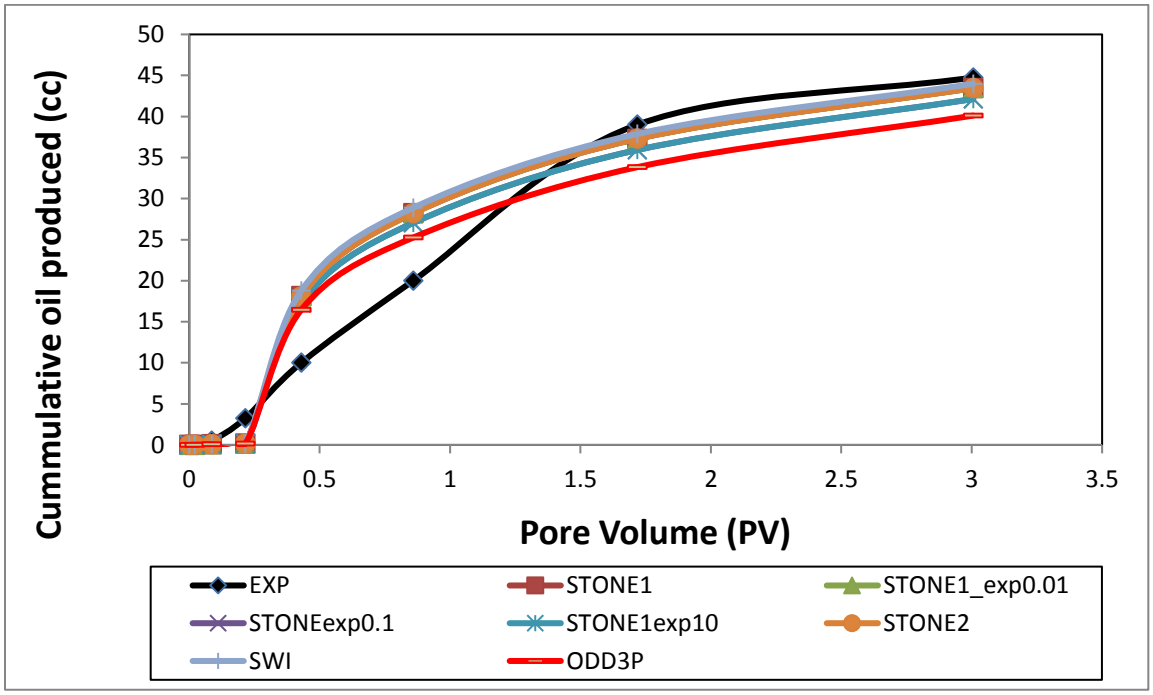

Figure 6.6: Cumulative oil recovery from the experiment and simulation (with different three phase relative permeability models) in the unsteady state core flood of crude J.

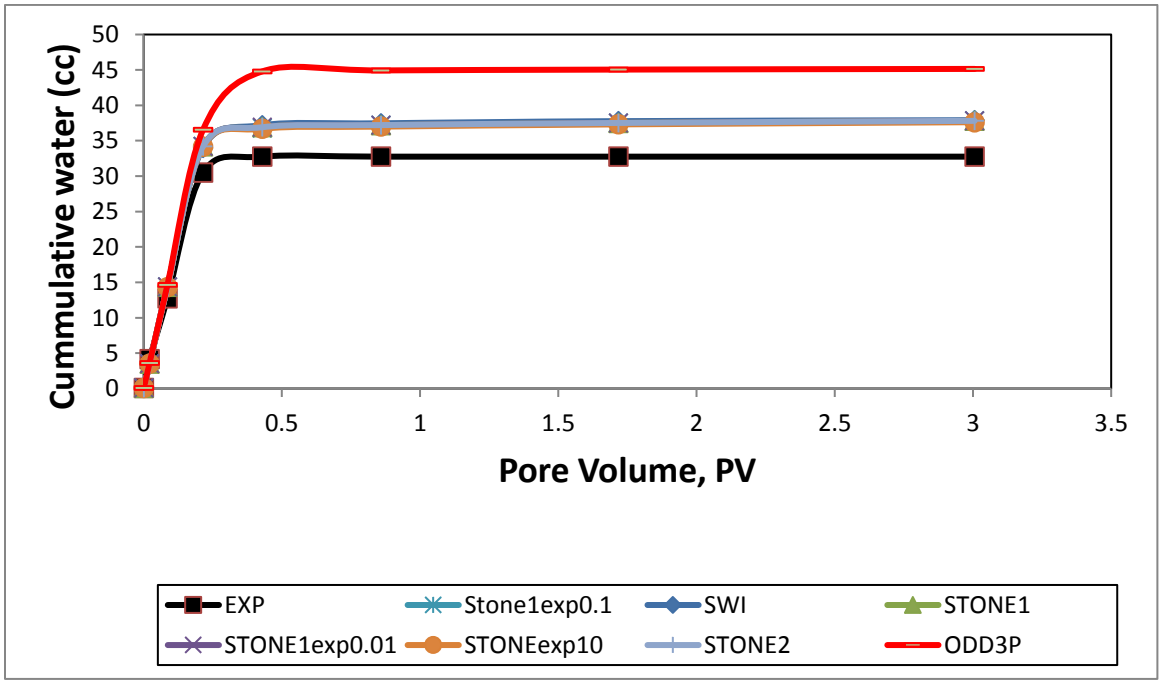

Figure 6.7: Cumulative water recovery from the experiment and simulation (with different three phase relative permeability models) in the unsteady state core-flood of crude J.

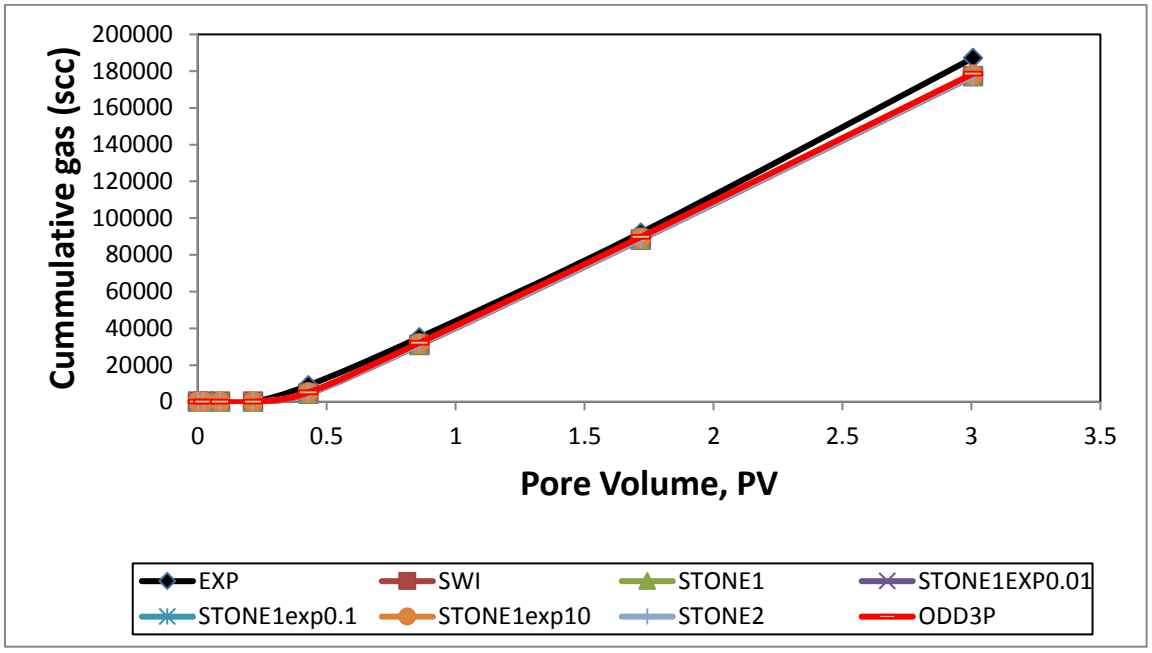

Figure 6.8: Cumulative gas recovery from the experiment and simulation (with different three phase relative permeability models) in the unsteady state core flood of crude J.

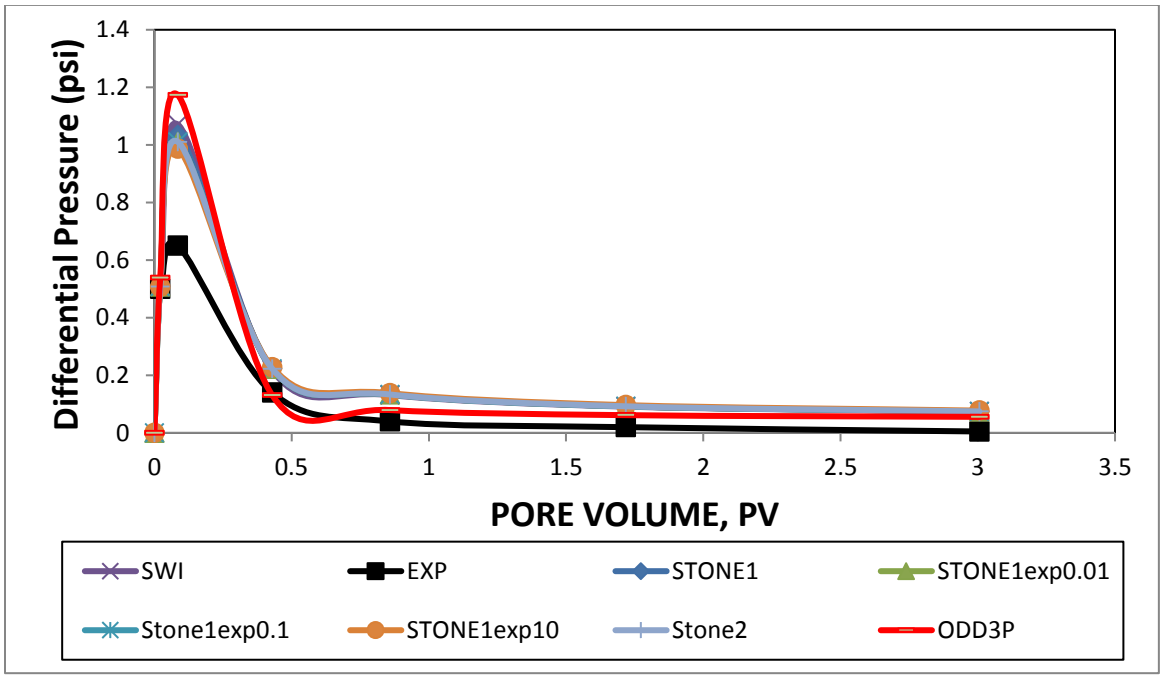

Figure 6.9: Differential pressure from the experiment and simulation (with different three phase relative permeability models) in the unsteady state core flood of crude J.

6.4.3 Three Phase Simulation for Crude C

For the secondary water experiment, the oil and water used were not pre-equilibrated with CO_2 hence the three phase flow in this experiment was simulated as a compositional system with the Eclipse 300 commercial simulator. Figure 6.10 is the PVT regression of the EOS used in the simulation. The two phase relative permeability used in the three phase simulation for crude C were estimated and reported in chapter two of this thesis. The three phase simulations were made with different 3-phase relative permeability models (Saturated Weighted Interpolation, STONE1, STONE2, STONE1-exponents and ODD3P) and their performances are compared with the experiment. Figure 6.11 to 6.14 present the comparison of the experimental results and the simulation results of the crude C WAG injection using different three phase relative permeability models for the for the cumulative oil, water, gas, and differential pressure respectively.

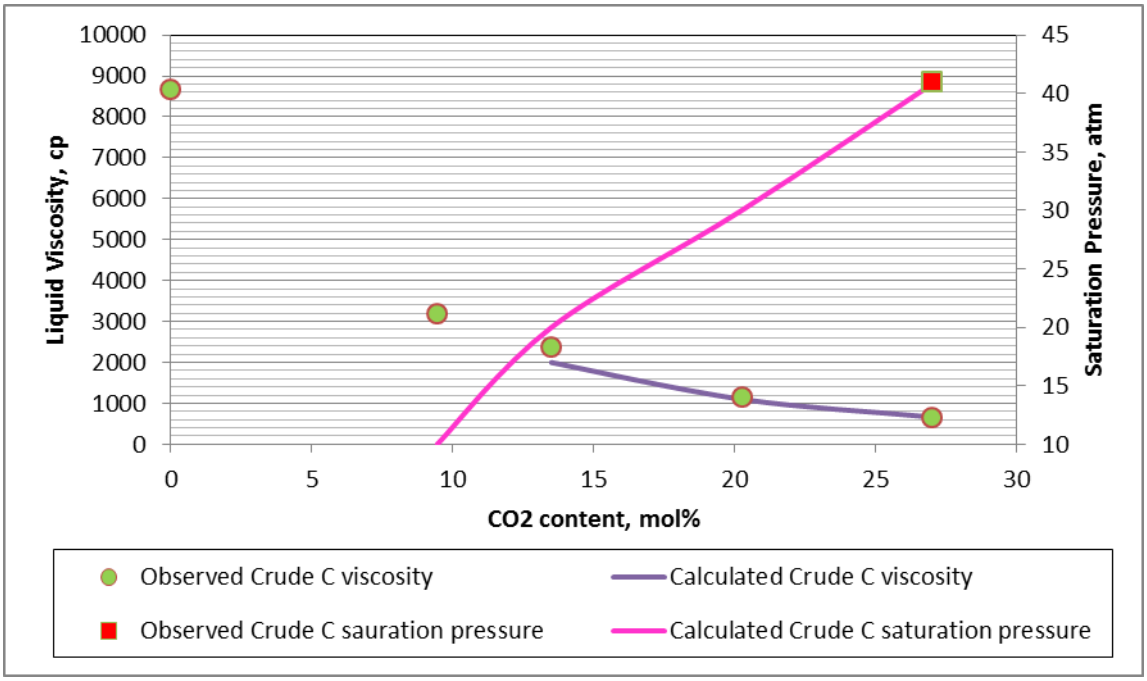

Figure 6.10: viscosity and saturation pressure match of crude C from the tuning of the Peng-Robinson equation of state model.

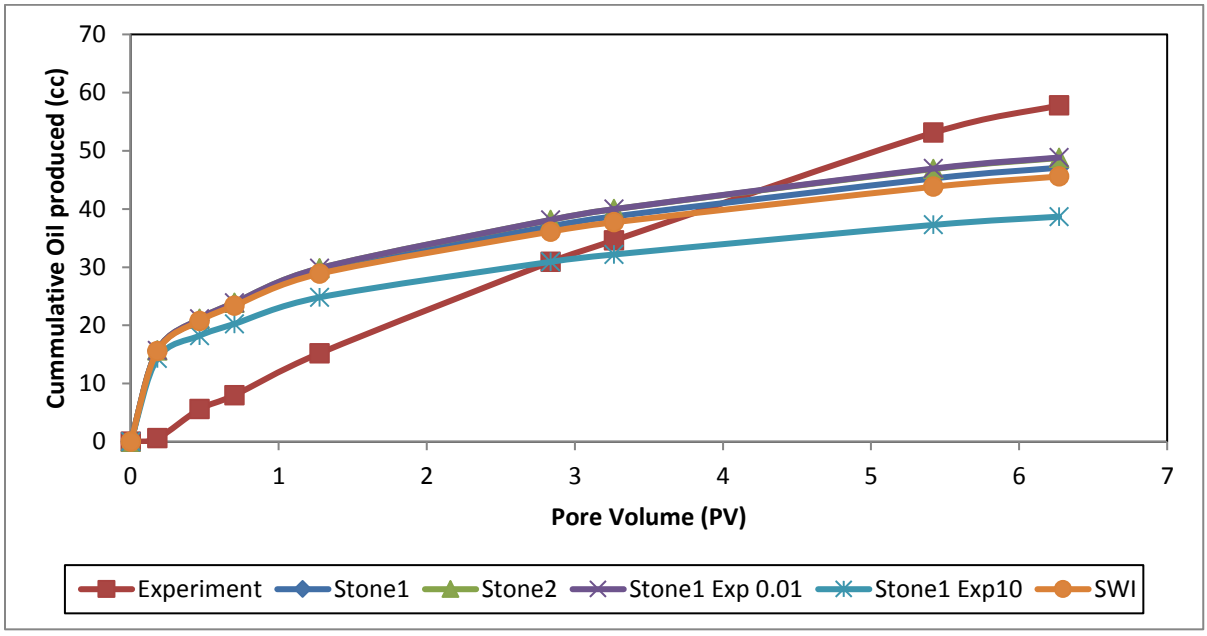

Figure 6.11: Cumulative oil recovery from the experiment and simulation (with different three phase relative permeability models) in the unsteady state core flood of crude C.

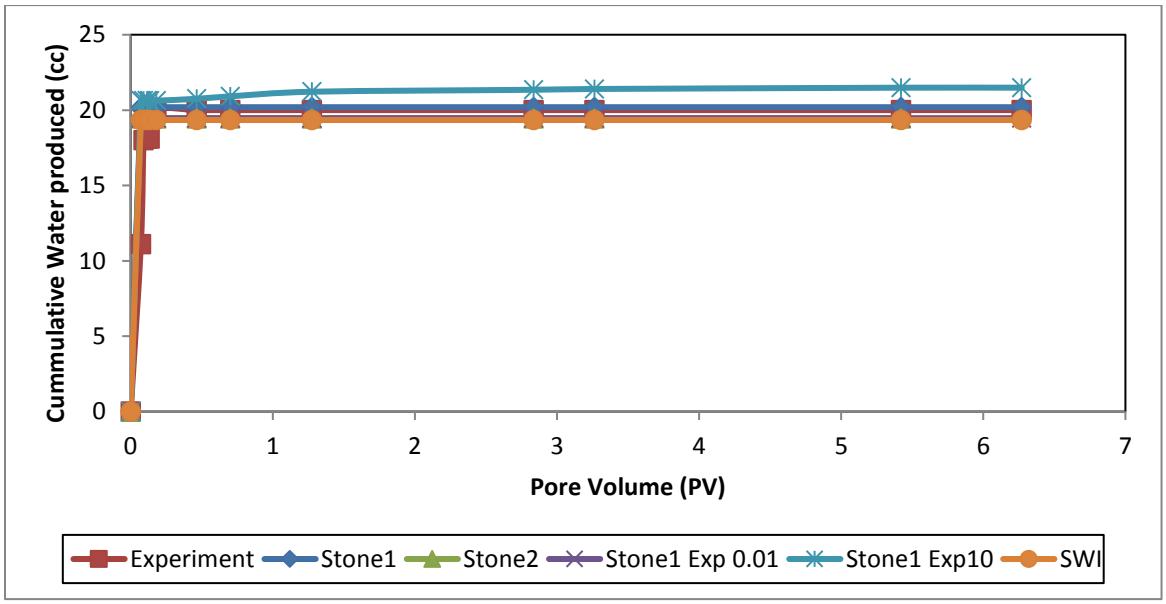

Figure 6.12: Cumulative water recovery from the experiment and simulation (with different three phase relative permeability models) in the unsteady state core-flood of crude C.

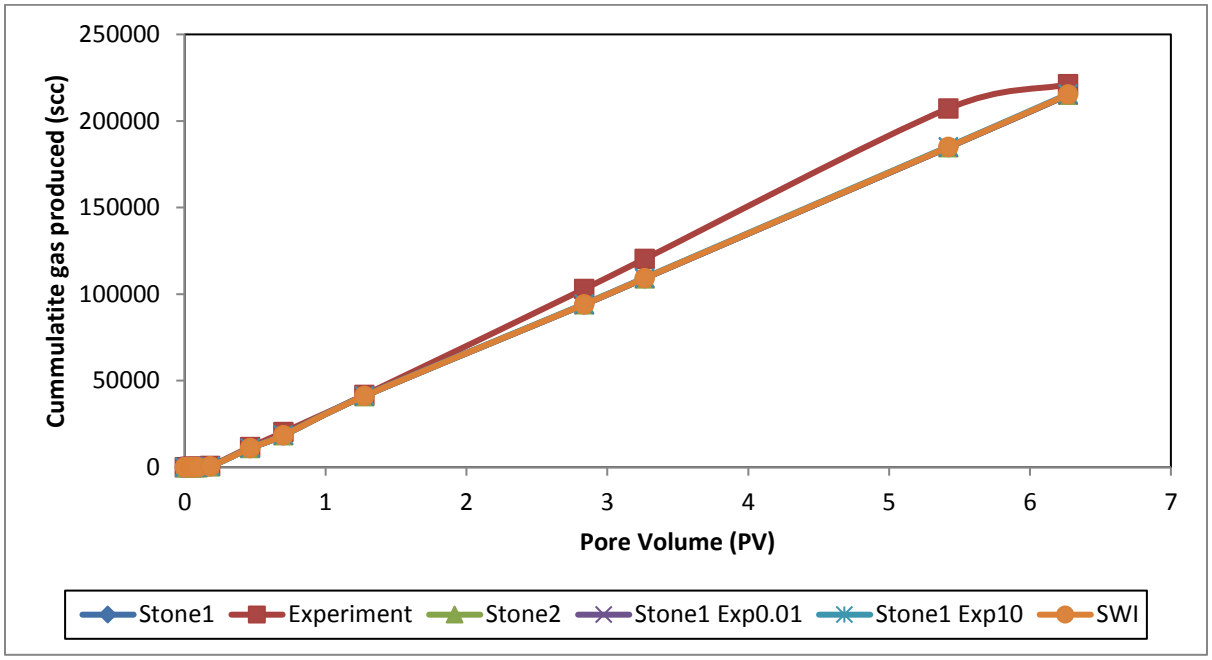

Figure 6.13: Cumulative gas recovery from the experiment and simulation (with different three phase relative permeability models) in the unsteady state core flood of crude C.

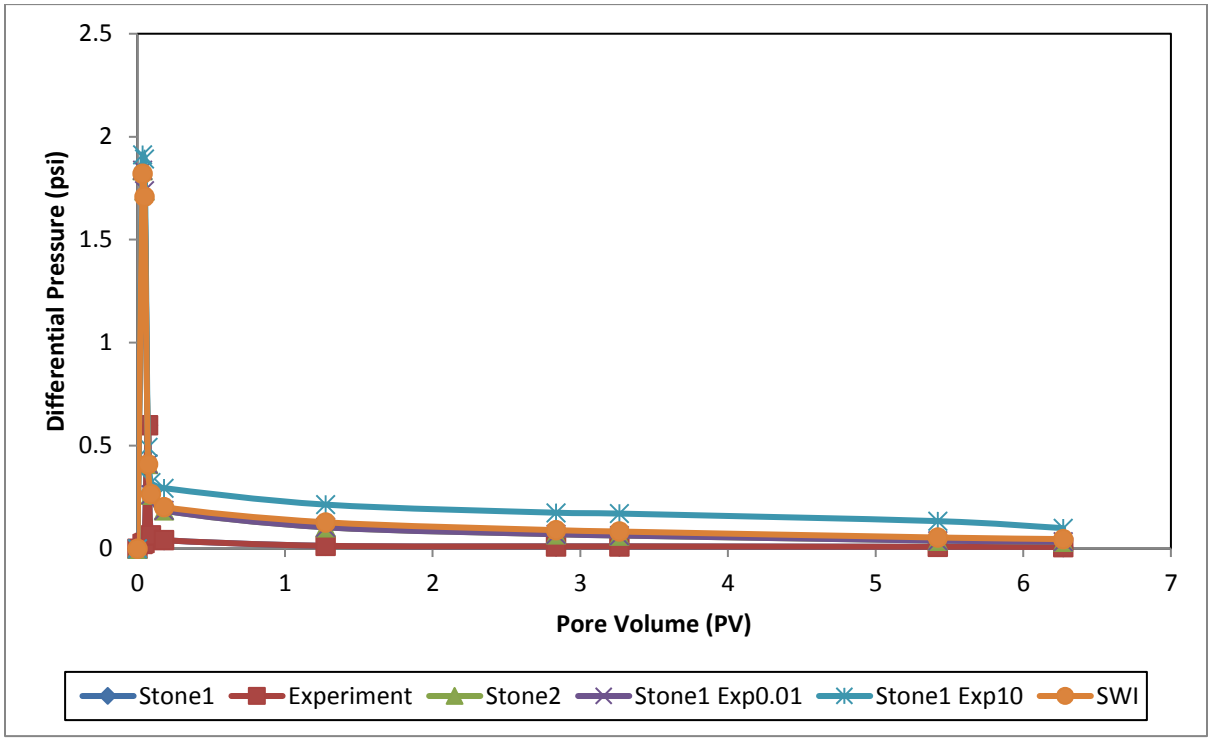

Figure 6.14: Differential pressure from the experiment and simulation (with different three phase relative permeability models) in the unsteady state core flood of crude C.

6.5 The Schrader Bluff Pool: tertiary CO_2 injection experiment

In order to investigate if the results so far seen in the three phase simulation of heavy oil in this project is applicable to other heavy oil projects reported in the literature, the three phase simulation of one of the Schrader bluff pool oil reservoir was conducted and reported in this thesis. The Schrader Bluff pool (Khataniar et al) is a heavy oil reservoir in the Alaskan North Slope. It is located in the Milne point unit of the West sak field. The reservoir is estimated to have over two billion barrels of heavy oil. The properties of the Schrader Bluff pool is shown in table 6.5.

Table 6.5: Reservoir and fluid properties for the Schrader Bluff Pool (Khataniar et al).

Depth	4000 - 5000 ft
Porosity	25 - 35 %
Permeability	100 - 6000 md
Reservoir Pressure	1300 psi
Reservoir Temperature	82 deg F
Oil Gravity	14 - 21 API
Oil Viscosity	200 - 600 cp

The coreflood experiment performed by Khatanir et al used a 4ft long and 2 inch diameter sandpack; and its porosity and permeability is 0.34 and 5100md respectively. In the experiment, conducted using live oil at 1300 psi and room temperature of 75 deg F, 0.05 PV of CO_2 at a rate of 4cc/min was injected into the oil-saturated core, followed by 1.15 PV of brine also injected at a rate of 4cc/min. The recovered oil and CO_2 were measured and recorded. Figure 6.17 shows the cumulative oil recovery result of the three-phase core-flood for the Schrader bluff reservoir.

6.5.1 Three Phase Simulation for Schrader Bluff Pool

The three phase flow in this experiment was simulated as a compositional system with the Eclipse 300 commercial simulator. Table 6.6 and 6.7, respectively, shows the fluid description and binary interaction coefficient of Schrader Bluff Pool oil used in this work.

Figure 6.15 and figure 6.16 are, respectively the Schrader Bluff oil/water and oil/CO2 relative permeability used in this three phase simulation. Simulations were made with different 3-phase relative permeability models (Saturated Weighted Interpolation, STONE1, STONE2, STONE1-exponents and ODD3P) and their performances are compared. Figure 6.17 shows the experimental and the simulation results of the cumulative oil recovery of the Schrader bluff pool oil reservoir WAG injection using different three phase relative permeability models. The results of the cumulative recovery of the other fluids were not reported in the literature.

Table 6.6: Fluid Description of Schrader Bluff Pool (Khataniar et al).

Component	z (mole fraction)	Pc (psi)	Tc (deg. R)	Vc (ft3/lb-mol)	Molecular Weight	Acentric Factor	Parachor
CO2	0.000436	1071.6	547.57	0.416	44.01	0.225	125.7429
C1	0.272149	667.8	343.04	1.602	16.04	0.013	45.8286
C2	0.004128	707.8	549.76	2.451	30.07	0.0986	85.9143
C3	0.010484	616.3	665.68	3.3	44.1	0.1524	126
nC4	0.02123	550.7	765.32	4.088	58.12	0.201	166.0571
nC5	0.02002	488.6	845.37	4.946	72.15	0.2539	206.1429
C6	0.022566	483.77	923	5.294	84	0.2583	240
C7-9	0.098746	415.41	1040.29	8.553	145.16	0.3165	311.8857
C10-13	0.100533	255.39	1199.64	13.11	223.26	0.4255	437.8857
C14-19	0.145138	203.91	1346.56	23.07	353.51	0.5768	638.6
C20-35	0.164159	158.03	1532.74	33.253	554.55	0.7659	1070.143
C36+	0.140411	94.8	1967.34	83.571	1052	1.1313	2062.857

Table 6.7: Binary Interaction Coefficient of Schrader Bluff Pool(Khataniar et al).

	CO2	C1	C2	C3	nC4	nC5	C6	C7-9	C10-13	C14-19	C20-35	C36+
CO2	0											
C1	0.07162	0										
C2	0.09399	0.00519	0									
C3	0.09759	0.01677	0.00394	0								
nC4	0.09397	0.03675	0.01226	0	0							
nC5	0.09034	0.04421	0.02316	0.00001	0	0						
C6	0.07454	0	0.03071	0.01065	0.00026	0.00003	0					
C7-9	0.09191	0.00001	0.0503	0.002209	0.00083	0.00045	0.00001	0				
C10-13	0.09863	0.00001	0.00497	0.00259	0.00205	0.00122	0.00001	0.00001	0			
C14-19	0.11636	0.1694	0.04511	0.02952	0.01012	0.01001	0.00001	0.00001	0	0		
C20-35	0.11636	0.17835	0.06547	0.005574	0.02093	0.01921	0.00002	0.00002	0	0	0	
C36+	0.16348	0.18222	0.13363	0.12456	0.05379	0.04953	0.00004	0.00002	0.00001	0.00001	0.00002	0

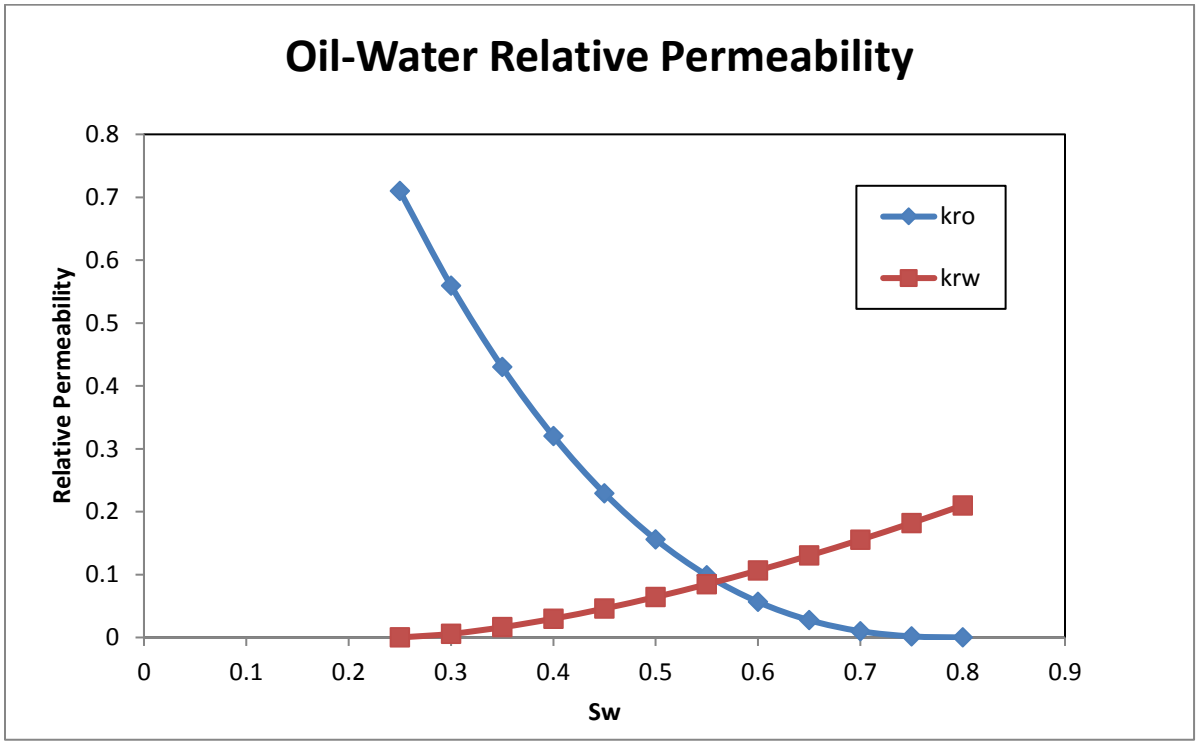

Figure 6.15: Schrader Bluff oil and Water relative permeability versus oil saturation (Khataniar et al).

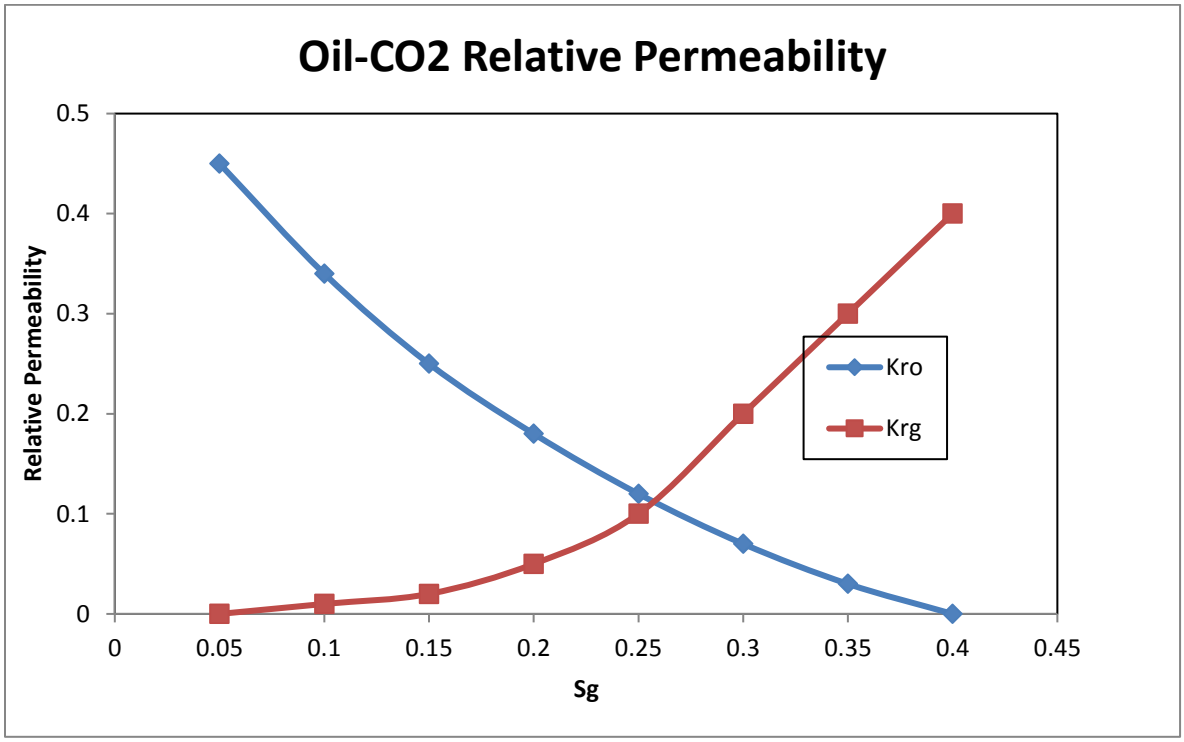

Figure 6.16: Schrader Bluff oil and CO_2 relative permeability versus oil saturation (Khataniar et al) .

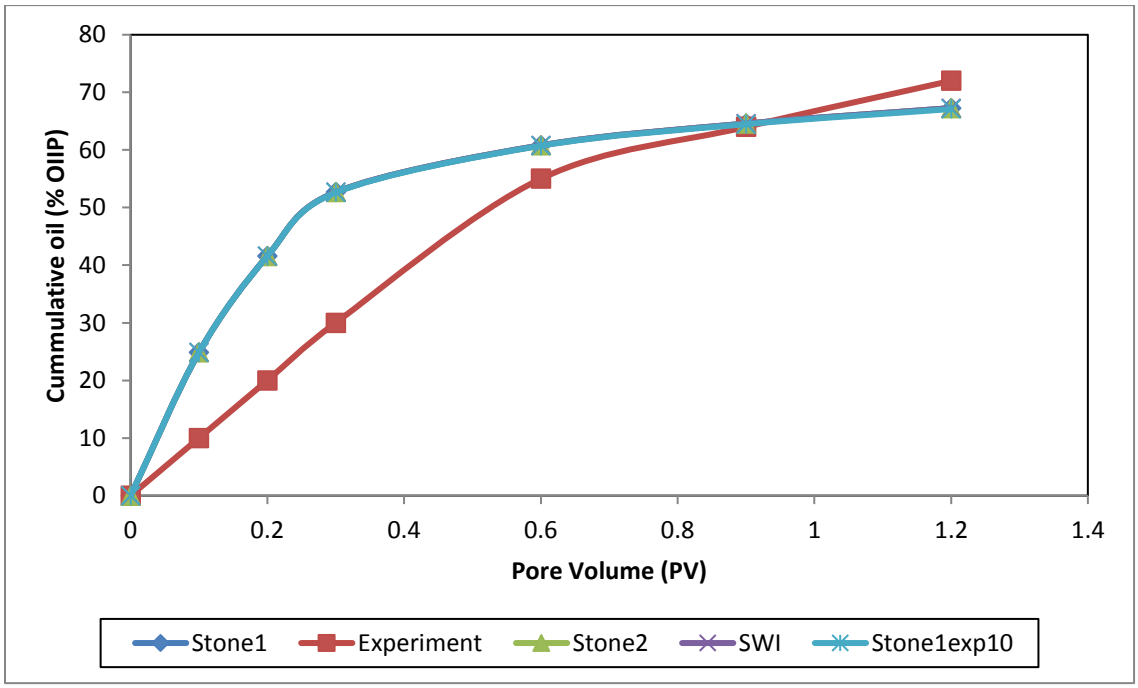

Figure 6.17: Cumulative oil recovery from the experiment and simulation (with different three phase relative permeability models) in the unsteady state core flood of Schrader Bluff oil.

6.6 Error Analysis

The standard error of estimate (shown below) is used to obtain the error value between the simulation and experimental results.

$$\text{SEE\%} = \sqrt{\frac{\sum_{i=1}^{n}\left(\frac{Q_{Exp} - Q_{Sim}}{Q_{Exp}}\right)^2}{n-1}} \tag{6.17}$$

where SEE % is the percentage of standard error of estimate, n is the data points number, and Q_{Exp} and Q_{Sim} are the experimental and simulation data respectively. The data are the production data (cumulative oil, cumulative water, cumulative gas) and the differential pressure data.

Figure 6.11 shows the error chart of the oil, water, gas and differential pressure obtained by comparing experimental and simulation results of WAG injection of pre-equilibrated crude J and all the average errors of all the production and pressure drop (SEE %) of pre-equilibrated crude J is shown in Figure 6.12. And similarly for crude J experiment, figure 6.13 shows error chart of oil, water, gas and differential pressure for different three phase relative permeability models; and figure 6.14 shows the average errors chart for crude J.

For the pre-equilibrated crude J, 13cp pre-equilibrated oil, where there is no mass transfer, the SWI three-phase model gives the lowest mismatch (7.7 %) in oil production while the Stone1exp0.1 gives the lowest average mismatch of 15.7 %. However, for crude B, with a viscosity of 600cp oil, the Stone1exp10 gives the lowest mismatch (37.6 %) in oil production and the lowest average mismatch of 26.7 %. For the 13 cp pre-equilibrated crude J system, the figures (especially the mismatch in oil production) fall within acceptable limits; however, for the 600cp crude J system, the mismatch values of 30% and above is clearly in the unacceptable realm. It seems from the above that the more viscous the crude is, the higher the level of mismatch, and hence the unsuitability of the existing correlations in commercial simulation software for predicting three-phase flows in highly viscous fluid.

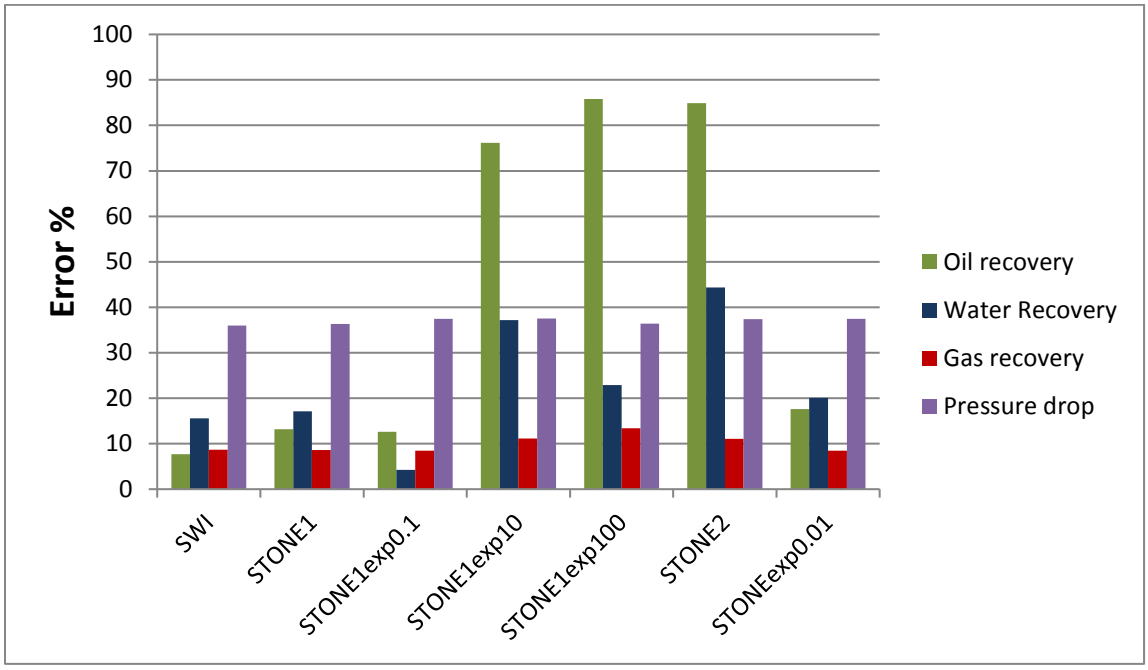

Figure 6.18: SEE% of oil, water, gas and differential pressure obtained by comparing experimental and simulation results of WAG injection of pre-equilibrated crude J *using the different three phase relative permeability models in Eclipse simulator*.

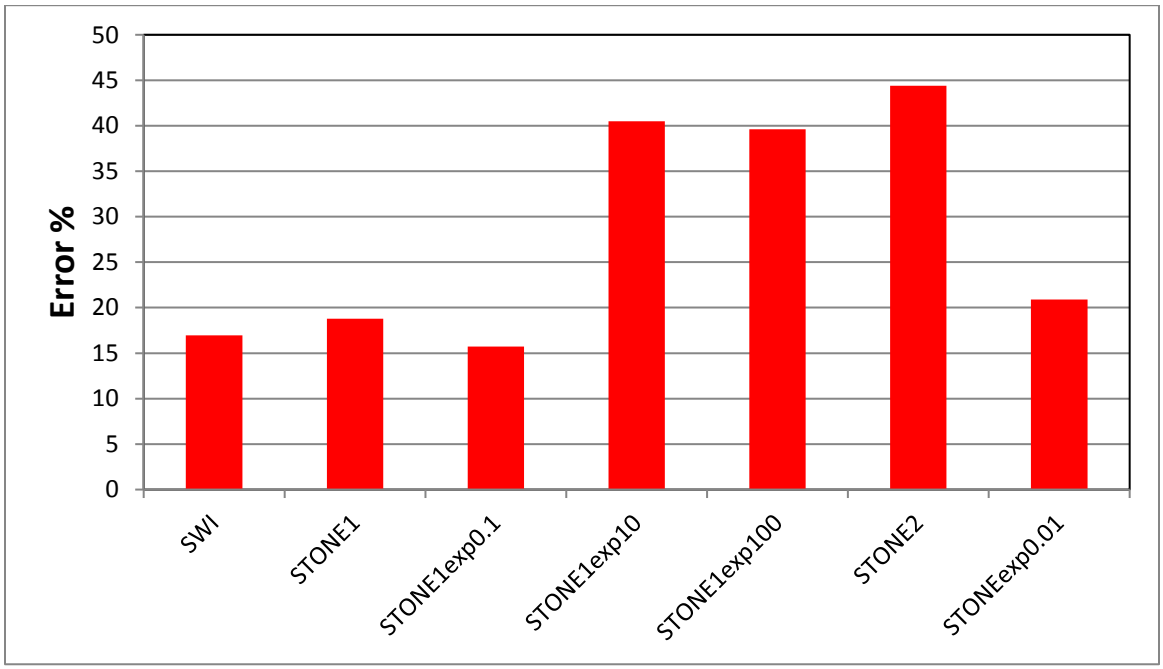

Figure 6.19: Average errors of all production and pressure drop (SEE %) obtained by comparing experimental and simulation results of WAG injection of pre-equilibrated crude J system *using the different three phase relative permeability models in Eclipse simulator.*

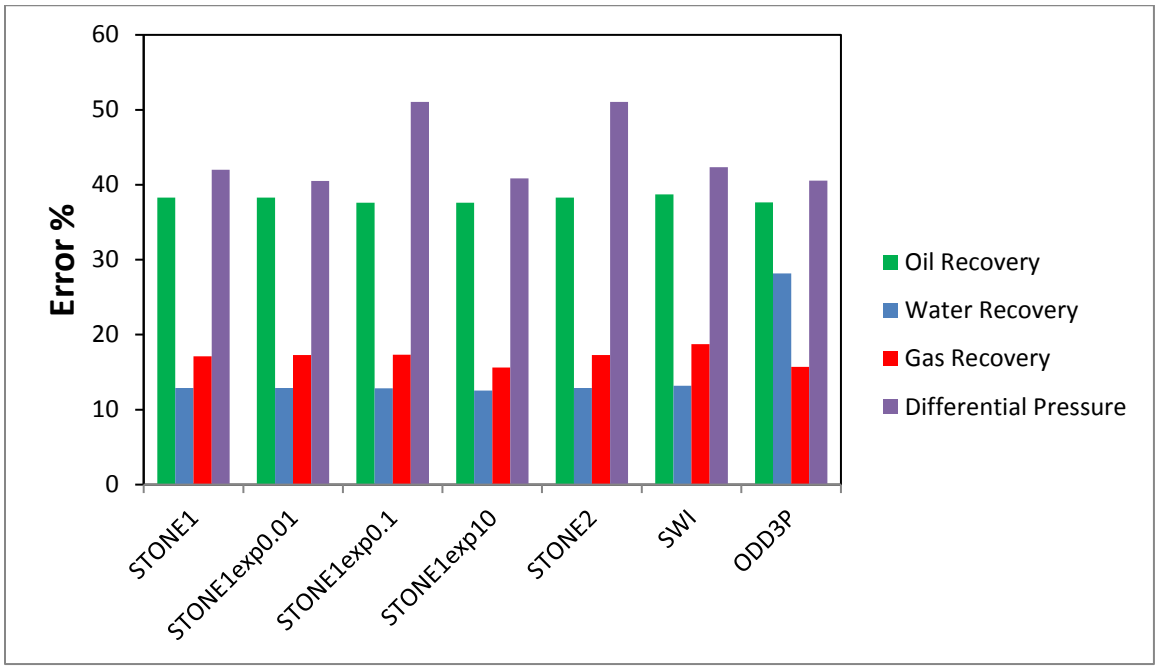

Figure 6.20: SEE% of oil, water, gas and differential pressure obtained by comparing experimental and simulation results of WAG injection of crude J using the different three phase relative permeability models in Eclipse simulator.

Figure 6.21: Average errors of all production and pressure drop (SEE %) obtained by comparing experimental and simulation results of WAG injection of crude J using the different three phase relative permeability models in Eclipse simulator.

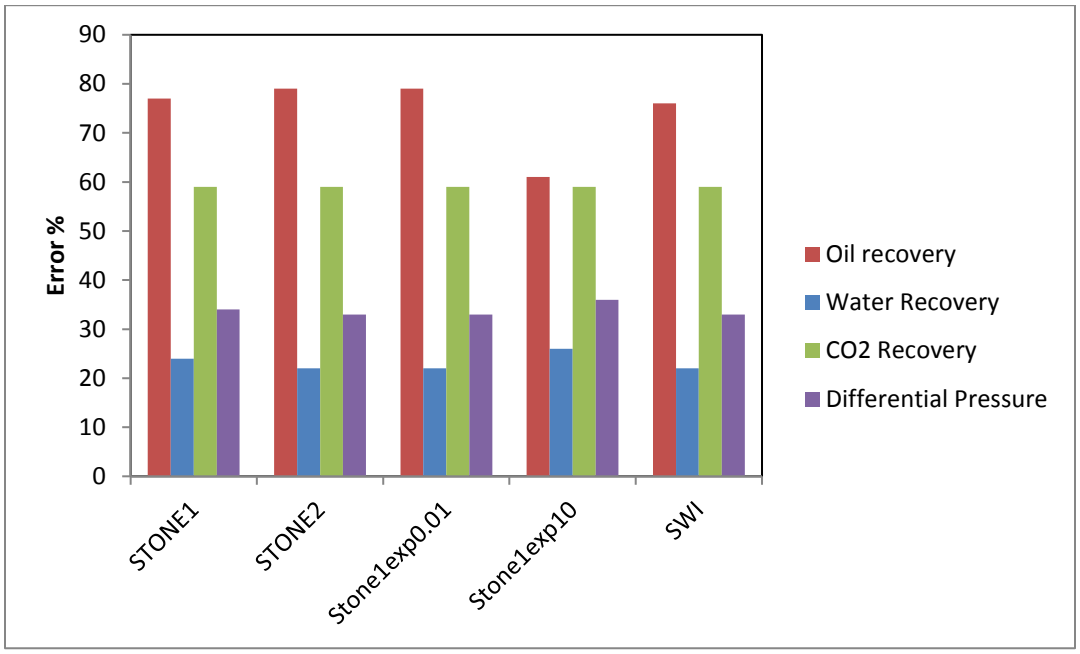

Figure 6.22: SEE% of oil, water, gas and differential pressure obtained by comparing experimental and simulation results of WAG injection of crude C using the different three phase relative permeability models in Eclipse simulator.

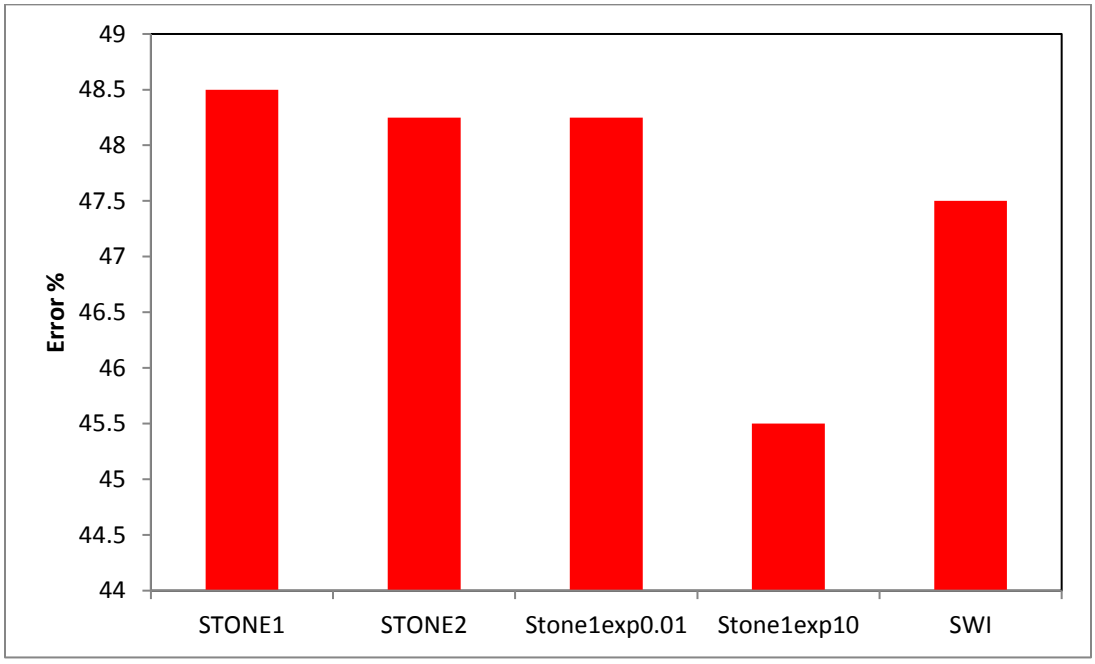

Figure 6.23: Average errors of all production and pressure drop (SEE %) obtained by comparing experimental and simulation results of WAG injection of crude C using the different three phase relative permeability models in Eclipse simulator.

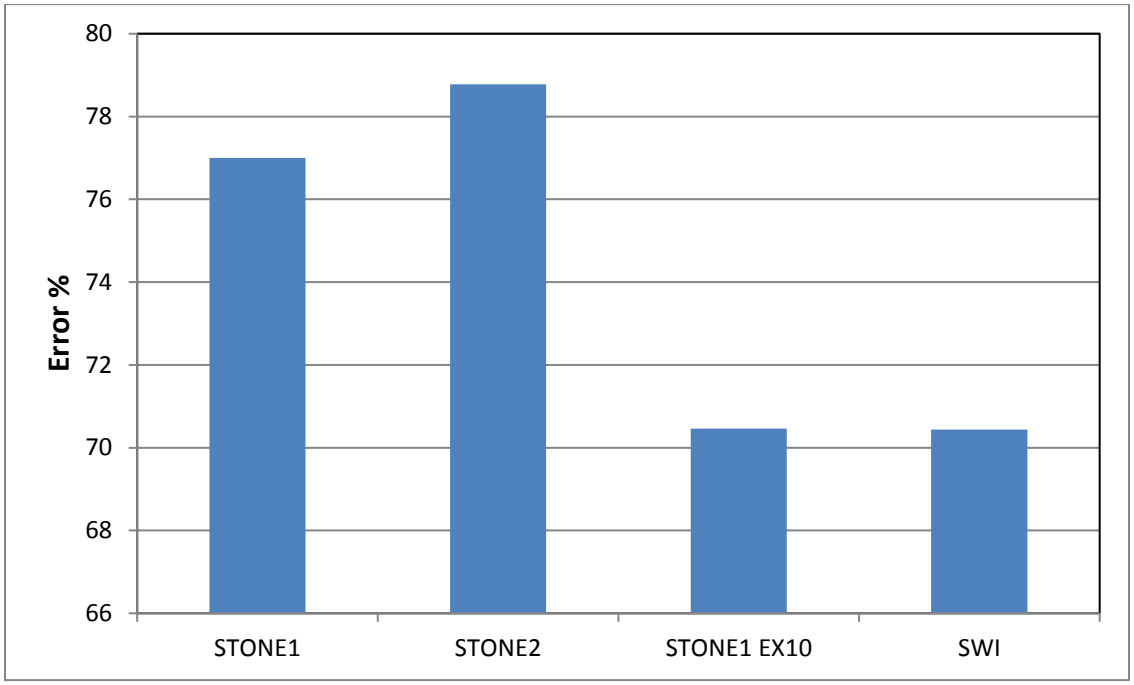

Figure 6.24: SEE% of oil obtained by comparing experimental and simulation results of WAG injection of Schrader Bluff Oil using the different three phase relative permeability models in Eclipse simulator.

6.7 Automatic History Matching Technique

From the simulation results, it is seen that none of the existing relative permeability models can predict satisfactorily the production and pressure performance of a three phase flow for heavy oil. It is also seen from the results that the three phase relative permeability models become less suitable as the viscosity of the oil increases. A computer optimization program, developed in the research group at the Institute of Petroleum Engineering, Heriot Watt University (Sharverdi, 2012) was used to obtain three phase relative permeability from unsteady state displacement experiments. This is an automatic History Matching technique that uses numerical iteration to match the three phase coreflood experimental data with the use of an optimization program that is linked to the Eclipse simulator. In this work the relative permeability of the three phases in crude A, are estimated in an optimization manner such that the difference between measured and simulated values is minimized. The program

gives an estimate of the relative permeability using a mathematical function (e.g Corey) that represents a relationship between relative permeability and phase saturations. The calculation always starts with an initial guess of relative permeability into the program, then the difference between modelling and experimental result is iteratively minimized by adjusting the parameters of the mathematical function till an error tolerance is reached. This method accommodates capillary pressure in the estimation of the relative permeability, and each relative permeability curve is assumed to be a function of two saturation values.

Using this program, the simulation result of the oil, CO_2, water recovery, and the corresponding pressure drop across the core when compared with the measured data for crude A three phase experiment is shown in Figure 6.15 to 6.18. The three phase relative permeability from the program is also shown in Figure 6.19 to Figure 6.21. It is evident from this comparison that there is good agreement between the experiment results and the simulation results thereby suggesting the suitability of the optimization program in predicting three phase flow in heavy oil system.

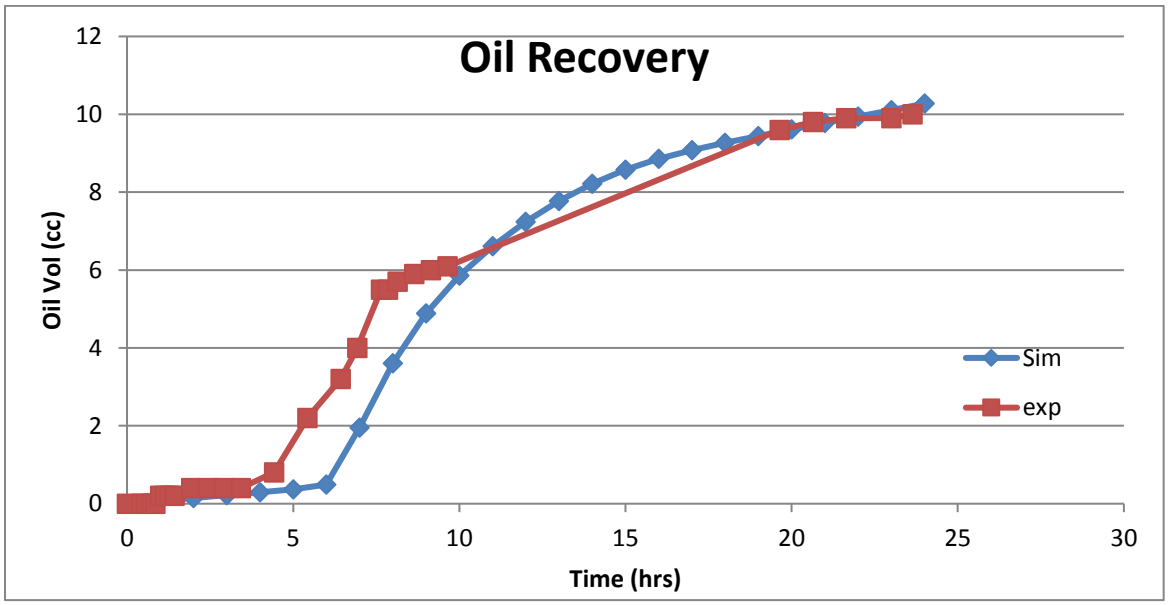

Figure 6.25: Cumulative oil recovery from the experiment and simulation (automatic history matching of the three phase experiment) in the unsteady state core flood of the pre-equilibrated crude J.

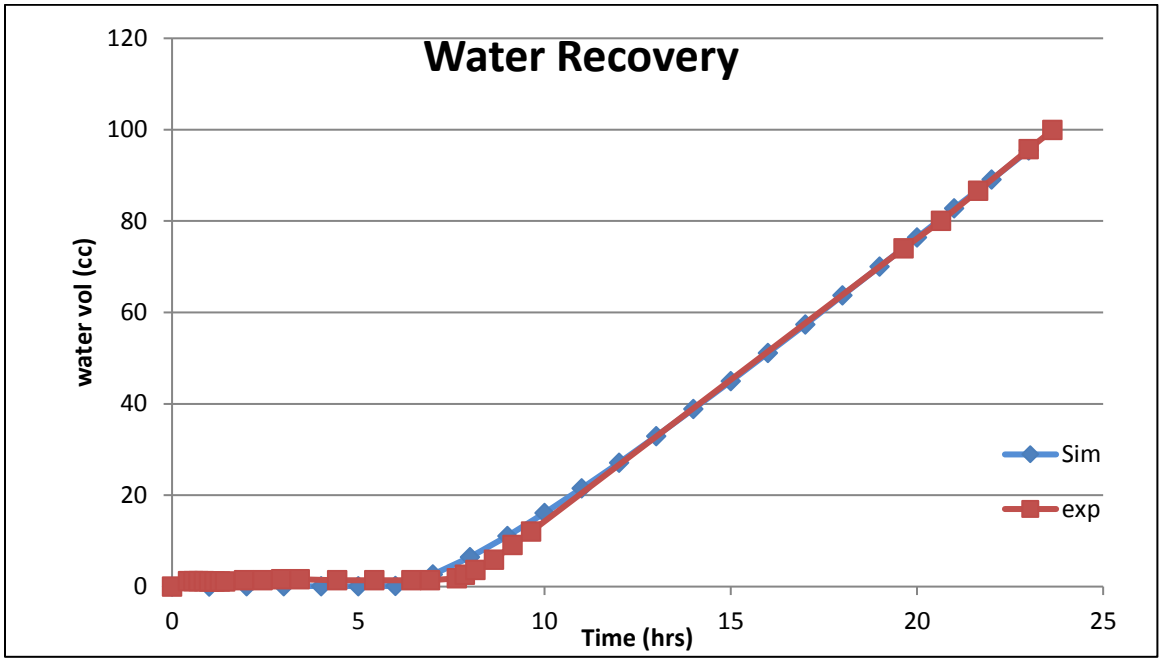

Figure 6.26: Cumulative water recovery from the experiment and simulation (automatic history matching of the three phase experiment) in the unsteady state core flood of the pre-equilibrated crude J.

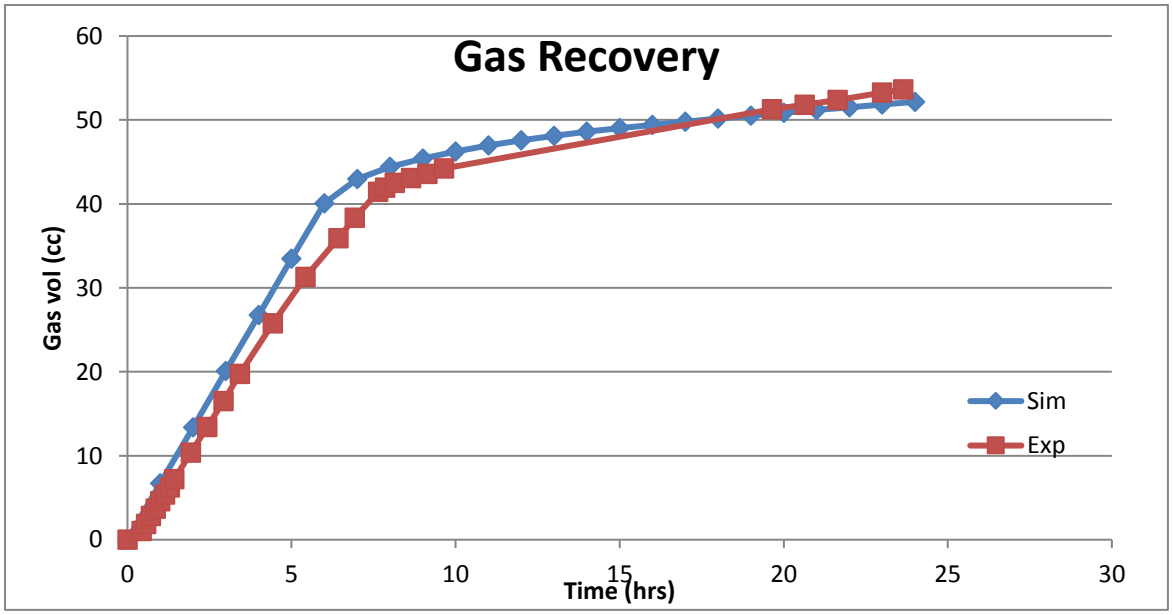

Figure 6.27: Cumulative gas recovery from the experiment and simulation (automatic history matching of the three phase experiment) in the unsteady state core flood of the pre-equilibrated crude J.

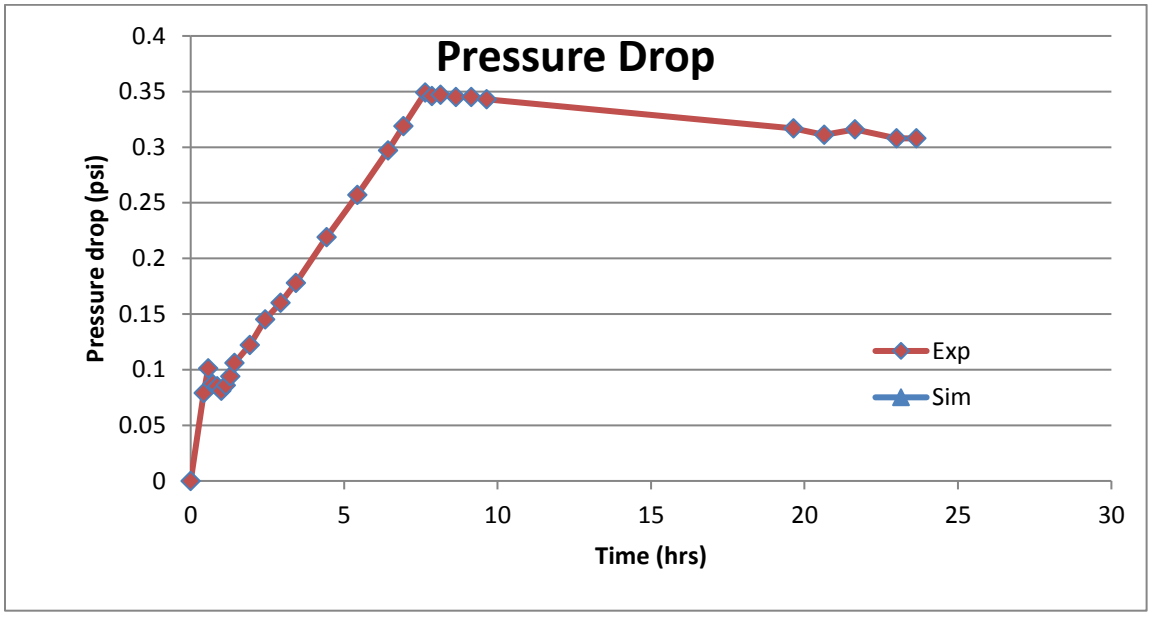

Figure 6.28: Differential pressure from the experiment and simulation (automatic history matching of the three phase experiment) in the unsteady state core flood of the pre-equilibrated crude J.

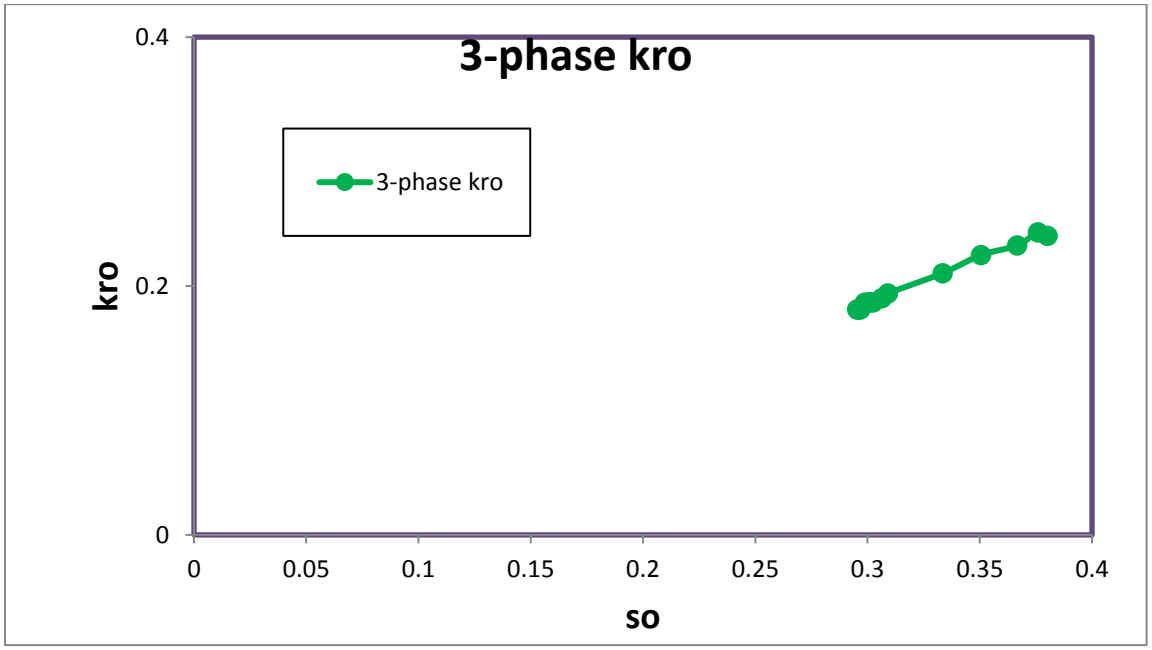

Figure 6.29: Oil relative permeability curve obtained from the automatic history matching of the three phase flow of the pre-equilibrated crude J.

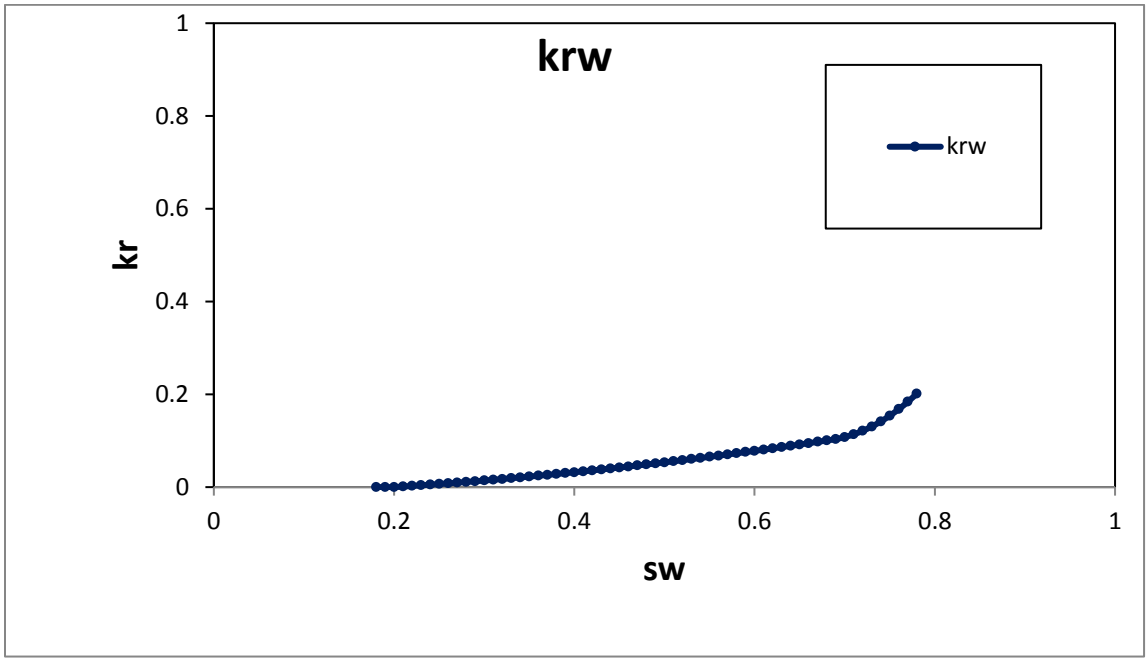

Figure 6.30: Water relative permeability curves obtained from the automatic history matching of the three phase flow of the pre-equilibrated crude J.

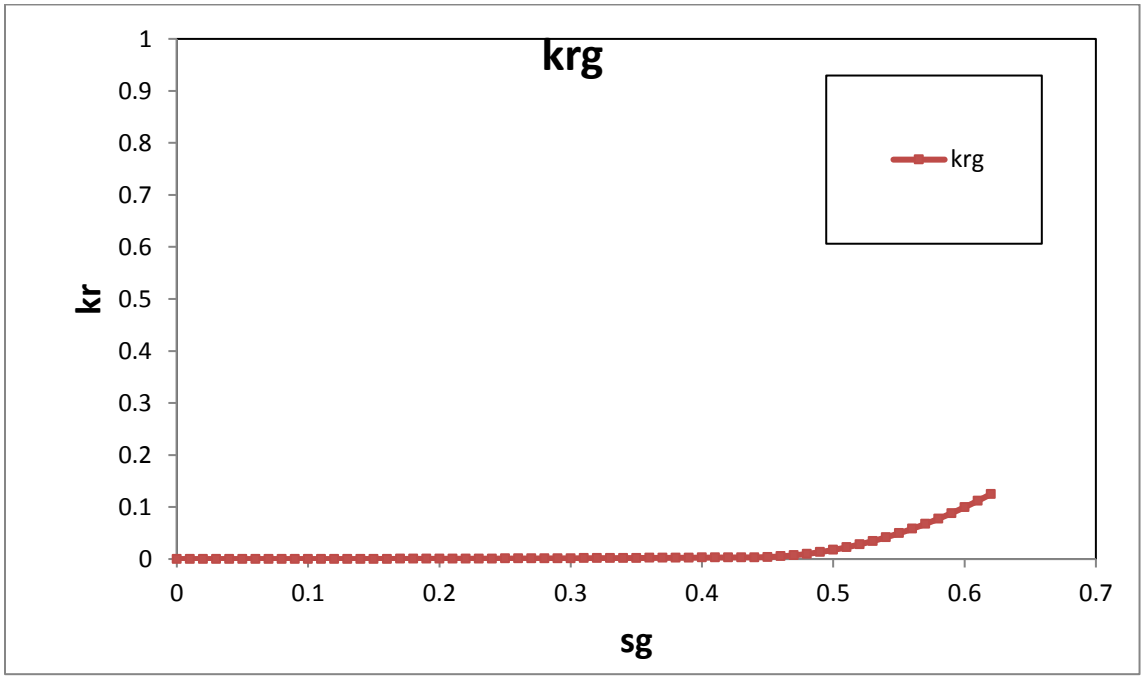

Figure 6.31: Gas relative permeability curves obtained from the automatic history matching of the three phase flow of the pre-equilibrated crude J.

6.7.1 JBN Relative Permeability

Two-phase relative permeabilities from unsteady-state core flooding data are usually computed explicitly using JBN method (Johnson et al, 1959) by neglecting capillary pressure effect. Li et al (1994) developed a new analytical method to calculate oil-water relative permeabilities with capillary pressure included. The water and oil relative permeability from this technique is given thus:

$$k_{rw} = f_{w2}\frac{d[\frac{1}{Q}]}{d[\frac{k(\Delta P+\rho_w gLsin\alpha)}{Q}]} \tag{6.18}$$

$$k_{ro} = \frac{\mu_o f_{o2}}{\frac{\mu_w f_{w2}}{k_{rw}} - \frac{k}{v(t)}[(\rho_w-\rho_o)gsin\alpha + \frac{dP_c}{dS_w}\frac{\partial S_w}{\partial x}]} \tag{6.19}$$

Where

And for three phase flow, the gas relative permeability, as derived by Sarem (1966) is used:

$$k_{rg} = k_{ro}\frac{\mu_g f_g}{\mu_o f_o} \tag{6.20}$$

The relative permeability from the JBN method for the three fluids is compared with relative permeability from the automatic history match technique, and the comparison is shown in Figure 6.22 to 6.24. The match in the water and gas relative permeability between the automatic history matching techniques is good but not good in the oil relative permeability. This match would have been worse if capillary forces had not been taken into consideration as in the conventional JBN method where capillary forces are always ignored because capillary forces can be very significant in heavy oil processes. The imperfect match seen in this case, however, suggests that the JBN method used in this work, despite the inclusion of capillary pressure, is less than perfect in predicting three-phase relative permeability curves for heavy oil flow processes. A possible explanation for this unsuitability might not be unconnected with the error-prone nature of the recovery data in heavy oil systems.

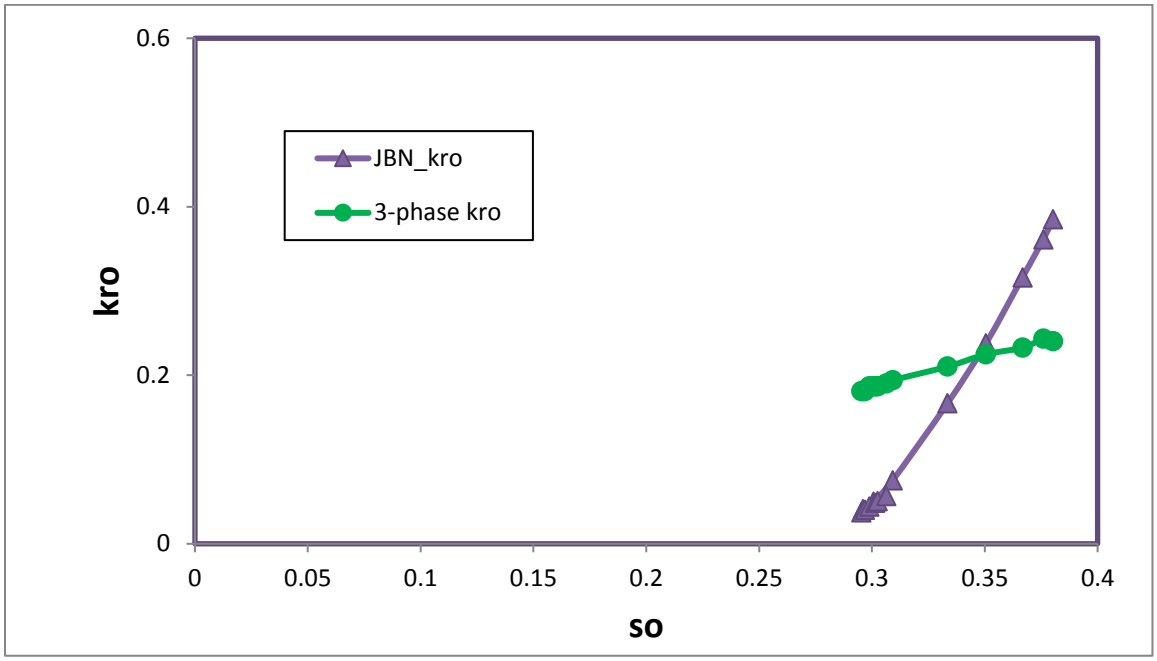

Figure 6.32: Comparison of Oil relative permeability curve obtained from JBN and oil relative permeability obtained from the automatic history matching of the three phase flow of the pre-equilibrated crude J.

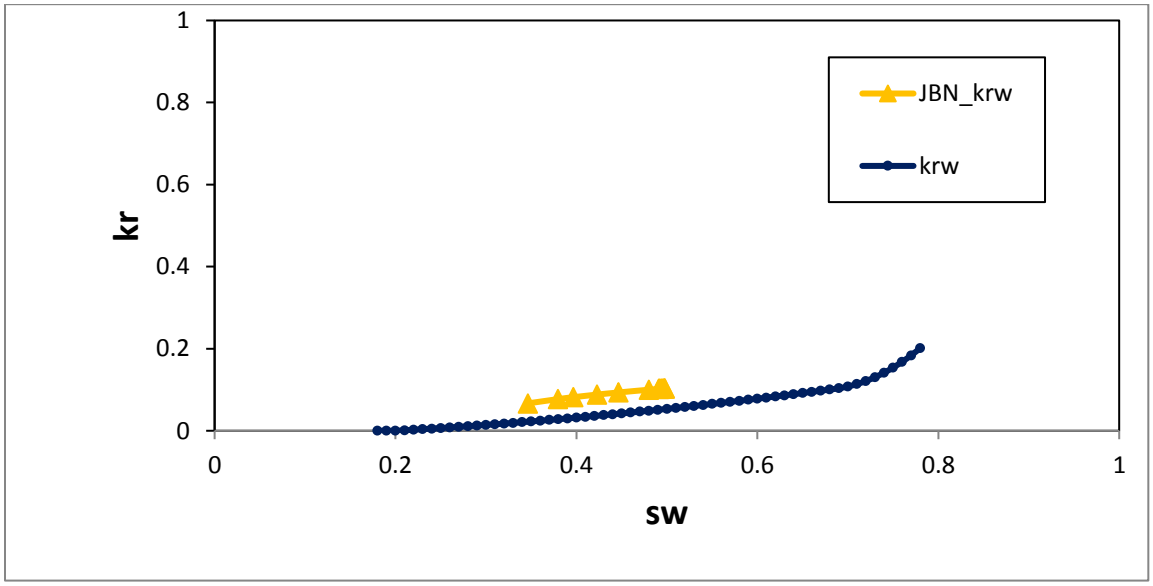

Figure 6.33: Comparison of Water relative permeability curves obtained from JBN and water relative permeability obtained from the automatic history matching of the three phase flow of the pre-equilibrated crude J.

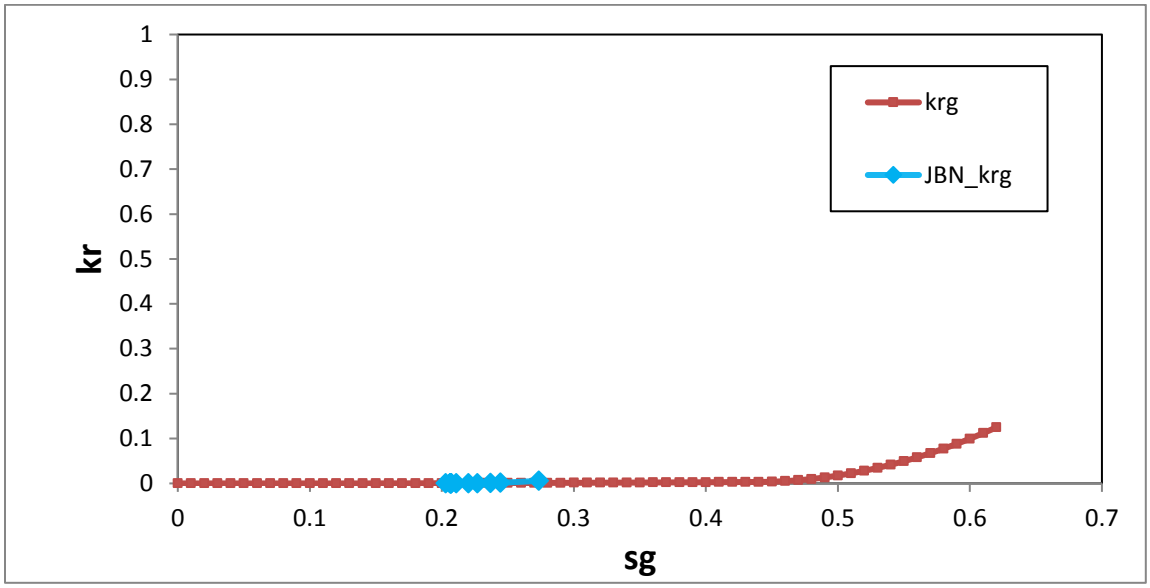

Figure 6.34: Comparison of Gas relative permeability curves obtained from JBN and gas relative permeability obtained from the automatic history matching of the three phase flow of the pre-equilibrated crude J.

6.8 Results and Discussion

Two Water Alternate CO_2 heavy oil core flood experiments were simulated using the existing three phase relative permeability models, and the comparisons of the simulation and the core flood experimental results were made. The modelling of the first experiment, the pre-equilibrated crude J, with a viscosity of 13cp, where both the gas and the oil were pre-equilibrated before injection into the core, achieved an acceptable match of the recoveries. The SWI three-phase model gives a mismatch of 7.7 % in oil production, which falls in the acceptable region. Exact matches were also in the water and gas recovery but their trends were accepted as representative of the displacement mechanisms in the system.

However, the modelling of the second experiment, Crude J, with a viscosity of 600cp, where both the gas and the oil were not pre-equilibrated before injection into the core, achieved a poorer match of the recoveries with the Stone1exp10 giving a mismatch of 37.6 % in oil production. This trend suggests that the more viscous the crude is, the higher the level of mismatch, and hence the unsuitability of the existing correlations in commercial simulation software for predicting three-phase flows in highly viscous fluid. This conclusion is

supported by the results of the three phase simulation of both crude C and the Schrader Bluff pool.

For displacement processes in the unstable region, the more viscous a fluid is, the more unstable the displacement process becomes, and the less the likelihood that the relative permeability from such displacement processes would conform to conventional relative permeability theories. The suitability of three phase relative permeability models to simulate three phase flow processes hence decreases as the viscosity of the fluids increases. This is also supported by the fact that the available three phase relative permeability models are developed through the observation of recovery mechanisms in conventional oil which to a large extent does not suffer the consequences of displacement instability like viscous fingering. It thus follows that since the recovery mechanism in conventional oil is different from that in heavy oil, the conventional relative permeability models cannot be used in simulating three phase flow processes in heavy oil.

As shown in figure 6.22 to 6.24, the JBN method (with capillary pressure) is not adequate in generating three-phase relative permeability curves for three phase processes especially in heavy oil processes. The use of the JBN method would be difficult in heavy oil processes because production data from heavy oil processes are by nature prone to error, and hence may introduce significant errors to the error-sensitive JBN relative permeabilities estimation method.

As a result of the inadequacy in the simulation capacity of the three phase relative permeability models and the JBN methods to simulate heavy oil processes, an alternative simulation approach, automatic history match approach, was sought. This approach produced a very good match between the experimental results and the simulation results thereby suggesting the suitability of the optimization program in predicting three phase flow in heavy oil system.

6.9 Conclusion

The adequacy of existing three phase relative permeability models to simulate three phase flow in heavy oil reservoirs has been investigated and the simulation results were compared with the experimental results. Though the channel flow assumption used in developing the

models was confirmed in a micro-model experiment for heavy oil processes, the models were found to be inadequate for the simulation of these processes. The other conclusions reached from this work are:

- In an unstable displacement process which is typical of heavy oil system, the more viscous the oil is, the less the suitability of the existing three phase models to simulate oil recovery in WAG and other three phase flow processes.
- Though exact matches were not obtained in the oil, water and gas recovery but their trends were accepted as representative of the displacement mechanisms in the system. This trends however worsen as the viscosity of the oil increases
- The JBN method of estimating relative permeability is not adequate in estimating three phase relative permeability in heavy oil processes
- The automatic history matching of the three phase experimental results of heavy oil can give very useful relative permeability results but it is laborious and it takes a long time to get a reasonable match of the experiment.

6.10 References

1. Al-Shuraiqi, H.S., Grattoni, C.A., Muggeridge, A.H., 2005, 'Numerical and Experimental Investigation into the effects of Viscosity and Injection rate on Relative Permeability and Oil Recovery'. SCA2005-40, International Symposium of the Society of Core Analysts held in Toronto, Canada; August 21−25.
2. Baker, L.E., 1998, 'Three phase relative permeability correlations,' paper SPE 17369 presented at the SPE enhanced oil recoverysymposium, Tulsa, Oklahoma.
3. Buckley, S. E., Leverett, M. C., 1942, "Mechanism of Fluid Displacement in Sands", Petroleum Transactions, AIME, Vol. 146, pp 107-116.
4. Cao, P., 2010, 'Three phase unsteady state relative permeability measurement' the international symposium of the society of core analyst, Halifax, Canada.
5. Carlson, F.M., 1981. 'Simulation of Relative Permeability Hysteresis to the Non-wetting Phase.' Paper SPE 10157 presented at the SPE annual Technical Conference and Exhibition, San Antonio, Texas, USA, 4-7 October. DOI:10.2118 /10157-MS.
6. Dake, L.P, 1978,'Fundamentals of Reservoir Engineering.',1st Edition, 100-125 Amsterdam, ELSEVIER.

7. Delshaid, M. And Pope, G.A., 1989, comparison of the three phase oil relative permeability models: transport in porous media, 4(1), p. 59-83.

8. Dietrich, J.K. and Bondor, P.L., 1976, 'Three phase oil relative permeability models,' SPE paper 6044, proceedings of 51st Fall Technical conference and Exhibition of Society of Petroleum Engineers and AIME, New Orleans, LA, Oct. 3-6.

9. Dyer, S.B., and Farouq Ali S.M. 1994. Linear Model Studies of the Immiscible CO_2 WAG Process for Heavy-Oil Recovery,' SPE 21162. *SPE Res Eval& Eng* 9 (2): 107-111.

10. Emadi, A., 2012 'Enhanced Heavy oil recovery by water and carbon dioxide flood' Phd thesis, PhD thesis, Heriot Watt University, IPE.

11. Huang, D.D., Honarpour, M.M., 1996, 'Capillary end effects in coreflood calculations'. SCA-9634, International Symposium of the Society of Core Analysts, Montpellier, France, September 8-10.

12. Hustard, O., and Holt, H., 1972, 'Gravity Stable Displacement of Oil and Gas after Water flooding' SPE paper 24116, SPE/DOE symposium on EOR, Tulsa, OK, April 22-24.

13. Hustard, O.S., & Hansen A.G., 1995, 'A consistent correlation for three phase relative permeabilities and phase pressures based on three sets of two phase data' 8th EAPG Improved Oil Recovery European Symposium, Vienna, 1: 289.

14. Johnson, E.F., Bossler, D.P., Naumann, V.O., 1958, 'Calculation of Relative Permeability from displacement Experiments', Petroleum Transactions, AIME, Vol. 216, pp 370-372.

15. Kamp, A.M., Joseph, D.D., Bai, R., 2001, 'A New Modelling Approach for Heavy Oil Flow in Porous Media' SPE 69720, SPE thermal operations and Heavy Oil Symposium, Poriar, Venezuella, March, 12-14.

16. Katayoun S. N., Eirik A.B., Jon K.R., 2011, 'Effect of Oil Viscosity on Water/Oil Relative Permeability' SCA2011-12, International Symposium of the Society of Core Analysts held in Austin, Texa, USA, September 18−21.

17. Khatanir, S., Kamath, V.A, Patil, S.L., Chandra, S., Inaganti, M.S., 1999, 'CO2 and Miscible Gas Injection for Enhanced Recovery of Schrader Bluff Heavy Oil' SPE 54085, SPE international Thermal Operations and Heavy Oil symposiums held in Bakersfield, California, 17-19 March.

18. Ko, S.C.M,, Domier, D.B., MacDermott, R.N., 1995, 'Waterflood Optimization of the Buffalo Coulee Bakken Heavy oil Pool of Southwestern Saskatchenwan' SPE 30285-MS, International Heavy Oil Symposium, Calgary, Alberta, Canada, June 19-21.

19. Li, K., Shen, P., Qing, T., 1994, 'A New Method for Calculating Oil-Water Relative Permeabilities with consideration of Capillary Pressure' Mechanics and Practice, V. 16, No. 2,1994

20. Mai, A., Kantzas, A., 2007, 'Heavy oil Waterflooding: Effects of Flowrate and Oil viscosity'. In the proceedings of the 8th Canadian International Petroleum Conference Calgary, Alberta, Canada; June 12-14.

21. Mai, A., Kantzas, A., 2008, 'Improved Heavy Oil Recovery by Low Rate Water flooding'. In the proceedings of the International Thermal Operations and Heavy Oil Symposium, , Calgary, Alberta, Canada; October 20−23 SPE Paper 117648.

22. Maini, B.B., 1995, 'Is It Futile to Measure Relative Permeability For Heavy Oil Reservoirs?', In the proceedings of the 46th Annual Technical Meeting, Petroleum Society of CIM, Banff, Canada, May 14-17.

23. Oak, M. J., Baker, L. E. and Thomas, D. C., 1990, Three-phase relative permeability of Berea sandstone,' J. Pet. Technol. 42(8), 1054–1061.

24. Oak, M.J, (1990) 'Three phase relative permeability of water-wet Berea,' SPE 20183, proceedings of the SPE/DOE Enhanced Oil Recovery Symposium, Tulsa, Oklahoma.

25. Odd Steve Hustard, 2002, 'A Coupled Model For Three-Phase Capillary Pressure and Relative Permeability' SPE paper -704705-PA. Society of Petroleum Engineers Journal.

26. Odd Steve Hustard, David J. Browning, 2010, 'A fully Coupled Three-Phase Model for Capillary Pressure and Relative Permeability for Implicit Compositional Reservoir Simulation' SPE paper -125429-PA. Society of Petroleum Engineers Journal.

27. Odeh, A.S., 1959,'Effect of Viscosity Ratio on Relative Permeability.' SPE-1189-G, Society of Petroleum Engineers.
28. Parish, D.R., (1966) 'Flooding process for recovery of oil.' US Patent No. 3,244,228.

29. Ruben Juanes, Blunt, M.J., 2007, 'Impact of viscous Fingering on the Prediction of Optimum WAG Ratio, SPE-99721-PA, Society of Petroleum Engineers Journal, Vol. 4, Issue 04.

30. Schlumberger 2011, Eclipse reservoir simulation Technical manual, version 2011.1.

31. Sharverdi, H., (2012), Characterization of three phase flow and WAG injection in oil reservoirs' PhD thesis, Heriot Watt University, IPE.

32. Sobers, L.E., 2012, 'Injection design for simultaneous enhanced oil recovery and carbon storage in a heavy oil reservoir' PhD thesis, Imperial College, London.

33. Sohrabi, M., Tehrani, D.H., Danesh, A., Henderson, G.D, 2000, 'Visualisation of Oil Recovery by Water Alternating Gas (WAG) Injection Using High Pressure Micro-

models – Water-Wet System' paper SPE 63000, Annual Technical Conference and Exhibition, Dallas, Texas, USA, October 1-4,

34. Spearing M.C, Davies A.S, Element D.J, Goodyear, S.G. and Law, E.J., 2002, 'A Focused Relative Permeability SCAL Study Driven by Reservoir Management Decisions', SCA2002-02.

35. Stalkup, F.I. Jr., 1983, 'Miscible Displacement, 'SPE Monograph Series,Vol. 8. Dallas: Society of Petroleum Engineers.

36. Stone, H.L., 1970 ' Estimation of three phase relative permeability and residual oil data,' PETSOC- 73-04-06, Journal of Canadian Petroleum Technology.

37. Stone, H.L., 1973 'Probability model for estimating three phase relative permeability,' SPE-2116, SPE Journal of Petroleum Technology.

38. Wang, J., Dong, M., Asghari, K., 2006, 'Effect of Oil Viscosity on Heavy Oil /Water Relative Permeability Curves ' Society of Petroleum Engineers. SPE 99763.

39. Weatherford Petroleum Consultants, 2005, Sendra user guide, version 2011.3

40. Wyckoff, R.D. and Botset, H.G., 1936, 'The Flow of Gas-Liquid Mixtures through Unconsolidated Sands," Journal of Applied Physics, Vol. 7, Issue 9.

Chapter 7: Summary and Conclusion

7.1 Summary

The scarcity of information on heavy oil relative permeability often leads to the erroneous application of the conventional oil relative-permeability assumptions in the simulation of heavy oil processes. This work investigated the suitability of these assumptions in estimating the relative permeability of heavy oil displacement processes. An assumption in the estimation of conventional oil relative permeability from experiments is that oil viscosity and core placement orientation have no influence on the estimates. However, heavy oil displacement processes often suffer from instability at the displacement front, and consequently viscous fingering.

The estimation of the relative permeability curves of conventional oil is always done through a 1D-model because of the negligibility of the changes in saturation in the other directions apart from the main flow direction. For heavy oil, however, the relative permeability from a 1D-model is a pseudo-relative permeability since it is impossible to capture effects of displacement front instability like viscous fingering in a 1D-system. In this work, the relative permeability curves from several heavy oil core flood experiments were estimated using 1D and 2D models.

These experiments involve different heavy oil viscosities, and different core orientations. The relative permeability curves estimated from these core flood experiments were found to vary with the oil viscosity, and the relative permeability curves obtained from cores in vertical direction during flooding were also observed to be different from those obtained from cores placed in the horizontal direction. The explanation for this is that for there is instability at the displacement front of most heavy oil systems leading to viscous fingering. Unlike in conventional oil systems where displacement is controlled by capillary forces, heavy oil systems beyond a particular instability number (13) are controlled by viscous forces and viscous forces vary with viscosity and their effects can be controlled by gravity forces. Instability numbers were computed for all the cases and a relationship between the instability numbers and the end point values was established. Furthermore, the comparison of the set of 1D and 2D relative permeability estimates from each experiment shows that below a certain instability number (13), there is no difference between the 1D and 2D relative permeability

curves. But beyond this number, there is a relationship between the instability numbers and the differences between the 1D and 2D curves.

This work also estimated relative permeability of heavy oil systems with the analytical method, and it was found that both the JBN and the graphical method can be used to estimate the relative permeability of heavy oil systems but they are still inadequate when compared with the automatic history matching method of estimating relative permeability for heavy oil.

Another challenge in estimating relative permeability in heavy oil systems involving CO_2 is that CO_2 is partially soluble in heavy oil thereby reducing its viscosity and interfacial tension, and hence making it unsusceptible to the standard industry practice of using the estimated gas and oil relative permeability curves from an immiscible core flood experiments. In this work it was demonstrated that substitute relative permeability like the one from N2/heavy oil and immiscible CO_2/ pre-equilibrated heavy oil system may not be adequate in simulating a partially soluble CO_2/heavy oil process. The use of nitrogen/heavy oil relative permeability curves to simulate CO_2 injection into heavy oil under-predicts the recovery since the estimation of these curves does not take into consideration the effect of the dynamic interfacial tension between CO_2 and heavy oil during the flooding process on its relative permeability curves. On the other hand, the use of the pre-equilibrated CO_2/heavy oil relative permeability curves for the simulation of the enhanced heavy oil recovery through CO_2 injection over-predicts the recovery. This is because as it has been explained above viscosity influences relative permeability for heavy oil, and the viscosity of the pre-equilibrated oil (saturated with CO_2) is not representative of the viscosity of the unsaturated heavy oil.

In this work, an analytical technique was used to correct for the difference in interfacial tension encountered when using substitute relative permeability from N2/heavy oil system, and the relative permeability curves from the analytical model compares well with the curves from the automatic history matching of the partially miscible CO_2 injection into heavy oil.

Another challenge in modelling heavy oil system is the representation of the three phase relative permeability that is often needed to model three phase flow system that is often encountered in enhanced heavy oil system. The modelling of three phase flow in existing commercial reservoir simulation uses three-phase relative permeability correlations to generate 3-phase relative permeability curves from 2-phase oil/water relative permeabilities

and 2-phase gas/oil relative permeabilities. This approach works satisfactorily for conventional oil since they were developed using conventional oils. In this study, this approach was used to model the WAG process in heavy oil, and a comparative analysis of the recovery performance from the heavy oil WAG experiment and these models was performed. The comparison shows that the existing three phase relative permeability models are inadequate in simulating three phase processes in heavy oil production. An alternative approach using an in-house three phase flow simulator was used in generating a three phase relative permeability curves suitable for heavy oil systems.

7.2 Conclusions

The main conclusions derived from this work are as follows:

1. The assumptions used in estimating the relative permeability curves for conventional oil are not valid in estimating heavy oil relative permeability curves. These assumptions like relative permeability being independent of viscosity is true for conventional oil systems because for all cases of oil viscosities encountered in the reservoirs for this system, the flow regime is always capillary-dominated; however, in the case of heavy oil systems, due to the large viscosities often encountered, the flow is often dominated by viscous force.
2. Increasing the displacement rate or increasing the viscosity of the displaced fluid in a coreflood experiment tends to shift the flow regime from a capillary dominated flow to a viscous dominated flow thereby aggravating instability at the displacement front with the consequent inefficient displacement.
3. The higher the instability at the displacement front, the worse is the resulting viscous fingering, and the smaller is the relative permeability of the displacing fluid.
4. For heavy oil systems with instability at displacement front, the water relative permeability from vertical coreflood is higher than the one from the horizontal corefloods. This is because gravity forces help in stabilizing coreflood experiments; thus vertical corefloods suffer from less instability than horizontal corefloods.
5. For stable displacement process, often encountered in conventional oil systems, relative permeability is only a function of the saturation of the fluid; whereas, for unstable displacement process, often encountered in heavy oil systems, relative

permeability is also a function viscosity ratio, flow rates, direction of flow, and interfacial tension.

6. The relative permeability curves for heavy oil with a tendency for instability are apparent relative permeability, and must be estimated at the exact reservoir condition, else may not be useful.
7. Though the JBN method and the graphical methods are analytical methods that can be easily used for estimating relative permeability for heavy oil because the high viscosity in this case makes the capillary terms negligible, the results of the relative permeability from these analytical methods are not as good as the result of the relative permeability estimated from history matching.
8. The Nitrogen-heavy oil relative permeability can be used as a substitute relative permeability to model CO_2/heavy oil system. This way, the challenge in estimating relative permeability in heavy oil systems involving CO_2 due to the partial solubility of CO_2 in heavy oil and the consequent reduction in the oil viscosity and interfacial tension can be overcome. However, to use this substitute relative permeability, it has to be corrected for the difference in interfacial tension in the N2/heavy oil system and CO_2/heavy oil system.
9. The three phase relative permeability models in existing reservoir simulation packages are not adequate in modelling three phase flow in heavy oil. The more unstable the flow process is, the less the suitability of the existing three phase models to simulate oil recovery in WAG and other three phase flow processes.
10. The automatic history matching of the three phase experimental results of heavy oil can give very useful relative permeability results but it is laborious and it takes a long time to get a reasonable match of the experiment.

7.3 Recommendations

1. Instability number should always be estimated for an heavy oil system to know if there is the possibility of viscous instability at the displacement front or not; thus knowing how best to approach the estimation of the relative permeability curves for the system.

2. If the instability number is high (higher than 13), there would be viscous instability; hence the experiments for estimating the relative permeability curves should be

performed at the exact condition in the reservoir as reservoir simulation studies results can be very sensitive to small changes in heavy oil relative permeability curves. The estimation from reservoir simulation should also be done with at least a 2D grid system.

3. For a thick heavy oil reservoir system with a high instability number, relative permeability for both horizontal and vertical flow should be estimated and used appropriately.

4. If the instability number is not high (not higher than 13), the relative permeability for heavy oil would be similar to that from conventional oil.

5. The three phase relative permeability for modelling heavy oil WAG and other three phase processes should be estimated from the automatic history matching of the three phase experimental results of heavy oil. The three phase relative permeabilities from these methods are more reasonable than those from existing three phase relative permeability models.

Appendix A: Experimental Facilities

A.1 Micro-model experiment facility

The micro-model experimental facility (micro-model rig) consists of the glass micro-model; fluid storage oven, micro-model oven, low rate pumps, and manual camera mount system. A schematic of the typical micro-model rig is shown in fig A-1. A glass micro-model is a transparent porous medium which consists of two glass plates. The first plate has a two dimensional pore pattern, generated by random sampling from a normal pore size distribution, etched onto its surface; and the second flat plate is then placed over the first etched one, covering the etched pattern and thus creating an enclosed pore space. This flat plate has an inlet hole and an outlet hole drilled at its either end, allowing fluids to be displaced through the network of pores. It is possible to observe the fluids as they flow along the pore channels and interact with each other because the structure is only one pore deep, and the containing walls are transparent glass. It can also be observed how the pattern of flow and trapping are influenced by the geometry of the pore network and the wettability of the glass wall.

The fluid storage oven is a temperature controlled air oven used to store the injection fluids, lines and connections at constant temperature; and the micro-model oven is an air oven used to maintain the overburden chamber which houses the micromodel. The low rate pumps are pumps used to inject and retract fluid to and from the glass micromodel and the overburden chamber; while the manual camera mount system is used to scan the micromodel for video and still image recording. The glass micromodel would first be saturated with distilled water before being injected with oil until it is fully saturated with oil.

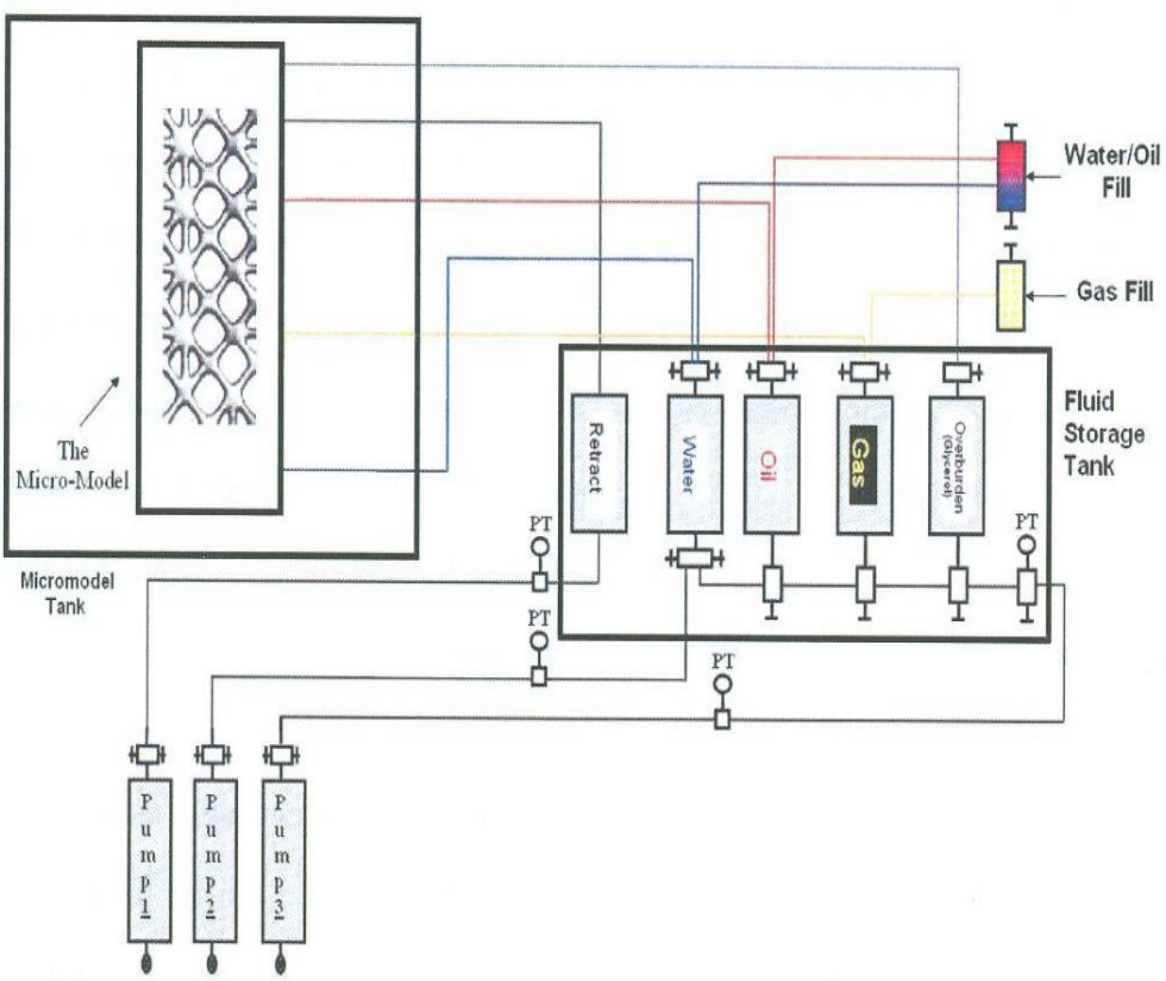

Fig A-1: Schematic diagram of the micromodel rig (Emadi, 2012).

A.2 Coreflood Experiments experiment facility

Figure A.2 is the schematic diagram of the coreflood rig used in this study. It consists of (1) high pressure, high temperature oven, (2) injection pumps, (3) pressure gauges, (4) the back pressure regulator, (5) the effluent collector, (6) the core, and (7) stainless piston cells for holding the test fluids. A fluid is circulated through the core by dedicating two cells (one initially empty, one initially full) to a fluid. With the aid of one of the injection pumps, a fluid is displaced from the cell initially filled with the fluid through the core to one of the effluent collector; while the differential pressure across the core is measured with the aid of the pressure gauges at the inlet and outlet of the core.

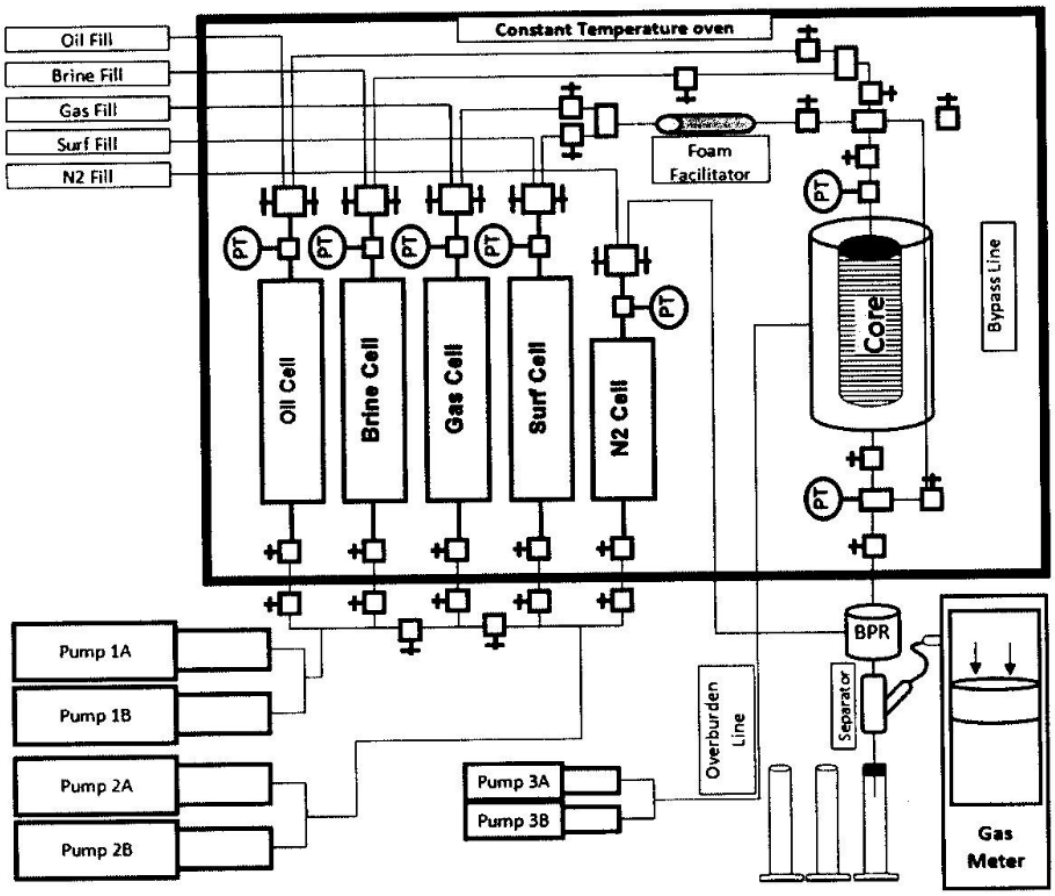

Fig A-2: Schematic diagram of the core flood rig (Emadi, 2012).

A.3 Viscosity Rig

A high pressure, high temperature 'capillary tube viscometer' rig was used for viscosity measurements. The pressure that forces the fluid to flow at a particular rate through a narrow tube is measured, and the viscosity of the fluid is then calculated through the Poiseulle's law.

The accurate measurement of fluid requires that the rig be calibrated with fluids of known density and viscosity

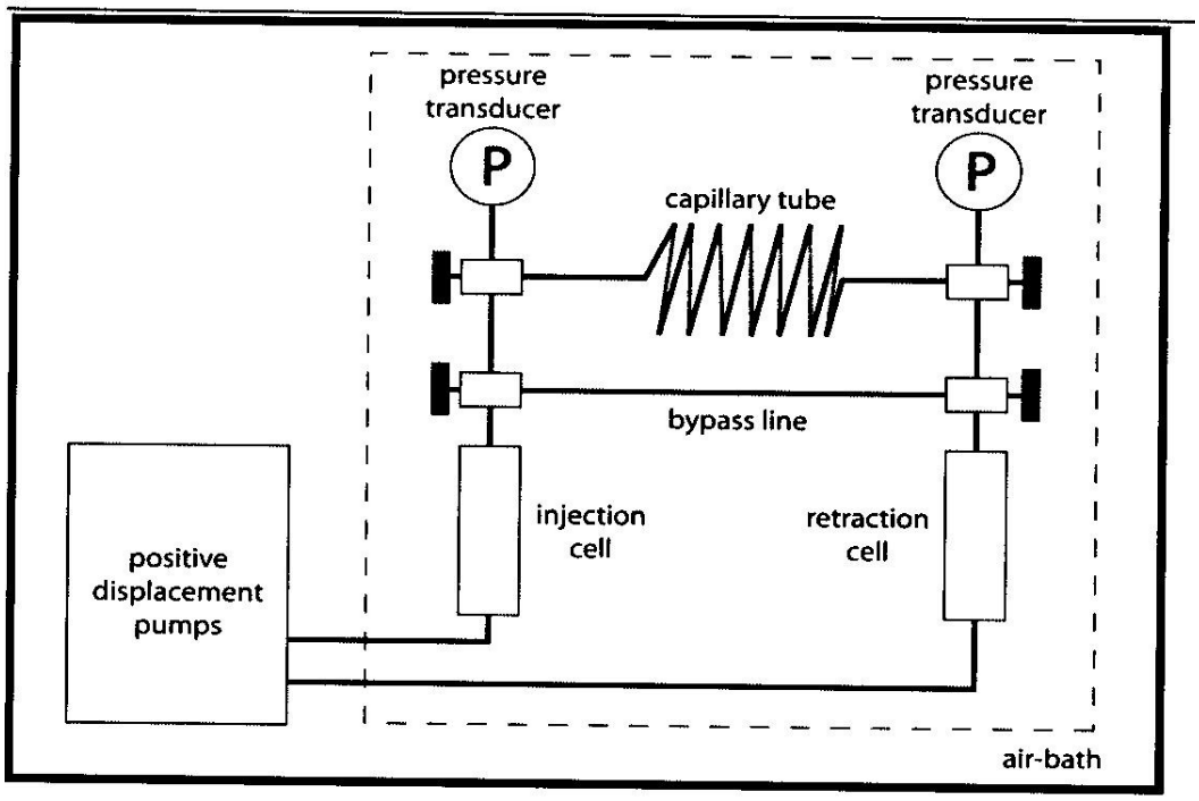

Fig A-3: Schematic diagram of the viscosity rig (Emadi, 2012).

Appendix B: Guideline for CMOST Two Phase Relative permeability History Matching

1. Be sure you have the CMG Technologies Launcher Open.

2. Open CMOST directly from the CMOST.exe or the shortcut, don't drag and drop the .dat file into the CMOST symbol in the CMG Technologies Launcher.

3. Create a folder and name it (this will be the main folder of your CMOST simulation).

4. Move the .dat file with the simulation you want to test into this folder

5. Open CMOST > File > New Project.

6. Project Name can be any, Base dataset you have to browse the .dat file in the folder of Step 1.

7. Select the "copy base case to project folder"

8. Click OK.

9. Now minimize CMOST and go to the folder from step 1, in there should have been created a folder with the same name chosen for the project (in step 4). Open that folder and Copy past into it all the simulation folders that correspond to the .dat file you have used in step 2 (this means .irf, .out, .mrf, .dat, etc…).

10. Now get back into CMOST and click in "New Study".

11. Give a Name.

12. Click on Browse and find the .dat set from Step 7.

13. Select “automatically create master dataset (.cmm)…

14. Click OK

Creation of .cmm and .fhf files

1. Inside the project folder should be a .cmm file.

2. Open it with notepad++.

3. Now for kr history matching you have to change the code bit correspondent to that in the following manner (you delete all the values for the kr curves and substitute for the code in red):

DENSITY OIL 58.058
DENSITY WATER 62.428

REFPW 1493.89

VWI 0.694

DENSITY GAS 0.113369

ROCKFLUID

RPT 1

**$ Sw krw krow Pcow

SWT

<cmost>OilWaterTable</cmost>

**$ Sl krg krog

SLT

<cmost>LiquidGasTable</cmost>

INITIAL

4. You must define what kr you want to history match or if you want to history match both. For exemple if it is a water injection into oil, then you only have to do <cmost>OilWaterTable</cmost> and for the SLT you leave the values as they are in the original simulation:

DENSITY GAS 0.113369

ROCKFLUID

RPT 1

**$ Sw krw krow Pcow

SWT

<cmost>OilWaterTable</cmost>

**$ Sg krg krog

SGT

0.26 0 0.3270637 ** 0.101795343

0.27 0.00556783 0.326725383 ** 0.100261925

0.28 0.00631168 0.32578864 ** 0.098790394

0.29 0.00711007 0.324252378 ** 0.097378738

0.3 0.007963 0.3221155 ** 0.09602495

0.31 0.00887047 0.319376913 ** 0.094727019

0.32 0.00983248 0.31603552 ** 0.093482934

0.33 0.01084903 0.312090228 ** 0.092290688

0.34 0.01192012 0.30753994 ** 0.091148269

0.35 0.01304575 0.302383563 ** 0.090053669

0.36 0.01422592 0.29662 ** 0.089004877

0.37 0.01546063 0.290248158 ** 0.087999884

0.38 0.01674988 0.28326694 ** 0.08703668

0.39 0.01809367 0.275675253 ** 0.086113255

0.4 0.019492 0.267472 ** 0.0852276

0.41 0.02094487 0.258656088 ** 0.084377705

0.42 0.02245228 0.24922642 ** 0.08356156

0.43 0.02401423 0.239181903 ** 0.082777156

0.44 0.02563072 0.22852144 ** 0.082022483

0.45 0.02730175 0.217243938 ** 0.081295531

0.46 0.02902732 0.2053483 ** 0.080594291

0.47 0.03080743 0.192833433 ** 0.079916752

0.48 0.03264208 0.17969824 ** 0.079260906

0.49 0.03453127 0.165941628 ** 0.078624741

0.5 0.036475 0.1515625 ** 0.07800625

0.51 0.03847327 0.136559763 ** 0.077403422

0.52 0.04052608 0.12093232 ** 0.076814246

0.53 0.04263343 0.104679078 ** 0.076236715

0.54 0.04479532 0.08779894 ** 0.075668817

0.55 0.04701175 0.070290812 ** 0.075108544

0.56 0.04928272 0.0521536 ** 0.074553885

0.57 0.05160823 0.033386208 ** 0.074002831

0.58 0.05398828 0.01398754 ** 0.073453372

0.59 0.05642287 0 ** 0.072903498

INITIAL

5. Also notice that in Step 3 the kr table is for liquid/gas, if you want for oil/gas if should be <cmost>OilGasTable</cmost>.

6. After doing these changes you can save the file and close the notepad++.

7. To create the .fhf file you only have to open a notepad++ file and write (considering that you want to history match with the oil production and differential pressure):

1999 01 05

'Actual Laboratory Data For CoreFlood #4'

1901 01 01

‘days’

2

‘Cumulative Oil SC’ ‘Well Bottom-hole Pressure’

‘bbl’ ‘psi’

2

‘IN’

0.002083333 0 1504.361163

0.004166667 0 1504.270231

0.008333333 0 1504.112587

‘OUT’

0.002083333 0.000003145 1495.376188

0.004166667 0.00000629 1495.383128

0.008333333 0.00001258 1495.411598

8. The red bits are the values corresponding to the time, cumulative oil and well bottom-hole pressure respectively for each line.

9. Also, you have to input these 3 parameters for each set of wells (the injectors “IN” and the producers “OUT”).

10. After that save the notepad++ file as “name.fhf” (you can chose the name) and move it to the project folder.

Setting up the History Matching in CMOST

1. You can now return to the CMOST.

2. Under the Study Tab you can click on General Properties.

3. Here the master and base data set should already be inputted automatically.

4. Verify if the Unit system in “field”.

5. Click in import .fhf file and browse for the .fhf file you created earlier.

6. Click “reload SR2”, Click “reload” (near the fhf).

7. Now, on the left side click on Fundamental data.

8. Click “insert” and select Wells > Out > Cum. Oil Production.

9. “insert” again > Wells > In > Well Bottom-hole pressure

10. “insert” again > Wells > Out > Well Bottom-hole pressure

11. (this will correspond to the data you have on the .fhf file and that is going to be history matched).

12. In this section you are basically defining which variables are going to change and in which range of values so that your kr curve can be generated using Corey.

13. For example if you wanted to use another method to generate kr instead of Corey you would have to insert the parameters necessary for that method.

14. Go to History Match Quality, insert the Cum oil production and the production and injection well bottom pressures (as in the example file) as follows:

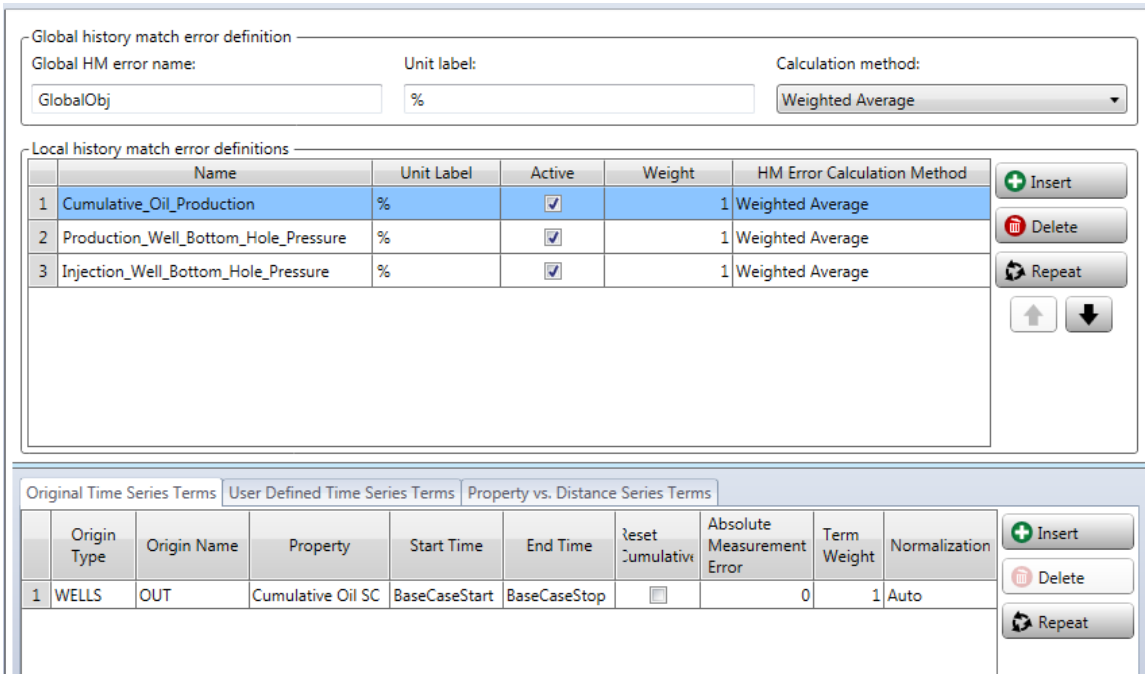

15. In the Control Center, go to Engine Settings and fill as follows:

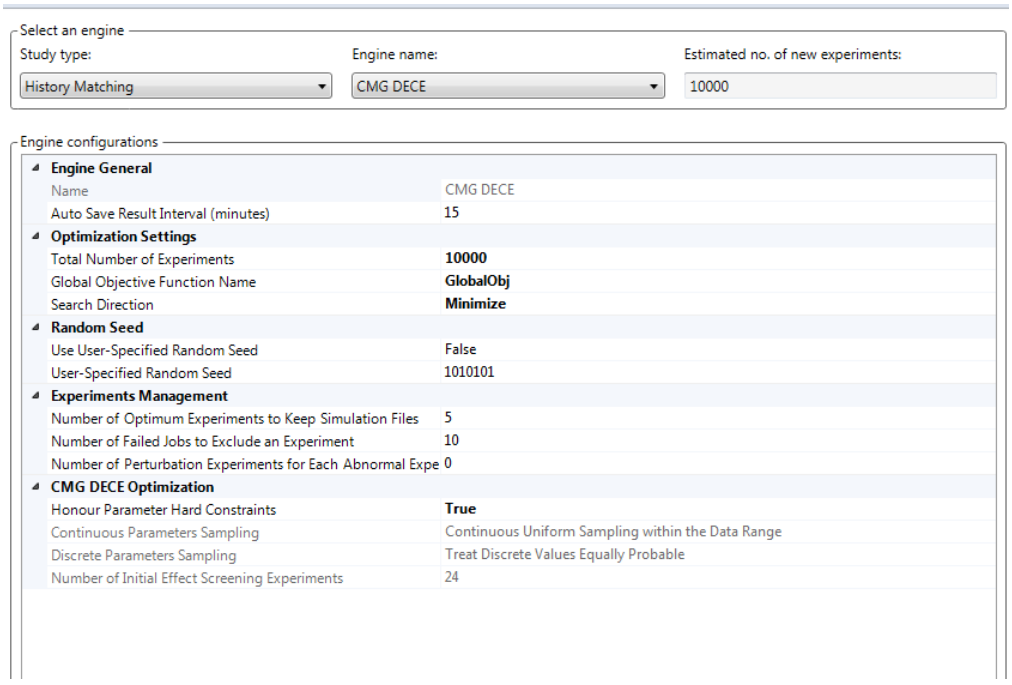

16. In Simulation Settings fill as follows:

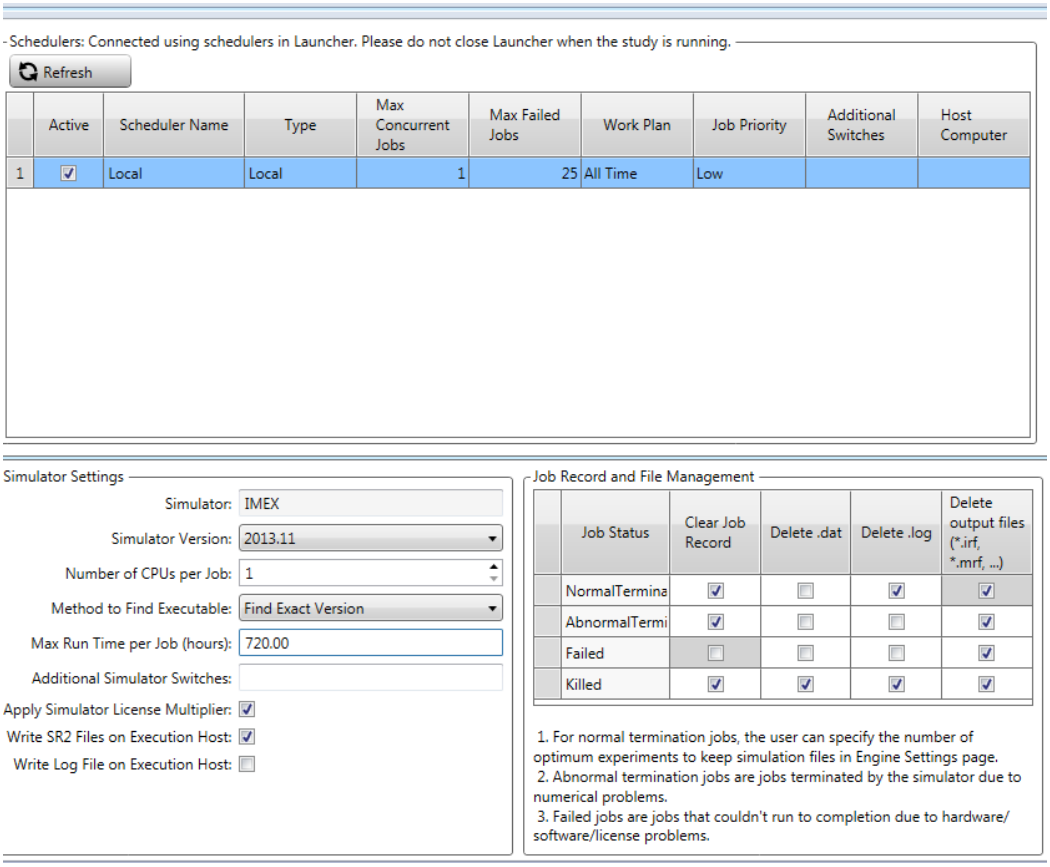

17. Now when everything is done you can go to “Control Center” and click in the green play to start your history matching process.

18. You can view in Real time the matching if you go to Results and analysis.

19. In Time series is presented the results in function of time, while in objective functions is presented as the minimum error for each parameter.

20. Now when you are satisfied with the results, for example the global objective function has a minimum and after several timesteps there isn’t an improvement:

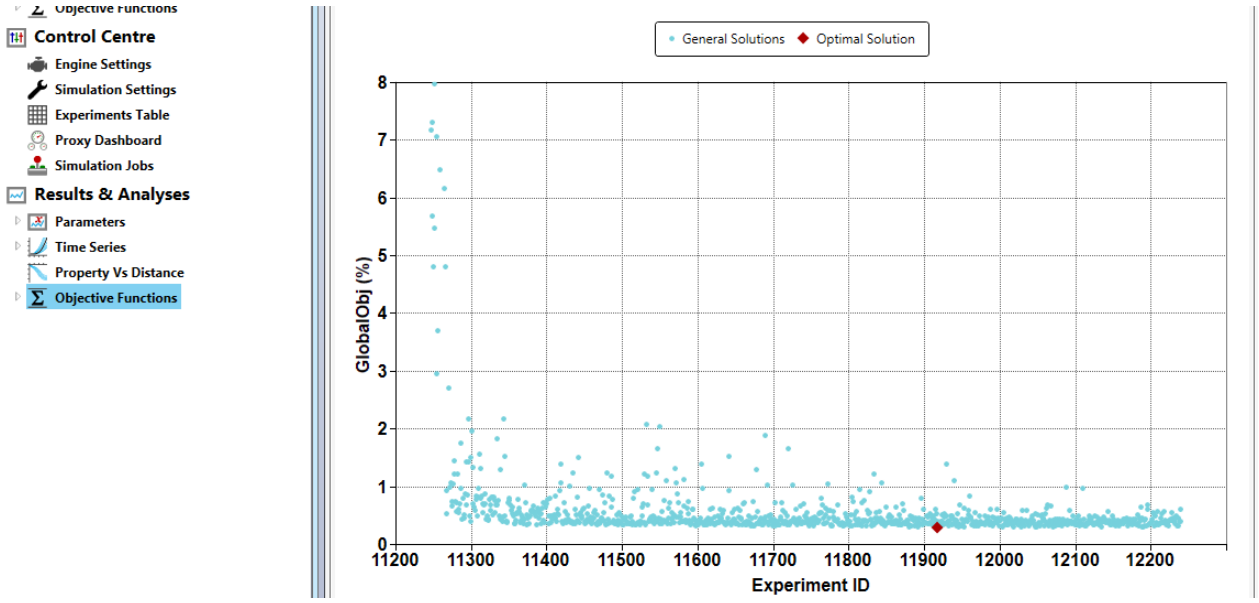

21. You can with the mouse see what is that optimum point correspondent to (or you can go see in the experiments Table under control centre) the number or ID of the simulation.

22. Then in the project folder you can find the corresponding .dat file.

23. If you open this .dat file in the CMG Builder, you can go into the relative permeability section to see what is the best kr for this case (alternatively you can go to the experiments table under control center in cmost and with the parameters value for that experiment ID calculate the kr curve using Corey, however this first method is easier).